# SYNTHESIS AND EVALUATION OF [2 + 1] Re(I) and $^{99m}$Tc(I) COMPLEXES

# SYNTHESIS AND EVALUATION OF [2 + 1] Re(I) and $^{99m}$Tc(I) COMPLEXES: NEW SYNTHONS FOR THE PREPARATION OF ISOSTRUCTURAL OPTICAL AND NUCLEAR PROBES

By

ABDOLREZA YAZDANI, B.Sc., M.Sc.

A Thesis

Submitted to the School of Graduate Studies

In Partial Fulfillment of the Requirements

For the Degree of

Doctor of Philosophy

Chemistry

McMaster University

DOCTOR OF PHILOSOPHY (2016) McMaster University

Chemistry Hamilton, Ontario

TITLE: Synthesis and Evaluation of [2 + 1] Re(I) and $^{99m}$Tc(I) Complexes: New Synthons for the Preparation of Isostructural Optical and Nuclear Probes

Author: Abdolreza Yazdani, B.Sc. (Tehran Azad University), M.Sc (University of Guelph)

Supervisor: Professor John F. Valliant

Number of Pages: XXVI, 260

**Abstract**

The synthesis, stability and photophysical properties of [2 + 1] Re(I) and Tc(I) complexes derived from bipyridine type ligands and a series of imidazole derivatives were investigated as a means of identifying complexes suitable for creating targeted isostructural optical/nuclear molecular imaging probes. The first generation complexes were prepared by combining $[Re(CO)_3(H_2O)_3]Br$ with 2,2'-bipyridine (bipy) to give $[Re(CO)_3(bipy)Br]$, which in turn was converted to the desired complexes by treatment with functionalized imidazoles. All products were fully characterized by conventional methods which included crystal structures of two new Re complexes. The corresponding $^{99m}Tc$ complexes $[^{99m}Tc(CO)_3(bipy)(L)]^n$ (L = imidazole derivatives) were prepared by combining $[^{99m}Tc(CO)_3(bipy)(H_2O)]Cl$ with the same series of monodentate ligands used with Re(I) and heating at 40 °C or 60 °C for 30 min. Quantitative transformation to the final products was confirmed in all cases by HPLC and the nature of the complexes verified by comparison to the authentic Re standards. Incubation in saline and plasma, and amino acid challenge experiments showed that N-substituted imidazole derivatives, bearing electron donating groups, exhibited superior stability to analogous metal complexes derived from less basic ligands. Imaging studies in mice revealed that with the appropriate choice of monodentate ligand, it is possible to prepare robust [2 + 1] Tc complexes that can be used as the basis for preparing targeted isostructural optical and nuclear probes.

The synthesis, stability, photophysical properties and *in vivo* biodistribution of $[M(CO)_3(BPS)(L)]^n$ (M = Re/$^{99m}Tc$, BPS = bathophenanthroline disulfonate, L =

imidazole derivatives) were investigated as a second generation of isostructural multimodal optical and nuclear probes. $[Re(CO)_3(BPS)(MeIm)]^-$ (MeIm = methylimidazole) was prepared in high yield as a model compound and showed enhanced optical properties to the corresponding bipy analogue. To prepare the radiolabeled compounds, BPS was added to $[^{99m}Tc(CO)_3(H_2O)_3]^+$ and the mixture heated to 40 °C for 15 min. The product, $[^{99m}Tc(CO)_3(BPS)(H_2O)]^-$ was immediately treated with N-methylimidazole (MeIm) and with heating at 40 °C for 15 min yielding $[^{99m}Tc(CO)_3(BPS)(MeIm)]^-$ **3b** in nearly quantitative radiochemical yield. A targeted analogue $[^{99m}Tc(CO)_3(BPS)(ImAln)]^{2-}$ (ImAln = imidazolealendronate) capable of binding regions of calcium turn-over associated with bone metabolism was also created. Biodistribution studies showed that the targeted $[^{99m}Tc(CO)_3(BPS)(ImAln)]^{2-}$ analogue cleared rapidly from non-target tissues and had significant accumulation in the shoulder (7.9 ± 0.2% ID/g) and knees (15.1 ± 0.9 % ID/g) by 6 h, with long residence in the skeleton, up to 24 h. The isostructural Re(I) analogue $[Re(CO)_3(BPS)(ImAln)]^{2-}$ was incubated with MCF-7 cells and fluorescence microscopy used to detect the probe that was located predominantly in the cytoplasm.

Having demonstrated *in vivo* targeting, [2 + 1] complexes of $^{99m}Tc(I)$ linked to a tetrazine were prepared and their utility for preparing radiopharmaceuticals using bioorthogonal chemistry was evaluated. Specifically, complexes of the type $[^{99m}Tc(CO)_3(N^N)(L)]^n$ (N^N = BPS and bipy), where the monodentate ligand (L) was a tetrazine linked to the metal through an imidazole group, were prepared in nearly quantitative radiochemical yield by adding $[^{99m}Tc(CO)_3(N^N)(H_2O)]^n$ to the imidazole-

tetrazine ligand and heating at 60 °C for 30 min. Measurement of the kinetics of the reaction between **10b** and *trans*-cyclooctenol showed a second rate order constant of 8.6 × $10^3$ $M^{-1}S^{-1}$ at 37 °C, which is suitable for pretargeting strategies that require rapid coupling to be effective *in vivo*. Stability studies showed that the products are resistant to ligand challenge and suitable for *in vivo* imaging. Biodistribution studies of the more water soluble BPS derivative in normal mice using pre-administered bisphosphonate conjugate of *trans*-cyclooctene (TCO-BP) showed high activity concentrations in the knee (9.27 ± 0.32% ID/g) and shoulder (5.28 ± 0.67% ID/g). SPECT/CT images showed that the [2 + 1] complex could also be used to visualize the damage associated with a bone tumor in a murine model further demonstrating the utility of this class of compounds for preparing new radiopharmaceuticals.

**Acknowledgements**

I would like to express my sincerest gratitude to an incredible group of people who have contributed to my success and made my Ph.D. experience most productive and stimulating. First and foremost, I extend my heartfelt appreciation and profound gratitude to my supervisor, Professor John Valliant who has always been an inspiring and relentless mentor. When I first joined the research group, I had very little experience working in a synthetic inorganic lab and even less experience with radiochemistry. Despite these challenges, Professor Valliant provided me not only with valuable opportunities to work on exciting projects, but extended generously his formidable guidance and encouragement when research was not going well. He celebrated the many accomplishments along the way and encouraged me to reach my potential. I was also offered numerous opportunities to participate at prestigious international conferences to discuss my research with some of the most eminent scientists in the field, to improve my communication skills and to further advance my professional network. For all of this and much more, I would like to acknowledge with sincere gratitude John's extraordinary support and guidance.

I would like to thank my committee members, Professor Ignacio Vargas-Baca and Professor David Emslie for their guidance throughout all phases of my project, for their constructive feedback and for taking their time to read my thesis. Their individual and collective feedback expedited the completion of my inquiry. This research would not have progressed as effectively without the support of the department research staff, particularly, Dr. Kirk Green and Dr. James Britten who continuously provided assistance

with instrumentation and in responding positively and productively to my questions. Thank you to the administrative staff in the Department of Chemistry and Chemical Biology for their administrative support.

A special note of thanks is extended to the members of the Valliant group, both past and present, who have all contributed to my valuable experience. I would like to offer gratitude to Dr. Mohamed El.Zaria, Dr. Dong Hyun Kim, Dr. Selvi Pitchumony, Dr. Joseph Ioppolo, Dr. Afaf Genady, Dr. Ramesh Patel, Dr. Denis Beckford, and the biologists in the group -- Shannon Czorny and Nancy Janzen for their respective valuable scientific insights and for welcoming and participating in great scientific discussions. I would like to thank Dr. Patricia Edem, Omid Beiraghi, Dr. Salma Al-Karmi, and Stephanie Rathmann not only for their help in the lab but for their valued friendship.

Last but not least, I would like to thank my wonderful family for all the love and encouragement. My partner has always been unwavering in her support and steadfast in her inspiration throughout the years. Thanks to my mother for her everlasting love, encouragement, support, and for all of the sacrifices she has made for my sister and me thereby enabling us to forge forward in life in positive and productive directions. I offer my warmest regards to all of those who supported me in any respect during the completion of the project. I have been truly blessed. Thank you all for everything.

## Publications

### Peer reviewed journal articles:

- Yazdani, A.; Vito, A.; Bilton, H.; Rathmann, S. M.; Genady, A. R.; Ahmad, Z.; Janzen, N.; Czorny, S.; Zeglis, B. M.; Francesconi, L. C.; Valliant, J. F. *J. Med. Chem.* **2016**, *59*, 9381-9389.

- Yazdani, A; Janzen, N.; Banevicius, L.; Czorny, S.; Valliant, J. F. *Inorg. Chem.* **2015**, *54*, 1728-1736.

### Manuscripts ready for submission:

- **Technetium(I) Complexes of Bathophenanthroline Disulfonic Acid**
  Yazdani, A; Janzen, N.; Czorny, S.; Valliant, J. F. *Inorg. Chem*.

- **Preparation of Tetrazine-Derived [2 + 1] Complexes of $^{99m}$Tc and *in vivo* Targeting using Inverse Electron Demand Diels-Alder Bioorthogonal Chemistry**
  Yazdani, A; Janzen, N.; Czorny, S.; Ungard, R.; Miladinovic, T.; Singh G.; Valliant, J. F. *Inorg. Chem*.

**Table of Contents**

**List of Figures**

**List of Supporting Figures**

**List of Supporting Tables**

**List of Schemes**

## List of Abbreviations

| | |
|---|---|
| BFC | Bifunctional chelating agent |
| Bipy | 2,2'-bipyridine |
| BODIPY | Boron-dipyrromethene |
| BPS | Bathophenanthroline disulfonic acid |
| Bq | Bequerel |
| CC | Calcium carbonate |
| CCAC | Canadian Council on Animal Care |
| $CD_3CN$ | Deuterated acetonitrile |
| δ | Chemical shift (NMR) |
| CO | Calcium oxalate |
| CPD | Calcium phosphate dibasic |
| CPP | Calcium pyrophosphate |
| CT | Computed Tomography |
| Cy5 | Cyanine 5 dye |
| Cys | Cysteine |
| $D_2O$ | Deuterated Water |
| DIPEA | Diisopropylethylamine |
| DOTA | 1,4,7,10-tetraazacyclododecane-1,4,7,10-tetraacetic acid |
| DTPA | Diethylenetriaminepentaacetic acid |
| EtOH | Ethanol |

| | |
|---|---|
| EtOHTrz | Ethanol triazole |
| eV | Electron volt |
| FDA | Food and Drug Administration |
| FITC | Fluorescein isothiocyanate |
| h | Hours(s) |
| HA | Hydroxyapatite |
| His | Histidine |
| HPLC | High Performance Liquid Chromatography |
| HRMS | High-resolution mass spectrometry |
| IAMC | Immobilized metal ion affinity chromatography |
| ICG | Indocyanine green |
| %ID/g | Percentage injected dose per gram |
| %ID/o | Percentage injected dose per organ |
| IEDDA | Inverse electron demand Diels-Alder |
| ImAln | Imidazole-alendronate |
| ImPA | Imidazole-pentanoic acid |
| ImPAMe | Imidazole-pentanoic acid methyl ester |
| ImTz | Imidazole-tetrazine |
| iv | Intravenous |
| $MAS_3$ | S-acetylmercaptoacetyltriglycine |
| MDP | Methylene diphosphonic acid |
| MeIm | N-methylimidazole |

| | |
|---|---|
| MeOH | Methanol |
| MI | Molecular imaging |
| min | Minute |
| MLCT | Metal-to-ligand charge transfer |
| mp | Melting point |
| NIRF | Near infrared fluorescence |
| NMR | Nuclear Magnetic Resonance |
| PBS | Phosphate-buffered saline |
| PET | Positron emission tomography |
| PSMA | Prostate specific membrane antigen |
| RCP | Radiochemical purity |
| RNA | Ribonucleic acid |
| $R_t$ | Retention time |
| SAAC | Single amino acid chelate |
| scFvs | Single-chain antibody fragments |
| SEM | Standard error mean |
| SNR | Signal-to-noise ratio |
| SPE | Solid phase extraction |
| SPECT | Single photon emission computed tomography |
| TBR | Target-to-background ratio |
| TCO | Trans-cyclooctene |
| TCO-BP | Trans-cyclooctene bisphosphonate |

| | |
|---|---|
| TEA | Triethylamine |
| TFA | Trifluoroacetic acid |
| THF | Tetrahydrofuran |
| β-t-C | β-tri-calcium phosphate |
| Trz | Triazole |
| 2D | Two-dimensional |
| Tz | Tetrazine |
| UV | Ultraviolet |
| ZA | Zoledronic acid |

# Chapter 1

## 1 Chapter 1. Introduction

### 1.1 Molecular Imaging

Molecular imaging (MI) aims to study non-invasively biological processes in cells, tissues, or living organisms through the use of instruments, endogenous contrast mechanisms and exogenous contrast agents.[1] From the clinical perspective, MI can be used to improve early detection of diseases, identify the presence of specific biomarkers, determine tumor margins, and monitor treatment efficiency. Two of the commonly used MI techniques, which are the foci of the work done in this thesis, are nuclear and optical imaging.[2]

#### 1.1.1 Nuclear Imaging – Positron Emission Tomography

Positron emission tomography (PET) is one of the two main nuclear imaging methods and is a sensitive MI technique that is used for quantitative measurements of physiological processes *in vivo*. In PET, a positron-emitting radionuclide after initial decay, produces two 511 keV γ-rays as a result of annihilation of the emitted positron with an electron. PET cameras detect the pairs of γ-rays which are oriented at approximately 180° from each other using a ring of detectors surrounding the patient.[3] Some common radioisotopes used in PET are O-15 (half-life 2 min), C-11 (20 min), N-13 (10 min), and F-18 (110 min) which are produced by a cyclotron and Rb-82 (76 s) which

is obtained from a generator.[4] Most radioisotopes are incorporated into molecules to generate radiotracers, also known as radiopharmaceuticals, which are then injected into patients prior to imaging. One of the most widely used PET radiopharmaceuticals is $^{18}$F-fluorodeoxyglucose ($^{18}$F-FDG); a glucose analogue that is readily taken up by tumors.[5] The main limitations of PET are its poor spatial resolution (approximately 3-5 mm), radiation dose to patients and most PET agents use short half-life radioisotopes which requires them to be used shortly after production.

### 1.1.2 Nuclear Imaging – Single photon emission computed tomography

Single photon emission computed tomography (SPECT) is another nuclear MI technique which employs γ-emitting radionuclides. γ-Rays emitted from SPECT isotopes are measured by one or more gamma detectors that are fitted with collimators. Collimators only allows entry of gamma rays that are perpendicular to the plane of the camera Modern SPECT machines are composed of rotating gamma cameras or multiple cameras where collected 2D images are combined to generate a 3D image.[6] Some common radionuclides used in SPECT are Tc-99m (half-life 6.01 h), I-123 (13.2 h), Ga-67 (78.3 h), and In-111 (2.8 days).[7] The main advantage of SPECT is the availability of low cost radioisotopes that have reasonably long half-lives. For example, $^{99m}$Tc is costs a few dollars per mCi and is accessible from a generator (see section 1.3).[8]

### 1.1.3 Optical Imaging

Optical imaging techniques exploit nonionizing photons and several different sources of contrast such as absorption, emission, reflectance, scattering, and fluorescence.[9] Fluorescence imaging requires administration of molecules that absorb energy within a specific energy window and re-emit typically at a longer wavelength.[10] Fluorescent imaging remains a sensitive and relatively low cost tool to study cellular structures, functions, and pathways in living cells organisms. However, the major disadvantage of this technique arises during *in vivo* applications due to the poor depth of penetration of light in tissues. The depth is limited to millimeters where signal quantification is challenging due to light attenuation and scattering differences in different tissues.[11] Despite these limitations, optical imaging agents are increasingly used for *in vivo* studies where indocyanine green (ICG) and fluorescein are approved by the FDA for hepatic function testing and ophthalmology respectively.[12]

## 1.2 Dual-Modality Imaging Agents

All imaging modalities have advantages and disadvantages in terms of resolution, sensitivity, tissue penetration, and cost amongst other key features. For example, nuclear techniques (PET and SPECT) have excellent sensitivity and tissue penetration, but very poor resolution (millimeters).[13] Optical imaging on the other hand, can have very high resolution (sub-millimeter), but very low tissue penetration and signal intensity due to tissue absorption, scattering, and autofluorescence.[14] Dual-modal imaging is the combination of two imaging techniques in order to benefit from their strengths and

overcome limitations of single modality imaging. To undertake dual-modal optical and nuclear imaging, contrast agents that can produce multiple signals are desirable.

### 1.2.1 PET/Optical Agents

Agents that can be used for both PET and optical imaging have been reported notably for image-guided surgery applications.[15] For example, a porphyrin-based photosensitizer was developed as a single agent for PET/optical imaging and photodynamic therapy (Figure 1.1, left). The compound exhibits strong absorption at 662 nm and emission at 667 nm in organic solvents ($CH_2Cl_2$, THF). The compound was labeled with the PET isotope $^{124}I$, which has a half-life of 4.2 days, and was therefore ideal for this study due to the long biological half-life of the parent compound.[16] More recently, F-18 labeling of bodipy dye has been reported for PET/fluorescent imaging.[15] The photophysical properties of this compound features a broad absorption band at 506 nm and an emission band at 528 nm (Figure 1.1, right). No bone uptake was observed even after 4 h indicating negligible release of free $^{18}F^-$ and good stability of the compound *in vivo*. *Ex vivo* fluorescent imaging indicated accumulation of the probe in liver and kidneys, which was consistent with the *in vivo* PET imaging data. Parallel efforts have been made to develop $^{11}C$-based PET/optical imaging agents despite the short half-life of $^{11}C$ (20 min).[17] For instance, a styryl dye labeled with carbon-11 has been used as a new probe to target RNA.[18,19]

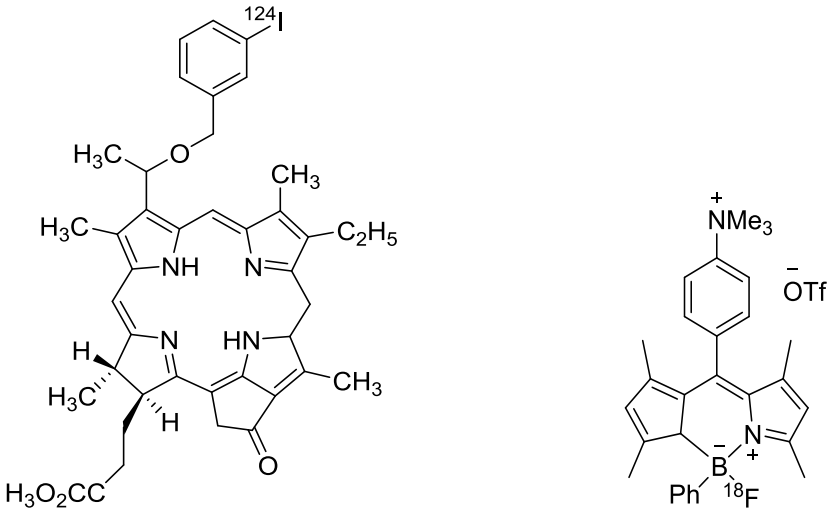


**Figure 1.1** A porphyrin-based photosensitizer (left)[16] and labeled bodipy dye for PET/optical imaging (right).[15]

Peptide derivatives have also been used to develop targeted PET/optical agents.[20] A dual-modality near infrared fluorescence (NIRF)/PET agent based on an engineered cystine knot peptide (knottin 2.5D) was prepared by conjugating Cy5.5 and $^{64}$Cu-DOTA to the N-terminus of the peptide (Figure 1.2).[21] NIRF and PET imaging results in tumor xenograft indicated that decreased wash-out and significantly better retention compared to a $^{64}$Cu-labeled single modality agent. Good linear correlation was observed over 1-24 h for both the optical and nuclear data indicating that the two labels are effectively delivered to the tumor.

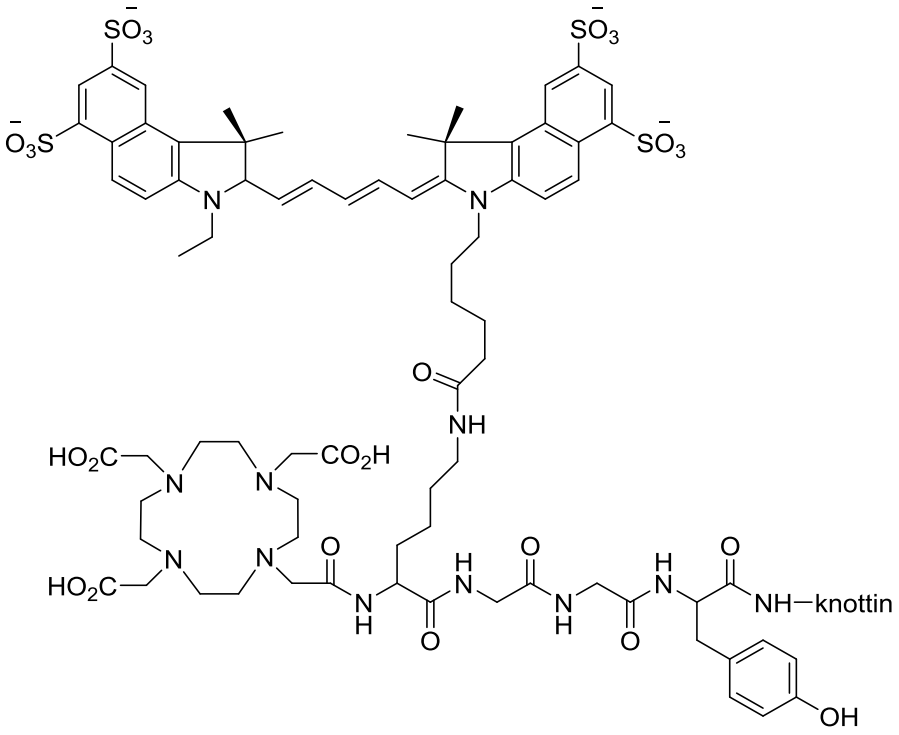


**Figure 1.2** NIRF/PET dual-modality PET probe derived from Cy5.5 and DOTA.[21]

As a second and related example, a cyclic peptide ($M_2$) that targets MMP-2/9 was combined with a NIRF dye (IRDye 800CW) followed by DOTA conjugation for $^{68}$Ga labeling.[22] Radiolabeling with $^{68}$Ga requires low pH (3.5-4) and elevated heating temperatures (95 °C). Therefore, additional stability studies were performed to evaluate the impact of $^{68}$Ga labeling on the optical properties. The results showed the labeling conditions did not adversely affect the optical and biological properties of the agent. In another report, octreotate was conjugated with DOTA chelating group and a near infrared (NIR) cypate fluorescent dye as a somatostatin (SSTr2) receptor-imaging agent.[23] The agent, which was labeled with both $^{64}$Cu and $^{177}$Lu, exhibited very low tumor uptake (less

than 1% ID/g) and predominant hepatobiliary clearance (more than 90% ID/g in the liver). Bombesin peptide analogues labeled with FITC and DOTA have been reported by the same research group.[24] It was found that the relative positions of the dye and chelator on the lysine linker had a major effect on receptor binding affinity.

### 1.2.2 SPECT/Optical Agents

Similar to the PET/optical agents, the combination of SPECT and optical imaging have been also explored.[25] It is known that bisphosphonates (BPs) binds to hydroxyapatite (HA) bone mineral surfaces and a NIRF imaging agent with bisphosphonate (Pam-800) have been developed to target HA.[26] A BP-based SPECT/optical imaging agent (Pam-Tc/Re-800) was used to target breast cancer microcalcification.[27] For this probe, the BP is labeled with an S-acetylmercaptoacetyltriglycine ($MAS_3$) chelator and IRDye800CW (Figure 1.3 A). NIRF and SPECT/CT *in vivo* imaging after labeling with $^{99m}Tc$ in a breast cancer model exhibited rapid clearance from the soft tissues and high tumor uptake of the agent indicating its usefulness for bone metastasis detection (Figure 1.3 B, C). A series of SPECT/optical dual-modality agents with the combination of fluorescent molecules such as acridine and flavone with $[^{99m}Tc(CO)_3]^+$ core were developed for cell-based studies; limited *in vivo* data has been reported.[28–31]

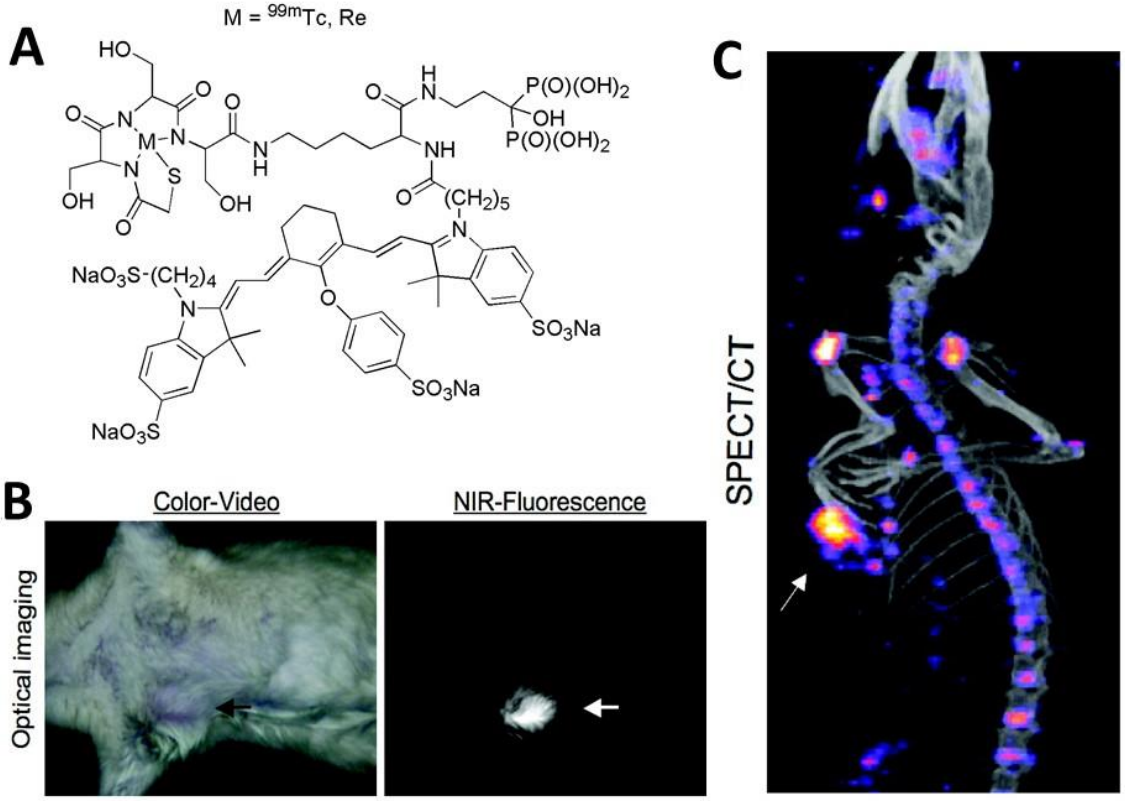


**Figure 1.3** Chemical structure of Pam-Tc-800 (A). NIRF (B) and SPECT/CT (C) *in vivo* imaging after administration of the probe in a breast cancer rat model for the detection of breast cancer microcalcification[27]

Several targeting peptide derivatives have also been reported for SPECT/optical imaging. A Caspase-3-sensitive SPECT/optical imaging agent was developed by linking $^{99m}$Tc-chelator to a fluorescent rhodamine-110 based DEVD peptide.[32] The probe is not fluorescent but it becomes fluorescent upon cleavage from DEVD in the presence of Caspase-3. In another study, a cyclic peptide [c(KRGDf)] was dual-labeled with $^{111}$In

(through DTPA), and a near-infrared dye, IRDye800.[33] It was found that target-to-background ratios (TBR) of nuclear and optical imaging at the targeted tumor site are similar. Furthermore, an analysis of signal-to-noise ratio (SNR) showed greater sensitivity of NIRF over SPECT imaging for the subcutaneous tumor targets. Another SPECT/optical dual-labeled imaging agent was developed by attaching a cyclic peptide c(CGRRAGGSC), which is known to target interleukin 11 receptor alpha-chain (IL-11RR) to DTPA ($^{111}$In labeling) and a fluorescent dye (IR-783-S-Ph-CO) via a lysine linker (Figure 1.4, A).[34] The cross validation and direct comparison of optical and nuclear imaging of the agent in a mice bearing human breast cancer xenograft (MDA-MB-231) using a single injection demonstrated the tumor targeting capabilities of the conjugate *in vivo* (Figure 1.4, B).

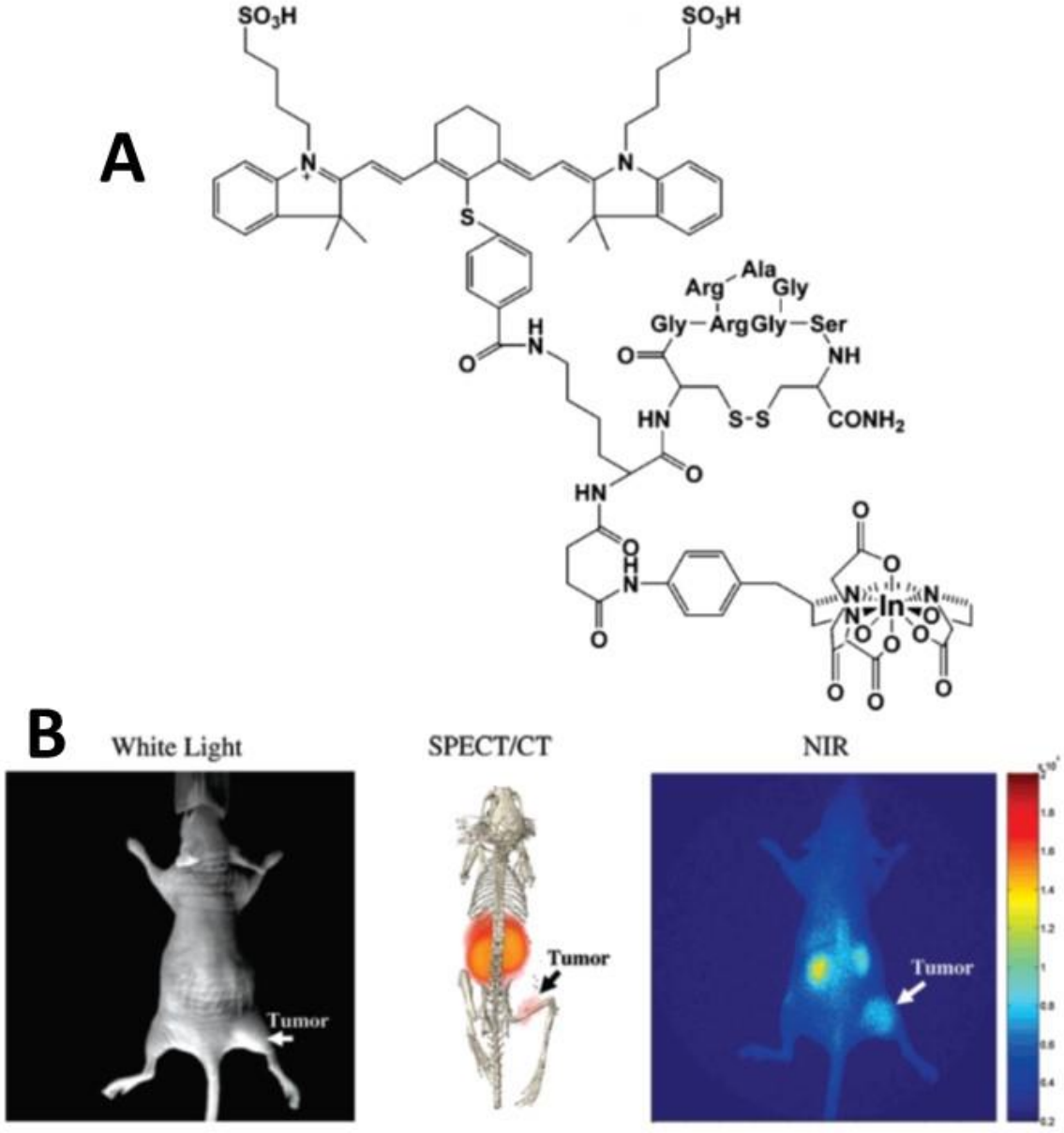


**Figure 1.4** Chemical structure of $^{111}$In-DTPA-(IR-783-S-Ph- CO)-c(CGRRAGGSC) (A). NIRF and SPECT/CT imaging 24 h after administration of the probe in a mice bearing human breast cancer xenograft (MDA-MB-231) (B).[34]

### 1.2.3 Isostructural Multimodal Agents

Nuclear/optical dual-modality imaging agents can be particularly useful clinically in cancer patient management. They make it possible to employ whole-body PET/SPECT imaging to identify the location of a disease and optical imaging to guide tumor resection. The ability to use one imaging agent for both applications instead of two separate compounds (the radiolabeled and fluorescent forms) can reduce development cost, facilitate clinical translations, and simplify lead discovery and validation efforts.[15] These multimodal optical and nuclear probes were traditionally prepared by modifying targeting vectors with a radionuclide binding prosthetic group and an optical dye.[35–37] The challenge with this approach is that the two groups can have a significantly detrimental impact on target affinity and ability to bind to the target of interest.

More recently, research has focused on developing a single construct that can be used as multimodal nuclear/optical agent. Radiolabeled dyes[38–43] for example, including $^{18}$F-labeled BODIPY have been reported as a PET/optical multimodal imaging probe that can be used for the labeling of small molecules as well as biological macromolecules.[44] As an another example, a modified DTPA-mannosyl-dextran (Lymphoseek) has been used for PET/NIRF imaging of sentinel lymph nodes (SLNs) in preclinical studies.[45] SLN imaging has attracted attention because changes in the lymph nodes are closely related to tumour metastasis, especially in breast and prostate carcinomas as well as melanomas. Lymphoseek was originally developed to locate the sentinel nodes for surgical resection.[46]

A related approach involves generating the radiolabeled analogue of luminescent metal complexes. Here the stable isotope of the metal is replaced with a radioactive

isotope or the same element or a transition metal congener to generate isostructural complexes.[47–53] For example, functionalized bis(thiosemi-carbazone) is an excellent tetradentate chelator which selectivity targets hypoxic tissues, particularly in the heart and brain.[54–56] When chelated to metals such as $Zn^{2+}$ and $Cu^{2+}$, the product is fluorescent and has been used in optical microscopy studies.[57] The radiolabeled $^{64}$Cu–bis(thiosemi-carbazonate) complex was prepared using facile transmetallation from the corresponding $Zn^{2+}$ analogues using $^{64}Cu(OAc)_2$ to give the isostructural nuclear probe.[58]

One of the first examples of isostructural SPECT/optical multimodal agent was based on the so called single amino acid quinoline (SAACQ) chelate. SAACQ contains two quinoline groups which form a luminescent complex with Re(I) and that can also be labeled with $^{99m}$Tc.[59–61] ReSAACQ has been used to image neurospheres *in vitro* while the $^{99m}$TcSAACQ was utilized to monitor cell transplantation using SPECT (Figure 1.5).

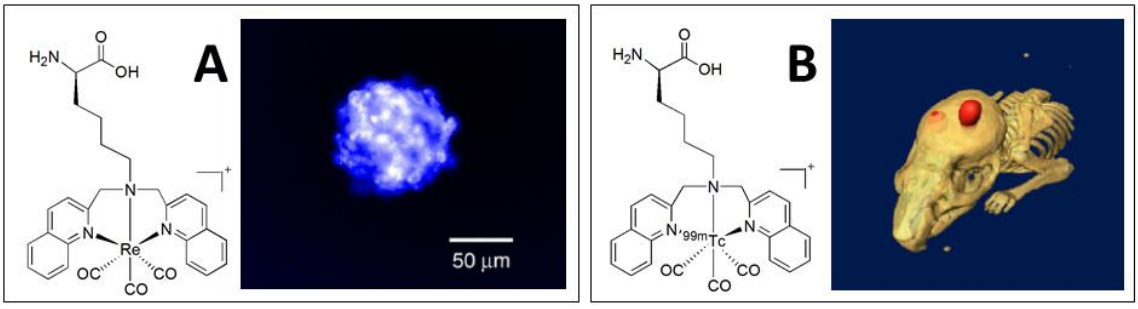


**Figure 1.5** Epifluorescent image of a single neurosphere incubated with a ReSAACQ-TAT peptide for 2 h at 37°C (A), SPECT/CT scan of cells labeled with the Tc analogue (image taken at 20 min post-transplantation) (B).[60]

## 1.3 The Chemistry of Re/Tc

$^{99m}$Tc is the most widely used radioisotope in diagnostic nuclear medicine due to its favorable properties and low cost. $^{99m}$Tc is readily available from $^{99}$Mo-$^{99m}$Tc generators[62] where the isotope can be isolated as $^{99m}TcO_4^-$ on a daily basis from the decay of $^{99}$Mo (Figure 1.6).[63] $^{99m}$Tc has a primary γ emission of 140 keV, which is within the desired range (30-300 keV) for commercial gamma cameras. For gamma rays that have energies below this range they are extensively absorbed by tissue. For those above 300 keV, commonly available scintillators are not able to detect the gamma rays effectively. The nature of the emissions from $^{99m}$Tc minimize the radiation dose to patients. Furthermore, the 6 h half-life of $^{99m}$Tc provides sufficient time to prepare, purify, and administer doses and to allow for optimal uptake and clearance from the target sites.

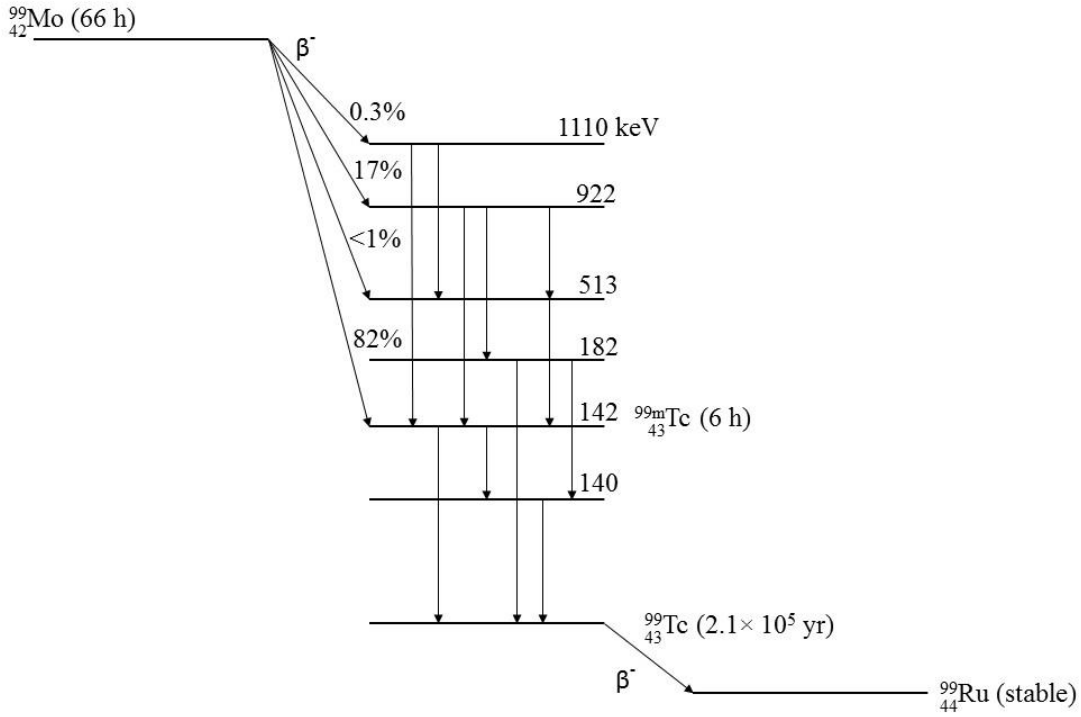


**Figure 1.6** Decay scheme of $^{99}$Mo to $^{99m}$Tc. Arrows going left to right indicate $\beta^-$ decay while vertical arrows show isomeric transitions ($\gamma$ or internal conversion). The energy levels are not shown to scale.[63]

Technetium (atomic number 43) is a transition metal in group 7 (Mn, Tc, and Re). Technetium forms compounds in a wide variety of oxidation states ranging from -1 to +7.[64,65] For nuclear medicine applications, complexes of Tc(V) and Tc(I) are the most common. Tc(V) complexes generally adopt square pyramidal geometries and often contain oxo, nitrido, imido, or hydrazido group in the axial position.[66] The chelates used

for Tc(V) are generally tri or tetradentate and contain a combination of oxygen, nitrogen, sulfur, and phosphorous atoms.[67]

Davison, Jones et al. prepared stable, water soluble Tc(I) complexes of hexakis (alkyl isocyanide) and hexakis (ary1 isocyanide) directly from $^{99m}TcO_4^-$ as the first examples of organometallic complexes that can be used for medical imaging.[68] They showed that the Tc(I) complex was a highly effective myocardial perfusion imaging agent.[69] The biodistribution characteristics were further refined by using a methoxybutyl isocyanide substituent to create Tc-MIBI, which was ultimately approved for clinical use under the trade name Cardiolite.[70,71] As an alternative starting material to prepare Tc(I) complexes, Alberto *et al.* reported a convenient method to prepare $[Tc(CO)_3(H_2O)_3]^+$ in aqueous media from pertechnetate. This complex reacts with a wide variety of ligands through displacement of the labile water molecules offering tremendous versatility when developing novel Tc radiopharmaceuticals (see sections **1.3.1**-**1.3.4**).[72–74]

Technetium has no stable isotopes consequently for most $^{99m}Tc$ radiopharmaceuticals, non-radioactive Re is often used for structural characterization and preliminary *in vitro* screening. Complexes of Re and Tc are typically the same size due to lanthanide contraction and relativistic effects.[75] The chemistry of the two elements can however differ particular with respect to redox potential and stability of complexes towards disproportionation. Re-complexes are thermodynamically more stable in higher oxidation states comparing their Tc counterparts. As a result, reducing rhenium from high oxidation states to lower oxidation states requires much harsher conditions. Re complexes

are also more inert than their Tc analogues while complexation type reactions often requires more forcing conditions.[76–77]

Notwithstanding the potential differences in their chemistry, to verify the formation of new $^{99m}$Tc complexes, which are produced in small (ng) quantities, the Re complex once fully characterized by traditional methods is often co-injected with the $^{99m}$Tc-species onto an HPLC equipped with UV and gamma detectors. Correlation of retention times is used to indicate the desired product has been formed. An additional advantage of using Re, is that it has two β-emitting radioisotopes $^{186}$Re and $^{188}$Re that can be used to create radiotherapeutic analogues of $^{99m}$Tc based diagnostics.[78]

### 1.3.1 Organometallic Complexes of Tc

$^{99m}$Tc is obtained from the $^{99}$Mo-$^{99m}$Tc generator as $^{99m}TcO_4^-$ in saline which necessitates that radiolabeling be performed in aqueous solutions. Alberto *et al.* developed a method to produce a precursor that can be used to generate organometallic complexes of $^{99m}$Tc in aqueous solutions at the tracer level. $[Tc(CO)_3(H_2O)_3]^+$ can be produced in water in a single step by direct reduction of pertechnetate with boranocarbonate.[79,80] The water molecules in $[Tc(CO)_3(H_2O)_3]^+$ are labile and can be displaced by a wide range of donor groups and used to create targeted organometallic radiopharmaceuticals.

Typically, the design of target-specific $^{99m}$Tc radiopharmaceutical involves the use of a bifunctional chelating agent (BFC) approach. A BFC consists of a $^{99m}$Tc-chelating unit and a reactive functional group for linking to a biomolecule.[81] An ideal

BFC should be able to form a stable complex with the radiometal in high radiochemical yield (RCY) and purity (RCP) at very low concentrations of a BFC-biomolecule conjugate.[82] The diverse coordination chemistry of $[Tc(CO)_3]^+$ core has led to development of a variety of BFCs based on bi- or tridentate ligand systems, and target-specific radiopharmaceuticals.[83–85]

A large array of tridentate Tc(I) chelates have been reported. For example, the so-called "click-to-chelate" method was developed in which functionalization of biomolecules and radiolabeling can be achieved in a convenient one-pot reaction.[86]. In the "click-to-chelate" strategy, the copper(I) catalyzed azide-alkyne cycloaddition (CuAAC; click reaction)[87] is used for the synthesis and conjugation of tridentate chelating systems that form stable complexes with the Re(I)/Tc(I)-tricarbonyl core.[88] Since its first report in 2006, "Click-to-chelate" has been applied to the development of numerous novel Re(I)/Tc(I) radiopharmaceuticals.[89,90] In one interesting example, isostructural $^{99m}$Tc-tricarbonyl folic acid radiotracers, one histidine-based and one triazole-based, were prepared.[91] The 1,2,3-triazole-containing folic acid derivative was prepared using the "click-to-chelate" approach, which was achieved in higher yield and in fewer steps than for the histidine derivative while stability and biological properties including the SPECT/CT images of the two agents were identical.

A facile synthetic route based on a tridentate chelating system with a pendent amino or carboxylic acid functionality for coupling to peptides and proteins via formation of an amide bond has been developed.[92] Our group was involved in preparing single amino acid chelates (SAACs) which are lysine derivatives capable of binding Re(I) and

Tc(I).[93,94] The tridentate chelating SAAC ligands have been prepared using a wide array of donors including pyridine, quinoline, imidazole and thiazole groups designed for effective coordination to the $[M(CO)_3]^+$ core. The other functional groups on the SAAC ligands allow for incorporation into peptide sequences using solid phase peptide synthesis (Figure 1.5).

Tridentate complexes of $^{99m}$Tc(I) have been used to create agents that are now in clinical trials. Several different $^{99m}$Tc(I)-labeled PSMA inhibitors have been previously reported.[95–97] Many of them however, have shown high liver uptake and clearance through intestine which is not ideal since prostate cancer usually metastasizes to the abdominal cavity. More recently, new $^{99m}$Tc(I)-labeled PSMA inhibitors based on a SAAC construct containing functionalized polar imidazole rings ($^{99m}$Tc-MIP-1404 and $^{99m}$Tc-MIP-1405) have been developed to reduce lipophilicity and to avoid gastrointestinal clearance (Figure 1.7).[98] Pharmacokinetics and biodistribution of these two agents have been studied in patients with metastatic prostate cancer.[99] They both showed rapid clearance from the blood, acceptable liver and kidney uptake, and high tumor-to-background ratios which range from 3:1 to 9:1.

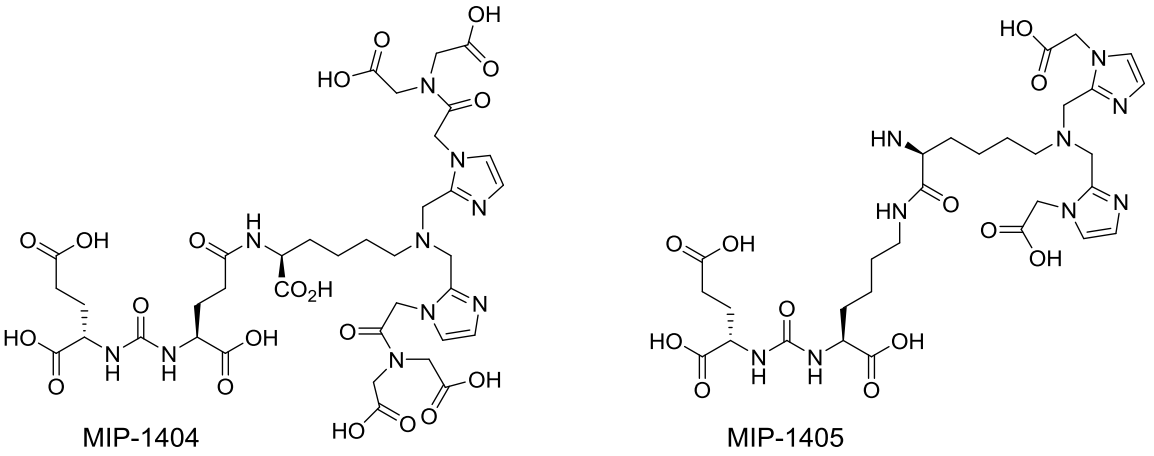


**Figure 1.7** Chemical structures of MIP-1404 and MIP-1405.

### 1.3.2 Rhenium(I) Polypyridine Complexes

Bipyridine and related bidentate pyridine type ligands coordinate to the **[**$Re(CO)_3]^+$ core and form complexes of the type $[Re(CO)_3(bipy)(L)]$. These complexes have been shown to have attractive photophysical properties.[100] They typically show excitation bands in the UV-Vis region (350-410 nm), which are associated with singlet metal-to-ligand charge transfer ($^1$MLCT), and broad emission bands (500-700 nm) attributed to $^3$MLCT.[101] The Re(I) complexes often exhibit long emission life-times (μs to ms) and large Stokes' shifts (> 100 nm) which allows for differentiation from autofluorescence.[102]

Compounds of the type $[Re(CO)_3(bipy)(L)]$ are commonly referred to as [2 + 1] complexes, where the "2" represents the bidentate ligand and the "1" the monodentate donor. This structure provides a great deal of versatility when designing novel probes.

The bidentate chelator can be used to optimize the photophysical properties, while the monodentate ligand in the axial position has been employed to modify cellular uptake and the intracellular target.[103] Furthermore, the solubility and stability can be tuned by altering substituents on the bidentate ligand and by changing the nature of the monodentate ligand.[104]

Rhenium polypyridyl complexes are typically prepared by combining a rhenium halide pentacarbonyl, $[Re(CO)_5X]$, with the chelating bisimine agent (NˆN). The resulting species $[Re(CO)_3(NˆN)X]$ is then activated to ligand exchange by precipitation of the halide with silver salt in an appropriate solvent. Finally, $[Re(CO)_3(NˆN)(sol)]X$ is converted to the target complex by treatment with the substituted monodentate ligand which has to date been largely pyridine based.

### 1.3.3 Rhenium(I) [2 + 1] Type Imaging Agents

Luminescent rhenium [2 + 1] systems have been utilized to prepare cell imaging agents.[105–108] The first example of Re polypyridyl application in cell imaging was reported in 2007, in which a variety of cationic, anionic, and neutral complexes were used to image parasitic flagellate associated with *spironucleus vortens.*[109] It was shown that the change in formal charge and lipophilicity was the driving force in controlling uptake and cellular localization. For example, the hydrophilic anionic $[Re(CO)_3(BPS)(L)]^-$ complex (BPS = bathophenanthroline disulphonate, L = 3-hydroxymethylpyridine) was incubated with MCF-7 cell line, which exhibited localization in the exterior plasma membrane (Figure 1.8). The lipophilic cationic

complexes appeared to reside mainly in the lipid membranes, while the neutral species showed cell uptake but also high cytotoxicity.

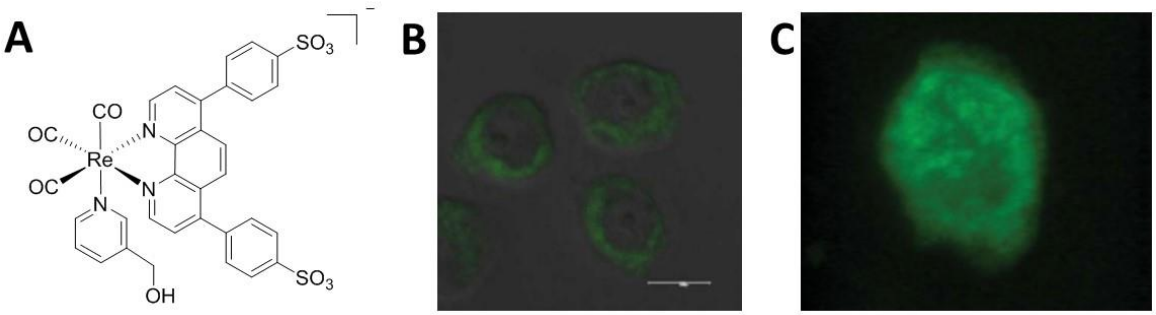


**Figure 1.8** Chemical structure of $[Re(CO)_3(BPS)(py\text{-}3\text{-}CH_2OH)]$ (A), Overlaid fluorescence and transmitted light images of the complex in MCF-7 cells showing localization in the exterior plasma membrane (B), and 3D reconstruction showing the complex in the plasma membrane of MCF-7 cells (C).[90]

A number of groups demonstrated that the uptake and localization of the rhenium [2 + 1] complexes can be controlled by small variation in ligand structure. For example, the $[Re(CO)_3(bipy)(L)]$ complex (bipy = 2,2′-bipyridine, L = 3-chloromethylpyridine) exhibited accumulation in mitochondria.[110] The chloromethyl unit is known to be thiol-reactive for which mitochondria are particularly rich (Figure 1.9). In another study, biotin-appended complexes have been studied as a method of promoting cell uptake.[111] *In vitro* studies showed that the complex was localized in the perinuclear region after internalization.

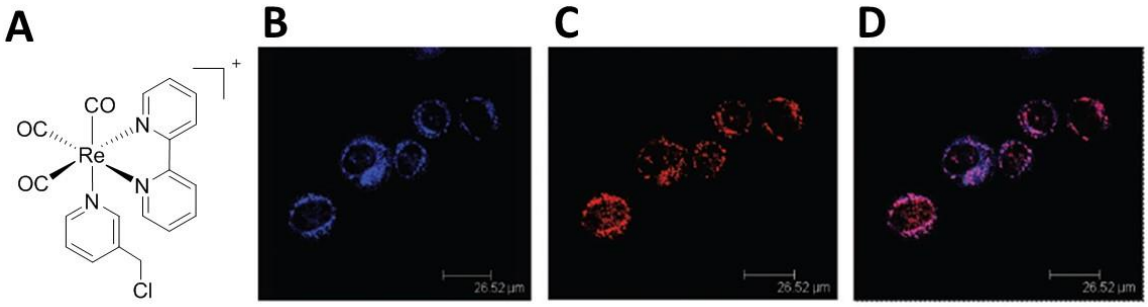


**Figure 1.9** Chemical structure of $[Re(CO)_3(bipy)(py\text{-}3\text{-}CH_2Cl)]$ (A), Fluorescent image of the complex (B), TMRE (C), and overlaid image (D) in MCF-7 cells.[110]

### 1.3.4 Technetium Polypyridine Complexes

Although rhenium (I) polypyridine complexes have been widely used to prepare luminescent probes, there have been limited investigation on their technetium(I) analogues for developing targeted MI probes.[112,113] That is due in part to concerns about premature loss of the monodentate ligand *in vivo*, which results in high protein binding and high background activity in the liver and blood stream.[114] Our hypothesis was that with the appropriate choice of monodentate ligand and the development of a convenient radiochemical synthesis method, compounds of the type $[M(CO)_3(N\hat{}N)L]^n$ (where M = Re, $^{99m}$Tc, N^N = bisimine, and L= monodentate ligand) could be used to create a new class of isostructural luminescent and nuclear probes with superior optical properties compared to existing isostructural agents.

## 1.4 References

(1) Herschman, H. R. *Science* **2003**, *302*, 605–608.

(2) Britz-Cunningham, S. H.; Adelstein, S. J. *J. Nucl. Med.* **2003**, *44*, 1945–1961.

(3) Cherry, S. R. *J. Clin. Pharmacol.* **2001**, *41*, 482–491.

(4) Pantaleo, M. A.; Nannini, M.; Maleddu, A.; Fanti, S.; Ambrosini, V.; Nanni, C.; Boschi, S.; Biasco, G. *Cancer Treat. Rev.* **2008**, *34*, 103–121.

(5) York, N.; Reivich, M. *J. Label . Compd. Radiopharm.* **1978**, *14*, 175–183.

(6) Buck, A. K.; Nekolla, S.; Ziegler, S.; Beer, A.; Krause, B. J.; Herrmann, K.; Scheidhauer, K.; Wester, H.; Rummeny, E. J.; Schwaiger, M.; Drzezga, A. *J. Nucl. Med.* **2016**, *49*, 1305–1319.

(7) Munley, M. T.; Kagadis, G. C.; Mcgee, K. P.; Kirov, A. S.; Jang, S.; Mutic, S.; Xing, L.; Bourland, J. D. *Med. Phys.* **2013**, *40*, 101501-1–23.

(8) Hong, H.; Sun, J.; Cai, W. *Biomark. Insights.* **2008**, No. 3, 435–451.

(9) Culver, J.; Akers, W.; Achilefu, S. *J. Nucl. Med.* **2008**, *49*, 169–172.

(10) Ntziachristos, V.; Ripoll, J.; Wang, L. V; Weissleder, R. *Nat. Biotechnol.* **2005**, *23*, 313–320.

(11) Taruttis, A.; Ntziachristos, V. *Am. J. Roentgenol.* **2012**, *199*, 263–271.

(12) Kobayashi, H.; Ogawa, M.; Alford, R.; Choyke, P. L.; Urano, Y. *Chem. Rev.* **2010**, *110*, 2620–2640.

(13) Weissleder, R.; Pittet, M. J. *Nature* **2008**, *452*, 580–589.

(14) Leblond, F.; Davis, S. C.; Valdés, P. A.; Pogue, B. W. *J. Photochem. Photobiol. B* **2010**, *98*, 77–94.

(15) Thorp-Greenwood, F. L.; Coogan, M. P. *Dalton Trans.* **2011**, *40*, 6129–6143.

(16) Pandey, S. K.; Gryshuk, A. L.; Sajjad, M.; Zheng, X.; Chen, Y.; Abouzeid, M. M.; Morgan, J.; Charamisinau, I.; Nabi, H. A.; Oseroff, A.; Pandey, R. K. *J. Med. Chem.* **2005**, *48*, 6286–6295.

(17) Ballou, B; Fisher, G.W.; Deng, J.S.; Hakala, T.R.; Srivastava, M.; Farkas, D. L. *Cancer Detect. Prev.* **1998**, *22*, 251–257.

(18) Li, Q.; Kim, Y.; Namm, J.; Kulkarni, A.; Rosania, G. R.; Ahn, Y.-H.; Chang, Y.-T. *Chem. Biol.* **2006**, *13*, 615–623.

(19) Wang, M.; Gao, M.; Miller, K. D.; Sledge, G. W.; Hutchins, G. D.; Zheng, Q. H. *Eur. J. Med. Chem.* **2009**, *44*, 2300–2306.

(20) Kuil, J.; Velders, A. H.; Van Leeuwen, F. W. B. *Bioconjugate Chem.* **2010**, *21*, 1709–1719.

(21) Kimura, R. H.; Miao, Z.; Cheng, Z.; Gambhir, S. S.; Cochran, J. R. *Bioconjugate Chem.* **2010**, *21*, 436–444.

(22) Azhdarinia, A.; Wilganowski, N.; Robinson, H.; Ghosh, P.; Kwon, S.; Lazard, Z. W.; Davis, A. R.; Olmsted-Davis, E.; Sevick-Muraca, E. M. *Bioorg. Med. Chem.* **2011**, *19*, 3769–3776.

(23) Edwards, W. B.; Xu, B.; Akers, W.; Cheney, P. P.; Liang, K.; Rogers, B. E.; Anderson, C. J.; Achilefu, S. *Bioconjugate Chem.* **2008**, *19*, 192–200.

(24) Achilefu, S.; Jimenez, H. N.; Dorshow, R. B.; Bugaj, J. E.; Webb, E. G.; Wilhelm, R. R.; Rajagopalan, R.; Johler, J.; Erion, J. L. *J. Med. Chem.* **2002**, *45*, 2003–2015.

(25) Jennings, L. E.; Long, N. J. *Chem. Commun.* **2009**, 3511–3524.

(26) Bhushan, K. R.; Tanaka, E.; Frangioni, J. V. *Angew. Chem. Int. Ed. Engl.* **2007**, *46*, 7969–7971.

(27) Bhushan, K. R.; Misra, P.; Liu, F.; Mathur, S.; Lenkinski, R. E.; Frangioni, J. V. *J. Am. Chem. Soc.* **2008**, *130*, 17648–17649.

(28) Agorastos, N.; Borsig, L.; Renard, A.; Antoni, P.; Viola, G.; Spingler, B.; Kurz, P.; Alberto, R. *Chem. Eur. J.* **2007**, *13*, 3842–3852.

(29) Esteves, T.; Xavier, C.; Gama, S.; Mendes, F.; Raposinho, P. D.; Marques, F.; Paulo, A.; Pessoa, J. C.; Rino, J.; Viola, G.; Santos, I. *Org. Biomol. Chem.* **2010**, *8*, 4104–4116.

(30) Tzanopoulou, S.; Sagnou, M.; Paravatou-Petsotas, M.; Gourni, E.; Loudos, G.; Xanthopoulos, S.; Lafkas, D.; Kiaris, H.; Varvarigou, A.; Pirmettis, I. C.; Papadopoulos, M.; Pelecanou, M. *J. Med. Chem.* **2010**, *53*, 4633–4641.

(31) Yang, Y.; Zhu, L.; Cui, M.; Tang, R.; Zhang, H. *Bioorg. Med. Chem. Lett.* **2010**, *20*, 5337–5344.

(32) Xiong, C.; Lu, W.; Zhang, R.; Tian, M.; Tong, W.; Gelovani, J.; Li, C. *Chem. Eur. J.* **2009**, *15*, 8979–8984.

(33) Houston, J. P.; Ke, S.; Wang, W.; Li, C.; Sevick-Muraca, E. M. *Proc. SPIE* **2005**, *5704*, 10–15.

(34) Wang, W.; Ke, S.; Kwon, S.; Yallampalli, S.; Cameron, A. G.; Adams, K. E.; Mawad, M. E.; Sevick-Muraca, E. M. *Bioconjugate Chem.* **2007**, *18*, 397–402.

(35) Hong, H.; Zhang, Y.; Severin, G. W.; Yang, Y.; Engle, J. W.; Niu, G.; Nickles, R. J.; Chen, X.; Leigh, B. R.; Barnhart, T. E.; Cai, W. *Mol. Pharm.* **2012**, *9*, 2339–

2349.

(36) Ghosh, S. C.; Ghosh, P.; Wilganowski, N.; Robinson, H.; Hall, M. A.; Dickinson, G.; Pinkston, K. L.; Harvey, B. R.; Sevick-Muraca, E. M.; Azhdarinia, A. *J. Med. Chem.* **2013**, *56*, 406–416.

(37) Xu, H.; Eck, P. K.; Baidoo, K. E.; Choyke, P. L.; Brechbiel, M. W. *Bioorg. Med. Chem.* **2009**, *17*, 5176–5181.

(38) Zhou, Y.; Kim, Y.-S.; Yan, X.; Jacobson, O.; Chen, X.; Liu, S. *Mol. Pharm.* **2011**, *8*, 1198–1208.

(39) Duheron, V.; Moreau, M.; Collin, B.; Sali, W.; Bernhard, C.; Goze, C.; Gautier, T.; Pais de Barros, J.-P.; Deckert, V.; Brunotte, F.; Lagrost, L.; Denat, F. *ACS Chem. Biol.* **2014**, *9*, 656–662.

(40) Zelenka, K.; Borsig, L.; Alberto, R. *Bioconjugate Chem.* **2011**, *22*, 958–967.

(41) Yan, R.; El-Emir, E.; Rajkumar, V.; Robson, M.; Jathoul, A. P.; Pedley, R. B.; Årstad, E. *Angew. Chem.* **2011**, *123*, 6925–6927.

(42) Heinrich, T. K.; Gottumukkala, V.; Snay, E.; Dunning, P.; Fahey, F. H.; Ted Treves, S.; Packard, A. B. *Appl. Radiat. Isot.* **2010**, *68*, 96–100.

(43) Priem, T.; Bouteiller, C.; Camporese, D.; Brune, X.; Hardouin, J.; Romieu, A.; Renard, P.-Y. *Org. Biomol. Chem.* **2013**, *11*, 469–479.

(44) Hendricks, J. A.; Keliher, E. J.; Wan, D.; Hilderbrand, S. A.; Weissleder, R.; Mazitschek, R. *Angew. Chem. Int. Ed.* **2012**, *51*, 4603–4606.

(45) Ting, R.; Aguilera, T. A.; Crisp, J. L.; Hall, D. J.; Eckelman, W. C.; Vera, D. R.; Tsien, R. Y. *Bioconjugate Chem.* **2010**, *21*, 1811–1819.

(46) Wallace, A. M.; Hoh, C. K.; Darrah, D. D.; Schulteis, G.; Vera, D. R. *Nucl. Med. Biol.* **2007**, *34*, 849–853.

(47) James, S.; Maresca, K. P.; Babich, J. W.; Valliant, J. F.; Doering, L.; Zubieta, J. *Bioconjugate Chem.* **2006**, *17*, 590–596.

(48) Nunes, P.; Morais, G. R.; Palma, E.; Silva, F.; Oliveira, M. C.; Ferreira, V. F. C.; Mendes, F.; Gano, L.; Miranda, H. V.; Outeiro, T. F.; Santos, I.; Paulo, A. *Org. Biomol. Chem.* **2015**, *13*, 5182–5194.

(49) Azad, B. B.; Cho, C.-F.; Lewis, J. D.; Luyt, L. G. *Appl. Radiat. Isot.* **2012**, *70*, 505–511.

(50) Connell, T. U.; Hayne, D. J.; Ackermann, U.; Tochon-Danguy, H. J.; White, J. M.; Donnelly, P. S. *J. Label. Compd. Radiopharm.* **2014**, *57*, 262–269.

(51) Botchway, S.; Dilworth, J. R.; Salichou, M. *Dalton Trans.* **2010**, *39*, 5219–5220.

(52) Thorp-Greenwood, F. L.; Coogan, M. P. *Dalton Trans.* **2011**, *40*, 6206–6209.

(53) Coogan, M. P.; Doyle, R. P.; Valliant, J. F.; Babich, J. W.; Zubieta, J. *J. Label Compd. Radiopharm* **2014**, *57*, 255–261.

(54) Cowley, A. R.; Dilworth, J. R.; Donnelly, P. S.; Heslop, J. M.; Ratcliffe, S. J. *Dalton Trans.* **2007**, 209–217.

(55) Bonnitcha, P. D.; Vavere, A. L.; Lewis, J. S.; Dilworth, J. R. *J. Med. Chem.* **2008**, *51*, 2985–2991.

(56) Holland, J. P.; Aigbirhio, F. I.; Betts, H. M.; Bonnitcha, P. D.; Burke, P.; Christlieb, M.; Churchill, G. C.; Cowley, A. R.; Dilworth, J. R.; Donnelly, P. S.; Green, J. C.; Peach, J. M.; Vasudevan, S. R.; Warren, J. E. *Inorg. Chem.* **2007**, *46*,

465–485.

(57) Pascu, S. I.; Waghorn, P. A.; Conry, T. D.; Betts, H. M.; Dilworth, J. R.; Churchill, G. C.; Pokrovska, T.; Christlieb, M.; Aigbirhio, F. I.; Warren, J. E. *Dalton Trans.* **2007**, 4988–4997.

(58) Holland, J. P.; Barnard, P. J.; Bayly, S. R.; Betts, H. M.; Churchill, G. C.; Dilworth, J. R.; Edge, R.; Green, J. C.; Hueting, R. *Eur. J. Inorg. Chem.* **2008**, 1985–1993.

(59) Stephenson, K. A.; Banerjee, S. R.; Besanger, T.; Sogbein, O. O.; Levadala, M. K.; McFarlane, N.; Lemon, J. A.; Boreham, D. R.; Maresca, K. P.; Brennan, J. D.; Babich, J. W.; Zubieta, J.; Valliant, J. F. *J. Am. Chem. Soc.* **2004**, *126*, 8598–8599.

(60) Schaffer, P.; Gleave, J. A.; Lemon, J. A.; Reid, L. C.; Pacey, L. K. K.; Farncombe, T. H.; Boreham, D. R.; Zubieta, J.; Babich, J. W.; Doering, L. C.; Valliant, J. F. *Nucl. Med. Biol.* **2008**, *35*, 159–169.

(61) Gasser, G.; Pinto, A.; Neumann, S.; Sosniak, A. M.; Seitz, M.; Merz, K.; Heumann, R.; Metzler-Nolte, N. *Dalton Trans.* **2012**, *41*, 2304–2313.

(62) Schwochau, K. *Angew. Chem. Int. Ed. Engl.* **1994**, *33*, 2258–2267.

(63) Saha, G. B. Physics and Radiobiology of Nuclear Medicine, 2nd ed.; Springer-Verlag: New York, 2001; p 1-251.

(64) Eckelman, W. C. *J. Am. Coll. Cardiol. Imag.* **2009**, *2*, 364–368.

(65) Lever, S. Z. *J. Cell. Biochem.* **2002**, *39*, 60–64.

(66) Johannsen, B.; Spies, H. *Transit. Met. Chem.* **1997**, *22*, 318–320.

(67) Dilworth, J. R.; Parrott, S. J. *Chem. Soc. Rev.* **1998**, *27*, 43–55.

(68) Abrams, M. J.; Davison, A.; Jones, A. G.; Costello, C. E.; Pang, H. *Inorg. Chem.* **1983**, *22*, 2798–2800.

(69) Holman, B. L.; Jones, A. G.; Lister-James, J.; Davison, A.; Abrams, M. J.; Kirshenbaum, J. M.; Tumeh, S. S.; English, R. J. *J. Nucl. Med.* **1984**, *25*, 1350–1355.

(70) Piwnica-Worms, D.; Kronauge, J. F.; Chiu, M. L. *Circulation* **1990**, *82*, 1826–1838.

(71) Chiu, M. L.; Kronauge, J. F.; Piwnica-Worms, D. *J. Nucl. Med.* **1990**, *31*, 1646–1653.

(72) Jurisson, S. S.; Lydon, J. D. *Chem. Rev.* **1999**, *99*, 2205–2218.

(73) Banerjee, S. R.; Maresca, K. P.; Francesconi, L.; Valliant, J.; Babich, J. W.; Zubieta, J. *Nucl. Med. Biol.* **2005**, *32*, 1–20.

(74) Abram, U.; Alberto, R. *J. Braz. Chem. Soc.* **2006**, *17*, 1486–1500.

(75) Deutsch, E.; Libson, K.; Vanderheyden, J. L.; Ketring, A. R.; Maxon, H. R. *Nucl. Med. Biol.* **1986**, *13*, 465–477.

(76) Vites, J. C.; Lynam, M. M. *Coord. Chem. Rev.* **1998**, *169*, 201–235.

(77) Vites, J. C.; Lynam, M. M. *Coord. Chem. Rev.* **1998**, *172*, 357–388.

(78) Volkert, W. A.; Hoffman, T. J. *Chem. Rev.* **1999**, *99*, 2269–2292.

(79) Alberto, R.; Schibli, R.; Egli, A.; Schubiger, A. P. *J. Am. Chem. Soc.* **1998**, *120*, 7987–7988.

(80) Alberto, R.; Ortner, K.; Wheatley, N.; Schibli, R.; Schubiger, A. P. *J. Am. Chem. Soc.* **2001**, *123*, 3135–3136.

(81) Lattuada, L.; Barge, A.; Cravotto, G.; Giovenzana, G. B.; Tei, L. *Chem. Soc. Rev.* **2011**, *40*, 3019–3049.

(82) Liu, S. *Adv. Drug Deliv. Rev.* **2008**, *60*, 1347–1370.

(83) Banerjee, S. R.; Levadala, M. K.; Lazarova, N.; Wei, L.; Valliant, J. F.; Stephenson, K. a; Babich, J. W.; Maresca, K. P.; Zubieta, J. *Inorg. Chem.* **2002**, *41*, 6417–6425.

(84) Causey, P. W.; Besanger, T. R.; Schaffer, P.; Valliant, J. F. *Inorg. Chem.* **2008**, *47*, 8213–8221.

(85) Schibli, R.; La Bella, R.; Alberto, R.; Garcia-Garayoa, E.; Ortner, K.; Abram, U.; Schubiger, P. A. *Bioconjugate Chem.* **2000**, *11*, 345–351.

(86) Mindt, T. L.; Struthers, H.; Brans, L.; Anguelov, T.; Schweinsberg, C.; Maes, V.; Tourwé, D.; Schibli, R. *J. Am. Chem. Soc.* **2006**, *128*, 15096–15097.

(87) Meldal, M.; Tornøe, C. W. *Chem. Rev.* **2008**, *108*, 2952–3015.

(88) Struthers, H.; Spingler, B.; Mindt, T. L.; Schibli, R. *Chem. Eur. J.* **2008**, *14*, 6173–6183.

(89) Struthers, H.; Mindt, T. L.; Schibli, R. *Dalton Trans.* **2010**, *39*, 675–696.

(90) Kluba, C. A.; Mindt, T. L. *Molecules* **2013**, *18*, 3206–3226.

(91) Mindt, T. L.; Müller, C.; Melis, M.; Jong, M. de; Schibli, R. *Bioconjugate Chem.* **2008**, *19*, 1689–1695.

(92) Stichelberger, A.; Waibel, R.; Dumas, C.; Schubiger, P. A.; Schibli, R. *Nucl. Med. Biol.* **2003**, *30*, 465–470.

(93) Bartholomä, M.; Valliant, J.; Maresca, K. P.; Babich, J.; Zubieta, J. *Chem.*

*Commun.* **2009**, *7345*, 493–512.

(94) Stephenson, K. A.; Zubieta, J.; Banerjee, S. R.; Levadala, M. K.; Taggart, L.; Ryan, L.; McFarlane, N.; Boreham, D. R.; Maresca, K. P.; Babich, J. W.; Valliant, J. F. *Bioconjugate Chem.* **2004**, *15*, 128–136.

(95) Banerjee, S. R.; Foss, C. A.; Castanares, M.; Mease, R. C.; Byun, Y.; Fox, J. J.; Hilton, J.; Lupold, S. E.; Kozikowski, A. P.; Pomper, M. G. *J. Med. Chem.* **2008**, *51*, 4504–4517.

(96) Kularatne, S. A.; Zhou, Z.; Yang, J.; Post, C. B.; Low, P. S. *Mol. Pharm.* **2009**, *6*, 790–800.

(97) Maresca, K. P.; Hillier, S. M.; Lu, G.; Marquis, J. C.; Zimmerman, C. N.; Eckelman, W. C.; Joyal, J. L.; Babich, J. W. *Inorg. Chim. Acta* **2012**, *389*, 168–175.

(98) Hillier, S. M.; Maresca, K. P.; Lu, G. L.; Merkin, R. D.; Marquis, J. C.; Zimmerman, C. N.; Eckelman, W. C.; Joyal, J. L.; Babich, J. W. *J. Nucl. Med.* **2013**, *54*, 1369–1376.

(99) Vallabhajosula, S.; Nikolopoulou, A.; Babich, J. W.; Osborne, J. R.; Tagawa, S. T.; Lipai, I.; Solnes, L.; Maresca, K. P.; Armor, T.; Joyal, J. L.; Crummet, R.; Stubbs, J. B.; Goldsmith, S. J. *J. Nucl. Med.* **2014**, *55*, 1791–1798.

(100) Balasingham, R. G.; Coogan, M. P.; Thorp-Greenwood, F. L. *Dalton Trans.* **2011**, *40*, 11663–11674.

(101) Thorp-Greenwood, F. L.; Balasingham, R. G.; Coogan, M. P. *J. Organomet. Chem.* **2012**, *714*, 12–21.

(102) Lo, K. K.-W.; Choi, A. W.-T.; Law, W. H.-T. *Dalton Trans.* **2012**, *41*, 6021–6047.

(103) Alberto, R.; Schibli, R.; Waibel, R.; Abram, U.; Schubiger, A. P. *Coord. Chem. Rev.* **1999**, *192*, 901–919.

(104) Alberto, R.; Pak, J. K.; van Staveren, D.; Mundwiler, S.; Benny, P. *Biopolymers* **2004**, *76*, 324–333.

(105) Fernandez-Moreira, V.; Thorp-Greenwood, F. L.; Amoroso, A. J.; Cable, J.; Court, J. B.; Gray, V.; Hayes, A. J.; Jenkins, R. L.; Kariuki, B. M.; Lloyd, D.; Millet, C. O.; Williams, C. F.; Coogan, M. P. *Org. Biomol. Chem.* **2010**, *8*, 3888–3901.

(106) Zhao, Q.; Huang, C.; Li, F. *Chem. Soc. Rev.* **2011**, *40*, 2508–2524.

(107) Lo, K. K.-W.; Louie, M.-W.; Zhang, K. Y. *Coord. Chem. Rev.* **2010**, *254*, 2603–2622.

(108) Clède, S.; Policar, C. *Chem. Eur. J.* **2014**, *20*, 1–18.

(109) Amoroso, A. J.; Coogan, M. P.; Dunne, J. E.; Fernández-Moreira, V.; Hess, J. B.; Hayes, A. J.; Lloyd, D.; Millet, C.; Pope, S. J. A.; Williams, C. *Chem. Commun.* **2007**, 3066–3068.

(110) Amoroso, A. J.; Arthur, R. J.; Coogan, M. P.; Court, J. B.; Fernández-Moreira, V.; Hayes, A. J.; Lloyd, D.; Millet, C.; Pope, S. J. A. *New J. Chem.* **2008**, *32*, 1097–1102.

(111) Lo, K. K. W.; Louie, M. W.; Sze, K. S.; Lau, J. S. Y. *Inorg. Chem.* **2008**, *47*, 602–611.

(112) Ellis, B. L.; Gorshkov, N. I.; Lumpov, A. a; Miroslavov, A. E.; Yalfimov, A. N.; Gurzhiy, V. V; Suglobov, D. N.; Braddock, R.; Adams, J. C.; Smith, A.-M.;

Prescott, M. C.; Sharma, H. L. *J. Label Compd. Radiopharm* **2013**, *56*, 700–707.

(113) Pitchumony, T. S.; Banevicius, L.; Janzen, N.; Zubieta, J.; Valliant, J. F. *Inorg. Chem.* **2013**, *52*, 13521–13528.

(114) Schibli, R.; Schubiger, P. A. *Eur. J. Nucl. Med.* **2002**, *29*, 1529–1542.

# Chapter 2

## 2 Chapter 2. Imidazole-Based [2 + 1] Re(I)/$^{99m}$Tc(I) Complexes as Isostructural Nuclear and Optical Probes

Abdolreza Yazdani, Nancy Janzen, Laura Banevicius, Shannon Czorny, John F. Valliant

The following chapter was published in the journal Inorganic Chemistry, under the citation:

Yazdani, A; Janzen, N.; Banevicius, L.; Czorny, S.; Valliant, J. F. *Inorg. Chem.* **2015**, *54*, 1728-1736.

I was responsible for the development and execution of the majority of the work described in this paper including drafting the initial manuscript and experimental. Biological testing and *in vivo* imaging studies have been done by Nancy Janzen and Shannon Czorny. Fluorescence measurements were performed by Laura Banevicius. Professor Valliant was the PI of the lab and responsible for the overall manuscript and project.

## 2.1 Abstract

The synthesis, stability and photophysical properties of [2 + 1] Re(I)/Tc(I) complexes derived from bipyridine and a series of imidazole derivatives were investigated as a means of identifying complexes suitable for creating targeted isostructural optical/nuclear molecular imaging probes. To prepare the desired complexes, $[Re(CO)_3(H_2O)_3]Br$ was combined with 2,2'-bipyridine (bipy) to give $[Re(CO)_3(bipy)Br]$, which in turn was converted to the desired complexes by treatment with functionalized imidazoles, yielding crystal structures of two new Re complexes. The corresponding $^{99m}Tc$ complexes $[^{99m}Tc(CO)_3(bipy)(L)]^+$ (L = imidazole derivatives) were prepared by combining $[^{99m}Tc(CO)_3(bipy)(H_2O)]Cl$ with the same series of ligands and heating at 40 °C or 60 °C for 30 min. Quantitative transformation to the final products was confirmed in all cases by HPLC and the nature of the complexes verified by comparison to the authentic Re standards. Incubation in saline and plasma, and amino acid challenge experiments showed that N-substituted imidazole derivatives, bearing electron donating groups, exhibited superior stability to analogous metal complexes derived from less basic ligands. Imaging studies in mice revealed that with the appropriate choice of monodentate ligand, it is possible to prepare robust [2 + 1] $^{99m}Tc$ complexes that can be used as the basis for preparing targeted isostructural optical and nuclear probes.

## 2.2 Introduction

Molecular imaging (MI) is being used increasingly to study specific biochemical pathways and drug targets non-invasively, and to enable early disease detection, selection of patients for targeted therapies and active monitoring of treatment efficacy.[1,2] Multi-modal MI makes it possible to combine the strengths of different imaging techniques.[3] For instance, nuclear and optical imaging strategies are being used for sentinel lymph node tumour detection and surgical guidance with impressive results.[4–6] The ability to link optical and nuclear imaging also provides the opportunity to use the former to validate the binding of a new radiopharmaceutical to a specific target and to study cellular uptake and distribution with high resolution.[7–9]

Multi-modal optical and nuclear probes are commonly prepared by modifying a targeting vector with a radionuclide and a fluorophore.[10–12] The challenge with this approach is that the two groups often have a detrimental impact on the ability of a targeting vector to reach and effectively bind to the target of interest consequently extensive optimization work is required. More recently the focus has shifted to developing radiolabeled fluorophores[13–25] and isostructural metal complexes as synthons for developing multi-modal probes.[26–31] The key advantage to the new approaches is that only one prosthetic group has to be added to the targeting vector of interest, which greatly simplifies lead discovery efforts.

In the case of $^{99m}$Tc, which is the workhorse of nuclear medicine[32] because of its widespread use, low cost and modest dose burden compared to other medical isotopes,[33] it is possible to use Re as a non-radioactive surrogate for $^{99m}$Tc, to create isostructural

luminescent probes. There has been extensive work done on the development of Re(I) based dyes for cellular imaging studies where complexes are typically derived from one bidentate heterocyclic arene ligand and one monodentate ligand.[34–36] These "[2 + 1]" systems typically exhibit broad excitation (350-410 nm) and emission (500-700 nm) bands with large Stokes shifts and long lifetimes where targeting specific cellular compartments can be achieved by attaching the appropriate vector to either the bidentate or monodentate ligand.[37–40]

Of particular interest to us were [2 + 1] Re bipyridine complexes containing imidazole-based donors as the monodentate ligand. Complexes of this nature have been used successfully as redox probes and luminescent labels for biomolecules,[41–44] by taking advantage of the sensitivity of their emissive properties to the nature of the donor ligands and environment. While they possess features that are attractive for developing targeted luminescent probes, one concern with their use as radiotracers is the premature loss of the monodentate ligand *in vivo*, which can result in high protein binding and uptake in non-target organs. Recently we reported that robust complexes such as $[^{99m}Tc(CO)_3(bipy)(DMAP)]^+$ can be produced using basic monodentate pyridine ligands, where analogous Re(I) complexes are effective luminescent probes (Figure 2.1).[45] Imidazole ligands are sufficiently basic that they should also form stable [2 + 1] $^{99m}$Tc complexes. However in contrast to the work on Re, there have been limited investigations of the chemistry of the analogous [2 + 1] bipyridyl-imidazole technetium(I) complexes.[46] We report here the synthesis and characterization of a series of novel $[M(CO)_3(bipy)(L)]^+$ complexes (M = $^{99m}$Tc, Re) where L represents N-alkyl imidazole ligands, which include

new bifunctional derivatives that can be used to prepare targeted isostructural optical and nuclear probes.

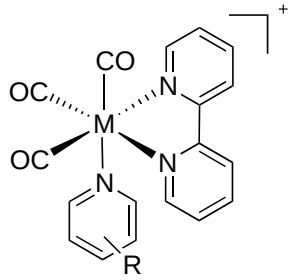


M = Tc, R = p-$NMe_2$ (**1a**)
M = Re, R = m-$CH_2C(O)OCy$ (**1b**)

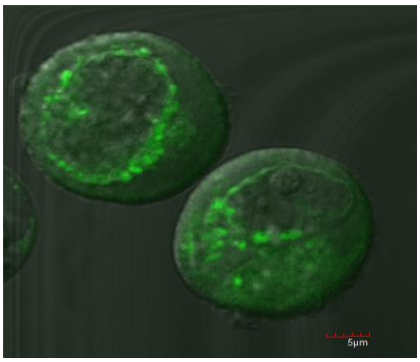

**Figure 2.1** $[^{99m}Tc(CO)_3(bipy)(DMAP)]^+$ **1a** and confocal images of the Re(I) complex **1b** incubated with MCF-7 cells for 1.5 h at room temperature (cy = cyclohexyl).[45]

## 2.3 Results and Discussion

### 2.3.1 Synthesis of $[M(CO)_3(bipy)(L)]^+$ Complexes (M = $^{99m}$Tc, Re)

The synthetic approach utilized $[^{99m}Tc(CO)_3(H_2O)_3]^+$, which can be prepared in a single step from $TcO_4^-$, following the method developed by Alberto *et al*.[47,48] Quantitative formation of $[^{99m}Tc(CO)_3(bipy)(H_2O)]Cl$ **4b** was achieved by the addition of $[^{99m}Tc(CO)_3(H_2O)_3]^+$ to bipy and heating the reaction mixture in a microwave reactor to 110 °C for 6 min (Scheme 2.1). While there are numerous classes of imidazole ligands to choose from for preparing the desired [2 + 1] complexes, we focused on N-substituted

imidazoles to avoid forming mixtures of products and to provide a convenient site for the attachment of different functional groups and targeting vectors. The archetypal ligand N-methylimidazole (MeIm) was combined with $[^{99m}Tc(CO)_3(bipy)(H_2O)]Cl$ resulting in the formation of $[^{99m}Tc(CO)_3(bipy)(MeIm)]^+$ **5b** in quantitative yield at 40 °C (Scheme 2.1). The retention time of the product matched that of the Re complex **5a**, which was prepared according to a literature method in 72% yield.[41] It was also possible to prepare the complex at room temperature using a reaction time of just 5 min.

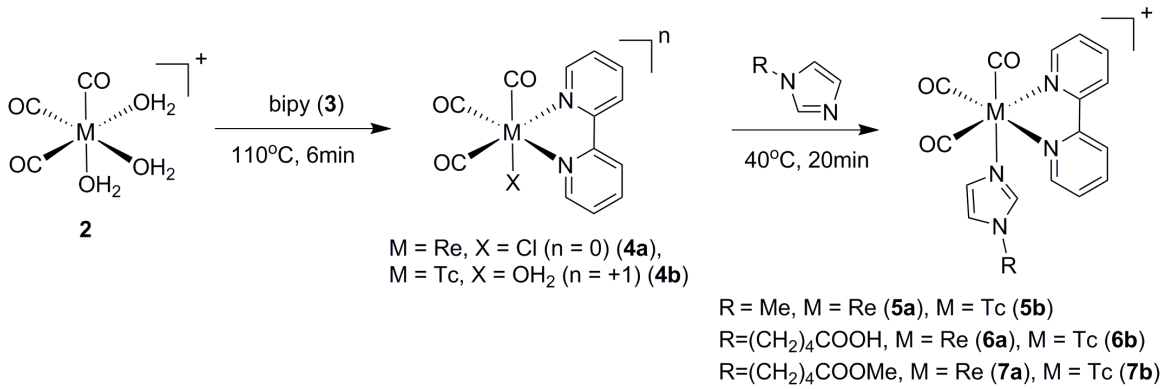


**Scheme 2.1** Synthesis of [2 + 1] Re(I) and $^{99m}Tc$ complexes from bipyridine and substituted imidazole ligands. The conditions shown are for the reactions performed at the tracer level.

Building on the success using N-methylimidazole, zoledronic acid (ZA) was investigated as an example of a bifunctional agent. This imidazole derived bisphosphonate has been used previously to treat osteoporosis and to target radiometals to bone metastases.[49–52] $[^{99m}Tc(CO)_3(bipy)(H_2O)]Cl$ **4b** was combined with ZA in water at

pH 7 and the mixture was heated in a microwave at 60 °C for 30 min, whereupon [$^{99m}$Tc(CO)$_3$(bipy)(ZA)] **8b** was isolated by HPLC in high yield (Scheme 2.2). The Re analogue **8a**, which had not been previously reported, was prepared by adding [Re(CO)$_3$(bipy)(H$_2$O)][CF$_3$SO$_3$] to ZA at pH 7 and heating the mixture to reflux overnight. The product was isolated in 77% yield by semi-preparative HPLC.

Single crystals of [Re(CO)$_3$(bipy)(ZA)] **8a** were obtained by slow diffusion of acetone into an aqueous solution of the complex. The molecular structure, which has a distorted octahedral geometry, is depicted in Figure 2.1 and the associated X-ray data is provided in the supporting information (Table S 6.1**)**. The imidazole moiety, as opposed to the bisphosphonate group, is coordinated to the metal through N1 with a Re-N distance of 2.175(6) Å (Table S 2.2 in the supporting information). The Re-N bonds to the bipy ligand are 2.180(5) and 2.173(8) Å, and C-O bond lengths vary from 1.147 to 1.164 Å, which is typical of [Re(CO)$_3$]$^+$ complexes of this nature.[53–55] The complex is oriented such that the bipyridine ligand is tilted to the center of the unit cell.

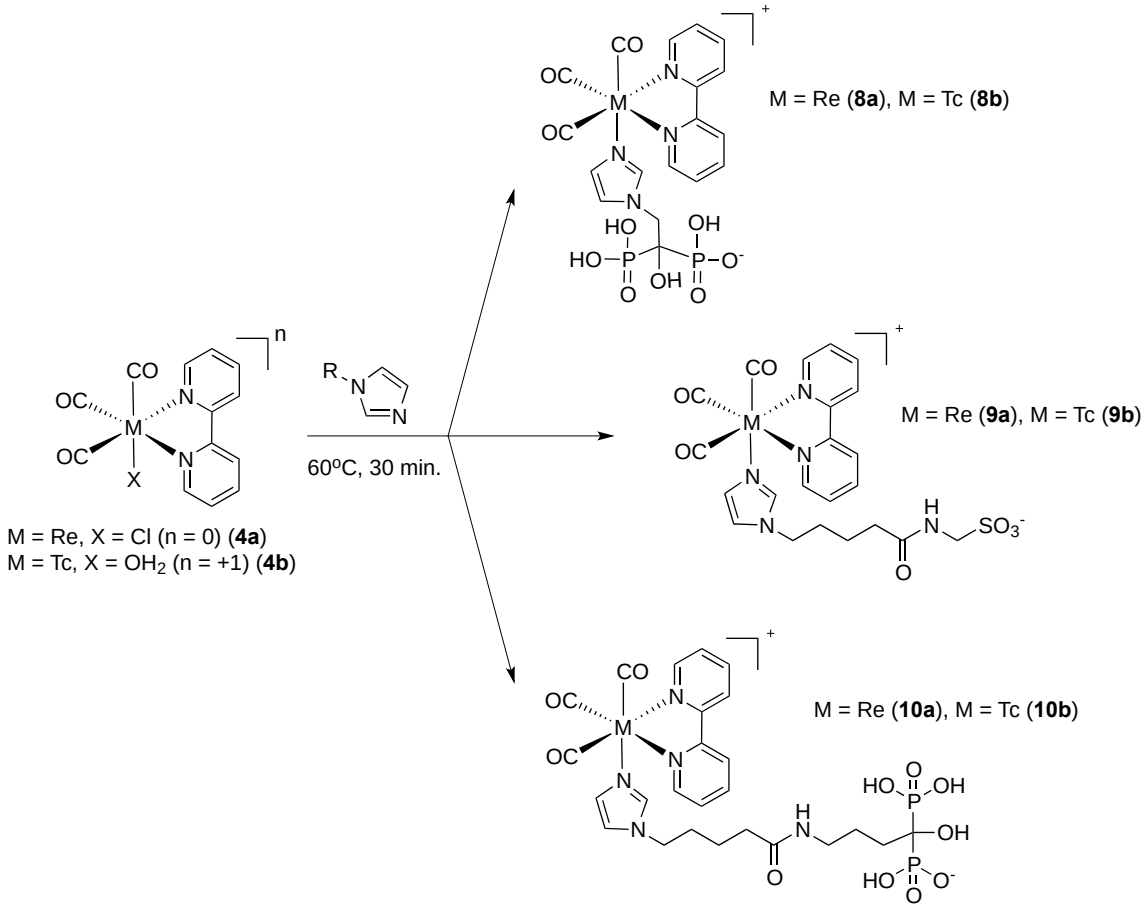


**Scheme 2.2** Synthesis of $[M(CO)_3(bipy)(ZA)]$ **8a/b**, $[M(CO)_3(bipy)(ImSfn)]$ **9a/b** and $[M(CO)_3(bipy)(ImAln)]$ **10a/b** (M = Re or $^{99m}Tc$). The reaction conditions shown are those used to prepare **8b** and **10b**.

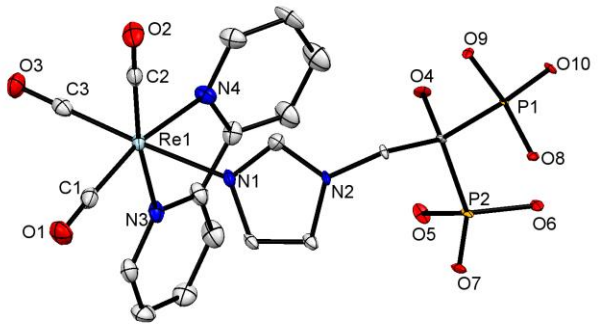


**Figure 2.2** ORTEP plot (50% thermal ellipsoid probability) for $[Re(CO)_3(bipy)(ZA)]$ **8a**. Hydrogen atoms have been omitted for clarity.

To provide a site for future attachment of targeting vectors, an imidazole derivative bearing a pentanoic acid linker was prepared by simple alkylation of imidazole with methyl 5-bromovalerate. The ligand was subsequently coupled to aminosulfonic acid to give **12** (ImSfn), or to alendronate (Aln) to give **13** (Scheme 2.3). The latter compound was chosen to allow for direct comparison of the *in vitro* stability and *in vivo* biodistribution with **8b**, while the addition of the sulfonate was done as part of a series of experiments to assess stability *in vivo* (*vide infra*).

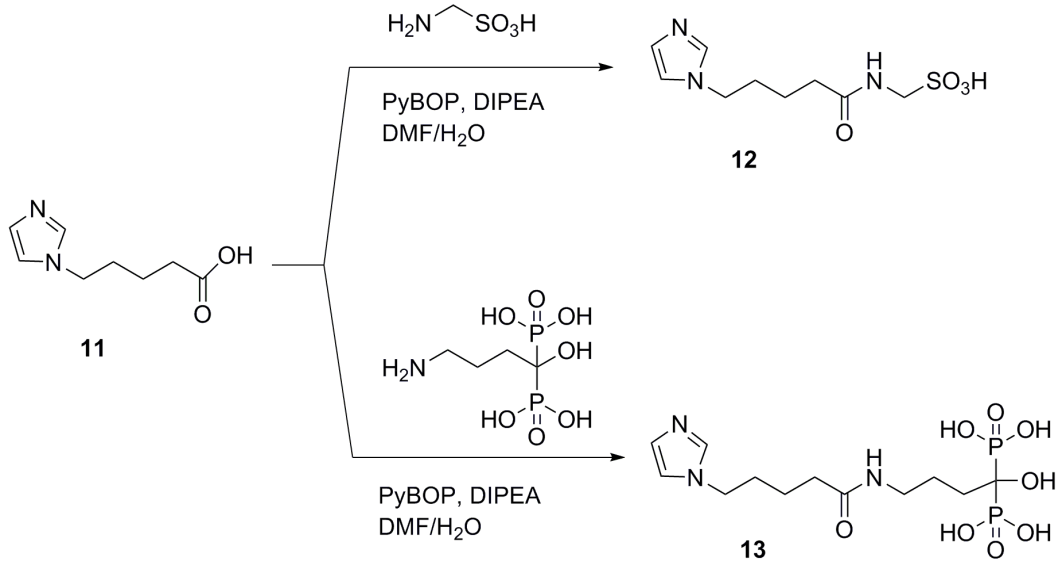


**Scheme 2.3** Synthesis of ImSfn **12** and ImAln **13**.

The Re complex of the sulfonate ligand (ImSfn, **12**) was prepared by combining it with **4a** and heating to reflux in MeOH overnight. The desired product was isolated in 45% yield by semi-preparative HPLC and single crystals of $[Re(CO)_3(bipy)(ImSfn)]$ **9a** were grown by slow evaporation of an acetonitrile-water solution. The molecular structure is depicted in Figure 2.3, where the imidazole ligand is again coordinated to the metal through N1 and the bond lengths and angles are within the ranges excepted for analogous complexes (Table S 6.2 in the supporting information). As was the case for **8a**, there was no evidence of a counter ion in the structure, which is consistent with the overall neutral charge of the complex. For the tracer level work, ImSfn was combined with $[^{99m}Tc(CO)_3(bipy)(H_2O)]Cl$ at 40 °C and resulted in the formation of $[^{99m}Tc(CO)_3(bipy)(ImSfn)]$ **9b** which was isolated by HPLC in quantitative yield.

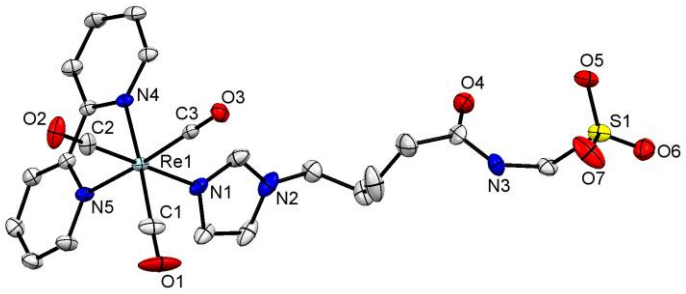


**Figure 2.3** ORTEP plot (50% thermal ellipsoid probability) for $[Re(CO)_3(bipy)(ImSfn)]$ **9a**. Hydrogen atoms have been omitted for clarity.

The Re complexes of other ligands containing spacer groups including **11** (ImPA), the corresponding methyl ester (ImPAMe), and **13** were obtained following the same conditions used to prepare **9a**. The desired products were isolated by semi-preparative HPLC, in 21% to 42% yield, respectively. The $^{31}P\{^{1}H\}$ NMR spectrum of **10a** showed a peak at 18.6 ppm, which was similar to that for **8a** (19.5 ppm), signifying the ligand was coordinated to the metal through the imidazole group and not the bisphosphonate. The Tc analogues $[^{99m}Tc(CO)_3(bipy)(ImPA)]^+$ **6b**, $[^{99m}Tc(CO)_3(bipy)(ImPAMe)]^+$ **7b** and $[^{99m}Tc(CO)_3(bipy)(ImAln)]$ **10b** were prepared under the same condition used to prepare **8b** and isolated by HPLC in nearly quantitative yield.

An attempt was also made to develop a one pot labeling method, whereby both the bidentate and monodentate ligands are present in the reaction mixture at the same

time, to simplify the radiolabelling procedure. Here the tendency of the two ligands to coordinate at different pH values was exploited.[45] $[^{99m}Tc(CO)_3(H_2O)_3]^+$ was added to a solution containing bipy and MeIm at pH 2 and the mixture heated to 40 °C. After 15 min the pH was adjusted to 9 and the reaction was allowed to proceed at 40 °C for a further 15 min, yielding the desired product in comparable yield to the two-step procedure. HPLC of the reaction mixture at pH 2 (Figure 2.4) clearly showed the formation of **4b**, whereupon raising the pH resulted in the formation of **5b**, which was confirmed through comparison of the retention times of both products to that of the corresponding Re standards.

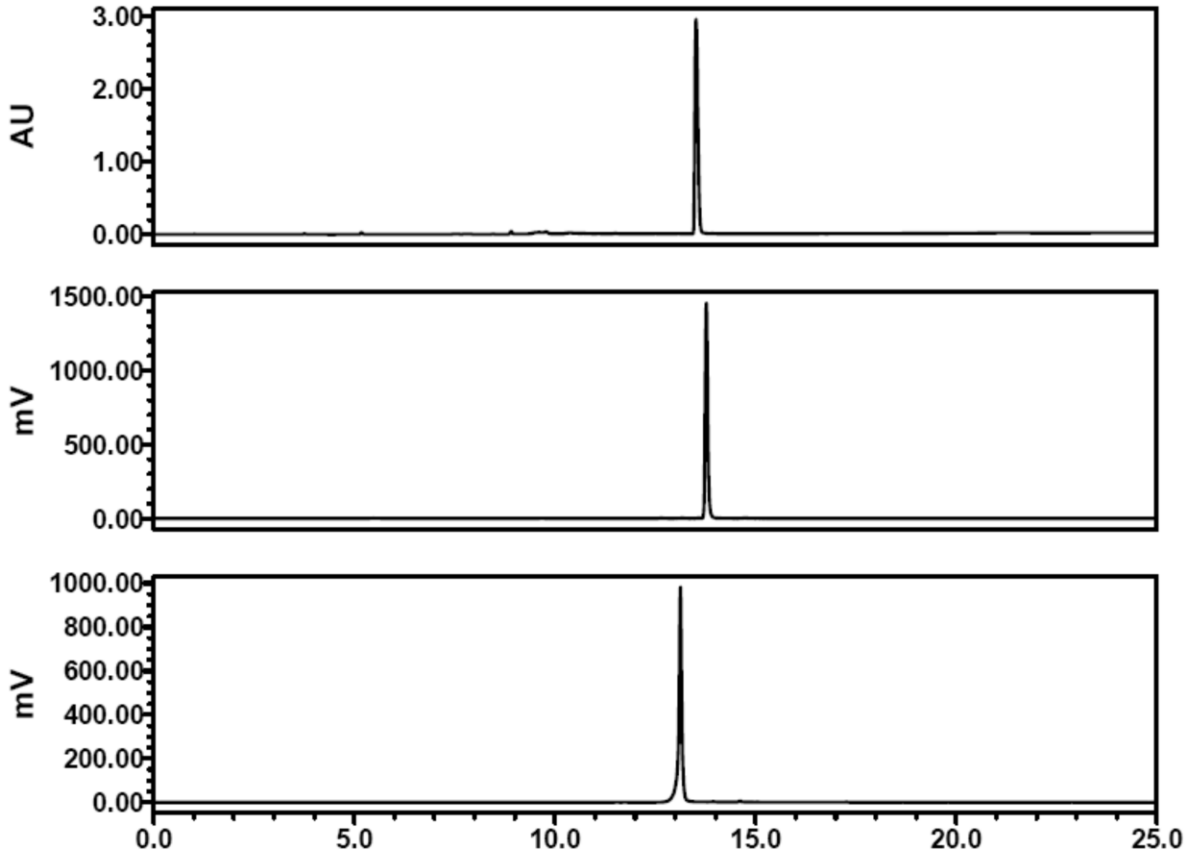


**Figure 2.4** HPLC chromatograms (UV and γ) of $[Re(CO)_3(bipy)(MeIm)]^+$ **5a** (top) co-injected with $[^{99m}Tc(CO)_3(bipy)(MeIm)]^+$ **5b** (middle), and $[^{99m}Tc(CO)_3(bipy)(H_2O)]Cl$ **4b** (bottom) prepared using a pH mediated one pot reaction.

### 2.3.2 Stability Studies

The stability of the Tc complexes was evaluated through amino acid challenge and by incubation in both isotonic saline and plasma. For the amino acid challenge experiments, **5b** was incubated separately with histidine and cysteine in PBS (pH = 7.4) at 37 °C. HPLC analysis (chromatograms provided in the supporting information) out to

6 h showed no sign of ligand substitution with either amino acid. After incubation in 0.9% saline, **5b** also showed no evidence of decomposition after 6 h. In contrast, compound [$^{99m}$Tc(CO)$_3$(bipy)(ZA)] **8b** showed 50% decomposition to the intermediate **4b** after incubation in saline for 6 h. However the compound was stable in the presence of a small amount of excess ligand (30 μg/mL). The same trend was observed in mouse plasma as a function of time (Figure 2.5), where if the monodentate ligand is lost, the resulting species [$^{99m}$Tc(CO)$_3$(bipy)(H$_2$O)]$^+$ exhibits high protein binding and the radioactivity precipitates upon the addition of acetonitrile. To verify that the activity associated with the complex in which the monodentate ligand was lost was precipitated quantitatively, HPLC analysis of the supernatant was performed. In all cases a single peak associated with the [2 + 1] complexes was observed confirming that products formed through loss of the monodentate ligand and subsequent protein binding were readily isolated by precipitation.

Despite being more polar (log P = -1.68 vs. 0.36), [$^{99m}$Tc(CO)$_3$(bipy)(ZA)] **8b** had higher protein binding than **5b** (23% versus 13%) at 6 h. The lower stability of the ZA complex compared to the MeIm derivative was attributed to the electron-withdrawing nature of the bisphosphonate group, which reduces the basicity of the donor ligand. Support for this hypothesis was that Tc complexes bearing a spacer group, which eliminated the electronic influence of the bisphosphonate in **10b** and the sulfonate in **9b** on the basicity of the amine, showed no sign of degradation over 6 h.

The results are somewhat surprising in that it had been previously reported that neutral bidentate ligands like bipy that form cationic complexes tend to favour

coordination to a halide over a neutral donor like imidazole.[56,57] In contrast [2 + 1] complexes derived from anionic bidentate ligands form neutral complexes where neutral monodentate ligands, such as imidazoles or isocyanides, are reported to form robust species.[58–62] Interestingly, a [2 + 1] $^{99m}$Tc complex derived from an anionic bidentate ligand (picolinate) and a N-substituted imidazole bearing an electron withdrawing substituent showed (similar to what we observed) reduced stability compared to a more basic imidazole derivative.[63] These results highlight one of the attractive features of the [2 + 1] system in that the properties of the metal complex including stability can be readily modified by judicious choice of mono and bidentate ligands, which is an important feature when designing and optimizing targeted molecular imaging probes.

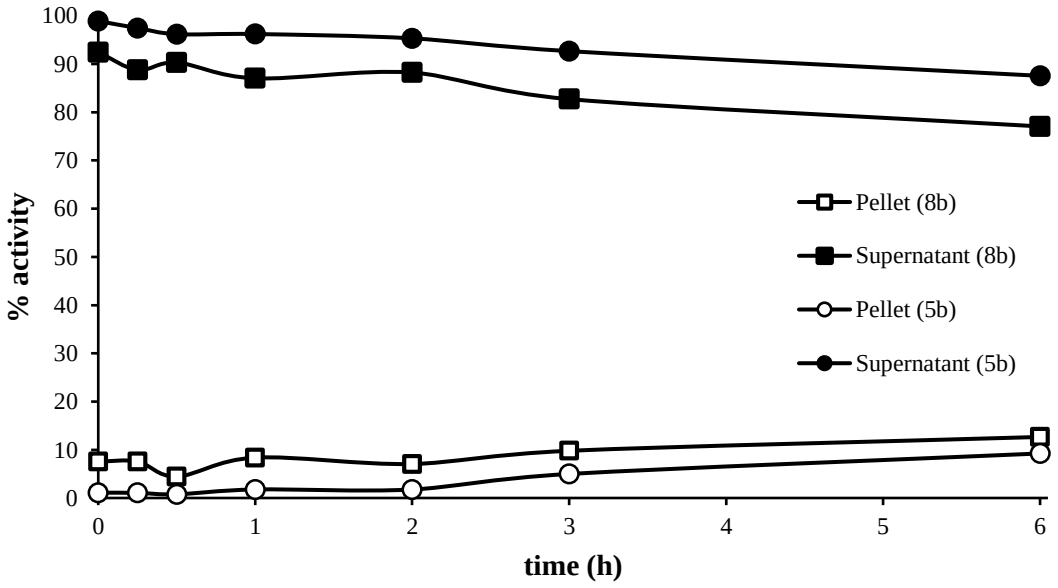


**Figure 2.5** Results of plasma binding studies for **5b** and **8b**.

### 2.3.3 Fluorescence Properties

Given the results of the stability studies and in consideration that a goal was to create isostructural optical and nuclear probes, the absorbance and emission spectra for the novel Re imidazole complexes were also measured. Experiments were performed in aqueous solutions at the same concentration to allow for comparison of the emission intensities (spectra provided in the supporting information). Compounds **8a-10a** showed a dominant absorption band at approximately 246 nm, which were attributed to intra-ligand $\pi \rightarrow \pi^*$ transitions and lower energy bands at 300 and 316 nm, which were attributed to metal-to-ligand charge transfer ($^1$MLCT).[64,65] Broad emission bands were observed with maxima typically around 600 nm, which were attributed to emission from triplet metal to ligand charge transfer ($^3$MLCT). The intensities varied significantly with the sulfonate (**9a)** being the most intense. This is not an unexpected result as sulfonate groups are often added to dyes to increase solubility and reduce intramolecular quenching. Interestingly the phosphonate derivatives were not nearly as intense. Nevertheless these measured values compare favorably to the literature values for this class of luminophores including those that have been used as cellular dyes.[38,53]

### 2.3.4 Biological Testing

Given the tendency of **8b** to lose the monodentate ligand in solution, prior to performing biodistribution studies we thought it would be prudent to first perform an *in*

*vitro* assay to see if the complex could adequately retain the ability to bind its target, prior to loss of the monodentate ligand. The study was performed using an established calcium salt binding assay for assessing radiolabeled bisphosphonates in direct comparison to $^{99m}$Tc-MDP, which is a clinically approved radiopharmaceutical used for imaging bone metastases.[66] $^{99m}$Tc-MDP is produced using an instant kit in the presence of excess ligand so to eliminate variability caused by the presence or absence of excess ligand, **8b** was prepared similarly (for both the *in vitro* assay and subsequent biodistribution studies). *In vitro* calcium salt binding of [$^{99m}$Tc(CO)$_3$(bipy)(ZA)] **8b** and $^{99m}$Tc-MDP is depicted in Figure 2.6 (HA = hydroxyapatite, β-t-C = β-tri-calcium phosphate, CPD = calcium phosphate dibasic, CO = calcium oxalate, CC = calcium carbonate, CPP = calcium pyrophosphate). Compound **8b** showed lower binding to calcium oxalate compared to MDP (15% vs. 61%) but superior binding to hydroxyapatite (72% vs. 52%), calcium phosphate (40% vs. 2%), calcium phosphate dibasic (55% vs. 5%), calcium carbonate (22% vs. 2%), and calcium pyrophosphate (14% vs. 4%). The binding data suggested that **8b** as formulated has sufficient affinity for calcium salts compared to MDP and stability to warrant assessing its distribution *in vivo*.

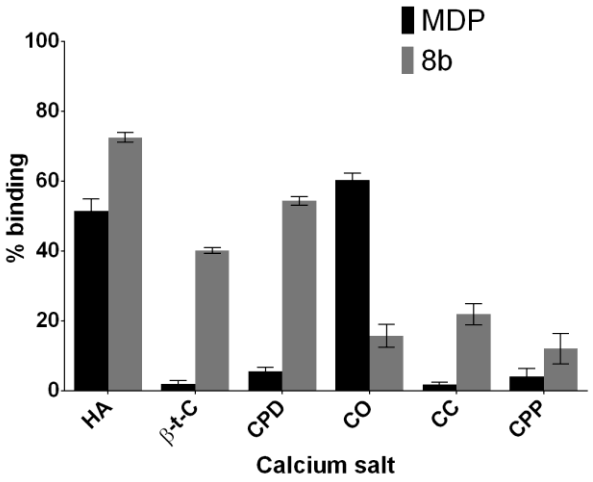


**Figure 2.6** *In vitro* calcium salt binding of [$^{99m}$Tc(CO)$_3$(bipy)(ZA)] **8b** (grey bars) and $^{99m}$Tc-MDP (black bars). (HA = hydroxyapatite, β-t-C = β-tri-calcium phosphate, CPD = calcium phosphate dibasic, CO = calcium oxalate, CC = calcium carbonate, CPP = calcium pyrophosphate).

### 2.3.5 *In vivo* Imaging Studies

One way to assess the utility of [2 + 1] complexes as platforms for developing probes is to compare their distribution to [$^{99m}$Tc(CO)$_3$(bipy)(H$_2$O)]Cl, which is the initial product that would form if the monodentate ligand were lost *in vivo*. As expected, SPECT/CT images of **4b** administered to Balb/c mice demonstrated high liver uptake, which is likely associated with the binding of the reactive complex with serum proteins (Figure 2.7a and b). The compound remains in the liver beyond 6 h providing a point of reference for assessing the stability of other [2 + 1] Tc complexes. The polar sulfonate ligand complex **9b** (Figure 2.7c and d) was a stark contrast to **4b** in that it was excreted

rapidly and predominantly through the kidneys and bladder with negligible liver uptake evident. Had the monodentate imidazole ligand been displaced within the time the agent was in circulation, significant liver uptake would have been expected, as was observed with **4b**.

In the case of **8b**, SPECT/CT images acquired at 1, 4, and 6 h after injection showed uptake in regions of high calcium turnover (e.g. knee and shoulder joints), consistent with MDP images. However despite the presence of excess ligand there was significant accumulation in the liver (Figure 2.8a). This suggested that a loss of the ZA ligand was occurring, as was seen in the *in vitro* stability studies. Compound **10b** was subsequently evaluated to study the impact of using a more basic imidazole ligand. SPECT/CT showed that the compound had modest liver uptake compared to **8b**, despite a higher log P and the absence of any excess ligand, but retained significant accumulation and long residence time in the bone, especially the larger joints (Figure 2.8b). The transverse images through the knees showed intense uptake for both complexes at 6 h (Figures 2.8c, d), where for **10b** activity in the bladder particularly at early time points was evident. While the goal here was not to develop a superior alternative to Tc-MDP, the results do demonstrate that with a suitable choice of monodentate ligand, robust [2 + 1] constructs can be prepared and used to develop targeted probes.

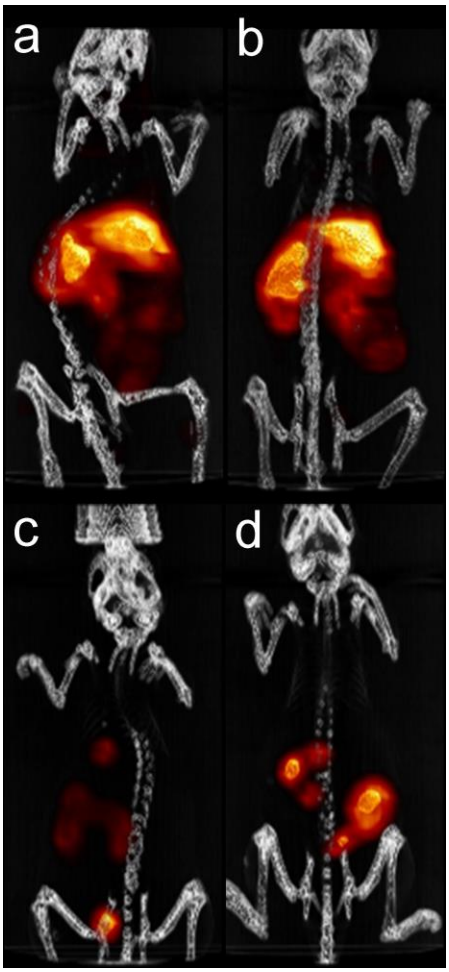


**Figure 2.7** Scintigraphic-CT images of Balb/c mice administered **4b** where images were obtained after (a) 1 h and (b) 6 h. Images of **9b** obtained after (c) 1 h and (d) 6 h.

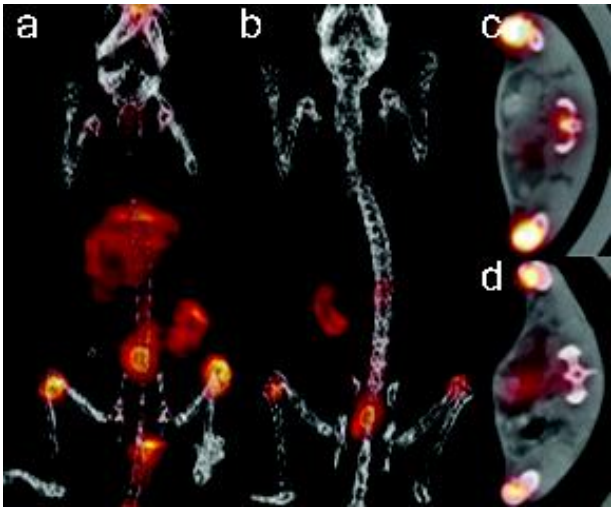


**Figure 2.8** Scintigraphic-CT images of Balb/c mice at 6 h post injection of (a) **8b** and (b) **10b** with images set to the same maximum threshold. The corresponding transverse images through the knees, spine and bladder for (c) **8b** and (d) **10b** at 6 h, set to the same maximum threshold.

## 2.4 Conclusion

A series of new Re(I)/Tc(I) [2 + 1] complexes derived from imidazole ligands were prepared and X-ray structures of two new Re(I) complexes were determined. A high yield method to prepare $^{99m}$Tc analogues of a class of rhenium luminophores was developed, which included a pH mediated one-pot reaction. *In vitro* and *in vivo* imaging studies determined that incorporation of a spacer group between the imidazole donor group and electron withdrawing substituents renders the complex suitably stable for use *in vivo*. In addition to being constructs that can be used to prepare targeted isostructural luminescent and nuclear probes, the [2 + 1] system has the benefit that the nature of the

monodentate ligand can be easily varied to optimize cell permeability and retention, pharmacokinetics and to select the preferred route of clearance. This will facilitate the discovery of new molecular imaging probes.

## 2.5 Experimental Section

### 2.5.1 Materials and Instrumentation

All solvents were purchased from Caledon. Chemicals were purchased from Sigma-Aldrich and used without further purification, unless otherwise stated. Compounds **4a**, **5a**, (5-imidazole-1-yl)pentanoic acid methyl ester (ImPAMe, **14**), and (5-imidazole-1-yl)pentanoic acid (ImPA, **11**) were prepared according to literature method.[41,67–69] Histidine and cysteine challenge studies were performed according to literature procedures.[70] Briefly, a solution of Tc(I) complex was incubated separately in 2 mM histidine and 2 mM cysteine in PBS (pH = 7.4) at 37 °C. Samples were taken at different time points up to 6 h and analyzed by HPLC to determine the degree of decomposition. Deuterated solvents for NMR samples were purchased from Cambridge Isotope Laboratories. Technetium-99m $[^{99m}TcO_4]^-$ was obtained from a $^{99}Mo/^{99m}Tc$ generator (Lantheus Medical Imaging) in saline (0.9% NaCl). *Caution: $^{99m}$Tc is a γ-emitter (Eγ = 140 keV, $t_{1/2}$ = 6 h) and should only be used in a licensed and appropriately shielded facility.*

Nuclear magnetic resonance spectra ($^1$H, $^{13}$C, $^{31}$P{$^1$H}) were recorded on a Bruker AV600 MHz spectrometer at ambient temperature. Microwave-assisted reactions were

performed on a Biotage Initiator 60 microwave reactor using crimp-sealed vials. Mass spectrometry analyses was provided by the McMaster Regional Centre for Mass Spectrometry on an Agilent 6340 Ion Trap LC/MS mass spectrometer operating in electrospray ionization (ES) mode. High resolution mass spectra (HRMS) were collected on a Waters/Micromass Q-Tof Global Ultima spectrometer. IR spectra were obtained on a Biorad FTS-40 FTIR spectrometer. The fluorescence spectra were collected with the Tecan Infinite M1000 plate reader and the concentration of the solutions were 50 μM. High performance liquid chromatography (HPLC) was performed on a Waters 1525 Binary (Midford, MA, USA) monitored simultaneously with 2998 Photodiode Array Detector at 220/254 nm and in-line radioactivity Bioscan gamma detector with NaI(Tl) scintillator using the Empower software package. Phenomenex Gemini C-18 analytical column (250 × 4.60 mm, 5 μm) and Phenomenex Synergy Polar-RP analytical column (250 × 4.60 mm, 5μm) operating at a flow rate of 1.0 ml/min, and Phenomenex Gemini C-18 semipreparative column (250 × 10 mm, 5 μm) operating at a flow rate of 4.0 ml/min were used for all analyses. The following solvent gradients were employed: *Method A* (solvent A = $H_2O$ + 0.1% TFA, solvent B = acetonitrile + 0.1% TFA): 0-2 min 2% B, 2-20 min 100% B; 20-22 min 100% B, 22-23 min 2% B, 23-25 min 2% B. *Method B* (solvent A = $H_2O$ + 0.005% TEA, solvent B = acetonitrile + 0.005% TEA): 0-2 min 2% B, 2-20 min 100% B; 20-22 min 100% B, 22-23 min 2%B, 23-25 min 2% B. *Method C* (solvent A = $H_2O$ + 0.1% FA, solvent B = acetonitrile + 0.1% FA): 0-2 min 2% B, 2-20 min 100% B; 20-22 min 100% B, 22-23 min 2%B, 23-25 min 2% B. *Method D* (solvent

A = $H_2O$ + 0.03% TFA, solvent B = acetonitrile + 0.03% TFA): 0-2 min 2% B, 2-20 min 100% B; 20-22 min 100% B, 22-23 min 2%B, 23-25 min 2% B.

### 2.5.2 X-ray crystallography

Suitable quality crystals were mounted in Paratone oil on a MiTeGen loop and placed in the cold stream of the diffractometer. Data were collected using 0.5 degree omega and phi scans on a Bruker Apex2 diffractometer using MoKα radiation. The data were integrated using SAINT, corrected for absorption with SADABS (face-indexing and redundancy) and solved in the space group P-1 for **8a** (CCDC 1041053) and P21/c for **9a** (CCDC 1041054).[71]

### 2.5.3 Synthetic Procedures

***[Re(CO)$_3$(bipy)(ImPA)][CF$_3$SO$_3$]*** **6a**

(5-Imidazole-1-yl)pentanoic acid (ImPA) **11** (34 mg, 0.2 mmol) was dissolved in MeOH (10 mL), and diisopropylethylamine (87 μL, 0.5 mmol) added to the solution. [Re(CO)$_3$(bipy)($H_2O$)][$CF_3SO_3$] (60 mg, 0.1 mmol) in MeOH (10 mL) was then added and the mixture heated to reflux overnight. The solution was subsequently evaporated to dryness under reduced pressure. The desired product was isolated by silica-gel column chromatography using MeOH:DCM (1:10 v/v) as a yellow solid (31 mg, 42%). m.p. 141-143 °C. IR ($\nu_{CO}$/cm$^{-1}$): 2020, 1892. $^1$H NMR (600 MHz, $CD_3OD$): δ (ppm) = 9.08 (d, *J* = 5.4 Hz, 2 H); 8.53 (d, *J* = 8.2 Hz, 2H); 8.22 (m, 2H); 7.86 (s, 1H); 7.66 (m, 2H); 7.14 (s,

2H); 3.81 (t, *J* = 7.1 Hz, 2H); 1.86 (t, *J* = 7.2 Hz, 2H); 1.37 (m, 2H); 1.08 (m, 2H). $^{13}$C NMR (150 MHz, $CD_3OD$): δ (ppm) = 180.85, 157.64, 154.78, 141.44, 141.13, 128.72, 128.39, 125.17, 124.79, 55.94, 36.87, 31.15, 24.16. HRMS: *m/z* calc for $C_{21}H_{20}N_4O_5Re$: 595.0991 found: 595.1003. HPLC (UV 254 nm, method A): $R_t$ = 12.1 min.

***[Re(CO)$_3$(bipy)(ImPAMe)][CF$_3$SO$_3$]*** **7a**

(5-Imidazole-1-yl)pentanoic acid methyl ester (ImPAMe, **14**) (21 mg, 0.12 mmol) in $CH_3CN$ (10 mL) was added to $[Re(CO)_3(bipy)(H_2O)][CF_3SO_3]$ (60 mg, 0.1 mmol) in $CH_3CN$ (10 mL) and the mixture heated to reflux overnight. The solution was then evaporated to dryness under reduced pressure. The desired product was isolated by silica-gel column chromatography using MeOH:DCM (1:10 v./v) as a yellow solid (28 mg, 37%). m.p. 185-187 °C. IR ($\nu_{CO}$/cm$^{-1}$): 2028, 1910. $^1$H NMR (600 MHz, $CD_3CN$): δ (ppm) = 9.14 (d, *J* = 5.4 Hz, 2 H); 8.41 (d, *J* = 8.1 Hz, 2H); 8.26 (m, 2H); 7.73 (m, 2H); 7.38 (s, 1H); 6.91 (s, 1H); 6.50 (s, 1H); 3.80 (t, *J* = 7.0 Hz, 2H); 3.59 (s, 3H); 2.17 (t, *J* = 7.3 Hz, 2H); 1.57 (m, 2H); 1.22 (m, 2H). $^{13}$C NMR (150 MHz, $CD_3CN$): δ (ppm) = 174.13, 156.59, 154.66, 141.83, 140.86, 129.68, 129.42, 125.49, 122.32, 51.96, 48.28, 33.43, 30.09, 21.97. HRMS: *m/z* calc for $C_{24}H_{24}NO_6Re$: 609.1161 found: 609.1165. HPLC (UV 254 nm, method A): $R_t$ = 15.5 min.

***[Re(CO)$_3$(bipy)(ZA)]*** **8a**

$[Re(CO)_3(bipy)(H_2O)][CF_3SO_3]$ (60 mg, 0.1 mmol) was dissolved in water (10 mL) and the pH adjusted to 7 with 0.1 M NaOH. Zoledronic acid (42 mg, 0.15 mmol) was

suspended in water (5 mL), the pH adjusted to 7 with 0.1 M NaOH, and added dropwise to the solution containing Re. The mixture was heated to reflux overnight and subsequently evaporated to dryness under reduced pressure. DCM (5 mL) was added and the precipitate removed by filtration. The product was isolated (65 mg, 77%) as a yellow solid by semipreparative HPLC (method C). m.p. 283-286 °C. IR ($\nu_{CO}$/cm$^{-1}$): 2026, 1910. $^{1}$H NMR (600 MHz, $D_2O$): δ (ppm) = 9.22 (d, *J* = 5.5 Hz, 2 H); 8.44 (d, *J* = 8.3 Hz, 2 H); 8.25 (m, 2 H); 7.72 (m, 2 H); 7.53 (s, 1 H); 7.01 (m, 1 H); 6.56 (m, 1 H); 4.30 (t, *J* = 10.1 Hz, 2 H). $^{13}$C NMR (150 MHz, $D_2O$): δ (ppm) = 196.79, 155.78, 153.35, 140.50, 127.89, 127.60, 124.13, 123.15, 73.03, 50.59. $^{31}$P{$^{1}$H} NMR (242 MHz, $D_2O$): δ (ppm) = 14.55. HRMS: *m/z* calc for $C_{18}H_{18}N_4O_{10}P_2Re$: 699.0056 found: 699.0072. HPLC (UV 254 nm, method B): $R_t$ = 7.8 min.

***[Re(CO)$_3$(bipy)(ImSfn)]*** **9a**

*(5-Imidazol-1-yl-pentanoylamino)methanesulfonic acid* (ImSfn) **12** (32 mg, 0.12 mmol) was dissolved in MeOH (10 mL) and diisopropylethylamine (104 µL, 0.6 mmol) added followed by [Re(CO)$_3$(bipy)($H_2O$)][$CF_3SO_3$] (60 mg, 0.1 mmol) in MeOH (10 mL) and the mixture heated to reflux overnight. The solution was then evaporated to dryness under reduced pressure and the desired product isolated by silica-gel chromatography using MeOH:DCM (1:3 v/v) as a yellow solid (32 mg, 38%). m.p. 250-253 °C. IR ($\nu_{CO}$/cm$^{-1}$): 2026, 1905. $^{1}$H NMR (600 MHz, $CD_3OD$): δ (ppm) = 9.22 (d, *J* = 5.6 Hz, 2 H); 8.63 (d, *J* = 8.2 Hz, 2H); 8.33 (m, 2H); 7.80 (m, 2H); 7.60 (s, 1H); 7.05 (s, 1H); 6.67 (s, 1H); 4.30 (s, 2H); 3.88 (t, *J* = 6.8 Hz, 2H); 2.09 (t, *J* = 7.2 Hz, 2H); 1.61 (m, 2H); 1.16 (m, 2H). $^{13}$C

NMR (150 MHz, $CD_3OD$): δ (ppm) = 174.74, 157.24, 154.82, 142.44, 141.28, 130.45, 129.77, 126.29, 122.71, 56.81, 48.50, 35.95, 30.86, 22.89. HRMS: *m/z* calc for $C_{22}H_{23}N_5O_7SRe$: 688.0876 found: 688.0883. HPLC (UV 254 nm, method A): $R_t$ = 12.6 min.

***[Re(CO)$_3$(bipy)(ImAln)]*** **10a**

$[Re(CO)_3(bipy)(H_2O)][CF_3SO_3]$ (60 mg, 0.1 mmol) was dissolved in water (10 mL) and the pH adjusted to 7 with 0.1 M NaOH. [1-Hydroxy-4-(5-imidazol-1-yl-pentanoylamino)-1-phosphono-butyl]-phosphonic acid (ImAln) **13** (43 mg, 0.11 mmol) was suspended in water (5 mL), the pH adjusted to 7 with 0.1 M NaOH and added dropwise to the solution containing Re. The mixture was heated to 80 °C overnight and then evaporated to dryness under reduced pressure. The desired product was isolated (19 mg, 21%) as a yellow solid by semi-preparative HPLC (method D). m.p. 142-145 °C. IR ($\nu_{CO}$/cm$^{-1}$): 2029, 1912. $^1$H NMR (600 MHz, $D_2O$): δ (ppm) = 9.07 (d, *J* = 5.3 Hz, 2 H); 8.26 (d, *J* = 7.5 Hz, 2 H); 8.09 (m, 2 H); 7.57 (m, 2 H); 7.38 (s, 1 H); 6.76 (s, 1H); 6.39 (s, 1 H); 3.68 (t, *J* = 6.3 Hz, 2 H); 3.03 (s, 2H); 1.84 (m, 2H); 1.79 (m, 2H); 1.67 (m, 2H); 1.38 (m, 2H); 0.88 (m, 2H). $^{13}$C NMR (150 MHz, $D_2O$): δ (ppm) = 175.85, 155.75, 153.53, 140.71, 139.84, 128.87, 128.00, 124.06, 121.10, 77.94, 47.28, 39.52, 34.72, 28.81, 23.27, 21.76, 20.69. $^{31}$P{$^1$H} NMR (242 MHz, $D_2O$): δ (ppm) = 18.62. HRMS: *m/z* calc for $C_{25}H_{31}N_5O_{11}P_2Re$: 826.1053 found: 826.1031. HPLC (UV 254 nm, method B): $R_t$ = 8.9 min.

***(5-Imidazol-1-yl-pentanoylamino)-methanesulfonic acid*** **(ImSfn) 12**

Aminomethanesulfonic acid (222 mg, 2.0 mmol) was dissolved in $H_2O$ (25 mL), and diisopropylethylamine (533 μL, 3.0 mmol) was added to the solution stirring at room temperature. After 30 min, the solution was added to a second premixed solution of (5-imidazole-1-yl)pentanoic acid **11** (168 mg, 1.0 mmol) and benzotriazole-1-yl-oxy-tris-(dimethylamino)phosphonium hexafluorophosphate (PyBOP, 775 mg, 1.5 mmol) in DMF (25 mL). The resulting solution was stirred overnight and then purified by semipreparative HPLC (method A). The pure product was isolated as colorless oil (122 mg, 47%). $^1$H NMR (600 MHz, $CD_3OD$): δ (ppm) = 9.01 (s, 1 H); 7.68 (s, 1 H); 7.54 (s, 1 H); 4.34 (s, 2 H); 4.28 (t, $J$ = 7.4 Hz, 2 H); 2.34 (t, $J$ = 6.8 Hz, 2 H); 1.99 (m, 2 H); 1.69 (m, 2 H). $^{13}$C NMR (150 MHz, $CD_3OD$): δ (ppm) = 175.09, 136.67, 123.41, 120.92, 56.53, 50.03, 35.82, 30.04, 23.05. HRMS: *m/z* calc for $C_9H_{14}N_3O_4S$: 260.0705 found: 260.0700.

***[1-Hydroxy-4-(5-imidazol-1-yl-pentanoylamino)-1-phosphono-butyl]-phosphonic acid*** **(ImAln) 13**

Alendronate sodium trihydrate (498 mg, 2.0 mmol) was dissolved in $H_2O$ (25 mL), and diisopropylethylamine (1.8 mL, 10.0 mmol) was added to the solution stirring at room temperature. After 30 min, the solution was added to a second premixed solution of (5-imidazole-1-yl)pentanoic acid **11** (168 mg, 1 mmol) and PyBOP (775 mg, 1.5 mmol) in DMF (25 mL). The resulting solution was stirred overnight and then purified by semipreparative HPLC (method A). The pure product was isolated as colorless oil (167

mg, 42%). $^{1}$H NMR (600 MHz, $D_2O$): δ (ppm) = 8.64 (s, 1 H); 7.42 (s, 1 H); 7.37 (s, 1 H); 4.16 (t, *J* = 6.9 Hz, 2 H); 3.12 (t, *J* = 6.7 Hz, 2 H); 2.20 (t, *J* = 7.2 Hz, 2 H); 1.91 (m, 2 H); 1.80 (m, 2 H), 1.73 (m, 2 H), 1.50 (m, 2 H). $^{13}$C NMR (150 MHz, $D_2O$): δ (ppm) = 176.00, 134.32, 121.75, 119.71, 73.01 (m), 48.95, 39.54, 34.97, 30.91, 28.68, 23.17, 22.00. $^{31}P\{^{1}H\}$ NMR (242 MHz, $D_2O$): δ (ppm) = 19.52. HRMS: *m/z* calc for $C_{12}H_{22}N_3O_8P_2$: 398.0882 found: 398.0883.

### 2.5.4 General Procedure for the Preparation of 5b-7b, 9b

Sodium boranocarbonate (10.0 mg, 0.10 mmol), sodium carbonate (15.0 mg, 0.14 mmol), sodium borate (20 mg, 0.05 mmol) and sodium potassium tartrate (22 mg, 0.08 mmol) were placed in a microwave vial and purged with argon for 10 min. To this mixture, Na[$^{99m}TcO_4$] (1 mL, 370-740 MBq) was added and the vial was heated in a microwave reactor at 110 °C for 3.5 min to form [$^{99m}Tc(CO)_3(H_2O)_3]^+$. The solution was then cooled and adjusted to pH 5.5-6.5 with aqueous hydrochloric acid (1.0 M). The solution was added to bipyridine (1 mg, 6 µmol) in a separate microwave vial that had been purged with argon, and the mixture heated to 110 °C for 6 min to form [$^{99m}Tc(CO)_3$(bipy)$(H_2O)$]Cl.[45] This solution was subsequently added to one of the monodentate ligands (30 – 120 µmol) under argon and the mixture stirred at 40 °C for 20 min. The formation of products was confirmed by analytical HPLC (method A). Quantitative conversion of [$^{99m}Tc(CO)_3(H_2O)_3]^+$ to the final product was achieved in all cases.

### 2.5.5 General Procedure for the Preparation of 8b and 10b

The pH of a solution of [$^{99m}$Tc(CO)$_3$(bipy)(H$_2$O)]Cl (1 mL, 370-740 MBq) was adjusted to 7 with 1 M NaOH and added to an argon purged solution of zoledronic acid or **13** in water (0.5 mL, 33 mM) whose pH was adjusted to 7 with 1M NaOH. The reaction mixture was heated in a microwave reactor at 60 °C for 30 min and the product isolated in quantitative yield by HPLC (Method B).

### 2.5.6 Specific Activity

Specific activity was determined by HPLC and calibration curves derived from the corresponding Re complexes. For the calibration curves, each calibration solution was evaluated in triplicate and the data analyzed by the least-squares method. The limit of detection was calculated using the standard deviation method.[72]

### 2.5.7 Purification of $^{99m}$Tc Complexes

Purification of [$^{99m}$Tc(CO)$_3$(bipy)(H$_2$O)]Cl and **5b**-**10b** was achieved by solid phase extraction (SPE) or semi-preparative HPLC. For SPE, the reaction mixture was diluted with water (2 mL) and the solution loaded on a Waters C18 Sep-Pak Plus cartridge, which had been previously activated with EtOH (1 × 6 mL) and H$_2$O (1 × 6 mL). After loading the reaction mixture, the column was washed with 15% CH$_3$CN in H$_2$O (2 × 6 mL), followed by 25% CH$_3$CN in 0.4% (w/v) aqueous ammonium formate (1

× 6 mL). The desired products were eluted with a 1:1 v/v mixture of 0.4% aqueous ammonium formate and $CH_3CN$. For HPLC, following isolation, the solution was evaporated to dryness and the desired compound reconstiuted in saline.

### 2.5.8 One-pot Synthesis of $[^{99m}Tc(CO)_3(bipy)(MeIm)]^+$ 5b

$[^{99m}Tc(CO)_3(H_2O)_3]^+$ was added to an argon purged solution of bipyridine (1 mg, 6 µmol) and MeIm (10 mg, 0.12 mmol) in water (0.5 mL). The pH of the solution was adjusted to 2 with 0.1 M HCl and the mixture stirred at 40 °C for 15 min. The pH of the solution was then adjusted to 9 with 1 M NaOH and the reaction mixture stirred at 40 °C for 15 min. A single product was observed in the gamma trace and the product was isolated in quantitative yield by HPLC (Method A).

### 2.5.9 Compound Testing and Evaluation

**Plasma Binding**

100 µL (111 MBq) of the labeled material was added to 900 µL of pre-warmed (37˚C) mouse plasma (Innovative Research, IMS-CD1-N), the mixture vortexed and then incubated at 37˚C. At multiple time points (t=0, 0.25, 0.5, 1, 2, 3, 6 h), 100 µL was removed and added to 200 µL ice cold acetonitrile. Samples were vortexed and then centrifuged at maximum speed for 10 min. The amount of activity in the whole sample was measured using a dose calibrator (Capintec Inc, CRC-25R). The supernatant was separated from the pellet and the activity in each was measured using a dose calibrator.

For all time points except t=0, pellets were washed with 200 µL of ice cold PBS. The experiment was repeated once with the percentage bound to blood proteins calculated as follows:

%bound = [(amount of activity in washed pellet)] / [(amount of activity in pellet) + (amount of activity in supernatant)] × 100%

Values are reported as an average of two experiments ± standard deviation.

**Calcium Salt Binding**

The method for *in vitro* calcium salt binding followed a literature procedure.[66] Briefly, 10 µL (0.8 MBq) of either the labeled compound or $^{99m}$Tc-MDP (as a positive control) was added to 1.5 mL of 1 mg/mL solutions of hydroxyapatite, β-tri-calcium phosphate, calcium phosphate dibasic, calcium oxalate, calcium carbonate and calcium pyrophosphate in 50 mM Tris buffer (pH 6.9). A no salt control was also included. Samples were incubated with gentle shaking for 1h at room temperature and then centrifuged for 5 min at 10 000 rpm. A 60 µL aliquot of the supernatant was measured using a gamma counter. The data is based on a minimum of three experiments done in triplicate. The percent binding was calculated using the following formula, (CPMs = counts per min of each sample; CPMc = counts per min for the no salt control):

$$\%\ binding = [1 - \left(\frac{CPMs}{CPMc}\right)] \times 100$$

**Imaging Studies**

Imaging was performed using female Balb/c mice (Senneville, QC, Canada). The mice were administered 200 µl of saline containing [$^{99m}$Tc(CO)$_3$(bipy)(H$_2$O)]Cl **4b** [$^{99m}$Tc(CO)$_3$(bipy)(ZA)] **8b**, [$^{99m}$Tc(CO)$_3$(bipy)(ImSfn)] **9b**, or [$^{99m}$Tc(CO)$_3$(bipy)(ImAln)] **10b**, (~35 MBq) via tail vein injection. Prior to imaging, mice were anaesthetized with 1% isoflurane and imaging conducted at approximately 1 and 6 h post injection for all the compounds. At each time point, CT images were acquired using a conebeam X-SPECT scanner (Gamma Medica, Northridge, USA) with a source voltage of 75 kVp and a current of 165 µA. Projection data was acquired with 1024 projection angles (1184×1120 pixels, 0.100 mm pixels) and reconstructed using a Feldkamp cone beam back projection algorithm in COBRA (Exxim Software, Pleasanton, CA, USA) into 512×512×512 arrays (0.155 mm isotropic voxels). SPECT images were acquired using dual sodium iodide crystals in combination with low-energy, high-resolution, parallel-hole collimators. A total of 64 projections over 360° were acquired with an energy window of 159 ± 10% keV and then reconstructed using an OSEM iterative reconstruction method (2 iterations/8 subsets) into 82×82×82 arrays (1.463 mm isotropic voxels) using in-house software. CT images were compressed to a $256^3$ matrix (0.31 mm isotropic voxels). Fusion was achieved by a rigid-body (linear) transformation of the SPECT image, during which, it is interpolated and resampled to the same matrix dimensions and voxel size as the compressed CT image. Imaging analysis was completed using AMIDE software.

*Note: All supporting information for this chapter can be found in Appendix 1.*

## 2.6 References

(1) Ametamey, S. M.; Honer, M.; Schubiger, P. A. *Chem. Rev.* **2008**, *108*, 1501–1516.

(2) Herschman, H. R. *Science* **2003**, *302*, 605–608.

(3) Kobayashi, H.; Longmire, M. R.; Ogawa, M.; Choyke, P. L. *Chem. Soc. Rev.* **2011**, *40*, 4626–4648.

(4) Spagnul, C.; Alberto, R.; Gasser, G.; Ferrari, S.; Pierroz, V.; Bergamo, A.; Gianferrara, T.; Alessio, E. *J. Inorg. Biochem.* **2013**, *122*, 57–65.

(5) Huang, M.; Xiong, C.; Lu, W.; Zhang, R.; Zhou, M.; Huang, Q.; Weinberg, J.; Li, C. *Mol. Imaging Biol.* **2013**, *16*, 74–84.

(6) Ray, P.; Wu, A. M.; Gambhir, S. S. *Cancer Res.* **2003**, *63*, 1160–1165.

(7) Backer, M. V; Levashova, Z.; Patel, V.; Jehning, B. T.; Claffey, K.; Blankenberg, F. G.; Backer, J. M. *Nat. Med.* **2007**, *13*, 504–509.

(8) Tzanopoulou, S.; Sagnou, M.; Paravatou-Petsotas, M.; Gourni, E.; Loudos, G.; Xanthopoulos, S.; Lafkas, D.; Kiaris, H.; Varvarigou, A.; Pirmettis, I. C.; Papadopoulos, M.; Pelecanou, M. *J. Med. Chem.* **2010**, *53*, 4633–4641.

(9) Yang, Y.; Zhu, L.; Cui, M.; Tang, R.; Zhang, H. *Bioorg. Med. Chem. Lett.* **2010**, *20*, 5337–5344.

(10) Bhushan, K. R.; Misra, P.; Liu, F.; Mathur, S.; Lenkinski, R. E.; Frangioni, J. V. *J. Am. Chem. Soc.* **2008**, *130*, 17648–17649.

(11) Agorastos, N.; Borsig, L.; Renard, A.; Antoni, P.; Viola, G.; Spingler, B.; Kurz, P.; Alberto, R. *Chem. Eur. J.* **2007**, *13*, 3842–3852.

(12) Esteves, T.; Xavier, C.; Gama, S.; Mendes, F.; Raposinho, P. D.; Marques, F.; Paulo, A.; Pessoa, J. C.; Rino, J.; Viola, G.; Santos, I. *Org. Biomol. Chem.* **2010**, *8*, 4104–4116.

(13) Jennings, L. E.; Long, N. J. *Chem. Commun.* **2009**, 3511–3524.

(14) Thorp-Greenwood, F. L.; Coogan, M. P. *Dalton Trans.* **2011**, *40*, 6129–6143.

(15) Ting, R.; Aguilera, T. A.; Crisp, J. L.; Hall, D. J.; Eckelman, W. C.; Vera, D. R.; Tsien, R. Y. *Bioconjugate Chem.* **2010**, *21*, 1811–1819.

(16) Priem, T.; Bouteiller, C.; Camporese, D.; Brune, X.; Hardouin, J.; Romieu, A.; Renard, P.-Y. *Org. Biomol. Chem.* **2013**, *11*, 469–479.

(17) Heinrich, T. K.; Gottumukkala, V.; Snay, E.; Dunning, P.; Fahey, F. H.; Ted Treves, S.; Packard, A. B. *Appl. Radiat. Isot.* **2010**, *68*, 96–100.

(18) Yan, R.; El-Emir, E.; Rajkumar, V.; Robson, M.; Jathoul, A. P.; Pedley, R. B.; Årstad, E. *Angew. Chem.* **2011**, *123*, 6925–6927.

(19) Li, Z.; Lin, T.-P.; Liu, S.; Huang, C.-W.; Hudnall, T. W.; Gabbaï, F. P.; Conti, P. S. *Chem. Commun.* **2011**, *47*, 9324–9326.

(20) Liu, S.; Lin, T.-P.; Li, D.; Leamer, L.; Shan, H.; Li, Z.; Gabbaï, F. P.; Conti, P. S. *Theranostics* **2013**, *3*, 181–189.

(21) Hendricks, J. A.; Keliher, E. J.; Wan, D.; Hilderbrand, S. A; Weissleder, R.; Mazitschek, R. *Angew. Chem. Int. Ed.* **2012**, *51*, 4603–4606.

(22) Zelenka, K.; Borsig, L.; Alberto, R. *Bioconjugate Chem.* **2011**, *22*, 958–967.

(23) Ranyuk, E.; Lebel, R.; Bérubé-Lauzière, Y.; Klarskov, K.; Lecomte, R.; van Lier, J. E.; Guérin, B. *Bioconjugate Chem.* **2013**, *24*, 1624–1633.

(24) Duheron, V.; Moreau, M.; Collin, B.; Sali, W.; Bernhard, C.; Goze, C.; Gautier, T.; Pais de Barros, J.-P.; Deckert, V.; Brunotte, F.; Lagrost, L.; Denat, F. *ACS Chem. Biol.* **2014**, *9*, 656–662.

(25) Zhou, Y.; Kim, Y.-S.; Yan, X.; Jacobson, O.; Chen, X.; Liu, S. *Mol. Pharm.* **2011**, *8*, 1198–1208.

(26) Schaffer, P.; Gleave, J. a; Lemon, J. a; Reid, L. C.; Pacey, L. K. K.; Farncombe, T. H.; Boreham, D. R.; Zubieta, J.; Babich, J. W.; Doering, L. C.; Valliant, J. F. *Nucl. Med. Biol.* **2008**, *35*, 159–169.

(27) Stephenson, K. A.; Banerjee, S. R.; Besanger, T.; Sogbein, O. O.; Levadala, M. K.; McFarlane, N.; Lemon, J. a; Boreham, D. R.; Maresca, K. P.; Brennan, J. D.; Babich, J. W.; Zubieta, J.; Valliant, J. F. *J. Am. Chem. Soc.* **2004**, *126*, 8598–8599.

(28) Azad, B. B.; Cho, C.-F.; Lewis, J. D.; Luyt, L. G. *Appl. Radiat. Isot.* **2012**, *70*, 505–511.

(29) Connell, T. U.; Hayne, D. J.; Ackermann, U.; Tochon-Danguy, H. J.; White, J. M.; Donnelly, P. S. *J. Label. Compd. Radiopharm.* **2014**, *57*, 262–269.

(30) Botchway, S.; Dilworth, J. R.; Salichou, M. *Dalton Trans.* **2010**, *39*, 5219–5220.

(31) Thorp-Greenwood, F. L.; Coogan, M. P. *Dalton Trans.* **2011**, *40*, 6206–6209.

(32) Saha, G. B. *Physics and Radiobiology of Nuclear Medicine*; 2nd ed.; Springer-Verlag: New York, 2001; pp. 1–201.

(33) Schwochau, K. *Angew. Chem. Int. Ed. Engl.* **1994**, *33*, 2258–2267.

(34) Balasingham, R. G.; Coogan, M. P.; Thorp-Greenwood, F. L. *Dalton Trans.* **2011**, *40*, 11663–11674.

(35) Bertrand, H. C.; Clède, S.; Guillot, R.; Lambert, F.; Policar, C. *Inorg. Chem.* **2014**, *53*, 6204–6223.

(36) Amoroso, A. J.; Arthur, R. J.; Coogan, M. P.; Court, J. B.; Fernández-Moreira, V.; Hayes, A. J.; Lloyd, D.; Millet, C.; Pope, S. J. A. *New J. Chem.* **2008**, *32*, 1097–1102.

(37) Fernández-Moreira, V.; Thorp-Greenwood, F. L.; Amoroso, A. J.; Cable, J.; Court, J. B.; Gray, V.; Hayes, A. J.; Jenkins, R. L.; Kariuki, B. M.; Lloyd, D.; Millet, C. O.; Williams, C. F.; Coogan, M. P. *Org. Biomol. Chem.* **2010**, *8*, 3888–3901.

(38) Lo, K. K.-W.; Choi, A. W.-T.; Law, W. H.-T. *Dalton Trans.* **2012**, *41*, 6021–6047.

(39) Fernández-Moreira, V.; Thorp-Greenwood, F. L.; Coogan, M. P. *Chem. Commun.* **2010**, *46*, 186–202.

(40) Thorp-Greenwood, F. L.; Balasingham, R. G.; Coogan, M. P. *J. Organomet. Chem.* **2012**, *714*, 12–21.

(41) Huertos, M. A; Pérez, J.; Riera, L. *J. Am. Chem. Soc.* **2008**, *130*, 5662–5663.

(42) Oriskovich, T. A.; White, P. S.; Thorp, H. H. *Inorg. Chem.* **1995**, *34*, 1629–1631.

(43) Zeng, Q.; Messaoudani, M.; Vlček Jr., A.; Hartl, F. *Eur. J. Inorg. Chem.* **2012**, *2012*, 471–474.

(44) El Nahhas, A.; Consani, C.; Blanco-rodríguez, A. M.; Lancaster, K. M.; Braem, O.; Cannizzo, A.; Towrie, M.; Clark, I. P.; Záliš, S.; Chergui, M.; Vlček Jr., A. *Inorg. Chem.* **2011**, *3*, 2932–2943.

(45) Pitchumony, T. S.; Banevicius, L.; Janzen, N.; Zubieta, J.; Valliant, J. F. *Inorg. Chem.* **2013**, *52*, 13521–13528.

(46) Ellis, B. L.; Gorshkov, N. I.; Lumpov, A. a; Miroslavov, A. E.; Yalfimov, A. N.; Gurzhiy, V. V; Suglobov, D. N.; Braddock, R.; Adams, J. C.; Smith, A.-M.; Prescott, M. C.; Sharma, H. L. *J. Label Compd. Radiopharm* **2013**, *56*, 700–707.

(47) Alberto, R.; Schibli, R.; Egli, A.; Schubiger, A. P. *J. Am. Chem. Soc.* **1998**, *120*, 7987–7988.

(48) Alberto, R.; Ortner, K.; Wheatley, N.; Schibli, R.; Schubiger, A. P. *J. Am. Chem. Soc.* **2001**, *123*, 3135–3136.

(49) Luis Costa; Major, P. P. *Nat. Clin. Pr. Oncol.* **2009**, *6*, 163–174.

(50) Roelofs, A. J.; Thompson, K.; Gordon, S.; Rogers, M. J. *Clin. Cancer Res.* **2006**, *12*, 6222s – 6230s.

(51) Lin, J.; Qiu, L.; Cheng, W.; Luo, S.; Ye, W. *Nucl. Med. Biol.* **2011**, *38*, 619–629.

(52) Lin, J.; Qiu, L.; Cheng, W.; Luo, S.; Xue, L.; Zhang, S. *Appl. Radiat. Isot.* **2012**, *70*, 848–855.

(53) Uppal, B. S.; Booth, R. K.; Ali, N.; Lockwood, C.; Rice, C. R.; Elliott, P. I. P. *Dalton Trans.* **2011**, *40*, 7610–7616.

(54) Palma, E.; Oliveira, B. L.; Correia, J. D. G.; Gano, L.; Maria, L.; Santos, I. C.; Santos, I. *J. Biol. Inorg. Chem.* **2007**, *12*, 667–679.

(55) Palma, E.; Correia, D. G.; Oliveira, B. L.; Gano, L.; Santos, I. C.; Santos, I. *Dalton Trans.* **2011**, 2787–2796.

(56) Alberto, R.; Pak, J. K.; van Staveren, D.; Mundwiler, S.; Benny, P. *Biopolymers* **2004**, *76*, 324–333.

(57) Mundwiler, S.; Kündig, M.; Ortner, K.; Alberto, R. *Dalton Trans.* **2004**, 1320–1328.

(58) Benny, P. D.; Fugate, G. a.; Ganguly, T.; Twamley, B.; Bučar, D.-K.; MacGillivray, L. R. *Inorg. Chim. Acta* **2011**, *365*, 356–362.

(59) Sagnou, M.; Tsoukalas, C.; Triantis, C.; Raptopoulou, C. P.; Terzis, A.; Pirmettis, I.; Pelecanou, M.; Papadopoulos, M. *Inorg. Chim. Acta* **2010**, *363*, 1649–1653.

(60) Gorshkov, N. I.; Schibli, R.; Schubiger, A. P.; Lumpov, A. a.; Miroslavov, A. E.; Suglobov, D. N. *J. Organomet. Chem.* **2004**, *689*, 4757–4763.

(61) Sagnou, M.; Benaki, D.; Triantis, C.; Tsotakos, T.; Psycharis, V.; Raptopoulou, C. P.; Pirmettis, I.; Papadopoulos, M.; Pelecanou, M. *Inorg. Chem.* **2011**, *50*, 1295–1303.

(62) Fuks, L.; Gniazdowska, E.; Kozminski, P.; Lyczko, M.; Mieczkowski, J.; Narbutt, J. *Appl. Radiat. Isot.* **2010**, *68*, 90–95.

(63) He, H.; Morely, J. E.; Silva-lopez, E.; Bottenus, B.; Montajano, M.; Fugate, G. A.; Twamley, B.; Benny, P. D. *Bioconjugate Chem.* **2009**, *20*, 78–86.

(64) Lin, R.-J.; Lin, K.-S.; Chang, I.-J. *Inorg. Chim. Acta.* **1996**, *242*, 179–183.

(65) Blanco-Rodríguez, A. M.; Towrie, M.; Sýkora, J.; Stanislav, Z.; Vlček Jr., A. *Inorg. Chem.* **2011**, *50*, 6122–6134.

(66) Torres Martin de Rosales, R.; Finucane, C.; Mather, S. J.; Blower, P. J. *Chem. Commun.* **2009**, *3*, 4847–4849.

(67) Kurz, P.; Probst, B.; Spingler, B.; Alberto, R. *Eur. J. Inorg. Chem.* **2006**, *2006*, 2966–2974.

(68) Probst, B.; Guttentag, M.; Rodenberg, A.; Hamm, P.; Alberto, R. *Inorg. Chem.* **2011**, *50*, 3404–3412.

(69) Hack, S.; Wörlein, B.; Höfner, G.; Pabel, J.; Wanner, K. T. *Eur. J. Med. Chem.* **2011**, *46*, 1483–1498.

(70) Maresca, K. P.; Hillier, S. M.; Femia, F. J.; Zimmerman, C. N.; Levadala, M. K.; Banerjee, S. R.; Hicks, J.; Sundararajan, C.; Valliant, J.; Zubieta, J.; Eckelman, W. C.; Joyal, J. L.; Babich, J. W. *Bioconjugate Chem.* **2009**, *20*, 1625–1633.

(71) APEX2 (version 2014.5-0); Bruker AXS; Madison; WI.

(72) Nayak, T. K.; Hathaway, H. J.; Ramesh, C.; Arterburn, J. B.; Dai, D.; Sklar, L. A; Norenberg, J. P.; Prossnitz, E. R. *J. Nucl. Med.* **2008**, *49*, 978–986.

# Chapter 3

## 3 Chapter 3. Technetium(I) Complexes of Bathophenanthroline Disulfonic Acid

Abdolreza Yazdani, Nancy Janzen, Shannon Czorny, John F. Valliant

The following chapter is formatted in a manuscript that is ready for submission to the journal Inorganic Chemistry. I was responsible for the development and execution of the majority of the work described in this paper including drafting the initial manuscript and experimental. Biodistribution and *in vivo* imaging studies have been done by Nancy Janzen and Shannon Czorny. Professor Valliant was the PI of the lab and responsible for the overall manuscript and project.

## 3.1 Abstract

Bathophenanthroline disulfonate (BPS) complexes of Tc(I) of the type $[Tc(CO)_3(BPS)(L)]^n$ (L = imidazole derivatives) were synthesized and evaluated *in vivo*. $[^{99m}Tc(CO)_3(BPS)(MeIm)]^-$ (MeIm = methylimidazole) was prepared in nearly quantitative yield using a convenient two step one pot labeling procedure. A targeted analogue capable of binding regions of calcium turnover associated with bone metabolism was also prepared. Here the bisphosphonate was linked to the metal through an imidazole group to give $[^{99m}Tc(CO)_3(BPS)(ImAln)]^{2-}$ (ImAln = imidazole-alendronate ligand) in high yield. Both complexes were stable *in vitro* and biodistribution studies of $[^{99m}Tc(CO)_3(BPS)(ImAln)]^{2-}$ exhibited rapid clearance from non-target tissues and significant accumulation in the shoulder (7.9 ± 0.2% ID/g) and knees (15.1 ± 0.9 % ID/g) by 6 h, with residence time in the skeleton reaching 24 h. In conjunction with the luminescent Re analogues, which were also prepared, the *in vitro* and *in vivo* data reported demonstrates the utility of this class of compounds for the creation of isostructural multimodal optical and nuclear probes.

## 3.2 Introduction

Optical imaging techniques can be used to generate high spatial resolution images of cells and tissues with real-time data acquisition,[1] while nuclear imaging methods, which include single photon emission computed tomography (SPECT), have the ability to generate tomographic whole body images. To access the unique features and strengths of

both optical and nuclear imaging, it is possible to create multimodal imaging probes that can be visualized by both methods.[2–4] This offers the means to generate complementary information from whole-body SPECT imaging and *in vitro* and intraoperative optical imaging, which has a number of important potential applications including surgical planning and guidance.[5–9] Multimodal probes for such applications are typically prepared by derivatizing a targeting vector with a radionuclide and a fluorophore.[10–17] The challenge with this approach is that the presence of multiple prosthetic groups on a single targeting molecule can have a significant and detrimental impact on target affinity and pharmacokinetics making it challenging to develop new multimodal probes.

An alternative strategy involves the use of a single prosthetic group that can exist in a luminescent or radiolabeled form that are identical in structure. This has been achieved using radiolabeled dyes[18–23] and luminescent radiometal complexes.[24–29] The latter employs a non-radioactive isotope or a transition metal congener of a radiometal to generate isostructural complexes.[30,31] For instance, Re(I) quinoline complexes have been used to prepare luminescent probes suitable for fluorescence microscopy studies on cells,[32–35] while the $^{99m}$Tc analogue can be employed to assess the *in vivo* distribution using SPECT and quantitative counting studies following necropsy. Unfortunately, the optical properties of Re complexes in this class are at present suboptimal including having low emission intensity and quantum yield.

Rhenium (I) polypyridine complexes of the general formula $[Re(CO)_3(N^N)(L)]^n$, which are also referred to as [2 + 1] type complexes,[32–35] have significantly higher quantum yields and have been used to great success as dyes for fluorescence

microscopy.[36–39] For instance, anionic $[Re(CO)_3(BPS)(L)]^n$ complexes (BPS = bathophenanthroline disulfonate, L = 3-substituted pyridines or chloride ion) were used to image the parasitic flagellate *Spironucleus vortens*, and human adenocarcinoma cells.[40,41] While the utility of Re(I)-BPS complexes for cellular imaging have been demonstrated, the Tc analogues have not been reported previously. The challenge is that the conditions used to prepare the Re(I)-BPS complexes are not appropriate when working with $^{99m}Tc$, where reactions are performed in aqueous solutions, with nanomolar concentrations of the radiometal, and reactions and the associated purification procedure should be complete within one half-life (approximately 6 h). Herein we report the synthesis of a family of Tc(I)-BPS complexes of the type $[Tc(CO)_3(BPS)(L)]^n$, where L is based on a series of imidazole derivatives. The stability and *in vivo* distribution of these complexes is also described as a way to assess the utility of Re/Tc [2 + 1] BPS complexes as a platform to create isostructural optical and nuclear probes.

## 3.3 Results and Discussion

### 3.3.1 Synthesis of $[M(CO)_3(BPS)(L)]^n$ Complexes (M = $^{99m}Tc$, Re)

We recently developed a method to prepare $[Tc(CO)_3(bipy)(L)]^n$ complexes (bipy = 2,2'-bipyridine), where L represents substituted imidazoles, as isostructural nuclear and optical probes.[42] Unfortunately, the Re analogues exhibited low emission intensity, and the Tc complexes showed non-specific binding *in vivo* because of the lipophilic bipy ligand. To address these issues, a method for creating complexes of the more water

soluble BPS ligand was pursued and the stability and biodistribution of the products assessed.

Prior to the preparation of the Tc complexes, it is necessary to generate the Re analogues as reference standards. This is a consequence of the fact that a typical labeling reaction uses amounts of technetium that are below the detection limit of most common characterization techniques (NMR, UV-HPLC etc.). For the present study, two new BPS based Re complexes were prepared; a model compound derived from methylimidazole (MeIm) and a second that contained imidazole derivatized with alendronate. Alendronate is a bisphosphonate that is known to target sites of calcium metabolism in bone. Radiolabeled bisphosphonates have been used extensively to image bone diseases and injuries as they are highly selective towards regions of calcium accretion. Bisphosphonates are therefore attractive targeting agents to assess new radiometal complexes *in vivo*.[43,44]

The complex containing MeIm was prepared by combining the monodentate ligand with $[Re(CO)_3(BPS)(Cl)]^{2-}$ **2a**, which can be prepared following a literature procedure,[40] and heating the solution to reflux in MeOH overnight (Scheme 3.1). The desired product $[Re(CO)_3(BPS)(MeIm)]^{-}$ **3a** was purified by column chromatography and isolated in 51% yield. To prepare the complex containing an imidazole alendronate derivative (ImAln), the ligand was added to **2a** in water at pH 7 and the reaction stirred overnight at 80 °C. $[Re(CO_3)(BPS)(ImAln)]^{2-}$ **4a** was isolated in 39% yield by semi-preparative HPLC. The $^{1}H$ NMR of **4a** showed the expected pattern of peaks, while the $^{31}P\{^{1}H\}$ NMR exhibited a single peak at 18.3 ppm (Supporting Information, Figures S

7.31-S 7.33). The HRMS for both complexes were consistent with the expected m/z values.

Photophysical properties were determined to verify the Re-labeled imidazole based compounds retained suitable properties for luminescence imaging. Fluorescent measurements were conducted at room temperature in water where both **3a** and **4a** showed an absorption band at 290 nm, which was attributed to intra-ligand $\pi \rightarrow \pi^*$ transitions, and two lower energy bands at 330 and 365 nm, which were assigned as $^1$MLCT. There was a broad emission band around 615 nm upon excitation at 365 nm (Supporting Information, Figures S 7.37, S 7.38), which are both red shifted compared to prior generations of isostructural Re(I) probes including analogous [2 + 1] complexes containing bipy in place of BPS.

To demonstrate that the imidazole derivatives can be visualized *in vitro*, **4a** was incubated with MCF-7 cells and fluorescence microscopy performed. Following incubation at room temperature for 1.5 h, binding and localization of 100 μM **4a** was evident and significantly different than the vehicle only control (Figure 3.1). Images, which were collected by exciting at 365 nm and by using a 550 nm long-pass emission filter, showed overall distribution in the cytoplasm.

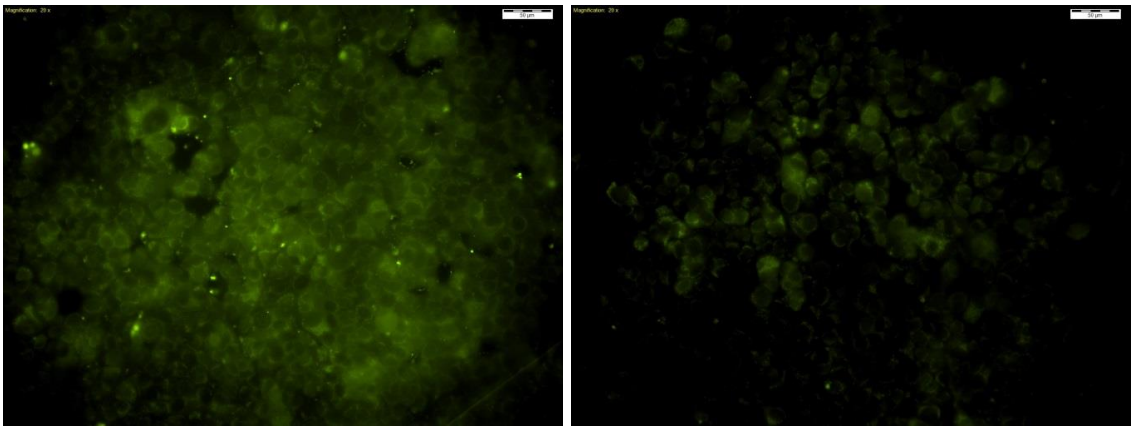

**Figure 3.1** Fluorescence microscopy images of MCF-7 cells incubated with **4a** (100 µM) for 1.5 h at room temperature (left). The autofluorescence control is also shown (right).

To prepare the technetium analogues, BPS was added to $[^{99m}Tc(CO)_3(H_2O)_3]^+$, which was generated from $TcO_4^-$ following a literature procedure,[45,46] and the mixture heated to 40 °C for 15 min. The product, $[^{99m}Tc(CO)_3(BPS)(H_2O)]^-$ **2b** was immediately treated with N-methylimidazole (MeIm) and the mixture heated to 40 °C for 15 min which produced $[^{99m}Tc(CO)_3(BPS)(MeIm)]^-$ **3b** in >99% radiochemical yield (Scheme 3.1). The formation of the product was verified by comparing the retention time of **3b** in the gamma HPLC chromatogram to the retention time of the Re-labeled analogue **3a** (Supporting Information, Figure S 7.5) in the corresponding UV trace. $[^{99m}Tc(CO)_3(BPS)(ImAln)]^{2-}$ **4b** was prepared under the same conditions where the radiochemical yield was also nearly quantitative, and HPLC retention time matched that of the Re-labeled analogue **4a** (Supporting Information, Figure S 7.36).

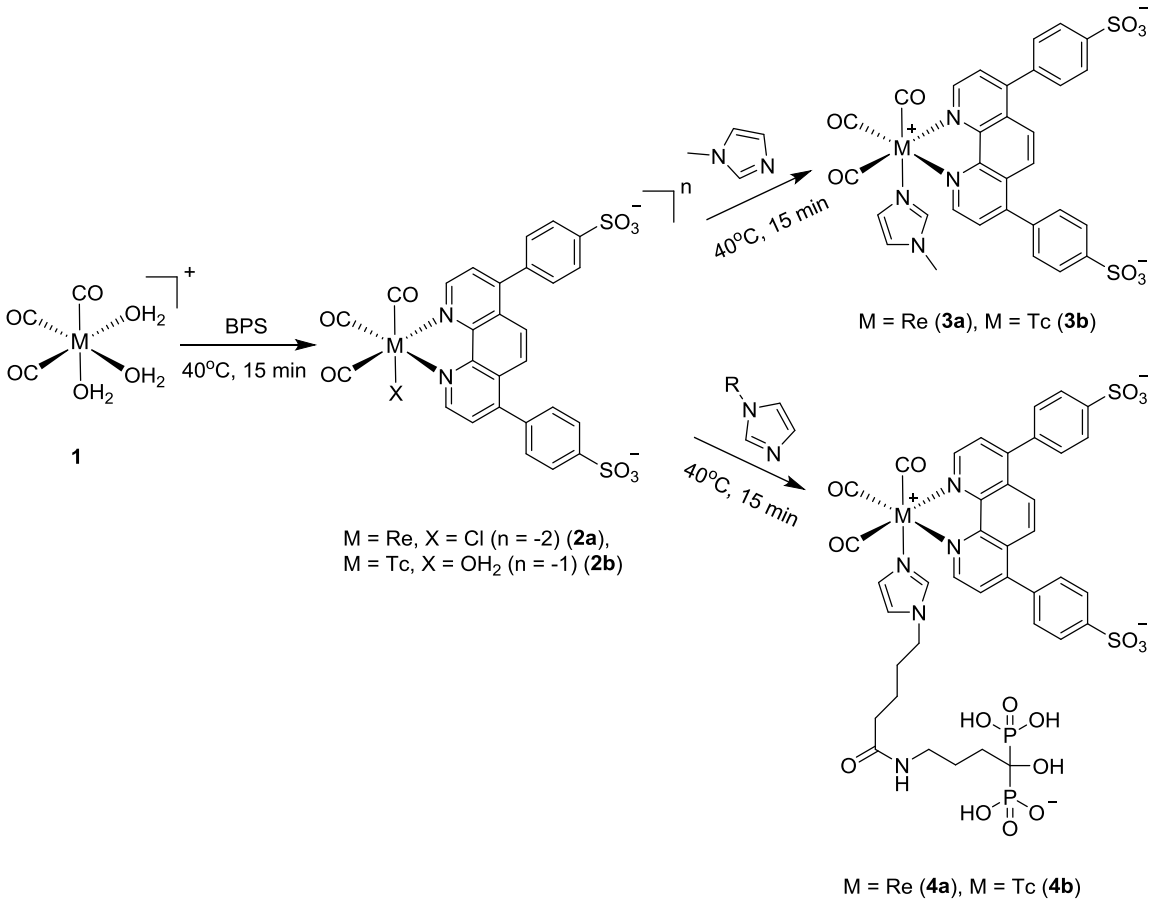


**Scheme 3.1** Synthesis of Re(I)/Tc(I) complexes **3a/b** and **4a/b**. The conditions shown are for the reactions performed at the tracer level.

### 3.3.2 Stability Studies

One concern with [2 + 1] type probes is the loss of the monodentate ligand *in vivo*.[47,48] We initially tested the stability of the Re-labeled compounds in water. The $d^6$, low spin complex **3a** (50 μM) at room temperature showed no evidence of loss of the monodentate ligand up to 24 h. To see if the radiolabeled analogue **3b** was similarly

robust, the stability of $^{99m}$Tc complexes were evaluated in saline and in an amino acid challenge study following an established literature procedure.[49] Briefly, a solution of **3b** was incubated separately in isotonic saline, 2 mM histidine, and 2 mM cysteine in PBS (pH = 7.4) at 37 °C. Samples were taken at different time points up to 6 h and analyzed by HPLC to determine the degree of decomposition (Supporting Information, Figures S 7.6-S 7.15). The complexes did not show any evidence of decomposition up to 6 h (Figure 3.2) even in the presence of amino acids. This timeline matches the half-life and optimal imaging window for imaging agents derived from $^{99m}$Tc. To ensure the analytical method was appropriate for this stability test, the amount of cysteine and histidine was increased 100 fold. Decomposition was evident by HPLC after two hours for both amino acid solutions (Supporting Information, Figures S 7.16-S 7.25).

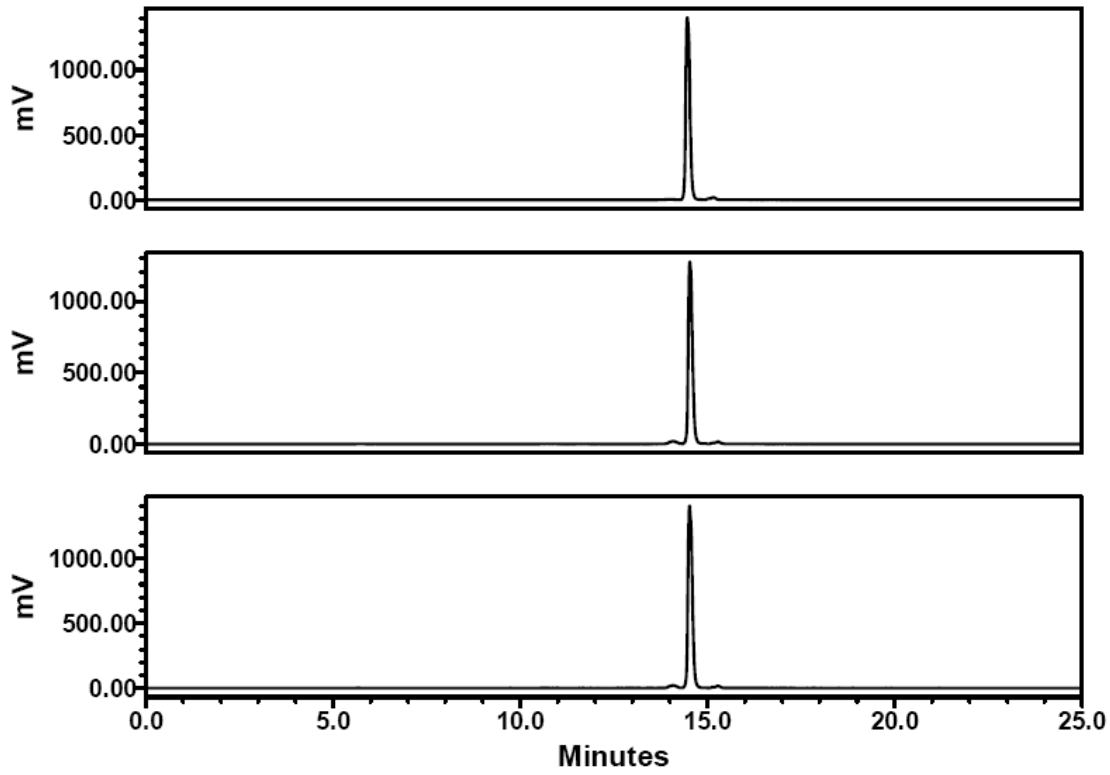


**Figure 3.2** γ-HPLC chromatogram of **3b** after incubation in saline (top), 2 mM cysteine (middle), and 2 mM histidine (bottom) for 6 h at 37 ºC.

### 3.3.3 Biodistribution and *in vivo* imaging studies

Radiolabeled bisphosphonates such as $^{99m}$Tc-methylenediphosphonic acid (MDP) are used clinically to image regions of calcium turnover or damage to bone.[50] As mentioned, bisphosphonates are a convenient way to evaluate the suitability of BPS complexes *in vivo.* With a bisphosphonate linked to the metal through the imidazole group, any loss of the monodentate ligand would eliminate the ability of the targeted [2 + 1] complex to bind to bone. The biodistribution study of **4b** was performed using healthy

female Balb/c mice, where regions of active bone metabolism (shoulder and knee) were collected along with other tissues, and radioactivity counted to determine the percent injected dose per gram of tissue (%ID/g). The results showed significant accumulation in the shoulder (7.9 ± 0.2% ID/g) and knees (15.1 ± 0.9 % ID/g) by 6 h (Figure 3.3). Compound **4b** exhibited prompt clearance from the blood and lower levels in soft tissues and major organs, including gut and gall bladder, when compared to the bipyridine analogue studied previously.[42] In a separate series of studies, mice were injected with **4b** and SPECT images were taken at 6 h and 24 h post injection. The resulting images confirmed that uptake was confined mainly to the joints, which is consistent with the higher bone remodeling activity at these sites. The imaging data also indicated that the compound cleared from non-target organs via the hepatobiliary system (Figure 3.4).

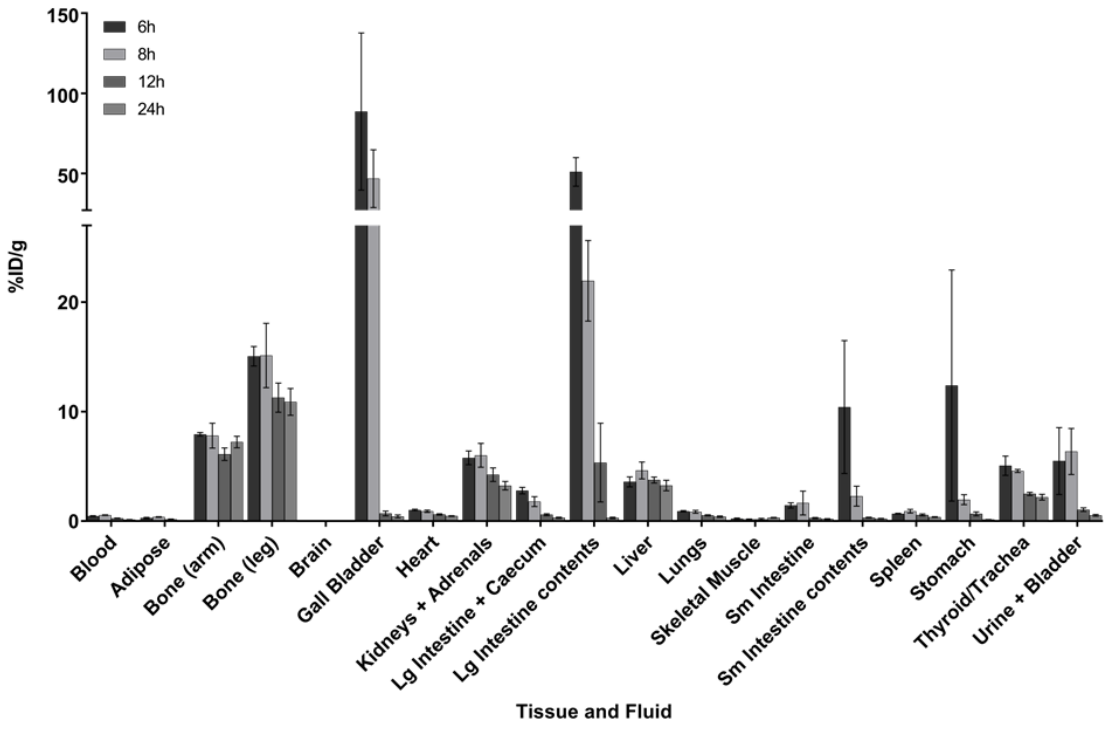


**Figure 3.3** Biodistrubution profile of **4b** in female Balb/c mice (%ID/g) at different time points in the tissues and fluids as shown. Data are mean %ID/g ± SEM.

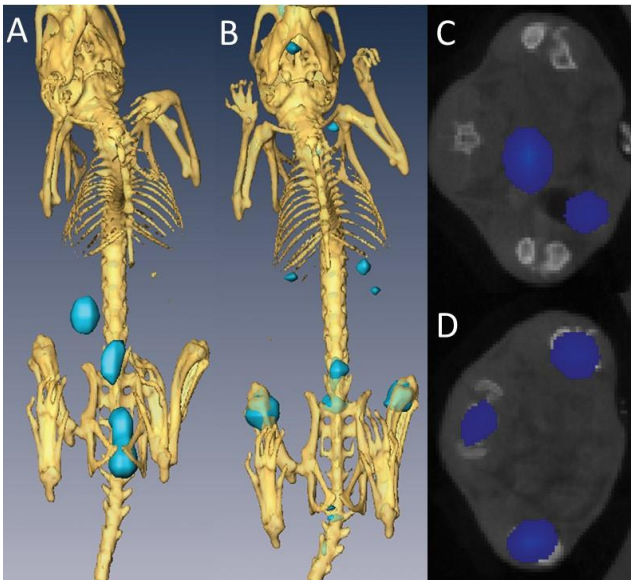


**Figure 3.4** SPECT-CT images of female Balb/c mice of **4b** at 6 h post injection (A) and at 24 h post injection (B), and corresponding transverse images through the knees, spine, and bladder at 6 h post injection (C) and at 24 h post injection (D). All images were set to the same maximum threshold.

If **4b** were to decompose *in vivo* after administration it would form **2b** by dissociative loss of the monodentate ligand. The resulting complex would then react with other donor groups including thiols found on proteins like albumin. If the decomposition occurs in the blood, any resulting protein conjugate of **2b** would be expected to localize to the liver. To test this, SPECT images of mice injected with **2b**, the complex lacking the bisphosphonate, were collected using the same protocol that was employed with **4b**. The resulting images showed almost exclusive uptake of **2b** in the liver and cecum with no evidence of binding to bone (Figure 3.5).

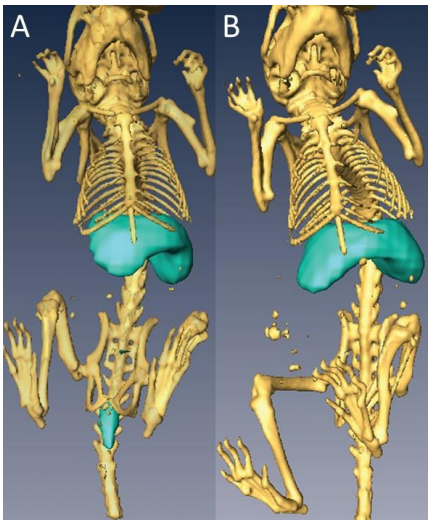


**Figure 3.5** SPECT-CT images of female Balb/c mice of **2b** at 6 h post injection (A) and at 24 h post injection (B). Images were set to the same maximum threshold.

Having established binding of **4b** to regions of active bone metabolism, the next step was to determine how long **4b** remained bound to those targets. Data from the biodistribution study using tissues taken at later time points (12 h and 24 h) indicated little change in **4b** uptake in the shoulder and only a slight decrease (3% decrease at 24 h) in the knee (Figure 3.3). The liver uptake remained constant and below 5%, from 6 h to 24 h. Over the 6 to 24 h time points there was also significant decrease in the amount of activity in the intestinal track. For instance, the ratios of the %ID/g for the skeleton (leg) and large intestine was 0.29 at 6 h, 2.1 at 12 h, and 36.3 at 24 h. Had compound **4b** decomposed substantially to form **2b** on the surface of the bone, one possibility would be increase in liver and gut uptake over time, which was not evident. Based on the

biodistribution data, it is likely that **4b** was internalized into osteoclasts by endocytosis which has been shown to occur for other labeled bisphosphonates.[51–53] This represents a potential advantage of the [2 + 1] type complexes over highly stable tridentate Tc(I) complexes where upon internalization of the former the monodentate ligand is likely replaced by intracellular proteins trapping the resulting radiometal conjugate within the cells. Over time, as clearance of non-internalized material progresses, the target to non-target ratios increase resulting in enhanced image contrast. Validation and exploitation of this mechanism is currently under investigation.

## 3.4 Conclusion

The preparation and evaluation of Tc(I)-BPS complexes and their Re analogues as a new type of isostructural luminescent and nuclear probes is reported. The Tc complexes were produced in high yield, and compounds **3b** and **4b** were shown to be stable *in vitro* and *in vivo* respectively, to the extent that they can be used to prepare targeted imaging probes. Given the ease with which imidazole derivatives of targeting molecules can be prepared, the reported chemistry is highly versatile and can be exploited to create a wide range of new multimodal probes. Studies on the utility of the bisphosphonate derivative reported here for imaging bone metastases and multimodal imaging of microcalcifications associated with breast cancer is ongoing.

## 3.5 Experimental Section

### 3.5.1 Materials and Instrumentation

All solvents were purchased from Caledon (Georgetown, ON). Chemicals were purchased from Sigma-Aldrich (Burlington, ON) and used without further purification, unless otherwise stated. Compounds [1-hydroxy-4-(5-imidazol-1-yl-pentanoylamino)-1-phosphono-butyl]-phosphonic acid (ImAln), and $[Re(CO_3)(BPS)(Cl)]^{2-}$ **2a** were prepared according to literature methods.[40,42] Histidine and cysteine challenge studies were performed according to literature procedures.[49] Deuterated solvents for NMR samples were purchased from Cambridge Isotope Laboratories. Technetium-99m $[^{99m}TcO_4]^-$ was obtained from a $^{99}Mo/^{99m}Tc$ generator (Lantheus Medical Imaging) in saline (0.9% NaCl). ***Caution: $^{99m}$Tc is a γ-emitter ($E_\gamma$ = 140 keV, $t_{1/2}$ = 6 h) and should only be used in a licensed and appropriately shielded facility.***

Nuclear magnetic resonance (NMR) spectra ($^1H$, $^{13}C$) were recorded on a Bruker AV600 MHz spectrometer at ambient temperature. Microwave-assisted reactions were performed on a Biotage Initiator 60 microwave reactor using crimp-sealed vials. Mass spectrometry analyses were provided by the McMaster Regional Centre for Mass Spectrometry on an Agilent 6340 Ion Trap LC/MS mass spectrometer, operating in electrospray ionization (ES) mode. High resolution mass spectra (HRMS) were collected on a Waters/Micromass Q-Tof Global Ultima spectrometer. IR spectra were obtained on a Biorad FTS-40 FTIR spectrometer. The fluorescence spectra were collected with the Tecan Infinite M1000 plate reader, with the concentration of the test solutions set at 50 μM. High performance liquid chromatography (HPLC) was performed on a Waters 1525 Binary (Midford, MA) monitored simultaneously with 2998 Photodiode Array Detector

at 220/254 nm and in-line radioactivity Bioscan gamma detector, with a NaI(Tl) scintillator using the Empower software package. Phenomenex Gemini C-18 analytical column (250 × 4.60 mm, 5 µm) operating at a flow rate of 1.0 mL/min, and Phenomenex Gemini C-18 semipreparative column (250 × 10 mm, 5 µm) operating at a flow rate of 4.0 mL/min were used for all analyses. HPLC methods employed the following solvent gradients: *Method A* (solvent A = $H_2O$ + 0.1% TFA, solvent B = $CH_3CN$ + 0.1% TFA): 0-2 min 2% B, 2-20 min 100% B; 20-22 min 100% B, 22-23 min 2% B, 23-25 min 2% B. *Method B* (solvent A = $H_2O$ + 0.005% TEA, solvent B = $CH_3CN$ + 0.005% TEA): 0-2 min 2% B, 2-20 min 100% B; 20-22 min 100% B, 22-23 min 2% B, 23-25 min 2% B.

### 3.5.2 Synthetic Procedures

*Synthesis of* $[Re(CO_3)(BPS)(MeIm)]^-$ **3a**

Compound **2a** $[Re(CO)_3(BPS)(Cl)]^{2-}$ (80 mg, 0.1 mmol) and silver triflate (26 mg, 0.1 mmol) were dissolved in MeOH (12 mL) and heated to reflux for 2 h. The solution was filtered through Celite, and *N*-methylimidazole (16 mg, 0.2 mmol) was added to the filtrate. The mixture was heated to reflux overnight, then evaporated to dryness under reduced pressure. The desired product was isolated by silica-gel column chromatography using MeOH:DCM (1:3 v/v) as an orange solid (43mg, 51%). mp 230-234 °C. IR ($\nu_{CO}$/$cm^{-1}$): 2025, 1905. $^1$H NMR (600 MHz, $CD_3OD$): δ (ppm) = 9.69 (d, *J* = 5.4 Hz, 2H); 8.16 – 8.04 (m, 8H); 7.79 – 7.69 (m, 5H); 6.95 (s, 1H); 6.73 (s, 1H); 3.55 (s, 3 H). $^{13}$C NMR (150 MHz, $CD_3OD$): δ (ppm) = 197.07, 193.17, 155.20, 152.81, 148.57,

148.06, 147.63, 141.95, 138.42, 136.87, 132.69, 131.09, 130.50, 130.33, 130.16, 128.48, 128.34, 127.81, 127.17, 123.99, 34.63. HRMS: *m/z* calcd for $C_{31}H_{22}N_4O_9S_2Re$ ($[M]^+$): 845.0384, found: 845.0406. HPLC (UV 254 nm, method A): $R_t$ = 12.8 min.

*Synthesis of [Re(CO$_3$)(BPS)(ImAln)][HNEt$_3$]$_2$* **4a**

$[Re(CO)_3(BPS)(Cl)]^{2-}$ **2a** (80 mg, 0.1 mmol) and silver triflate (26 mg, 0.1 mmol) were dissolved in MeOH (12 mL) and heated to reflux for 2 h. The solution was filtered through Celite, and evaporated to dryness under reduced pressure. The yellow residue was then suspended in water (15 mL) and stirred at room temperature for 3 h. The insoluble residue was collected by filtration and the solution was concentrated under reduced pressure, and the pH was adjusted to 7 with 0.1 M NaOH. [1-Hydroxy-4-(5-imidazol-1-yl-pentanoylamino)-1-phosphono-butyl]-phosphonic acid (ImAln) (43 mg, 0.11 mmol) was then suspended in water (5 mL), the pH adjusted to 7 with 0.1 M NaOH and added dropwise to the solution containing the Re complex with constant stirring. The mixture was heated to 80 °C overnight and then concentrated to dryness under reduced pressure. The desired product was isolated (53 mg, 39%) as a yellow solid by semi-preparative HPLC (method B). m.p. 163-165 °C. IR ($\nu_{CO}$/cm$^{-1}$): 2027, 1915. $^1$H NMR (600 MHz, $D_2O$): δ (ppm) = 9.43 (d, *J* = 5.4 Hz, 2H); 7.98 – 7.80 (m, 5H); 7.69 – 7.47 (m, 8H); 6.71 (s, 1H); 6.30 (s, 1H); 3.65 (t, *J* = 7.1 Hz, 2H); 3.11 (q, *J* = 7.4 Hz, 12H); 2.98 (t, *J* = 6.6 Hz, 2H); 1.88 (m, 2 H), 1.81 (m, 2 H), 1.66 (m, 2 H), 1.40 (m, 2 H), 1.19 (t, *J* = 7.3 Hz, 18H); 1.00 (m, 2 H). $^{13}$C NMR (150 MHz, $D_2O$): δ (ppm) = 196.12, 175.54, 153.68, 150.38, 146.95, 143.58, 139.90, 137.74, 135.60, 132.53, 130.36, 130.07,

129.94, 128.46, 128.22, 126.79, 126.55, 126.19, 125.35, 120.94, 73.95, 47.09, 46.70, 39.92, 34.67, 31.05, 28.94, 23.39, 21.65, 8.22. $^{31}P\{^{1}H\}$ NMR (242 MHz, $D_2O$): δ (ppm) = 18.30. HRMS: *m/z* calcd for $C_{39}H_{37}N_5O_{17}P_2S_2Re$ ($[M-2H]^{2-}$): 1160.0658, found: 1160.0662. HPLC (UV 254 nm, method B): $R_t$ = 8.1 min.

### 3.5.3 General Procedure for Preparation of $^{99m}$Tc-labelled Compounds 3b and 4b

Sodium boranocarbonate (10 mg, 0.10 mmol), sodium carbonate (15 mg, 0.14 mmol), sodium borate (20 mg, 0.05 mmol) and sodium potassium tartrate (22 mg, 0.08 mmol) were placed in a microwave vial and purged with argon for 10 min. To this mixture, $Na[^{99m}TcO_4]$ (1 mL, 370-740 MBq) was added and the vial was heated in a microwave reactor at 110 °C for 3.5 min to form $[^{99m}Tc(CO)_3(H_2O)_3]^+$. The solution was cooled to room temperature and adjusted to pH 5.5-6.5 with aqueous hydrochloric acid (HCl) (1.0 M). Bathophenanthroline disulfonic acid (BPS) (1 mg, 2 µmol) was added as a solid and the reaction mixture was heated to 40 °C for 15 min to form $[^{99m}Tc(CO)_3(BPS)(H_2O)]^-$. This solution was adjusted to pH 7.5-8.5 and then added to the monodentate ligand (1 mg) whose pH was adjusted to 7.5-8.5 with 1 M NaOH and the mixture stirred at 40 °C for 15 min. The formation of products was confirmed by analytical HPLC (method A). Quantitative conversion of $[^{99m}Tc(CO)_3(H_2O)_3]^+$ to the final product was achieved in all cases.

### 3.5.4 Purification of $^{99m}$Tc Complexes

Purification of **3b** was achieved by solid phase extraction. The reaction mixture was diluted with water (2 mL) and the solution loaded on a Waters C18 Sep-Pak Plus cartridge, which had been previously activated with EtOH (6 mL) and $H_2O$ (6 mL). After loading the reaction mixture, the cartridge was washed with 15% $CH_3CN$ in $H_2O$ (12 mL), followed by 25% $CH_3CN$ in 0.4% (w/v) aqueous ammonium formate (6 mL). The desired product were eluted with a 1:1 v/v mixture of 0.4% aqueous ammonium formate and $CH_3CN$. Product **4b** was isolated in quantitative yield by HPLC (method B).

### 3.5.5 Fluorescence Microscopy

MCF-7 breast cancer cells (ATCC; Manassas, VA) were grown in DMEM medium, supplemented with 10% fetal bovine serum, 100 U/mL penicillin and 100 µg/mL streptomycin, and maintained at 37 °C and 5% $CO_2$. Cells were grown on coverslips in 24 well plates at a density of $2.7 \times 10^5$ cells per well. Approximately 48 hours after plating, media was removed and wells were rinsed twice with warm PBS. Cells were incubated in varying concentrations of compound **4a** in a volume of 300 µL of vehicle, for 1.5 h, at room temperature. Following incubation, media was aspirated and cells were washed twice with warm PBS. Cells were maintained in PBS and mounted onto slides immediately prior to imaging. Images were collected using an Olympus BX53F Upright Brightfield and Fluorescence Microscope, equipped with a filter set

consisting of a 360 nm excitation filter, a 400 mm dichroic long-pass filter, and a 550 nm long-pass emission filter.

### 3.5.6 Biodistribution Studies

All animal studies were approved by the Animal Research Ethics Board at McMaster University in accordance with Canadian Council on Animal Care (CCAC) guidelines. Biodistribution studies were performed on healthy female Balb/c mice, 5-6 weeks old purchased from Charles River Laboratories (Kingston, NY), ($n$ = 3 per time point at t = 6, 8, 12, 24 h). Mice were injected with approximately 0.74 MBq of $[^{99m}Tc(CO)_3(BPS)(ImAln)]^{2-}$ **4b** (100µL in saline) via the tail vein. At various time points, animals were anesthetized with 3% isoflurane and following blood collection, euthanized by cervical dislocation. Blood, adipose, adrenals, bone (femur), brain, gall bladder, heart, kidneys, large intestine and caecum (with contents), liver, lungs, pancreas, skeletal muscle, small intestine (with contents), spleen, stomach (with contents), thyroid/trachea, urinary bladder + urine and tail were collected, weighed, and counted in a Perkin Elmer Wizard 1470 Automatic Gamma Counter. Decay correction was used to normalize organ activity measurements to time of dose preparation for data calculations with respect to injected dose (i.e., %ID/g).

### 3.5.7 SPECT-CT Imaging

Imaging was completed using female Balb/c mice (Senneville, QC, Canada). The mice were administered 200 µl of saline containing either $[^{99m}Tc(CO)_3(BPS)(H_2O)]^-$ **2b**, or $[^{99m}Tc(CO)_3(BPS)(ImAln)]^{2-}$ **4b**, (~35 MBq) via tail vein injection. Prior to imaging, mice were anaesthetized with 1% isoflurane and maintained under same conditions for the length of the SPECT and CT scans. Imaging was conducted on the mice at 1, 6 and 24 h post injection for both compounds and also at 4 h post injection for **4b**. At each time point, CT images were acquired using a conebeam X-SPECT scanner (Gamma Medica, Northridge, CA) with a source voltage of 75 kVp and a current of 165 µA. Projection data was acquired with 1024 projection angles (1184×1120 pixels, 0.100 mm pixels) and reconstructed using a Feldkamp cone beam back projection algorithm in COBRA (Exxim Software, Pleasanton, CA) into 512×512×512 arrays (0.155 mm isotropic voxels). SPECT images were acquired using dual sodium iodide crystals in combination with low-energy, high-resolution, parallel-hole collimators. A total of 64 projections over 360° were acquired with an energy window of 159 ± 10% keV and then reconstructed using an OSEM iterative reconstruction method (2 iterations/8 subsets) into 82×82×82 arrays (1.463 mm isotropic voxels) using in-house software. CT images were compressed to a $256^3$ matrix (0.31 mm isotropic voxels). Fusion was achieved by a rigid-body (linear) transformation of the SPECT image, during which, it is interpolated and resampled to the same matrix dimensions and voxel size as the compressed CT image. Imaging analysis was completed using Amira.

*Note: All supporting information for this chapter can be found in Appendix 2.*

## 3.6 References

(1) Thorp-Greenwood, F. L.; Balasingham, R. G.; Coogan, M. P. *J. Organomet. Chem.* **2012**, *714*, 12–21.

(2) Baker, M. *Nature* **2010**, *463*, 977–980.

(3) Jennings, L. E.; Long, N. J. *Chem. Commun.* **2009**, 3511–3524.

(4) Thorp-Greenwood, F. L.; Coogan, M. P. *Dalton Trans.* **2011**, *40*, 6129–6143.

(5) François, A.; Auzanneau, C.; Le Morvan, V.; Galaup, C.; Godfrey, H. S.; Marty, L.; Boulay, A.; Artigau, M.; Mestre-Voegtlé, B.; Leygue, N.; Picard, C.; Coulais, Y.; Robert, J.; Benoist, E. *Dalton Trans.* **2014**, *43*, 439–450.

(6) Backer, M. V; Levashova, Z.; Patel, V.; Jehning, B. T.; Claffey, K.; Blankenberg, F. G.; Backer, J. M. *Nat. Med.* **2007**, *13*, 504–509.

(7) Tzanopoulou, S.; Sagnou, M.; Paravatou-Petsotas, M.; Gourni, E.; Loudos, G.; Xanthopoulos, S.; Lafkas, D.; Kiaris, H.; Varvarigou, A.; Pirmettis, I. C.; Papadopoulos, M.; Pelecanou, M. *J. Med. Chem.* **2010**, *53*, 4633–4641.

(8) Wallace, A. M.; Hoh, C. K.; Darrah, D. D.; Schulteis, G.; Vera, D. R. *Nucl. Med. Biol.* **2007**, *34*, 849–853.

(9) Hosseini, A.; Baker, J. L.; Tokin, C. A.; Qin, Z.; Hall, D. J.; Stupak, D. G.; Hayashi, T.; Wallace, A. M.; Vera, D. R. *J. Surg. Res.* **2014**, *190*, 528–534.

(10) Xiong, C.; Lu, W.; Zhang, R.; Tian, M.; Tong, W.; Gelovani, J.; Li, C. *Chem. Eur. J.* **2009**, *15*, 8979–8984.

(11) Xu, H.; Eck, P. K.; Baidoo, K. E.; Choyke, P. L.; Brechbiel, M. W. *Bioorg. Med. Chem.* **2009**, *17*, 5176–5181.

(12) Azhdarinia, A.; Wilganowski, N.; Robinson, H.; Ghosh, P.; Kwon, S.; Lazard, Z. W.; Davis, A. R.; Olmsted-Davis, E.; Sevick-Muraca, E. M. *Bioorg. Med. Chem.* **2011**, *19*, 3769–3776.

(13) Kuil, J.; Velders, A. H.; Van Leeuwen, F. W. B. *Bioconjugate Chem.* **2010**, *21*, 1709–1719.

(14) Wang, W.; Ke, S.; Kwon, S.; Yallampalli, S.; Cameron, A. G.; Adams, K. E.; Mawad, M. E.; Sevick-Muraca, E. M. *Bioconjugate Chem.* **2007**, *18*, 397–402.

(15) Edwards, W. B.; Xu, B.; Akers, W.; Cheney, P. P.; Liang, K.; Rogers, B. E.; Anderson, C. J.; Achilefu, S. *Bioconjugate Chem.* **2008**, *19*, 192–200.

(16) Ghosh, S. C.; Ghosh, P.; Wilganowski, N.; Robinson, H.; Hall, M. a.; Dickinson, G.; Pinkston, K. L.; Harvey, B. R.; Sevick-Muraca, E. M.; Azhdarinia, A. *J. Med. Chem.* **2013**, *56*, 406–416.

(17) Hong, H.; Zhang, Y.; Severin, G. W.; Yang, Y.; Engle, J. W.; Niu, G.; Nickles, R. J.; Chen, X.; Leigh, B. R.; Barnhart, T. E.; Cai, W. *Mol. Pharm.* **2012**, *9*, 2339–2349.

(18) Priem, T.; Bouteiller, C.; Camporese, D.; Brune, X.; Hardouin, J.; Romieu, A.; Renard, P.-Y. *Org. Biomol. Chem.* **2013**, *11*, 469–479.

(19) Li, Z.; Lin, T.-P.; Liu, S.; Huang, C.-W.; Hudnall, T. W.; Gabbaï, F. P.; Conti, P.

S. *Chem. Commun.* **2011**, *47*, 9324–9326.

(20) Heinrich, T. K.; Gottumukkala, V.; Snay, E.; Dunning, P.; Fahey, F. H.; Ted Treves, S.; Packard, A. B. *Appl. Radiat. Isot.* **2010**, *68*, 96–100.

(21) Yan, R.; El-Emir, E.; Rajkumar, V.; Robson, M.; Jathoul, A. P.; Pedley, R. B.; Årstad, E. *Angew. Chem.* **2011**, *123*, 6925–6927.

(22) Liu, S.; Lin, T.-P.; Li, D.; Leamer, L.; Shan, H.; Li, Z.; Gabbaï, F. P.; Conti, P. S. *Theranostics* **2013**, *3*, 181–189.

(23) Hendricks, J. A.; Keliher, E. J.; Wan, D.; Hilderbrand, S. A.; Weissleder, R.; Mazitschek, R. *Angew. Chem. Int. Ed.* **2012**, *51*, 4603–4606.

(24) Nunes, P.; Morais, G. R.; Palma, E.; Silva, F.; Oliveira, M. C.; Ferreira, V. F. C.; Mendes, F.; Gano, L.; Miranda, H. V.; Outeiro, T. F.; Santos, I.; Paulo, A. *Org. Biomol. Chem.* **2015**, *13*, 5182–5194.

(25) Schaffer, P.; Gleave, J. A.; Lemon, J. A.; Reid, L. C.; Pacey, L. K. K.; Farncombe, T. H.; Boreham, D. R.; Zubieta, J.; Babich, J. W.; Doering, L. C.; Valliant, J. F. *Nucl. Med. Biol.* **2008**, *35*, 159–169.

(26) Azad, B. B.; Cho, C.-F.; Lewis, J. D.; Luyt, L. G. *Appl. Radiat. Isot.* **2012**, *70*, 505–511.

(27) Connell, T. U.; Hayne, D. J.; Ackermann, U.; Tochon-Danguy, H. J.; White, J. M.; Donnelly, P. S. *J. Label. Compd. Radiopharm.* **2014**, *57*, 262–269.

(28) Botchway, S.; Dilworth, J. R.; Salichou, M. *Dalton Trans.* **2010**, *39*, 5219–5220.

(29) Zelenka, K.; Borsig, L.; Alberto, R. *Bioconjugate Chem.* **2011**, *22*, 958–967.

(30) Stephenson, K. A.; Banerjee, S. R.; Besanger, T.; Sogbein, O. O.; Levadala, M. K.; McFarlane, N.; Lemon, J. A.; Boreham, D. R.; Maresca, K. P.; Brennan, J. D.; Babich, J. W.; Zubieta, J.; Valliant, J. F. *J. Am. Chem. Soc.* **2004**, *126*, 8598–8599.

(31) Coogan, M. P.; Doyle, R. P.; Valliant, J. F.; Babich, J. W.; Zubieta, J. *J. Label Compd. Radiopharm* **2014**, *57*, 255–261.

(32) Lo, K. K.-W.; Choi, A. W.-T.; Law, W. H.-T. *Dalton Trans.* **2012**, *41*, 6021–6047.

(33) Lo, K. K.-W.; Louie, M.-W.; Zhang, K. Y. *Coord. Chem. Rev.* **2010**, *254*, 2603–2622.

(34) Zhao, Q.; Huang, C.; Li, F. *Chem. Soc. Rev.* **2011**, *40*, 2508–2524.

(35) Thorp-Greenwood, F. L.; Platts, J. A.; Coogan, M. P. *Polyhedron* **2014**, *67*, 505–512.

(36) Balasingham, R. G.; Coogan, M. P.; Thorp-Greenwood, F. L. *Dalton Trans.* **2011**, *40*, 11663–11674.

(37) Fernández-Moreira, V.; Thorp-Greenwood, F. L.; Coogan, M. P. *Chem. Commun.* **2010**, *46*, 186–202.

(38) Coogan, M. P.; Fernández-Moreira, V. *Chem. Commun.* **2014**, *50*, 384–399.

(39) Thorp-Greenwood, F. L. *Organometallics* **2012**, *31*, 5686–5692.

(40) Amoroso, A. J.; Coogan, M. P.; Dunne, J. E.; Fernández-Moreira, V.; Hess, J. B.;

Hayes, A. J.; Lloyd, D.; Millet, C.; Pope, S. J. A.; Williams, C. *Chem. Commun.* **2007**, 3066–3068.

(41) Fernández-Moreira, V.; Thorp-Greenwood, F. L.; Amoroso, A. J.; Cable, J.; Court, J. B.; Gray, V.; Hayes, A. J.; Jenkins, R. L.; Kariuki, B. M.; Lloyd, D.; Millet, C. O.; Williams, C. F.; Coogan, M. P. *Org. Biomol. Chem.* **2010**, *8*, 3888–3901.

(42) Yazdani, A.; Janzen, N.; Banevicius, L.; Czorny, S.; Valliant, J. F. *Inorg. Chem.* **2015**, *54*, 1728–1736.

(43) Zhang, S.; Gangal, G.; Uludağ, H. *Chem. Soc. Rev.* **2007**, *36*, 507–531.

(44) Drake, M. T.; Clarke, B. L.; Khosla, S. *Mayo Clin. Proc.* **2008**, *83*, 1032–1045.

(45) Alberto, R.; Schibli, R.; Egli, A.; Schubiger, A. P. *J. Am. Chem. Soc.* **1998**, *120*, 7987–7988.

(46) Alberto, R.; Ortner, K.; Wheatley, N.; Schibli, R.; Schubiger, A. P. *J. Am. Chem. Soc.* **2001**, *123*, 3135–3136.

(47) Alberto, R.; Schibli, R.; Waibel, R.; Abram, U.; Schubiger, A. P. *Coord. Chem. Rev.* **1999**, *192*, 901–919.

(48) Schibli, R.; Schubiger, P. A. *Eur. J. Nucl. Med.* **2002**, *29*, 1529–1542.

(49) Jiang, H.; Kasten, B. B.; Liu, H.; Qi, S.; Liu, Y.; Tian, M.; Barnes, C. L.; Zhang, H.; Cheng, Z.; Benny, P. D. *Bioconjugate Chem.* **2012**, *23*, 2300–2312.

(50) Ben-Haim, S.; Israel, O. *Semin. Nucl. Med.* **2009**, *39*, 408–415.

(51) Junankar, S.; Shay, G.; Jurczyluk, J.; Ali, N.; Down, J.; Pocock, N.; Parker, A.; Nguyen, A.; Sun, S.; Kashemirov, B.; McKenna, C. E.; Croucher, P. I.; Swarbrick, A.; Weilbaecher, K.; Phan, T. G.; Rogers, M. J. *Cancer Discov.* **2015**, *5*, 35–42.

(52) Wong, K. K.; Piert, M. *J. Nucl. Med.* **2013**, *54*, 590–599.

(53) Sato, M.; Grasser, W.; Endo, N.; Akins, R.; Simmons, H.; Thompson, D. D.; Golub, E.; Rodan, G. A. *J. Clin. Invest.* **1991**, *88*, 2095–2105.

# Chapter 4

## 4 Chapter 4. Preparation of Tetrazine-Derived [2 + 1] Complexes of $^{99m}$Tc and *in vivo* Targeting using Bioorthogonal Inverse Electron Demand Diels-Alder Chemistry

Abdolreza Yazdani, Nancy Janzen, Shannon Czorny, Robert Ungard, Tanya Miladinovic, Gurmit Singh, John F. Valliant

The following chapter is formatted in a manuscript that is ready for submission to the journal Inorganic Chemistry. I was responsible for the development and execution of the majority of the work described in this paper including drafting the initial manuscript and experimental. Biodistribution and *in vivo* imaging studies have been done by Nancy Janzen and Shannon Czorny. Tumour inoculation was done by Robert Ungard and Tanya Miladinovic. Professor Valliant was the PI of the lab and responsible for the overall manuscript and project.

## 4.1 Abstract

[2 + 1] complexes of $^{99m}$Tc(I) containing a tetrazine were synthesized and their utility for preparing targeted radiopharmaceuticals using bioorthogonal chemistry evaluated. The reported complexes were of the type $[^{99m}Tc(CO)_3(N^N)(L)]^n$ (N^N = bathophenanthroline disulfonate (BPS) and 2,2-bipyridine (bipy)) where the monodentate ligand (L) was a tetrazine linked to the metal through an imidazole group. The desired products could be obtained in nearly quantitative radiochemical yield by adding $[^{99m}Tc(CO)_3(N^N)(H_2O)]^n$ to the imidazole-tetrazine ligand and heating at 60 °C for 30 min. Measurement of the kinetics of the reaction with *trans*-cyclooctenol showed a second rate order constant of $8.6 \times 10^3$ $M^{-1}S^{-1}$ at 37 °C, which is suitable for pretargeting strategies that require rapid coupling to be effective *in vivo*. Stability studies showed that the metal complexes are resistant to ligand challenge and they exhibit moderate protein binding *in vitro*. Biodistribution studies of the more water-soluble BPS derivative in normal mice one hour after administration of a bisphosphonate derivative of *trans*-cyclooctene (TCO-BP) revealed high activity concentrations in the knee (9.27 ± 0.32% ID/g) and shoulder (5.28 ± 0.67% ID/g). Using the same approach, SPECT/CT imaging showed that the [2 + 1] tetrazine complex was also able to visualize damage to the skeleton associated with a bone tumor in a murine model derived from 4T1 cells. The data demonstrates the potential of this class of compounds for preparing targeted radiopharmaceuticals using bioorthogonal chemistry.

## 4.2 Introduction

Bioorthogonal coupling reactions are highly selective chemical transformations that can take place *in vitro* and *in vivo*. They are generally insensitive to the biological surrounding and do not interfere with ongoing biochemical processes.[1,2] As a result, bioorthogonal chemistry in conjunction with pre-targeting strategies have been used to develop a wide range of different targeted imaging probes. Here, one reaction component is coupled to a targeting agent which is administered and allowed to localize at the site of interest. This is followed by administration of the second reaction component that is linked to a signaling moiety such as a fluorophore or a radiolabel that selectively couples to the first reagent. This approach can result in enhanced image contrast and in the case of certain radiolabeled compounds, the delivery of higher therapeutic doses of medical isotopes compared to conventional "actively" targeted constructs.[3,4]

Of the bioorthogonal chemical reactions available, the inverse electron demand Diels-Alder (IEDDA) cycloaddition reaction between tetrazines and strained alkenes such as *trans*-cyclooctene (TCO) have proven to be particularly effective.[5–9] Their success is driven largely by rapid reaction kinetics, high selectivity, compatibility with biological media, and the ease of synthesis of TCO and tetrazine derivatives.[10–16] A wide range of radiolabeled tetrazines have been reported including those containing $^{11}$C, $^{18}$F, $^{64}$Cu, $^{89}$Zr, $^{99m}$Tc, and $^{111}$In.[17–22]

In addition to radiolabeled tetrazines, there has been a number of reports of fluorophore-tetrazine derivatives for optical imaging applications. Tetrazines have been used to prepare highly sensitive 'turn-on' optical probes for visualization of cellular processes where fluorescent emission increases upon reaction with the complementary

TCO derived component.[23–30] One benefit of this feature for optical imaging is that it can be used to reduce background fluorescence (higher signal-to-noise ratio), enabling real time fluorescence imaging without the requirement for a washing step.[31] Recently, a Re(I) polypyridine complex containing a tetrazine was shown to have significant dienophile induced emission enhancement.[32] Re(I) complexes are actively used as *in vitro* probes for cellular imaging[33] and have the added feature that the corresponding $^{99m}$Tc(I) analogues, which have the identical structure, can be used to create the complementary nuclear imaging agent. [34,35] Isostructural Re and Tc complexes containing a tetrazine, which have not been reported previously, could be used to create pairs of targeted optical and nuclear probes using pretargeting and bioorthogonal chemistry.

Herein we report the preparation and *in vitro* and *in vivo* testing of a new class of Re(I)/ Tc(I) tetrazine [2 + 1] type complexes. The tetrazine was linked to the metal through a monodentate imidazole ligand and the impact of changing the bidentate ligand on the optical properties, stability and extent of protein binding in plasma evaluated. The ability of the lead construct to localize to areas of active bone turnover and tumor invasion using pretargeting and the IEDDA reaction were also assessed *in vivo*.

## 4.3 Results and Discussion

### 4.3.1 Synthesis of $[M(CO)_3(bipy)(ImTz)]^+$ and $[M(CO)_3(BPS)(ImTz)]^-$

Recently, we reported that [2 + 1] complexes of $^{99m}$Tc of the type $[M(CO)_3(bipy)(L)]^n$ and $[M(CO)_3(BPS)(L)]^n$ (bipy = 2,2'-bipyridine, BPS =

bathophenanthroline disulfonate L = substituted-imidazoles) can be synthesized in aqueous media in nearly quantitative yield.[46] The resulting imidazole complexes are sufficiently stable *in vivo* that they can be used to prepare targeted isostructural nuclear and optical probes.[35] To prepare [2 + 1] Re complexes containing a tetrazine, which are needed as reference standards for the work with $^{99m}$Tc, a new monodentate ligand derived from imidazole was developed (Scheme 4.1). The first step involved adding a pentanoic acid linker (**4**) through alkylation of **2** and subsequent deprotection, which was achieved in 29% overall yield. Compound **4** was subsequently coupled to the commercially available amino tetrazine **5** to form **6** (ImTz) in 73% yield.

One potential concern was that tetrazines would decompose under the conditions typically used to prepare [2 + 1] Tc/Re complexes or that they could act as competing donor groups reducing yields and complicating purification.[36] The desired Re complexes, $[Re(CO)_3(bipy)(ImTz)]^+$ and $[Re(CO)_3(BPS)(ImTz)]^-$ were prepared by combining ImTz **6** with **8a** or **9a** and heating the mixtures to reflux in either acetone or methanol for 6 h. The desired products **10a** and **11a** were purified by column chromatography in 48% and 37% yield, respectively. The $^1$H NMR and $^{13}$C NMR data of all products showed the expected pattern of peaks and the HRMS for all complexes were consistent with the expected m/z values. The ν(CO) stretching bands appear at ~2025 and ~1910 cm$^{-1}$ which are within the range reported for comparable complexes containing the $[Re(CO)_3]^+$ core.[37]

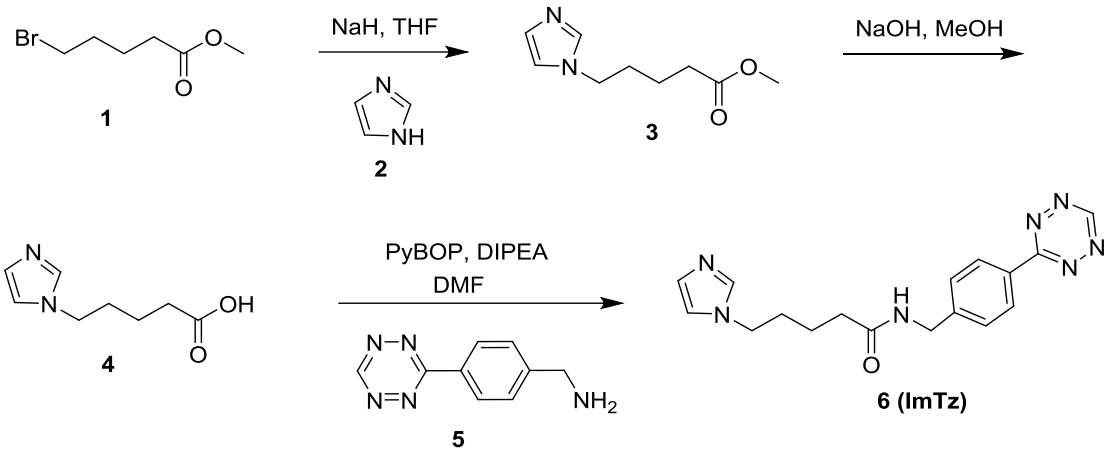


**Scheme 4.1** Synthesis of imidazole-tetrazine **6**.

### 4.3.2 Photophysical Properties

An attractive feature of using tetrazines is that they can act as a fluorescence quencher, in which fluorophore emission is restored upon reaction with its bioorthogonal counterpart.[38–40] Though the primary focus of the work was to prepare and evaluate the $^{99m}$Tc complexes, for completeness the optical properties and turn-on ratio for **10a** and **11a** were determined. Compounds **10a** and **11a** showed dominant absorption bands at 290 nm attributed to intraligand transitions and lower energy $^{1}$MLCT absorption bands at 330 and 365 nm respectively. In the presence of excess *trans*-cyclooctenol (TCO-OH), **10a** and **11a** had a 2.5 and 9-fold increase in the emission intensity ($\lambda_{max}$ = 597 nm for **10a**, and $\lambda_{max}$ = 625 nm for **11a**) respectively. These turn-on ratios are significant but modest compared to other tetrazine-fluorophore derivatives. This is due to the distance of

the tetrazine from the Re-complex and its ability to freely rotate relative to the bidentate metal complex.[31]

### 4.3.3 Radiochemistry and the Synthesis of $[^{99m}Tc(CO)_3(bipy)(ImTz)]^+$ and $[^{99m}Tc(CO)_3(BPS)(ImTz)]^-$

To prepare the $^{99m}Tc$ analogues, $[^{99m}Tc(CO)_3(H_2O)_3]^+$ was combined with 2,2'-bipyridine (bipy) and the mixture heated to 110 °C for 6 min to give $[^{99m}Tc(CO)_3(bipy)(H_2O)]^+$ **8b** (Scheme 2). The more water soluble ligand, bathophenanthroline disulfonic acid (BPS) was combined with **7** and the mixture heated at 40 °C for 15 min to produce $[^{99m}Tc(CO)_3(BPS)(H_2O)]^-$ **9b**. Both intermediates were in turn converted to the desired final products through the treatment with the ImTz ligand (**6)** and heating at 60 °C for 30 min (Scheme 4.2). The formation of desired products **10b** and **11b** were confirmed by comparison of the HPLC retention times to that for the Re standards. The products could be readily isolated in nearly quantitative yield by simple solid phase extraction (SPE). The log P values were measured and were consistent with the more hydrophilic nature of the BPS ligand (log P for **10b** = 0.33; log P for **11b** = -0.39).

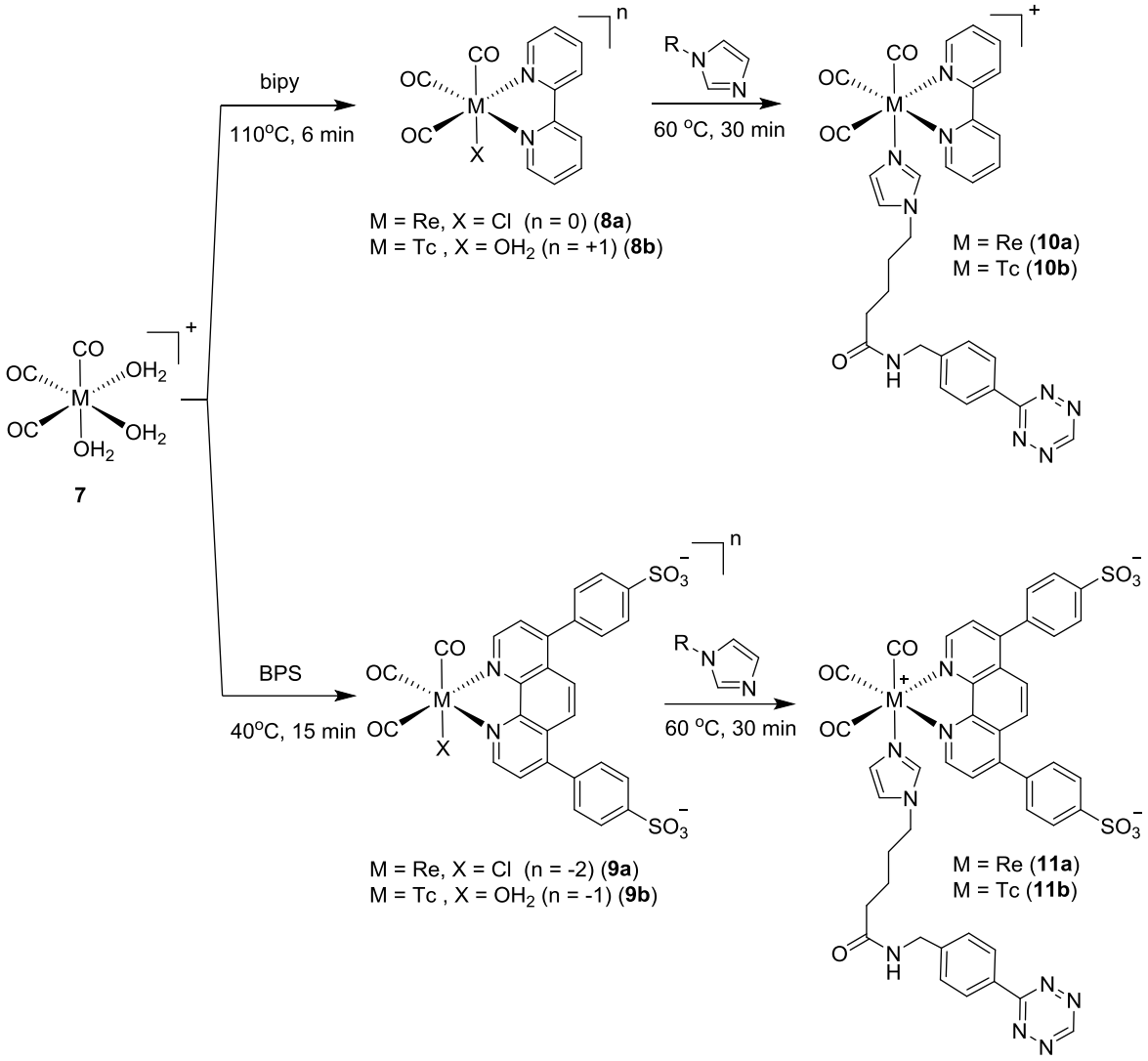


**Scheme 4.2** Synthesis of $[M(CO)_3(bipy)(ImTz)]^+$ **10a/b** and $[M(CO)_3(BPS)(ImTz)]^-$ **11a/b** (M = Re or $^{99m}$Tc). The reaction conditions shown are those used to prepare **10b** and **11b**. [46]

### 4.3.4 Stability Studies

One potential concern with using [2 + 1] complexes to create imaging probes is associated with premature loss of the monodentate ligand *in vivo.* This can result in high protein binding and elevated background activity in the liver.[41] In the case of the tetrazine derivatives, loss of the ligand would preclude the complex from being able to undergo the IEDDA reaction and ligate to the targeting molecule *in vivo*. The stability of the $^{99m}$Tc tetrazine complexes was assessed *in vitro* by amino acid challenge and plasma stability studies. For the amino acid challenge, **10b** and **11b** were incubated with 2 mM cysteine and histidine in PBS (pH = 7.4) at 37 °C for 6 h.[42] This is higher than the concentration of these amino acids in the blood and is a convenient way to assess stability prior to *in vivo* studies.[43] Samples were periodically analyzed by radio-HPLC (chromatograms provided in the supporting information) which showed that the metal complexes were resistant to ligand challenge where there was no evidence of decomposition up to 6 h.

The stability of Tc complexes and extent of protein binding were subsequently evaluated by incubation in plasma. Compounds **10b** and **11b** were added to mouse plasma at 37 °C and the stability of the complexes along with the extent of protein binding determined (Figure 4.1). The data showed increasing but modest levels of protein binding over time reaching a maximum value of approximately 30% at 6 h. At 1h, more than 80% of both metal complexes were still intact, which based on *in vivo* data for other radiolabeled tetrazines is sufficient to achieve efficient coupling to TCO-derived biomolecules.[11,44] The HPLC chromatograms did not show any evidence of loss of the monodentate ligands (i.e. there was no evidence of the formation of

$[^{99m}Tc(CO)_3(bipy)(H_2O)]^+$, **8b** or $[^{99m}Tc(CO)_3(BPS)(H_2O)]^-$, **9b)** where the observed decomposition is more likely associated with the reactive tetrazine moiety.

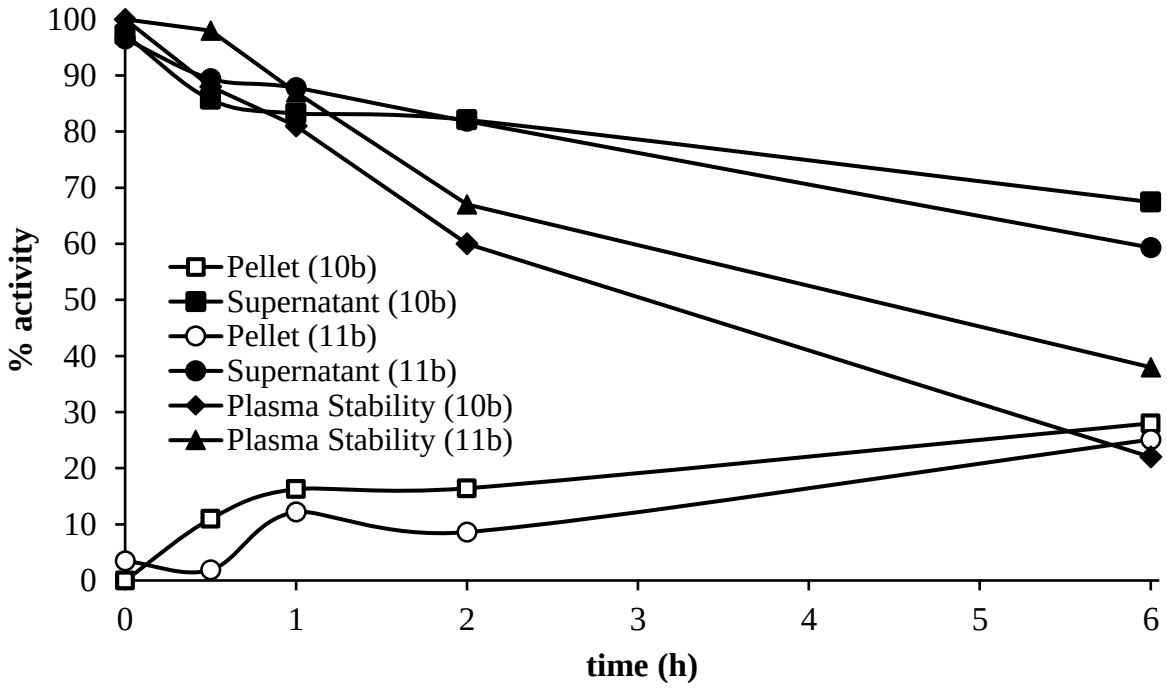


**Figure 4.1** Results for plasma stability and plasma binding studies for **10b** and **11b**. Plasma stability data was determined by HPLC analysis of samples of the supernatant. Activity in the pellet is an indicator of protein binding.

### 4.3.5 Kinetics

Inverse electron demand Diels-Alder reactions between tetrazine and *trans*-cyclooctenes typically have second order rate constants > $10^3$ $M^{-1}S^{-1}$.[45] In order to study

the impact of the Tc-complex on the reactivity of the appended tetrazine, the rate of reaction of a [2 + 1] $^{99m}$Tc-tetrazine complex with a model *trans*-cyclooctene derivative was studied. $[^{99m}Tc(CO)_3(bipy)(ImTz)]^+$ **10b** was combined with increasing concentration of TCO-OH. At the selected times, sample were quenched by adding an excess of the tetrazine **5** and the extent of formation of the product determined by HPLC. The data was fitted to a first order exponential and a pseudo first order rate constant ($K_{obs}$) calculated. The second order rate constant was determined by plotting the $K_{obs}$ vs. the concentration of TCO-OH and was found to be $8.6 \times 10^3$ $M^{-1}S^{-1}$ at 37 °C. This rate is comparable to other radiolabeled tetrazines that have been used successfully *in vitro* and *in vivo*.[17]

### 4.3.6 Biodistribution Studies

For *in vivo* testing, we opted to employ the more polar BPS complex **11b**, which we have shown previously for actively targeted derivatives, has lower non-specific binding *in vivo*.[46] Biodistribution studies were performed in female Balb/c mice using a TCO-derivative of a bisphosphonate (alendronate) which is capable of binding sites of calcium metabolism in bone.[21] A solution of the TCO-bisphosphonate (TCO-BP, approximately 20 mg/kg in saline) was administered intravenously followed 1 h later by **11b**. The mice were sacrificed at 6 and 12 h after injection of **11b** and radioactivity in various tissues and fluids counted. Biodistribution data at 6 h showed significant activity concentrations at the sites of high calcium accretion including in the knee (9.27 ± 0.32% ID/g) and shoulder (5.28 ± 0.67% ID/g). High concentrations were also seen in the gall

bladder (54.32 ± 5.45% ID/g), large intestine and caecum (27.70 ± 4.63% ID/g) which decreased to (7.94 ± 2.75% ID/g) and (2.95 ± 0.68% ID/g) at 12 h, respectively (Figure 4.2). The data clearly demonstrate that **11b** is sufficiently stable to be able to ligate with the bound TCO-BP *in vivo*. Had the compound lost the tetrazine ligand prior to coupling with the TCO-BP derivative, the biodistribution results would have showed no uptake in the bone. This is based on an imaging study performed previously on **9b**[46] in the same animal model, which showed almost exclusive uptake in the liver and no obvious uptake in the bone. SPECT/CT imaging studies with **11b** were carried out at 6 h and 24 h with Balb/c mice using the same TCO-BP pretargeting strategy. The resulting images were consistent with the biodistribution results and clearly showed high uptake and long residence time at the site of calcium accretion, especially the knee joints (Figure 4.3). The significant gut uptake is likely due to the non-polar tetrazine ligand since polar derivatives of the BPS complex show significantly lower non-specific binding.[46]

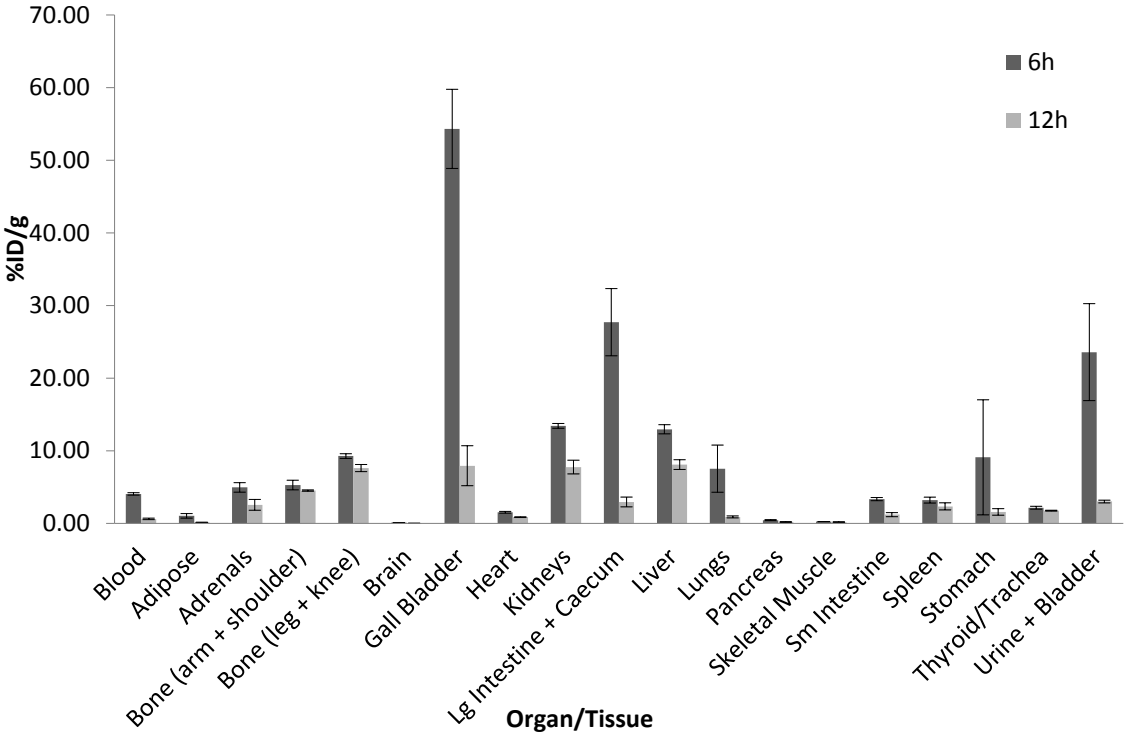


**Figure 4.2** Biodistribution data for select fluids and tissues for pretargeting with 20 mg/kg of TCO-BP administered 1 h prior to **11b**. Experiments were performed using Balb/c mice (n = 3 per time point) with tissues collected at 6 h and 12 h post administration of the labeled compound. Data are expressed as mean percent injected dose per gram (%ID/g) ± SEM.

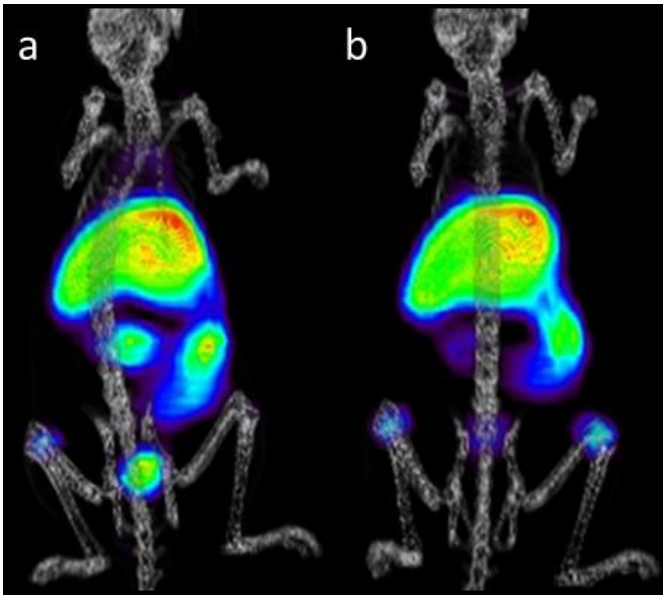


**Figure 4.3** SPECT/CT images of healthy Balb/c mice administered **11b** 1h after a TCO-derived bisphosphonate were obtained at (a) 6 and (b) 24 h.

### 4.3.7 Imaging Bone Tumors

Building on the promising biodistribution results in normal mice, the ability of **11b** and TCO-BP to image calcium liberation associated with formation of a tumor in bone was assessed using SPECT/CT. First, a solution of TCO-BP (approximately 20 mg/kg in saline) was administered intravenously to a Balb/c mice that had been injected with 4T1 mouse breast cancer cells into head of the right femur as a bone metastasis model (Figure 4.4, a-d).[47] For comparison, imaging studies were also performed using $^{99m}$Tc-MDP (Figure 4.4, e-h), which is used clinically for imaging bone metastases. In both cases, significant accumulation was observed in the right femur in addition to the joints, where the latter was also observed in normal mice. There was significant non-

target binding of **11b** in the gut, which as noted previously is likely due to the lipophilic nature of the complex compared to the highly polar Tc-MDP. The goal here was not to make an agent that is superior to Tc-MDP but rather to show that [2 + 1] complexes bearing a tetrazine have sufficient stability and reactivity to effectively undergo *in vivo* coupling reactions. Based on the data, future efforts will focus on fine-tuning the pharmacokinetics by modifying the polarity of the tetrazine-imidazole component.

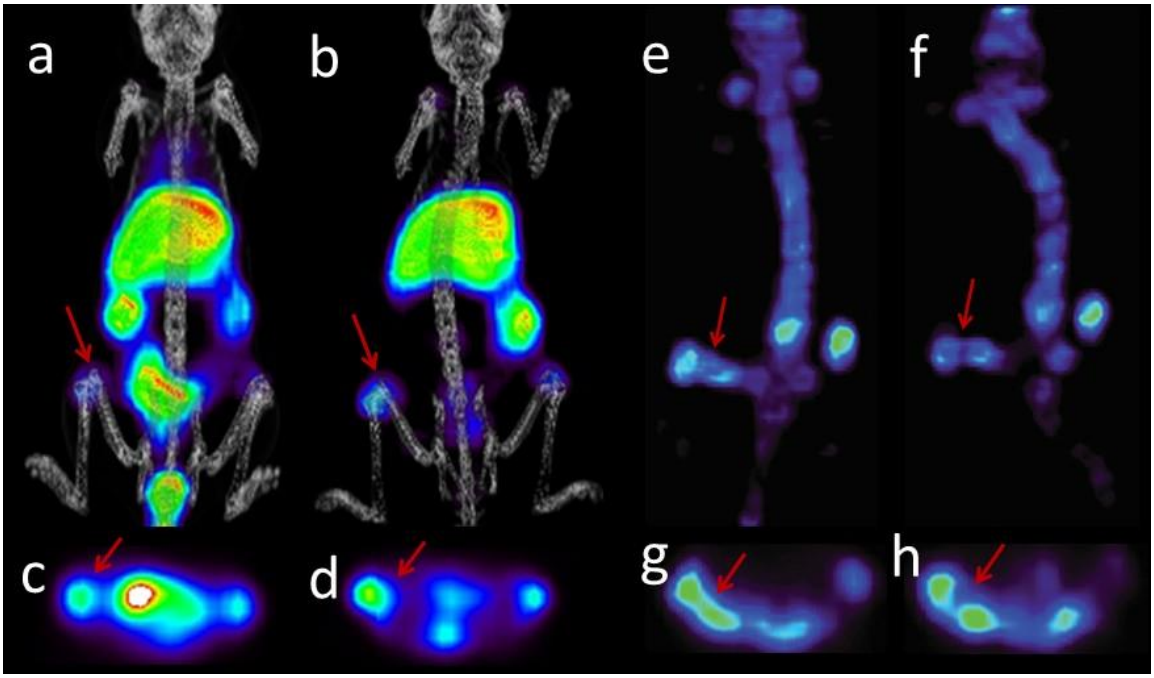


**Figure 4.4** SPECT/CT images of Balb/c mice bearing 4T1 tumour administered TCO-BP 1 h prior to **11b** where images were obtained at (a) 6 h, (b) 24 h post administration of the radiolabeled compound. The corresponding transverse images through the knees, spine, and bladder (c, d) are also shown. SPECT images of Balb/c mice bearing 4T1 tumour administered $^{99m}$Tc-MDP where images were obtained at (e) 4 h and (f) 6 h post-

injection, and the corresponding transverse images through the knees, spine, and bladder (g, h). Arrows show the right femur which contained the 4T1 derived tumour.

## 4.4 Conclusion

In summary, [2 + 1] complexes of Re(I) and Tc(I) containing a tetrazine were developed to create multimodal probes that can be targeted using bioorthoogonal chemistry. Both Tc complexes reported showed good *in vitro* stability and moderate protein binding in plasma. The metal complexes selectively coupled to a bisphosphonate-modified *trans*-cyclooctene *in vivo* at sites of active bone remodeling in normal mice and bone injury in a preclinical tumor model.

## 4.5 Acknowledgements

The authors gratefully acknowledge funding support from the Natural Science and Engineering Research Council (NSERC) of Canada, Canadian Cancer Society (CCS), and the Ontario Institute for Cancer Research (OICR).

## 4.6 Experimental Section

### 4.6.1 Materials and Instrumentation

All solvents were purchased from Caledon. Chemicals were purchased from Sigma-Aldrich and used without further purification, unless otherwise stated. Compounds

(5-imidazole-1-yl)pentanoic acid methyl ester (**3**), (5-imidazole-1-yl)pentanoic acid (**4**), $[Re(CO_3)(bipy)(Cl)]$ **8a**, and $[Re(CO_3)(BPS)(Cl)]^{2-}$ **9a** were prepared according to literature methods.[48–50] Histidine and cysteine challenge studies were performed according to literature procedures.[42] Deuterated solvents for NMR samples were purchased from Cambridge Isotope Laboratories. $[^{99m}TcO_4]^-$ was obtained from a $^{99}Mo/^{99m}Tc$ generator (Lantheus Medical Imaging) in saline (0.9% NaCl). *Caution: $^{99m}Tc$ is a γ-emitter ($E_\gamma$ = 140 keV, $t_{1/2}$ = 6 h) and should only be used in a licensed and appropriately shielded facility.*

Nuclear magnetic resonance (NMR) spectra ($^1H$, $^{13}C$) were recorded on a Bruker AV600 MHz spectrometer at ambient temperature. Microwave-assisted reactions were performed on a Biotage Initiator 60 microwave reactor using crimp-sealed vials. Mass spectrometry analyses were provided by the McMaster Regional Centre for Mass Spectrometry on an Agilent 6340 Ion Trap LC/MS mass spectrometer operating in electrospray ionization (ES) mode. High resolution mass spectra (HRMS) were collected on a Waters/Micromass Q-Tof Global Ultima spectrometer. IR spectra were obtained on a Biorad FTS-40 FTIR spectrometer. The fluorescence spectra were collected with the Tecan Infinite M1000 plate reader and the concentration of the solutions were 50 μM. High performance liquid chromatography (HPLC) was performed on a Waters 1525 Binary (Midford, MA, USA) monitored simultaneously with 2998 Photodiode Array Detector at 220/254 nm and in-line radioactivity Bioscan gamma detector with NaI(Tl) scintillator using the Empower software package. Phenomenex Gemini C-18 analytical column (250 × 4.60 mm, 5 μm) operating at a flow rate of 1.0 mL/min, and

Phenomenex Gemini C-18 semipreparative column (250 × 10 mm, 5 µm) operating at a flow rate of 4.0 mL/min were used for all analyses. The following solvent gradient was employed: (solvent A = $H_2O$ + 0.1% TFA, solvent B = $CH_3CN$ + 0.1% TFA): 0-2 min 2% B, 2-20 min 100% B; 20-22 min 100% B, 22-23 min 2% B, 23-25 min 2% B.

### 4.6.2 Synthetic Procedures

*5-Imidazol-1-yl-pentanoic acid 4-[1,2,4,5]tetrazin-3-yl-benzylamide* (ImTz) (**6**)

4-(1,2,4,5-Tetrazin-3-yl)phenyl)methanamine hydrochloride (8.0 mg, 0.045 mmol) in DMF (3 mL) was added to a premixed solution of (5-imidazole-1-yl)pentanoic acid (ImPA) (15 mg, 0.09 mmol), diisopropylethylamine (16 µL, 0.09 mmol), and PyBOP (62 mg, 0.12 mmol) in DMF (3 mL). The resulting solution was stirred overnight, the solvent was evaporated, and then subsequently purified by silica-gel column chromatography using MeOH:DCM (1:10 v/v). The pure product was isolated as a pink solid. (11 mg, 73%). mp 140-142 °C. $^1$H NMR (600 MHz, $CD_3OD$): δ (ppm) = 10.26 (s, 1H); 8.51 (d, $J$ = 8.3 Hz, 2H); 7.65 (s, 1H); 7.53 (d, $J$ = 8.3 Hz, 2H); 7.14 (s, 1H); 7.05 (s, 1H); 6.94 (s, 1 H); 4.45 (d, $J$ = 6.14 Hz, 2H); 4.00 (t, $J$ = 6.95 Hz, 2H); 2.25 (m, 2H); 1.79 (m, 2H); 1.56 (m, 2H). $^{13}$C NMR (150 MHz, $CD_3OD$): δ (ppm) = 174.66, 167.30, 158.95, 145.71, 138.06, 131.84, 129.32, 129.16, 128.12, 120.72, 47.66, 43.35, 35.99, 31.06, 23.38. HRMS: *m/z* calc for $C_{17}H_{20}N_7O$: 338.1729 found: 338.1719. HPLC (UV 220 nm): $R_t$ = 8.4 min.

*[Re(CO$_3$)(bipy)(ImTz)][CF$_3$SO$_3$]* **10a**

AgOTf (26 mg, 0.10 mmol) was added to a solution of [Re($CO_3$)(bipy)(Cl)] **8a** (46 mg, 0.10 mmol) in acetone (15 mL), and the mixture was heated to reflux for 2 h. The solution was filtered through Celite, and the solvent was evaporated under vacuum. The yellow residue was re-dissolved in acetone (10 mL) and ImTz **6** (34 mg, 0.1 mmol) added and the solution heated to reflux for 6 h prior to evaporation of the solvent to dryness. The desired product was isolated by silica-gel column chromatography using MeOH:DCM (1:10 v/v) as an orange solid (44 mg, 48%). mp 160-162 °C. IR ($\nu_{CO}$/$cm^{-1}$): 2029, 1916. $^1$H NMR (600 MHz, $CD_3OD$): δ (ppm) = 10.34 (s, 1H); 9.23 (d, *J* = 5.6 Hz, 2H); 8.61 (d, *J* = 8.2 Hz, 2H); 8.52 (d, *J* = 8.4 Hz, 2H); 8.31 (m, 2H); 7.81 (m, 2H); 7.78 (s, 1 H); 7.54 (d, *J* = 8.4 Hz, 2H); 7.05 (s, 1 H); 6.57 (s, 1 H); 4.48 (s, 1H); 3.92 (t, *J* = 7.0 Hz, 2H); 2.22 (t, *J* = 7.4 Hz, 2H); 1.64 (m, 2H); 1.34 (m, 2H). $^{13}$C NMR (150 MHz, $CD_3OD$): δ (ppm) = 197.00, 175.32, 167.61, 159.29, 157.11, 154.80, 145.72, 142.19, 141.40, 132.30, 129.94, 129.76, 129.45, 129.33, 125.87, 122.68, 48.52, 43.73, 35.96, 30.96, 23.38. HRMS: *m/z* calc for $C_{30}H_{27}N_9O_4Re$: 764.1744 found: 764.1722. HPLC (UV 254 nm): $R_t$ = 15.1 min.

*[Re($CO_3$)(BPS)(ImTz)]$^-$* **11a**

[Re$(CO)_3$(BPS)(Cl)]$^{2-}$ **9a** (80 mg, 0.1 mmol) and silver triflate (26 mg, 0.1 mmol) were dissolved in MeOH (12 mL) and heated to reflux for 2 h. The solution was filtered through Celite, and ImTz **6** (68 mg, 0.2 mmol) added to the filtrate. The mixture was heated to reflux for 6 h, then evaporated to dryness under vacuum. The desired product was isolated by silica-gel column chromatography using MeOH:DCM (1:3 v/v) as an

orange solid (46 mg, 37%). mp 230-234 °C. mp 241-243 °C. IR ($\nu_{CO}$/cm$^{-1}$): 2025, 1906. $^{1}$H NMR (600 MHz, $CD_3OD$): δ (ppm) = 10.30 (s, 1H); 9.50 (t, *J* = 4.4 Hz, 2H); 8.50 (d, *J* = 8.3 Hz, 2H); 8.17 – 8.01 (m, 8H); 7.80 – 7.67 (m, 5H); 7.52 (d, *J* = 8.3 Hz, 2H); 7.13 (s, 1H); 6.96 (s, 1H); 4.48 (s, 2H); 4.05 (t, *J* = 6.9 Hz, 2H); 2.32 (t, *J* = 7.3 Hz, 2H); 1.82 (m, 2H); 1.64 (m, 2H). $^{13}$C NMR (150 MHz, $CD_3OD$): δ (ppm) = 198.45, 190.53, 175.63, 167.56, 159.24, 154.36, 154.28, 151.97, 148.81, 147.75, 147.45, 145.62, 138.88, 138.29, 137.25, 132.71, 132.27, 131.02, 130.42, 130.18, 129.40, 129.30, 128.31, 128.26, 127.78, 127.70, 126.85, 120.65, 47.73, 43.79, 36.26, 31.62, 23.88. HRMS: *m/z* calc for $C_{44}H_{35}N_9O_{10}ReS_2$: 1098.1444 found: 1098.1478. HPLC (UV 254 nm): $R_t$ = 14.7 min.

### 4.6.3 General Procedure for the Preparation of 8b-11b

Sodium boranocarbonate (10 mg, 0.10 mmol), sodium carbonate (15 mg, 0.14 mmol), sodium borate (20 mg, 0.05 mmol) and sodium potassium tartrate (22 mg, 0.08 mmol) were placed in a microwave vial and purged with argon for 10 min. To this mixture, Na[$^{99m}TcO_4$] (1 mL, 370-740 MBq) was added and the vial was heated in a microwave reactor at 110 °C for 3.5 min to form [$^{99m}Tc(CO)_3(H_2O)_3]^+$. The solution was cooled to RT and adjusted to pH 5.5-6.5 with 1.0M HCl(aq). Bipyridine (1 mg, 6 µmol) was then added to the solution in a new microwave vial that had been purged with argon, and the mixture heated to 110 °C for 6 min to form [$^{99m}Tc(CO)_3$(bipy)$(H_2O)$]Cl. In case of bathophenanthroline disulfonic acid (BPS) (1 mg, 2 µmol) was added as a solid and the reaction mixture was heated to 40 °C for 15 min to form [$^{99m}Tc(CO)_3$(BPS)$(H_2O)]^-$. The **8b** and **9b** solutions were subsequently added to the monodentate ligand **6** (1 mg)

under argon and the mixture stirred at 60 °C for 30 min. The formation of products was confirmed by analytical HPLC. Conversion of $[^{99m}Tc(CO)_3(H_2O)_3]^+$ to the final product was >99% for both products.

### 4.6.4 Purification of $^{99m}$Tc Complexes

Purification of the $^{99m}$Tc complexes was achieved by solid phase extraction (SPE). The reaction mixture was diluted with water (2 mL) and the solution loaded on a Waters C18 Sep-Pak Plus cartridge, which had been previously activated with EtOH (6 mL) and $H_2O$ (6 mL). After loading the reaction mixture, the cartridge was washed with 15% $CH_3CN$ in $H_2O$ (12 mL), followed by 25% $CH_3CN$ in 0.4% (w/v) aqueous ammonium formate (6 mL). The desired products were eluted with a 1:1 v/v mixture of 0.4% aqueous ammonium formate and $CH_3CN$. For biological studies, the product was was evaporated to dryness and reconstituted in saline to the desired activity concentration.

### 4.6.5 Compound Testing and Evaluation

**Plasma Binding**

$^{99m}$Tc complexes **10b** or **11b** (100 µL, 111 MBq) was added to pre-warmed (37 ˚C) mouse plasma (900 µL) (Innovative Research, IMS-CD1-N), and the mixture vortexed prior to incubation at 37 ˚C. At multiple time points (t=0, 0.25, 0.5, 1, 2, 3, 6 h), 100 µL was removed and added to 200 µL ice cold $CH_3CN$. Samples were vortexed and

then centrifuged at maximum speed for 10 min. The amount of activity in the whole sample was measured using a dose calibrator (Capintec Inc, CRC-25R). The supernatant was separated from the pellet and the activity in each was measured using a dose calibrator. For all time points except t=0, pellets were washed with 100 µL of ice cold PBS and the percentage bound to blood proteins calculated by:

%bound = [(amount of activity in the wash pellet)]/[(amount of activity in pellet) + (amount of activity in supernatant)] × 100%

Values are reported as an average of two experiments ± standard deviation.

### 4.6.6 Kinetics

$[^{99m}Tc(CO)_3(bipy)ImTz]^+$ **10b** was combined with increasing concentration of TCO-OH (3, 4, and 5 µM) in 200 µL saline for 5 min. At the selected times (15, 30, 45, 60, 120, 180, 300 sec), a 20 µL sample was taken and quenched by the addition of **5** (1.5 µL, 5 mg/mL in DMF), and analyzed by HPLC. The data was fitted to a first order exponential to determine the pseudo first order rate constant ($K_{obs}$). A plot of $K_{obs}$ vs. TCO concentration was used to determine the second order rate constant.[11]

### 4.6.7 Biodistribution studies

Animal studies were approved by the Animal Research Ethics Board at McMaster University in accordance with Canadian Council on Animal Care (CCAC) guidelines. Biodistribution studies were performed using female Balb/c mice (Charles River

Laboratories, Kingston, NY) at the indicated time points. The mice were administered all compounds via tail vein injection with final volume not exceeding 200 µL. A 5 mg/mL solution of TCO-BP in saline was administered at a dose of 20 mg/kg. One hour after the TCO-BP injection, the mice were administered approx. 0.2 MBq of **11b**. At 6 h and 12 h post-injection of **11b**, animals were anesthetized with 3% isoflurane and euthanized by cervical dislocation. Fluids, bone (knee, shoulder), and select tissues were collected, weighed, and counted in a PerkinElmer Wizard 1470 Automatic Gamma Counter. Decay correction was used to normalize organ activity measurements to time of dose preparation for data calculations. Data is expressed as percent injected dose per gram (%ID/g) or percent injected dose per organ (%ID/O).

### 4.6.8 Cell Culture

Mycoplasma free 4T1 cells (ATCC, Manassas, Va) were maintained at sub-confluent densities in a humidified incubator with 5% $CO_2$ in room air at 37 °C using high glucose RPMI (Life Technologies, Carlsbad, CA) supplemented with 10% fetal bovine serum (FBS) and antibiotics (100 U/mL penicillin sodium and 100 µg/mL streptomycin sulfate) (Invitrogen).

### 4.6.9 Animal Care

Female Balb/c immunocompetent mice (Charles River, St. Constant, QC, Canada) at 4–6 weeks of age were sterile housed and maintained at 24 °C with a 12-hour light/dark cycle

and were provided autoclaved food and water *ad libitum*. All procedures were conducted according to the guidelines of the Committee for Research and Ethical Issues of the International Association for the Study of Pain, and guidelines established by the Canadian Council on Animal Care with ethical approval from the McMaster University Animal Research Ethics Board.

### 4.6.10 Tumour inoculation

On day 0, mice were anaesthetized by isoflurane inhalation and injected subcutaneously with buprenorphine (0.05 mg/kg) (Schering-Plough, Welwyn Garden City, Hertfordshire, UK) to reduce discomfort due to the surgical procedure. Animals were inoculated with $2\times10^5$ 4T1 cells in 25 μL sterile phosphate-buffered saline percutaneously into the right distal femur. To minimize tissue damage, mice were laid supine with the ipsilateral stifle joint bent at 90° to provide clearance of the patella. A 26-gauge needle was then manually inserted between the medial and lateral condyles of the distal epiphysis parallel to the longitudinal axis of the femur to penetrate the cortical bone and enter the epiphysis. The injectate was infused slowly over 1 minute. The contralateral hind limbs served as a negative control specific to each animal. This method of intrafemoral injection results in little damage to the surrounding tissues. Imaging of tumour inoculated mice was done on day 12.

### 4.6.11 Imaging Study

A 5 mg/mL solution of TCO-BP in saline was administered (20 mg/kg) 1 h prior to either **11b** or Tc-MDP (~35 MBq) via tail vein injection. Prior to imaging, mice were anaesthetized with 1.5-2.0% isoflurane and maintained under same conditions for the length of the SPECT and CT scans. Imaging was conducted at 6, 24 h post injection for **11b**, and 4, 6 h for Tc-MDP. At each time point, imaging was conducted on a GammaMedica Ideas X-SPECT system (North Ridge, California). CT acquisition (for **11b**) consisted of 512 projections acquired over 360˚ with 75 Kvp, 205 mA cone beam CT system. Cobra Exxim software (Feldkamp filtered backprojection cone beam reconstruction software) was used to reconstruct the images at a voxel size of 155 microns and a matrix size of $512^3$. An OS-EM interactive reconstructed method (2 iterations/8 subsets) was used to reconstruct the SPECT data which was fused to the CT data using in house software. AMIDE software was used to analyze all images.

*Note: All supporting information for this chapter can be found in Appendix 3.*

## 4.7 References


(1) Sletten, E. M.; Bertozzi, C. R. *Angew. Chem. Int. Ed.* **2009**, *48*, 6974–6998.

(2) Jewett, J. C.; Bertozzi, C. R. *Chem. Soc. Rev.* **2010**, *39*, 1272–1279.

(3) Goldenberg, D. M.; Sharkey, R. M.; Paganelli, G.; Barbet, J.; Chatal, J. F. *J. Clin. Oncol.* **2006**, *24*, 823–834.

(4) Goldenberg, D. M.; Rossi, E. a; Sharkey, R. M.; McBride, W. J.; Chang, C.-H. *J. Nucl. Med.* **2008**, *49*, 158–163.

(5) Blackman, M. L.; Royzen, M.; Fox, J. M. *J. Am. Chem. Soc.* **2008**, *130*, 13518–13519.

(6) Denk, C.; Svatunek, D.; Filip, T.; Wanek, T.; Lumpi, D.; Fröhlich, J.; Kuntner, C.; Mikula, H. *Angew. Chem. Int. Ed.* **2014**, *53*, 9655–9659.

(7) Denk, C.; Svatunek, D.; Mairinger, S.; Stanek, J.; Filip, T.; Matscheko, D.; Kuntner, C.; Wanek, T.; Mikula, H. *Bioconjugate Chem.* **2016**, *27*, 1707–1712.

(8) Nichols, B.; Qin, Z.; Yang, J.; Vera, D. R.; Devaraj, N. K. *Chem. Commun.* **2014**, *50*, 5215–5217.

(9) García, M. F.; Zhang, X.; Shah, M.; Newton-Northup, J.; Cabral, P.; Cerecetto, H.; Quinn, T. *Bioorg. Med. Chem.* **2016**, *24*, 1209–1215.

(10) Devaraj, N. K.; Upadhyay, R.; Haun, J. B.; Hilderbrand, S. a.; Weissleder, R. *Angew. Chem. Int. Ed.* **2009**, *48*, 7013–7016.

(11) Rossin, R.; Verkerk, P. R.; van den Bosch, S. M.; Vulders, R. C. M.; Verel, I.; Lub, J.; Robillard, M. S. *Angew. Chem.* **2010**, *49*, 3375–3378.

(12) Zeglis, B. M.; Sevak, K. K.; Reiner, T.; Mohindra, P.; Carlin, S. D.; Zanzonico, P.; Weissleder, R.; Lewis, J. S. *J. Nucl. Med.* **2013**, *54*, 1389–1396.

(13) Seitchik, J. L.; Peeler, J. C.; Taylor, M. T.; Blackman, M. L.; Rhoads, T. W.; Cooley, R. B.; Refakis, C.; Fox, J. M.; Mehl, R. A. *J. Am. Chem. Soc.* **2012**, *134*, 2898–2901.

(14) Liu, D. S.; Tangpeerachaikul, A.; Selvaraj, R.; Taylor, M. T.; Fox, J. M.; Ting, A. Y. *J. Am. Chem. Soc.* **2012**, *134*, 792–795.

(15) Versteegen, R. M.; Rossin, R.; Ten Hoeve, W.; Janssen, H. M.; Robillard, M. S. *Angew. Chem. Int. Ed.* **2013**, *52*, 1–6.

(16) Patterson, D. M.; Nazarova, L. A.; Prescher, J. A. *ACS Chem. Biol.* **2014**, *9*, 592–605.

(17) Rossin, R.; Robillard, M. S. *Curr. Opin. Chem. Biol.* **2014**, *21*, 161–169.

(18) Herth, M. M.; Andersen, V. L.; Lehel, S.; Madsen, J.; Knudsen, G. M.; Kristensen, J. L. *Chem. Commun.* **2013**, *49*, 3805–3807.

(19) Li, Z.; Cai, H.; Hassink, M.; Blackman, M. L.; Brown, R. C. D.; Conti, P. S.; Fox, J. M. *Chem. Commun.* **2010**, *46*, 8043–8045.

(20) Zeglis, B. M.; Mohindra, P.; Weissmann, G. I.; Divilov, V.; Hilderbrand, S. A.; Weissleder, R.; Lewis, J. S. *Bioconjugate Chem.* **2011**, *22*, 2048–2059.

(21) Yazdani, A.; Bilton, H.; Vito, A.; Genady, A. R.; Rathmann, S. M.; Ahmad, Z.; Janzen, N.; Czorny, S.; Zeglis, B. M.; Francesconi, L. C.; Valliant, J. F. *J. Med. Chem.* **2016**, *59*, 9381–9389.

(22) Rossin, R.; Van Den Bosch, S. M.; Ten Hoeve, W.; Carvelli, M.; Versteegen, R. M.; Lub, J.; Robillard, M. S. *Bioconjugate Chem.* **2013**, *24*, 1210–1217.

(23) Devaraj, N. K.; Weissleder, R. *Acc. Chem. Res.* **2011**, *44*, 816–827.

(24) Yang, J.; Šečkute, J.; Cole, C. M.; Devaraj, N. K. *Angew. Chem. Int. Ed.* **2012**, *51*, 7476–7479.

(25) Devaraj, N. K.; Weissleder, R.; Hilderbrand, S. A. *Bioconjugate Chem.* **2008**, *19*, 2297–2299.

(26) Lang, K.; Davis, L.; Wallace, S.; Mahesh, M.; Cox, D. J.; Blackman, M. L.; Fox, J. M.; Chin, J. W. *J. Am. Chem. Soc.* **2012**, *134*, 10317–10320.

(27) Meimetis, L. G.; Carlson, J. C. T.; Giedt, R. J.; Kohler, R. H.; Weissleder, R. *Angew. Chem. Int. Ed.* **2014**, *53*, 7531–7534.

(28) Wu, H.; Yang, J.; Šečkute, J.; Devaraj, N. K. *Angew. Chem. Int. Ed.* **2014**, *53*, 5805–5809.

(29) Wieczorek, A.; Buckup, T.; Wombacher, R. *Org. Biomol. Chem.* **2014**, *12*, 4177–4185.

(30) Murrey, H. E.; Judkins, J. C.; Am Ende, C. W.; Ballard, T. E.; Fang, Y.; Riccardi, K.; Di, L.; Guilmette, E. R.; Schwartz, J. W.; Fox, J. M.; Johnson, D. S. *J. Am. Chem. Soc.* **2015**, *137*, 11461–11475.

(31) Carlson, J. C. T.; Meimetis, L. G.; Hilderbrand, S. A.; Weissleder, R. *Angew. Chem. Int. Ed.* **2013**, *52*, 6917–6920.

(32) Choi, A. W.-T.; Tso, K. K.-S.; Yim, V. M.-W.; Liu, H.-W.; Lo, K. K.-W. *Chem. Commun.* **2015**, *51*, 3442–3445.

(33) Lo, K. K.-W.; Choi, A. W.-T.; Law, W. H.-T. *Dalton Trans.* **2012**, *41*, 6021–6047.

(34) Pitchumony, T. S.; Banevicius, L.; Janzen, N.; Zubieta, J.; Valliant, J. F. *Inorg. Chem.* **2013**, *52*, 13521–13528.

(35) Yazdani, A.; Janzen, N.; Banevicius, L.; Czorny, S.; Valliant, J. F. *Inorg. Chem.* **2015**, *54*, 1728–1736.

(36) Li, G.; Parimal, K.; Vyas, S.; Hadad, C. M.; Flood, A. H.; Glusac, K. D. *J. Am. Chem. Soc.* **2009**, *131*, 11656–11657.

(37) Palma, E.; Correia, D. G.; Oliveira, B. L.; Gano, L.; Santos, I. C.; Santos, I. *Dalton*

*Trans.* **2011**, 2787–2796.

(38) Dumas-Verdes, C.; Miomandre, F.; Lépicier, E.; Galangau, O.; Vu, T. T.; Clavier, G.; Méallet-Renault, R.; Audebert, P. *Eur. J. Org. Chem.* **2010**, 2525–2535.

(39) Devaraj, N. K.; Hilderbrand, S.; Upadhyay, R.; Mazitschek, R.; Weissleder, R. *Angew. Chem. Int. Ed.* **2010**, *49*, 2869–2872.

(40) Wu, H.; Alexander, S. C.; Jin, S.; Devaraj, N. K. *J. Am. Chem. Soc.* **2016**, *138*, 11429–11432.

(41) Schibli, R.; Schubiger, P. A. *Eur. J. Nucl. Med.* **2002**, *29*, 1529–1542.

(42) Jiang, H.; Kasten, B. B.; Liu, H.; Qi, S.; Liu, Y.; Tian, M.; Barnes, C. L.; Zhang, H.; Cheng, Z.; Benny, P. D. *Bioconjugate Chem.* **2012**, *23*, 2300–2312.

(43) Bridgeman, M. M.; Marsden, M.; MacNee, W.; Flenley, D. C.; Ryle, A. P. *Thorax* **1991**, *46*, 39–42.

(44) Meyer, J. P.; Houghton, J. L.; Kozlowski, P.; Abdel-Atti, D.; Reiner, T.; Pillarsetty, N. V. K.; Scholz, W. W.; Zeglis, B. M.; Lewis, J. S. *Bioconjugate Chem.* **2016**, *27*, 298–301.

(45) Wang, M.; Svatunek, D.; Rohlfing, K.; Liu, Y.; Wang, H.; Giglio, B.; Yuan, H.; Wu, Z.; Li, Z.; Fox, J. *Theranostics* **2016**, *6*, 887–895.

(46) Yazdani, A.; Janzen, N.; Czorny, S.; Valliant, J. F. *Inorg. Chem.* submitted.

(47) Blankenberg, F. G.; Backer, M. V.; Levashova, Z.; Patel, V.; Backer, J. M. *Eur. J. Nucl. Med. Mol. Imaging* **2006**, *33*, 841–848.

(48) Hack, S.; Wörlein, B.; Höfner, G.; Pabel, J.; Wanner, K. T. *Eur. J. Med. Chem.* **2011**, *46*, 1483–1498.

(49) Huertos, M. a; Pérez, J.; Riera, L. *J. Am. Chem. Soc.* **2008**, *130*, 5662–5663.

(50) Amoroso, A. J.; Coogan, M. P.; Dunne, J. E.; Fernández-Moreira, V.; Hess, J. B.; Hayes, A. J.; Lloyd, D.; Millet, C.; Pope, S. J. A.; Williams, C. *Chem. Commun.* **2007**, 3066–3068.

# Chapter 5

## 5 Chapter 5. Summary and Future Work

### 5.1 Summary

The overall objective was to develop and study the chemistry and chemical biology of a new class of isostructural optical and nuclear probes. The work reported was based on [2 + 1] Re(I)/Tc(I) complexes which required careful selection of the monodentate and bidentate ligands to give the best possible chemical, optical and *in vivo* properties. In chapter 2, a series of new [2 + 1] Re(I)/$^{99m}$Tc(I) complexes derived from bipyridine and imidazole derivatives were developed and X-ray structures of two new Re(I) complexes were determined. A high yielding method to prepare the $^{99m}$Tc(I) analogues was developed, which included a pH mediated one-pot reaction. Plasma stability and *in vivo* imaging studies revealed that incorporation of a spacer group between the imidazole donor group and electron-withdrawing substituents renders the complex suitably stable for use *in vivo*. Therefore, with the appropriate choice of monodentate ligand, it is possible to prepare robust [2 + 1] Tc complexes that can be used to prepare targeted isostructural optical/nuclear molecular imaging probes.

In chapter 3, new [2 + 1] Re(I)/$^{99m}$Tc(I) complexes derived from bathophenanthroline disulfonate (BPS) were developed in order to enhance solubility and photophysical properties of the resulting complexes. The binding and uptake of the Re(I) complex, $[Re(CO)_3(BPS)(ImAln)]^{2-}$ (ImAln = an imidazole-alendronate derivative) in MCF-7 cells showed cytoplasmic localization by fluorescence microscopy. The Tc(I)

analogue, $[^{99m}Tc(CO)_3(BPS)(ImAln)]^{2-}$ exhibited high bone uptake and rapid clearance from non-target tissues. Re(I)/Tc(I) complexes with BPS had superior water solubility, optical properties and lower non-specific binding *in vivo* compared to those prepared using bipy as the bidentate ligand.

In chapter 4, [2 + 1] Re(I)/Tc(I) complexes derived from bipy and BPS which contained an imidazole-tetrazine (ImTz) monodentate ligand were developed as complementary pairs of optical and nuclear probes that could be used to develop new probes via pretargeting and bioorthogonal chemistry. Stability studies of both $^{99m}Tc(I)$ complexes showed moderate protein binding and resistance to ligand challenge and are therefore suitable for *in vivo* imaging. Measurement of the kinetics of the reaction between $[^{99m}Tc(CO)_3(bipy)(ImTz)]^+$ and *trans*-cyclooctenol (TCO-OH) showed a second rate order constant of $8.6 \times 10^3$ $M^{-1}S^{-1}$ at 37 °C, which is suitable for pretargeting strategies. The biodistribution of the more polar complex $[^{99m}Tc(CO)_3(BPS)(ImTz)]^-$ which was administered to normal mice 1h after a transcyclooctene-bisphosphonate derivative showed high activity concentrations in the knee (9.27 ± 0.32% ID/g) and shoulder (5.28 ± 0.67% ID/g). The SPECT/CT images of the same complex in a bone cancer model demonstrated high accumulation at the site of tumor invasion where there was elevated metabolic activity in bone. These results clearly demonstrated that $[^{99m}Tc(CO)_3(BPS)(ImTz)]^-$ effectively underwent bioorthogonal chemical reactions *in vivo*. An additional attractive feature was that the Re(I) analogue exhibited a 9-fold enhancement in its fluorescence emission upon addition of a *trans*-cyclooctene

derivative. This can be used to improve signal-to-noise ratios, which is particularly important for cell and tissue imaging studies.

## 5.2 Future Work

Having established the model constructs and developed new Tc(I) labeling and purification procedures, the next step is to expand the use of the platform for labeling biomolecules. One approach is to ligate the intermediate complex $[M(CO)_3(BPS)(H_2O)]^-$ to his-tags found on proteins leveraging the work presented here which demonstrated the stability of the corresponding imidazole complexes. A second potential approach, in which some preliminary studies are described in section 5.4-5.7, is to utilize triazoles formed through Click chemistry as both monodentate ligands and linker groups to biomolecules.

## 5.3 Labeling His Tagged Proteins

His-tags are often added to proteins to facilitate their purification using immobilized metal ion affinity chromatography (IAMC).[1] The presence of his-tags offers an opportunity to use proteins as targeting vectors for radiometals such as Re(I)/Tc(I)-tricarbonyl, and avoid the need to introduce a separate chelating group on free lysine or cysteine residues.[2] The approach has been applied to a range of single-chain antibody fragments (scFvs) such as affibodies.[3]

Despite the success of this strategy for labeling and purification of proteins with $[^{99m}Tc(CO)_3]^+$, several variants of his-tags have been developed to reduce non-specific binding in the liver.[4,5] There are also no examples of isostructural optical and nuclear probes derived from his-tagged proteins, where the products could be used to assess the cellular and whole body distribution of proteins. Since we demonstrated that [2 + 1] complexes are robust when the monodentate ligand are imidazoles, there is the opportunity to label his-tagged proteins with $[M(CO)_3(BPS)X]^n$ to create isostructural optical and nuclear probes. The first step would be to determine the stability of the complex labeled with typical his-tags used in IAMC. This would be done by combining a penta-his-tag with $[M(CO)_3(BPS)X]^n$ (Figure 5.1) and then assess the stability of the complex to ligand exchange by HPLC. Assuming the complex showed sufficient resistance to histidine and cysteine challenge and moderate protein binding, test reactions with a model his-tagged protein such as scFvs would be attempted. The key here would be to ensure that reactions are done below 37 °C and that the metal selectively coordinates to the his tag and that the product is both stable and maintains its affinity for its target.

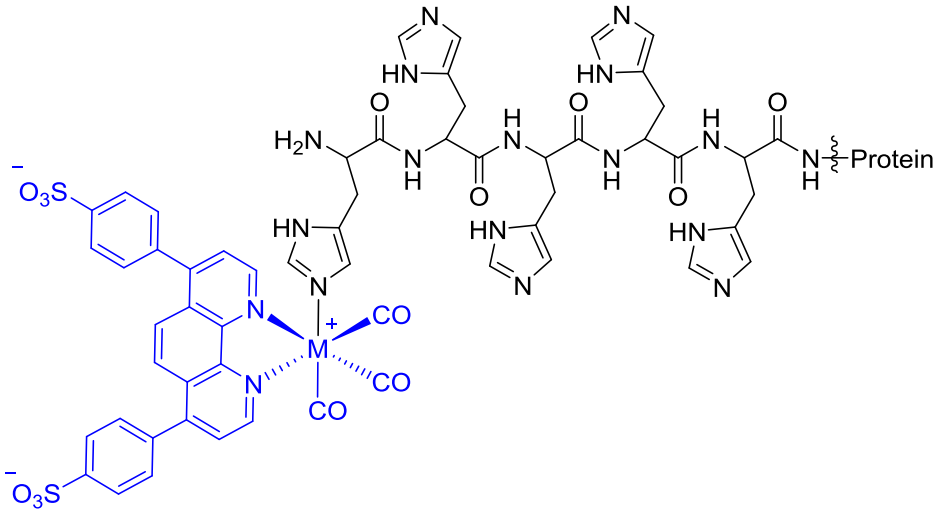


**Figure 5.1** Proposed structure of $[M(CO)_3(BPS)X]^n$ – labeled protein with penta-his-tags

## 5.4 Triazole-Based [2 + 1] Re(I)/$^{99m}$Tc(I) Complexes as Isostructural Nuclear and Optical Probes

As an alternative to imidazoles it may be possible to generate new [2 + 1] complexes of Tc(I)/Re(I) complexes derived from bipy or BPS and triazole ligands. 1,4-Disubstituted imidazoles which are known to be efficient ligand for $[M(H_2O)_3(CO)_3]^+$ (M = Re/$^{99m}$Tc) share similar coordinative properties with 1,4-disubstituted 1,2,3-triazoles, while providing the opportunity of using "Click chemistry" to link the complexes to biomolecules.[6] Schibli *et al.* reported a comparative study of the labeling of a imidazole-containing histidine-based folate and its triazole analogue with $[M(H_2O)_3(CO)_3]^+$ (M = Re/$^{99m}$Tc) where the products were evaluated *in vitro* and *in vivo*.[7,8] The results showed that while synthesis of the clicked triazole tracer is shorter and more efficient, the

stability and biological affinity of the $^{99m}$Tc-labeled derivatives *in vitro* and their pharmacological profiles *in vivo* are identical. The approach supports the idea that triazoles can be utilized not only as a linker strategy (to connect radioisotopes to the targeting vector), but they can also act as an efficient donor group to the technetium-tricarbonyl core (Figure 5.2).

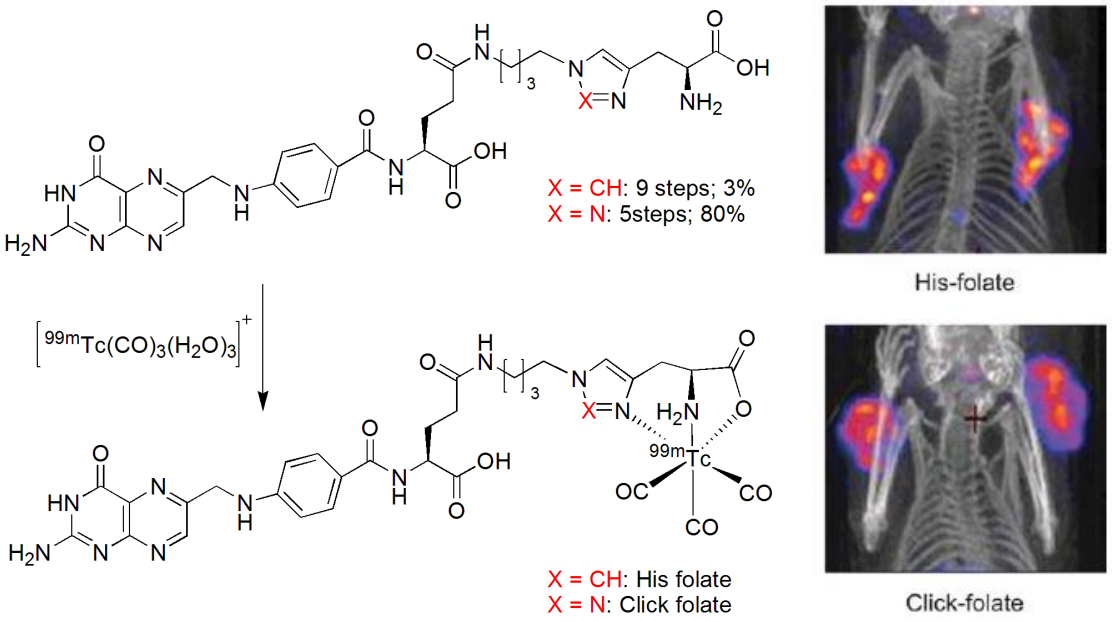


**Figure 5.2** Synthesis and comparison of the structure and tumor uptake of two folate derivatives; one histidine-based and one triazole-based (left); combined small animal SPECT/CT 24 h post injection of each radiotracer (right)[8]

The use of triazoles for the preparation of [2 + 1] complexes of Tc(I) has not been studied extensively while [2 + 1] type rhenium(I) polypyridine complexes containing a triazole have been used as fluorescence imaging agents.[9–12] One of the concerns

associated with using triazoles as the monodentate ligand, as is the case with all [2 + 1] type complexes, is the tendency of the Tc complex to undergo ligand exchange *in vivo*. As a preliminary assessment of the suitability of triazoles, a series of model complexes were prepared and their stability *in vitro* evaluated.

To prepare the desired Re(I) triazole complexes, **2a** was treated with a series of functionalized triazoles and the mixtures heated to reflux overnight. The first triazole used was 1H-1,2,3-triazole-1-ethanol (EtOHTrz), where the Re complex **3a** was isolated by column chromatography in 61% yield. The reactions were repeated using *N*-methyltriazole (MeTrz) which was selected because of possibility of direct comparison with *N*-methylimidazole which was used successfully in chapter 2 to prepare stable [2 + 1] complexes. $[Re(CO)_3(bipy)(MeTrz)]^+$ **5a**, was isolated in 82% yield by column chromatography. The HRMS and $^1H$ NMR spectra of the material were consistent with the target products.

The corresponding $^{99m}Tc$ complexes $[^{99m}Tc(CO)_3(bipy)(L)]^+$ (L = triazole), were obtained by adding **2b** to the triazole ligands and heating at 40 °C for 30 min (Scheme 5.1). Quantitative transformation to the final product was obtained for **3b** and **5b**, which contained either EtOHTrz or MeTrz as shown by HPLC and through comparison to the retention times of authentic Re standards. When **2b** was combined with a more hindered triazole, 4-phenyl-1-methyl-1,2,3-triazole, the corresponding $^{99m}Tc$ complex $[^{99m}Tc(CO)_3(bipy)(MePhTrz)]^+$ **4b** was not observed. The reaction mixture was heated to 150 °C in a microwave reactor for different time intervals where the maximum yield was

40%. HPLC indicated the reaction did not go to completion under any of the conditions tested which is likely due to the steric hindrance and electron withdrawing nature of the phenyl group. Unlike for the Tc complex, the Re complex **4a** was prepared in high yield following a literature method.[15] Nevertheless the poor yield of the Tc complex and stability issues that were observed during *in vitro* testing (vide infra) suggested that (like imidazoles) the nature of the groups attached to the triazole can drastically affect the stability of the final complex.

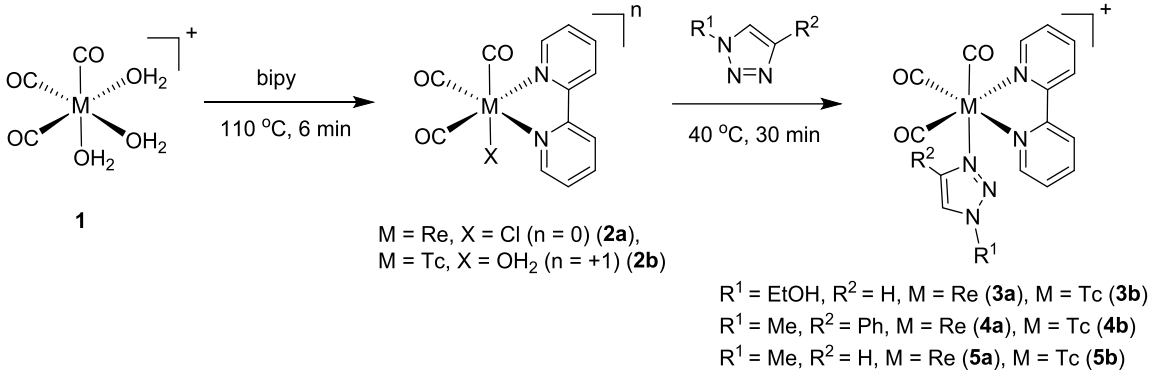


**Scheme 5.1** Synthesis of isostructural [2 + 1] Re (I) and $^{99m}$Tc complexes. The conditions shown are for the reactions performed at the tracer level.

### 5.4.1 Stability Studies

The stability of the Tc complexes was initially studied in isotonic saline. For $[^{99m}Tc(CO)_3(bipy)(EtOHTrz)]^+$ **3b** after 3 h approximately 50% of the complex converted to $[^{99m}Tc(CO)_3(bipy)(H_2O)]^+$, **2b**. $[^{99m}Tc(CO)_3(bipy)(MeTrz)]^+$ **5b** was observed to

partially dissociate during incubation in saline to yield the intermediate compound **2b** as identified by comparing the retention time to the Re standard (roughly 37% of the parent complex **5b** converted to the intermediate **2b** after 3 h incubation in saline). Histidine and cysteine challenge studies were performed subsequently. A solution of $[^{99m}Tc(CO)_3(bipy)(MeTrz)]^+$ **5b** was incubated separately by histidine and cysteine in PBS (pH = 7.4) at 37 °C. Samples were taken at different time points up to 6 h and analyzed by HPLC to determine the degree of decomposition. The results indicated that when **5b** was incubated in cysteine about 53% decomposed. When **5b** was incubated in histidine nearly 50% of the complex decomposed.

In summary, a method to prepare $^{99m}Tc(I)$ [2 + 1] complexes containing triazoles was developed. The stability results of Tc complexes was not as good as for the imidazole derivatives. Nevertheless it may be possible to exploit the labile monodentate ligand such that following targeting and internalization, the monodentate ligand could be substituted by intracellular proteins which could enhance target to non-target ratios. The latter would require complexes to be found that are sufficiently robust in the blood that they can clear the body if they are not taken up at the site of interest. The advantage of using triazoles as a way to link [2 + 1] complexes to biomolecules is significant and warrants further study of this class of compounds.

## 5.5 Experimental Section

All solvents were purchased from Caledon. Chemicals were purchased from Sigma-Aldrich and used without further purification, unless otherwise stated. Compound

1-methyl-1,2,3-triazole was purchased from Enamine and used without further purification. Compounds **2a**, **4a**, and 4-phenyl-1-methyl-1,2,3-triazole were prepared following an established method in good yields.[15–17] Histidine and cysteine challenge studies were performed according to literature procedures.[18] Deuterated solvents for NMR samples were purchased from Cambridge Isotope Laboratories. Technetium-99m $[^{99m}TcO_4]^-$ was obtained from a $^{99}Mo/^{99m}Tc$ generator (Lantheus Medical Imaging) in saline (0.9 % NaCl). *Caution: $^{99m}Tc$ is a γ-emitter (Eγ = 140 keV, $t_{1/2}$ = 6 h) and should only be used in a licensed and appropriately shielded facility.*

Nuclear magnetic resonance (NMR) spectra ($^1H$, $^{13}C$) were recorded on a Bruker AV600 MHz spectrometer at ambient temperature. Microwave-assisted reactions were performed on a Biotage Initiator 60 microwave reactor using crimp-sealed vials. Mass spectrometry analyses were provided by the McMaster Regional Centre for Mass Spectrometry on an Agilent 6340 Ion Trap LC/MS mass spectrometer operating in electrospray ionization (ES) mode. High resolution mass spectra (HRMS) were collected on a Waters/Micromass Q-Tof Global Ultima spectrometer. IR spectra were obtained on a Biorad FTS-40 FTIR spectrometer. The fluorescence spectra were collected with the Tecan Infinite M1000 plate reader and the concentration of the solutions were 50 μM. High performance liquid chromatography (HPLC) was performed on a Waters 1525 Binary (Midford, MA, USA) monitored simultaneously with 2998 Photodiode Array Detector at 220/254 nm and in-line radioactivity Bioscan gamma detector with NaI(Tl) scintillator using the Empower software package. Phenomenex Gemini C-18 analytical column (250 × 4.60 mm, 5 μm) operating at a flow rate of 1.0 mL/min, and

Phenomenex Gemini C-18 semipreparative column (250 × 10 mm, 5 μm) operating at a flow rate of 4.0 mL/min were used for all analyses. The following solvent gradients were employed: *Method A* (solvent A = $H_2O$ + 0.1% TFA, solvent B = $CH_3CN$ + 0.1% TFA): 0-2 min 2% B, 2-20 min 100% B; 20-22 min 100% B, 22-23 min 2% B, 23-25 min 2% B. *Method B* (solvent A = $H_2O$ + 0.1% FA, solvent B = $CH_3CN$ + 0.1% FA): 0-2 min 2% B, 2-20 min 100% B; 20-22 min 100% B, 22-23 min 2% B, 23-25 min 2% B.

### 5.5.1 Synthetic Procedures

*$[Re(CO)_3(bipy)(EtOHTrz)][CF_3SO_3]$* ***3a***

$[Re(CO)_3(bipy)(H_2O)][CF_3SO_3]$ (60mg, 0.1mmol) was dissolved in DCM (10 mL) and 1H-1,2,3-triazole-1-ethanol (17mg, 0.15mmol) in DCM (5mL) was added to the solution, and the mixture was refluxed overnight. The solution was then evaporated to dryness under reduced pressure. The crude reaction mixture was purified by silica-gel column chromatography using MeOH:DCM = 1:10 as eluent to yield a yellow solid (41mg, 61%). m.p. 115-117 °C. $^1$HNMR (600 MHz, $CD_3CN$): δ (ppm) = 9.09 (d, *J* = 5.7 Hz, 2 H); 8.42 (d, *J* = 8.2 Hz, 2 H); 8.25 (m, 2 H); 7.78 (s, 1 H); 7.68 (m, 2 H); 7.64 (s, 1 H); 4.13 (t, *J* = 5.0 Hz, 2 H); 3.56 (q, *J* = 5.1 Hz, 2 H); 2.90 (t, *J* = 5.7 Hz, 1 H). $^{13}$CNMR (150 MHz, $CD_3CN$): δ (ppm) = 157.17, 154.85, 141.86, 137.95, 129.09, 128.80, 125.22, 60.51, 54.89. HRMS: *m/z* calc for $C_{18}H_{17}N_5O_4Re(M^+)$: 540.0695 found: 540.0707.

*$[Re(CO)_3(bipy)(MeTrz)][CF_3SO_3]$* ***5a***

$[Re(CO)_3(bipy)(H_2O)][CF_3SO_3]$ (60mg, 0.1mmol) was dissolved in THF (10 mL) and *N*-methyltriazole (12mg, 0.15mmol) in THF (5mL) was added to the solution, and the mixture was refluxed overnight. The solution was then evaporated to dryness under reduced pressure. The crude reaction mixture was purified by silica-gel column chromatography using MeOH:DCM = 1:20 as eluent to yield a yellow solid (42mg, 82%). m.p. 108-111 °C. $^1$HNMR (600 MHz, $CD_3OD$): δ (ppm) = 9.18 (d, *J* = 5.3 Hz, 2 H); 8.62 (d, *J* = 8.2 Hz, 2 H); 8.32 (m, 2 H); 7.97 (s, 1 H); 7.81 (s, 1 H); 7.77 (m, 2 H); 3.88 (s, 3 H). $^{13}$CNMR (150 MHz, $CD_3CN$): δ (ppm) = 157.57, 154.94, 142.16, 138.44, 129.54, 129.43, 125.50, 38.10. HRMS: *m/z* calc for $C_{16}H_{13}N_5O_3Re(M^+)$: 510.0576 found: 510.0584.

### 5.5.2 General Procedure for the Preparation of $[^{99m}Tc(CO)_3(bipy)(L)]^+$

Sodium boranocarbonate (10.0 mg, 0.10 mmol), sodium carbonate (15.0 mg, 0.14 mmol), sodium borate (20 mg, 0.05 mmol) and sodium potassium tartrate (22 mg, 0.08 mmol) were placed in a microwave vial and purged with argon for 10 min. To this mixture, $Na[^{99m}TcO_4]$ (1 mL) was added and the vial was heated in a microwave reactor at 110 °C for 3.5 min to form $[^{99m}Tc(CO)_3(H_2O)_3]^+$. The solution was then cooled, and neutralized to pH 5.5-6.5 with aqueous hydrochloric acid (1.0 M). The solution was added to bipyridine (1 mg, 6 µmol) in a separate microwave vial, which had been purged with argon, heated to 110°C for 6 min to form the intermediate $[^{99m}Tc(CO)_3(bipy)(H_2O)]^+$ and the solution added to one of the monodentate ligands (30 – 120 µmol) under argon and the mixture stirred at 40 °C for 20 min to give $[^{99m}Tc(CO)_3(bipy)(L)]^+$. The formation

of products was confirmed by analytical HPLC. In case of **4b** poor yield of metal complex was observed. In contrast, quantitative conversion of $[^{99m}Tc(CO)_3(H_2O)_3]^+$ to **3b**, and **5b** was achieved.

### 5.5.3 Purification of $^{99m}$Tc Complexes

Purification of **3b**-**5b** was achieved by solid phase extraction (SPE). The reaction mixture was diluted with water (2 mL) and the solution loaded on a Waters C18 Sep-Pak Plus cartridge, which had been previously activated with EtOH (1 × 6 mL) and $H_2O$ (1 × 6 mL). After loading the reaction mixture, the column was washed with 15% $CH_3CN$ in $H_2O$ (2 × 6 mL), followed by 25% $CH_3CN$ in 0.4% (w/v) aqueous ammonium formate (1 × 6 mL). The desired products were eluted with a 1:1 v/v mixture of 0.4% aqueous ammonium formate and $CH_3CN$.

*Note: All supporting information for this chapter can be found in Appendix 4.*

## 5.6 References


(1) Novak-Hofer, I.; Waibel, R.; Zimmermann, K.; Schibli, R.; Grünberg, J.; Chester, K. a; Murray, A.; Lo, B. K. C.; Perkins, A. C.; Schubiger, P. A. *Methods Mol. Biol.* **2004**, *248*, 481–494.

(2) Waibel, R.; Alberto, R.; Willuda, J.; Finnern, R.; Schibli, R.; Stichelberger, A.; Egli, A.; Abram, U.; Mach, J. P.; Plückthun, A.; Schubiger, P. A. *Nat. Biotechnol.* **1999**, *17*, 897–901.

(3) Hofström, C.; Orlova, A.; Altai, M.; Wangsell, F.; Gräslund, T.; Tolmachev, V. *J. Med. Chem.* **2011**, *54*, 3817–3826.

(4) Hofström, C.; Altai, M.; Honarvar, H.; Strand, J.; Malmberg, J.; Hosseinimehr, S. J.; Orlova, A.; Gräslund, T.; Tolmachev, V. *J. Med. Chem.* **2013**, *56*, 4966–4974.

(5) Tolmachev, V.; Hofström, C.; Malmberg, J.; Ahlgren, S.; Hosseinimehr, S. J.; Sandström, M.; Abrahmsén, L.; Orlova, A.; Gräslund, T. *Bioconjugate Chem.* **2010**, *21*, 2013–2022.

(6) van Staveren, D. R.; Mundwiler, S.; Hoffmanns, U.; Pak, J. K.; Spingler, B.; Metzler-Nolte, N.; Alberto, R. *Org. Biomol. Chem.* **2004**, *2*, 2593–2603.

(7) Mindt, T. L.; Müller, C.; Melis, M.; Jong, M. de; Schibli, R. *Bioconjugate Chem.* **2008**, *19*, 1689–1695.

(8) Struthers, H.; Mindt, T. L.; Schibli, R. *Dalton Trans.* **2010**, *39*, 675–696.

(9) Lo, K. K.-W.; Choi, A. W.-T.; Law, W. H.-T. *Dalton Trans.* **2012**, *41*, 6021–6047.

(10) Lo, K. K.-W.; Louie, M.-W.; Zhang, K. Y. *Coord. Chem. Rev.* **2010**, *254*, 2603–2622.

(11) Balasingham, R. G.; Coogan, M. P.; Thorp-Greenwood, F. L. *Dalton Trans.* **2011**, *40*, 11663–11674.

(12) Zhao, Q.; Huang, C.; Li, F. *Chem. Soc. Rev.* **2011**, *40*, 2508–2524.

(13) Pitchumony, T. S.; Banevicius, L.; Janzen, N.; Zubieta, J.; Valliant, J. F. *Inorg. Chem.* **2013**, *52*, 13521–13528.

(14) Yazdani, A.; Janzen, N.; Banevicius, L.; Czorny, S.; Valliant, J. F. *Inorg. Chem.* **2015**, *54*, 1728–1736.

(15) Uppal, B. S.; Booth, R. K.; Ali, N.; Lockwood, C.; Rice, C. R.; Elliott, P. I. P. *Dalton Trans.* **2011**, *40*, 7610–7616.

(16) Kurz, P.; Probst, B.; Spingler, B.; Alberto, R. *Eur. J. Inorg. Chem.* **2006**, *2006*, 2966–2974.

(17) Probst, B.; Guttentag, M.; Rodenberg, A.; Hamm, P.; Alberto, R. *Inorg. Chem.* **2011**, *50*, 3404–3412.

(18) Jiang, H.; Kasten, B. B.; Liu, H.; Qi, S.; Liu, Y.; Tian, M.; Barnes, C. L.; Zhang,

H.; Cheng, Z.; Benny, P. D. *Bioconjugate Chem.* **2012**, *23*, 2300–2312.

# 6 Appendix 1 (Supporting Information for Chapter 2)

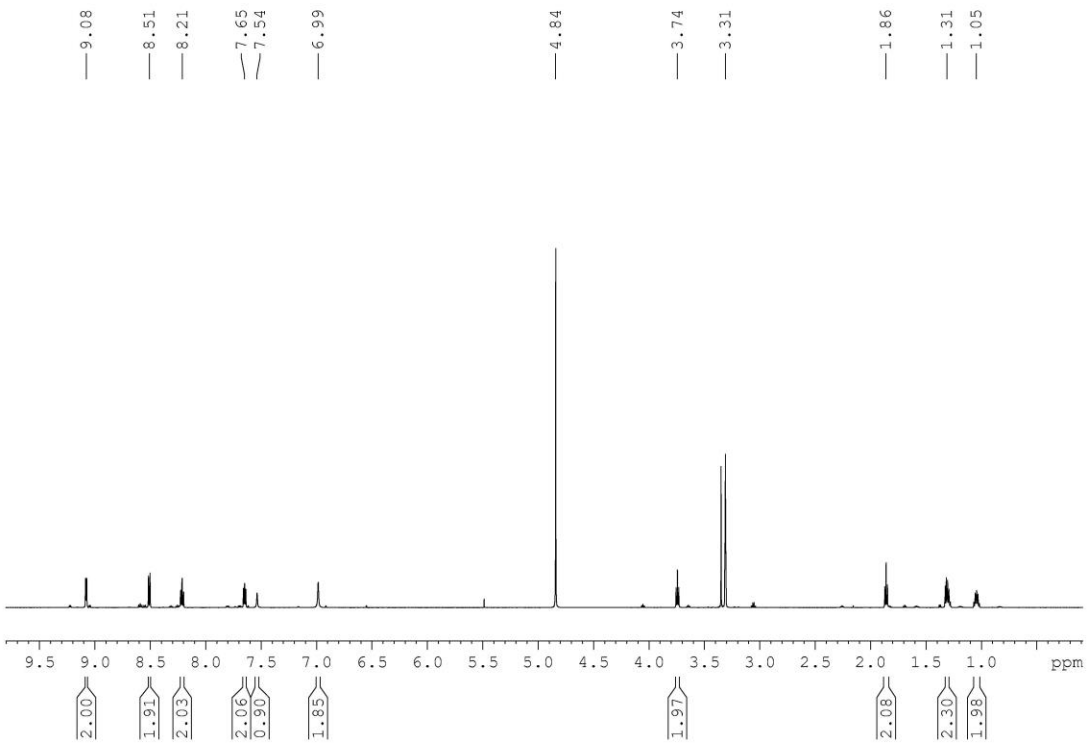


**Figure S 6.1** $^{1}$H NMR spectrum ($CD_3OD$, 600 MHz) of **6a**.

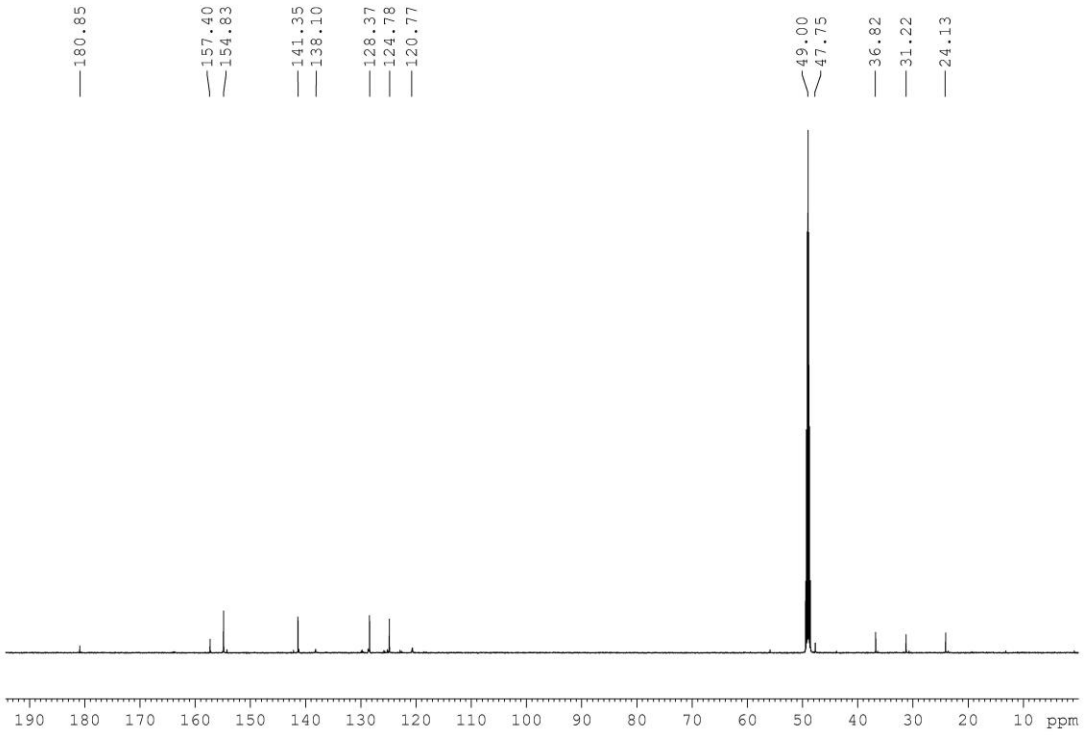


**Figure S 6.2** $^{13}C$ NMR spectrum ($CD_3OD$, 150 MHz) of **6a**.

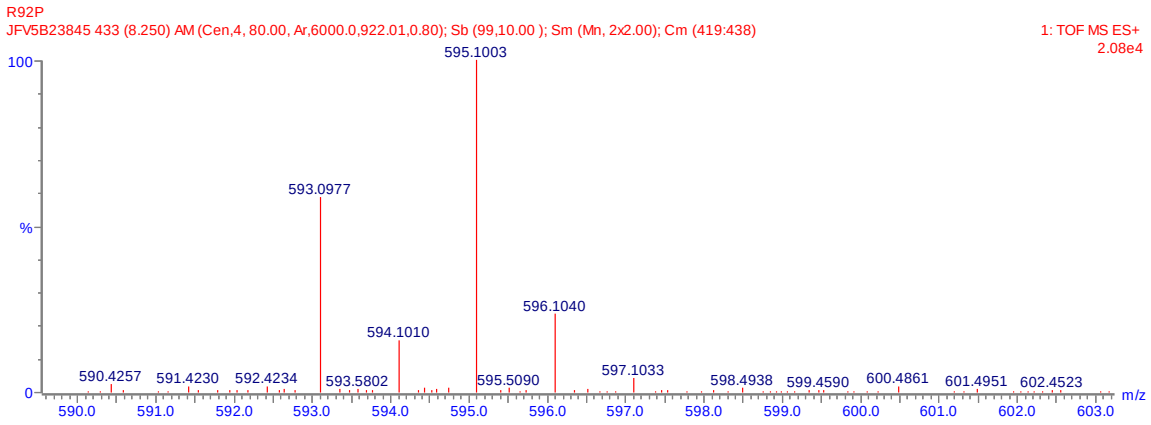


**Figure S 6.3** HRMS of **6a**.

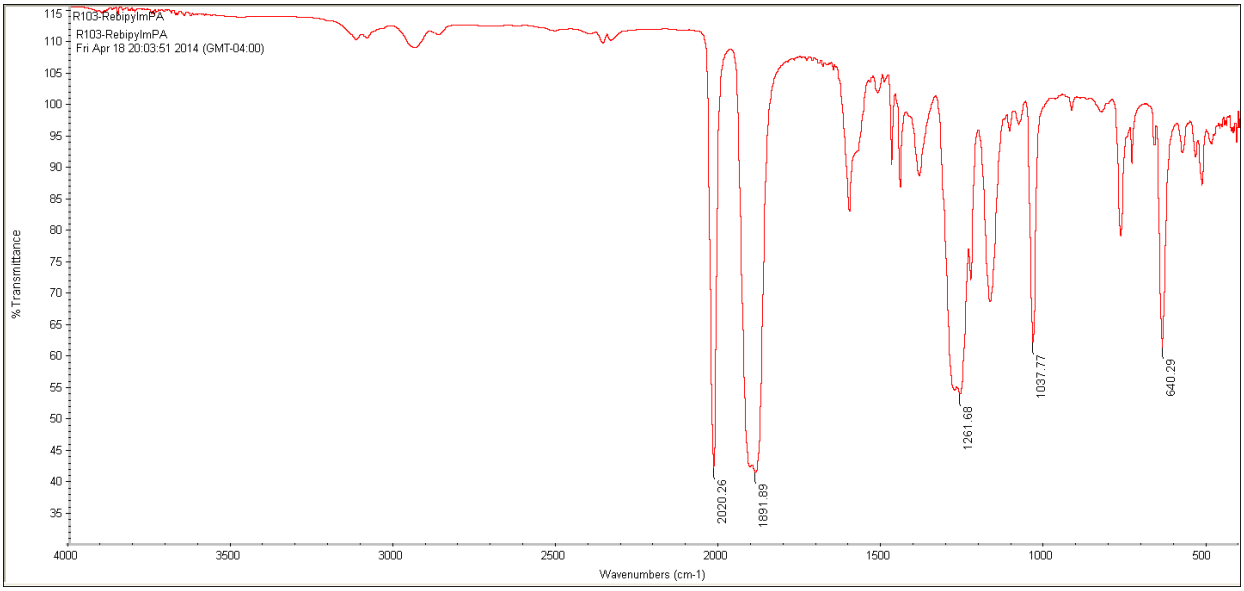


**Figure S 6.4** IR spectrum of **6a**.

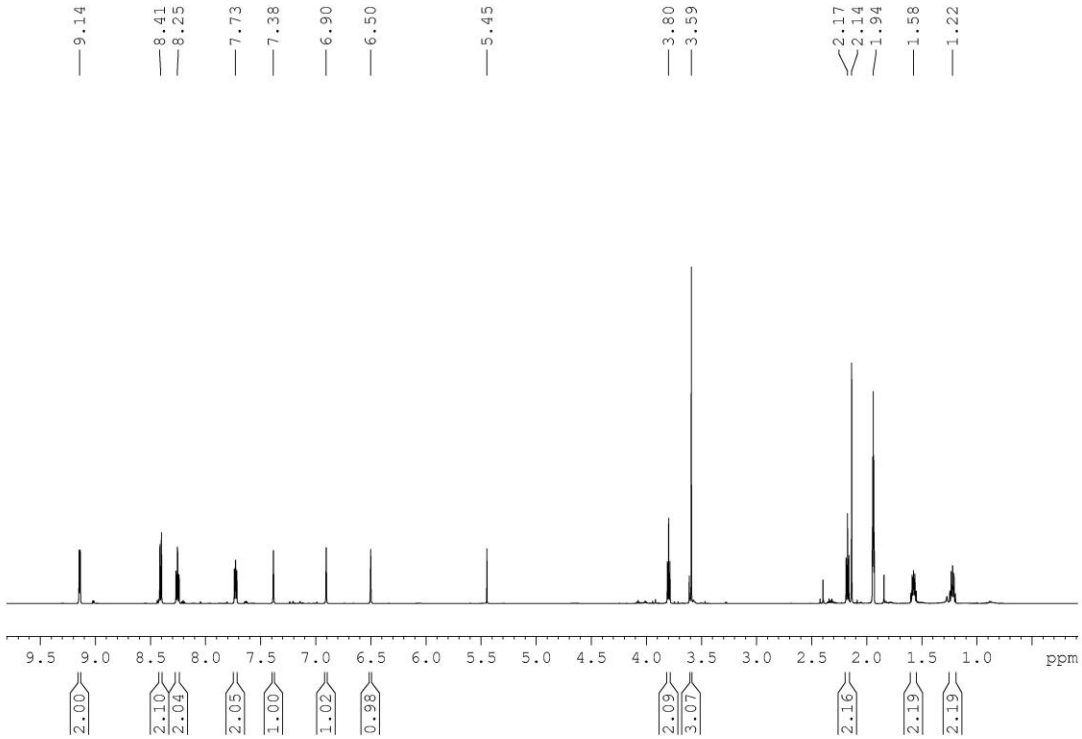


**Figure S 6.5** $^{1}$H NMR spectrum ($CD_3CN$, 600 MHz) of **7a**.

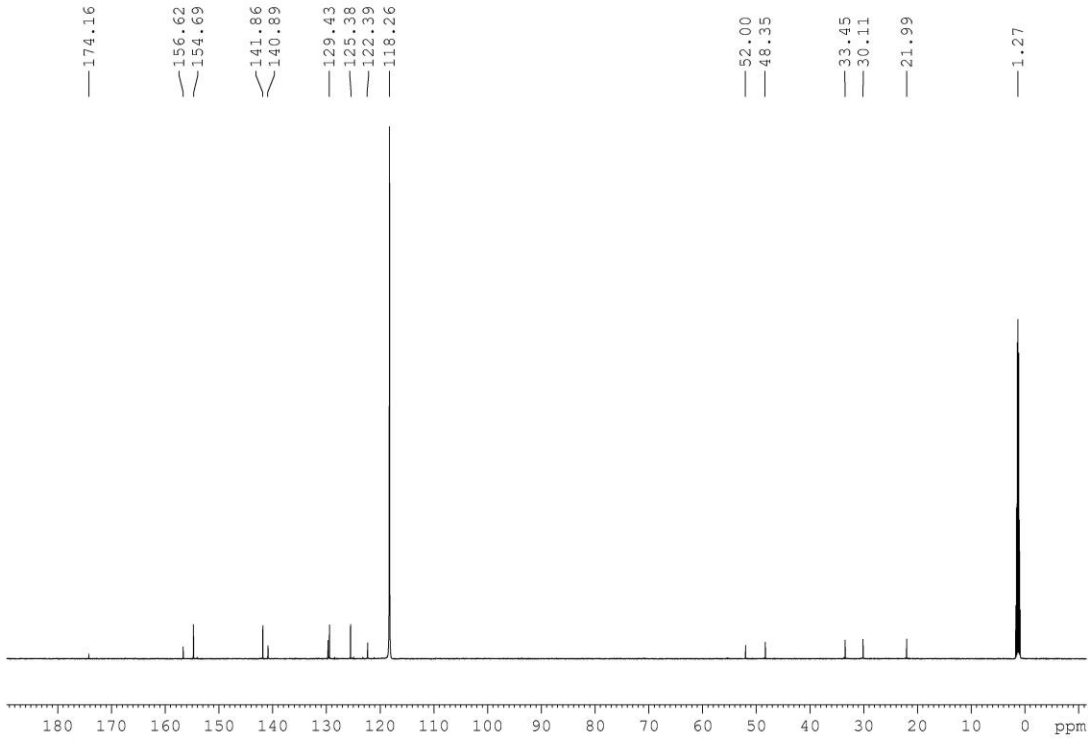


**Figure S 6.6** $^{13}C$ NMR spectrum ($CD_3CN$, 150 MHz) of **7a**.

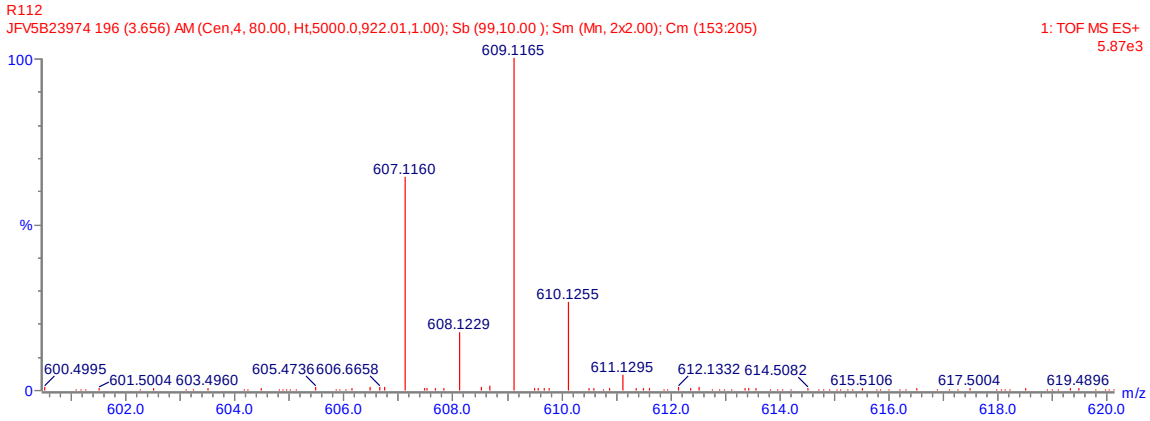


**Figure S 6.7** HRMS of **7a**.

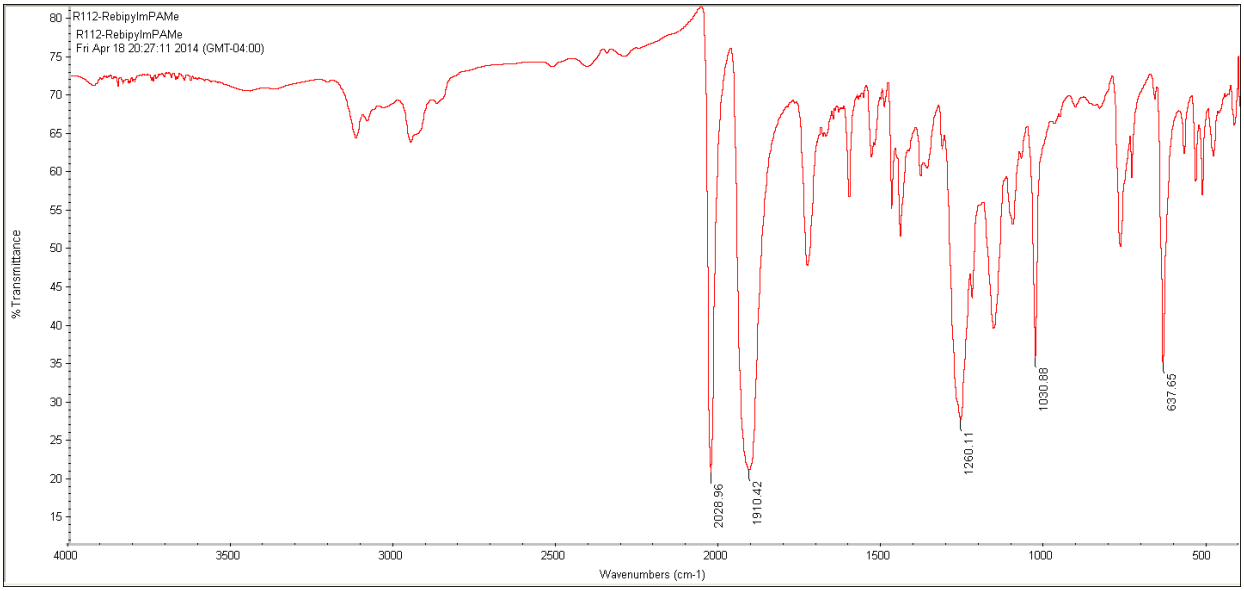


**Figure S 6.8** IR spectrum of **7a**.

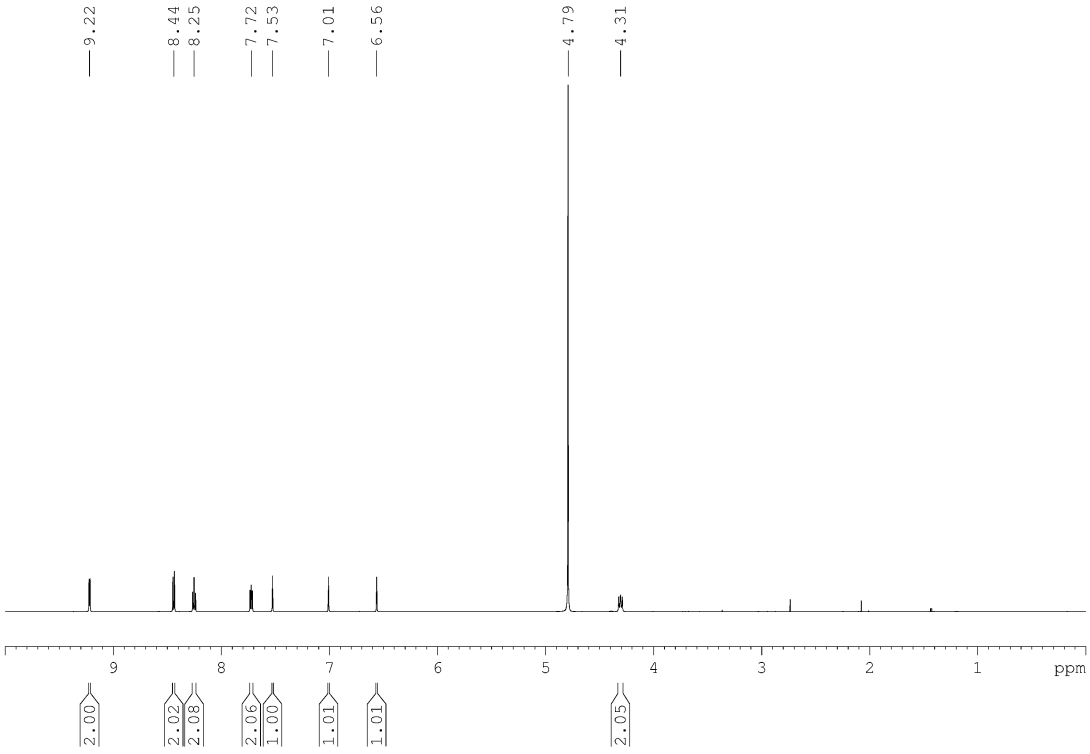


**Figure S 6.9** $^{1}$H NMR spectrum ($D_2O$, 600 MHz) of **8a**.

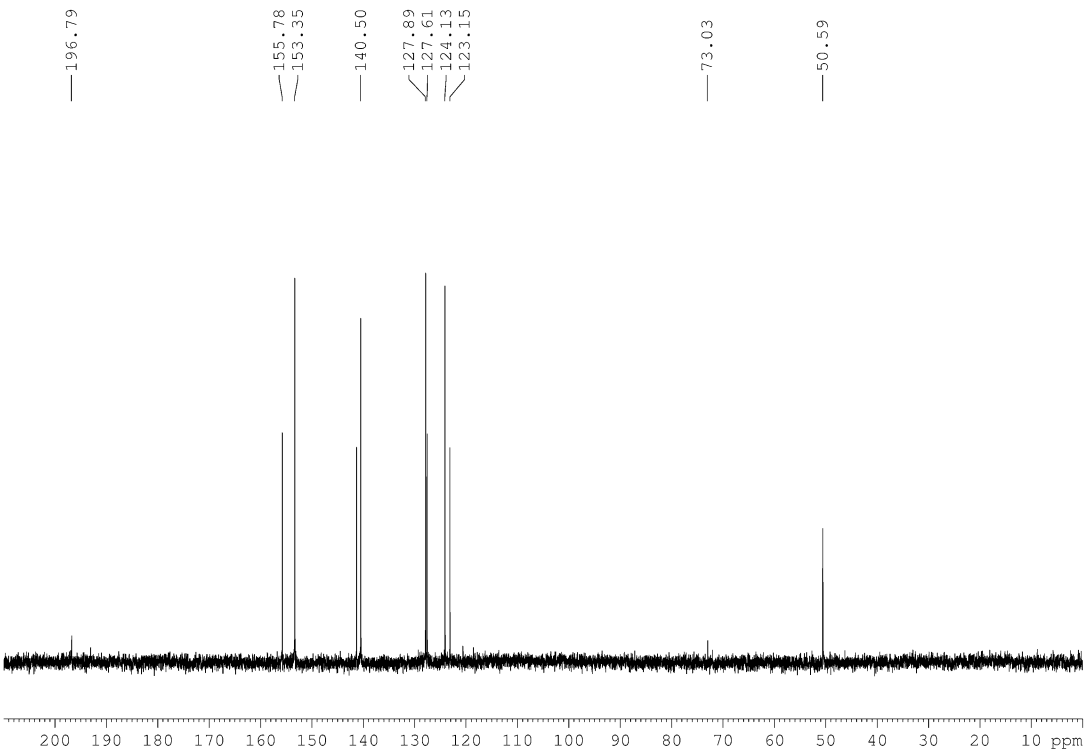


**Figure S 6.10** $^{13}C$ NMR spectrum ($D_2O$, 150 MHz) of **8a**.

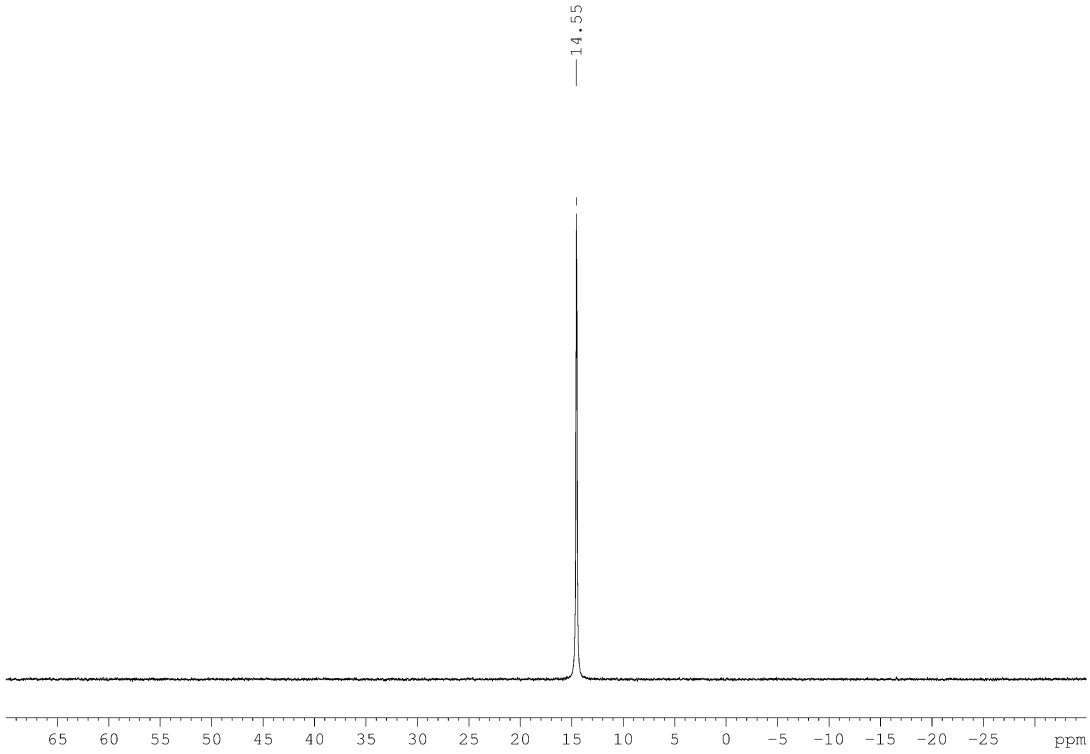


**Figure S 6.11** $^{31}$P NMR spectrum ($D_2O$, 242 MHz) of **8a**.

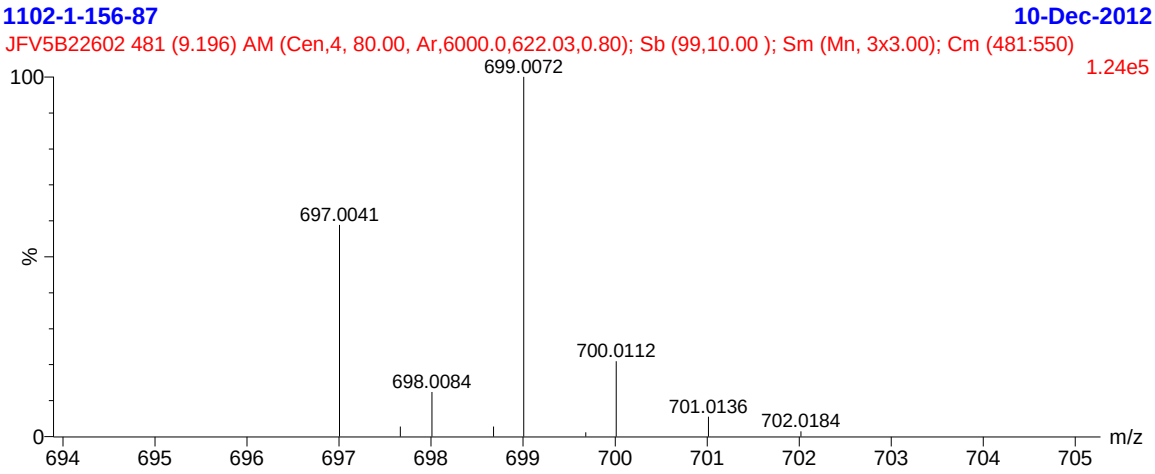


**Figure S 6.12** HRMS of **8a**.

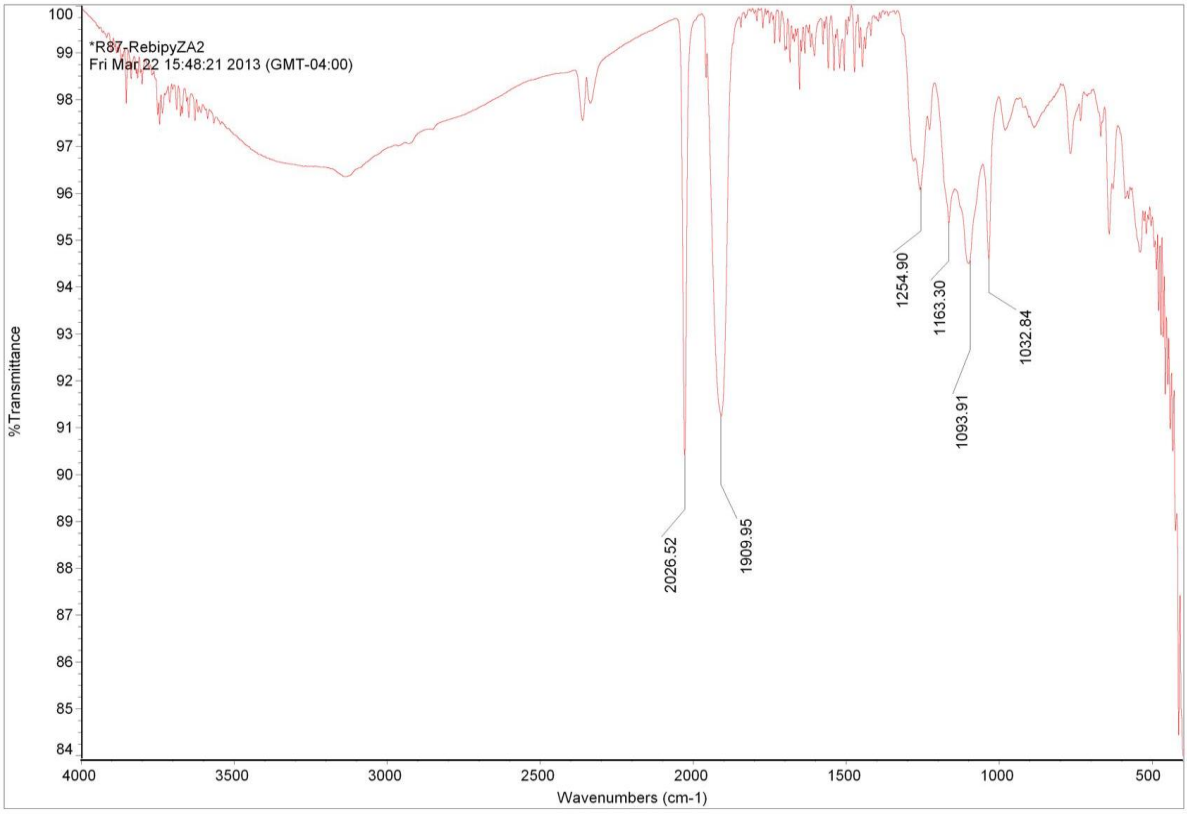


**Figure S 6.13** IR spectrum of **8a**.

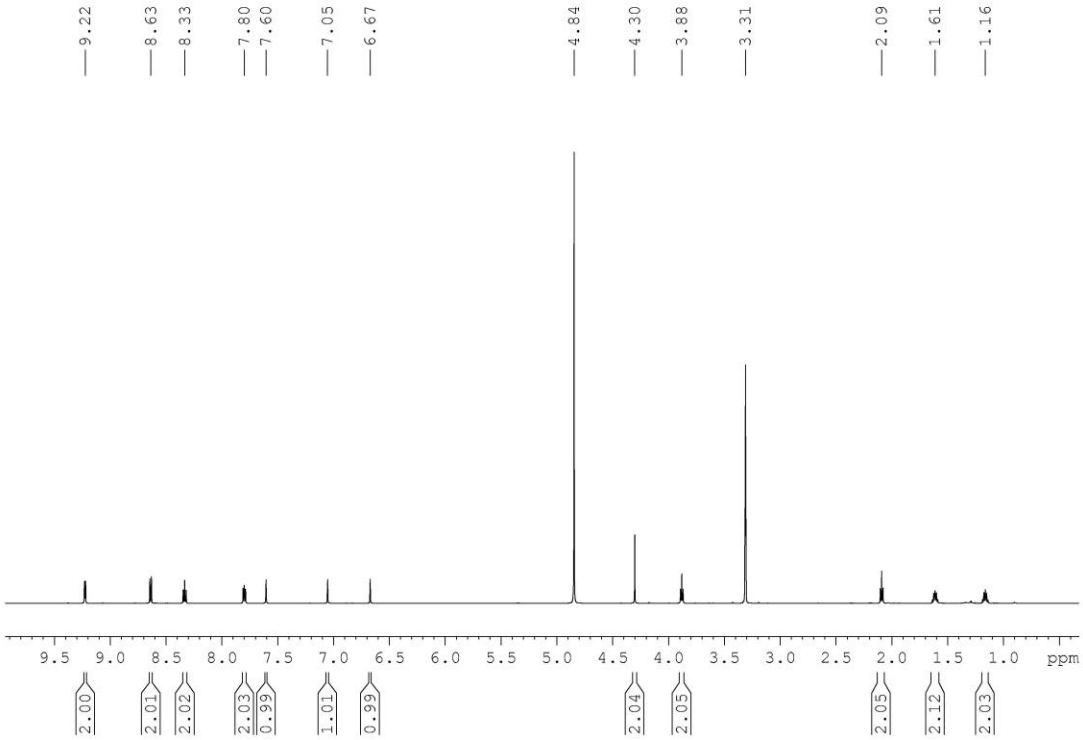


**Figure S 6.14** $^{1}$H NMR spectrum ($CD_3OD$, 600 MHz) of **9a**.

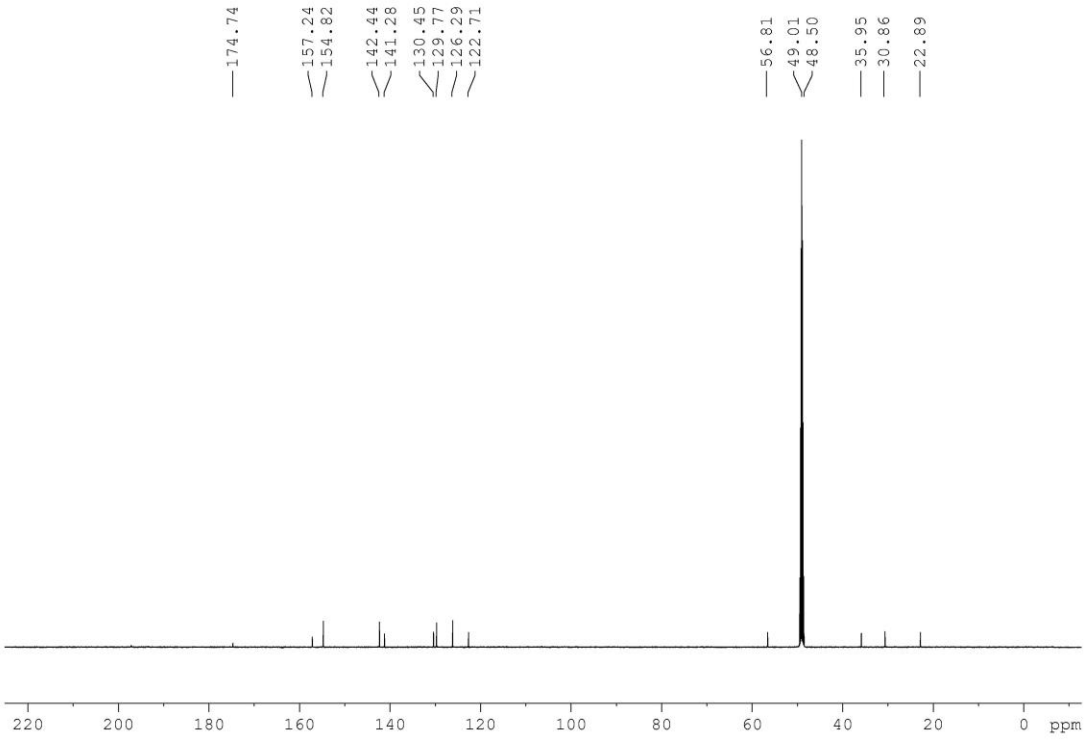


**Figure S 6.15** $^{13}$C NMR spectrum ($CD_3OD$, 150 MHz) of **9a**.

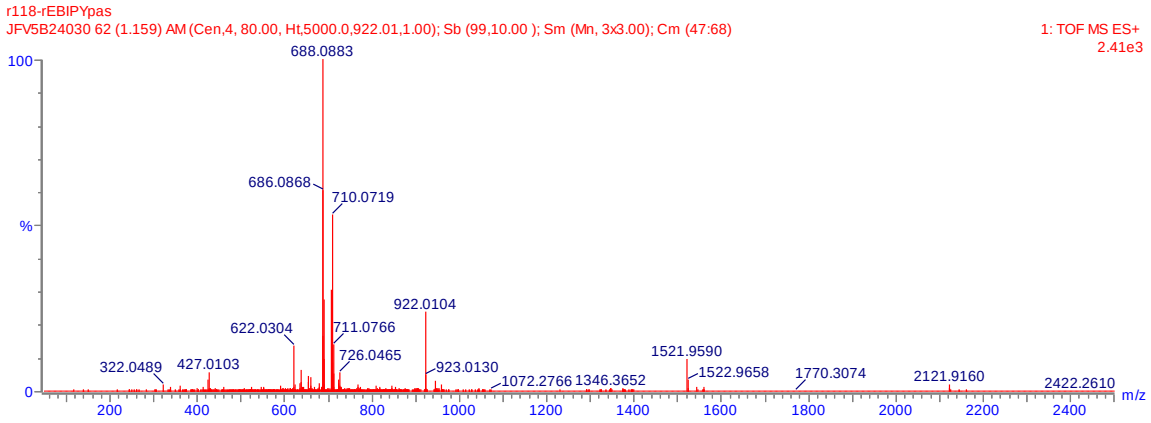


**Figure S 6.16** HRMS of **9a**.

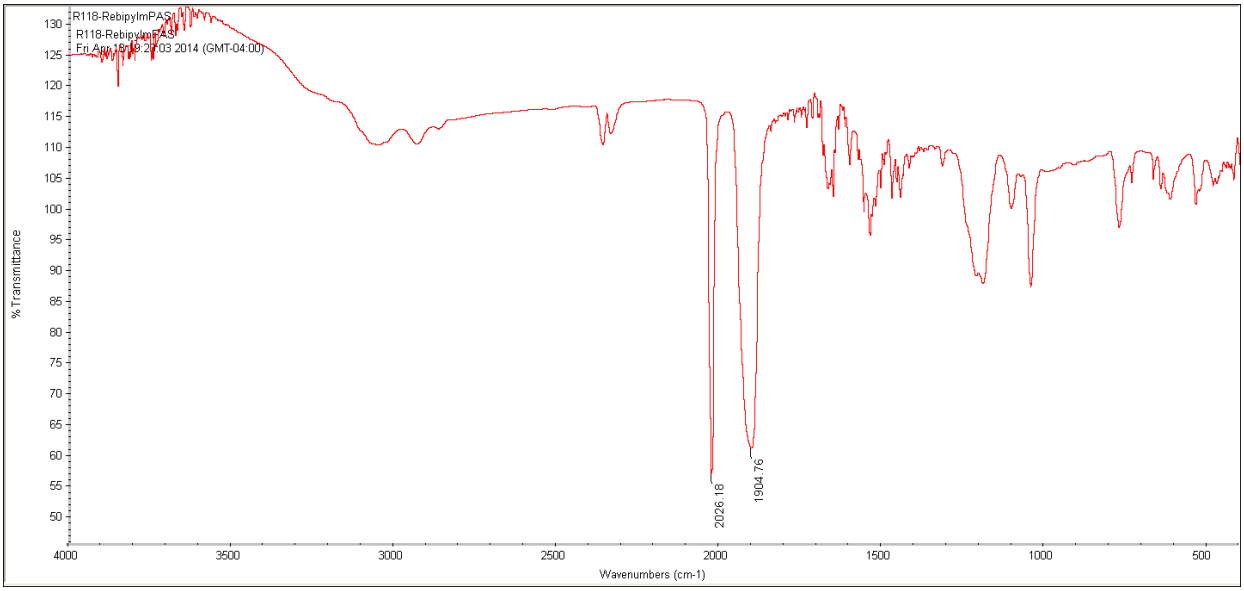


**Figure S 6.17** IR spectrum of **9a**.

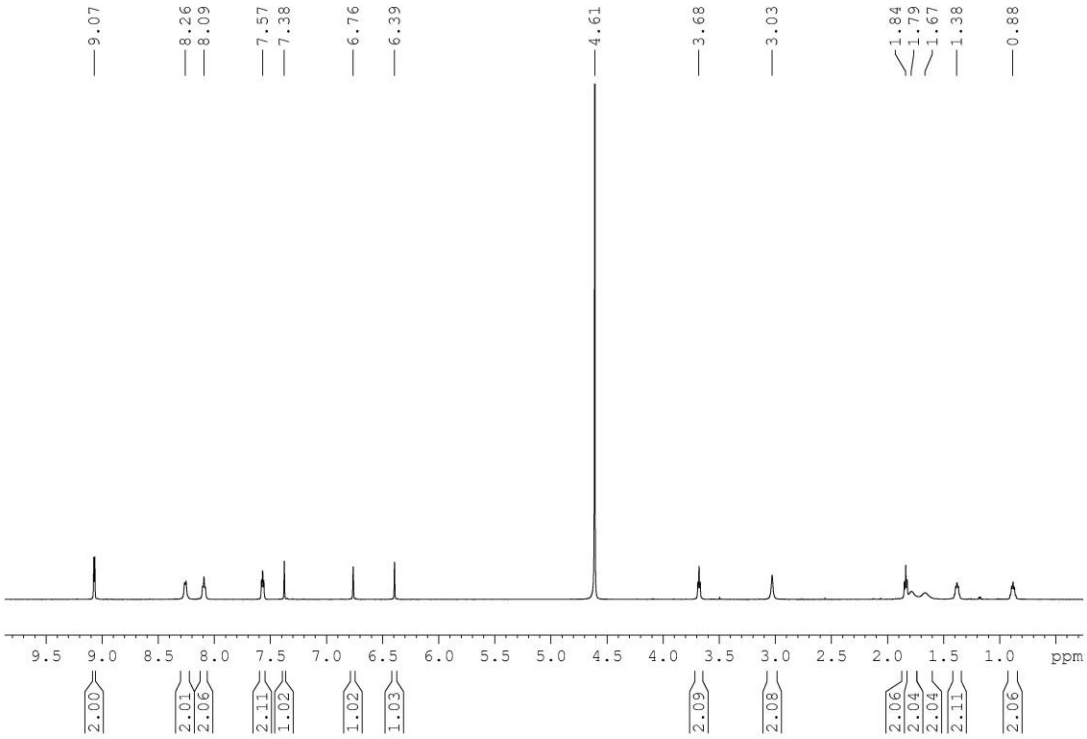


**Figure S 6.18** $^{1}$H NMR spectrum ($D_2O$, 600 MHz) of **10a**.

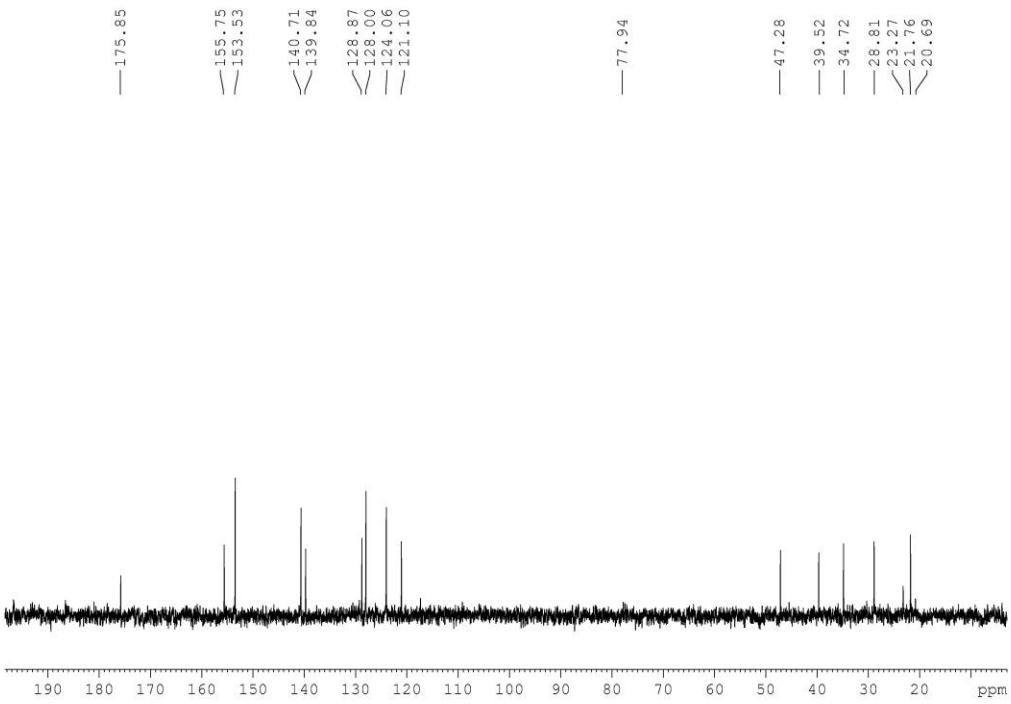


**Figure S 6.19** $^{13}C$ NMR spectrum ($D_2O$, 150 MHz) of **10a**.

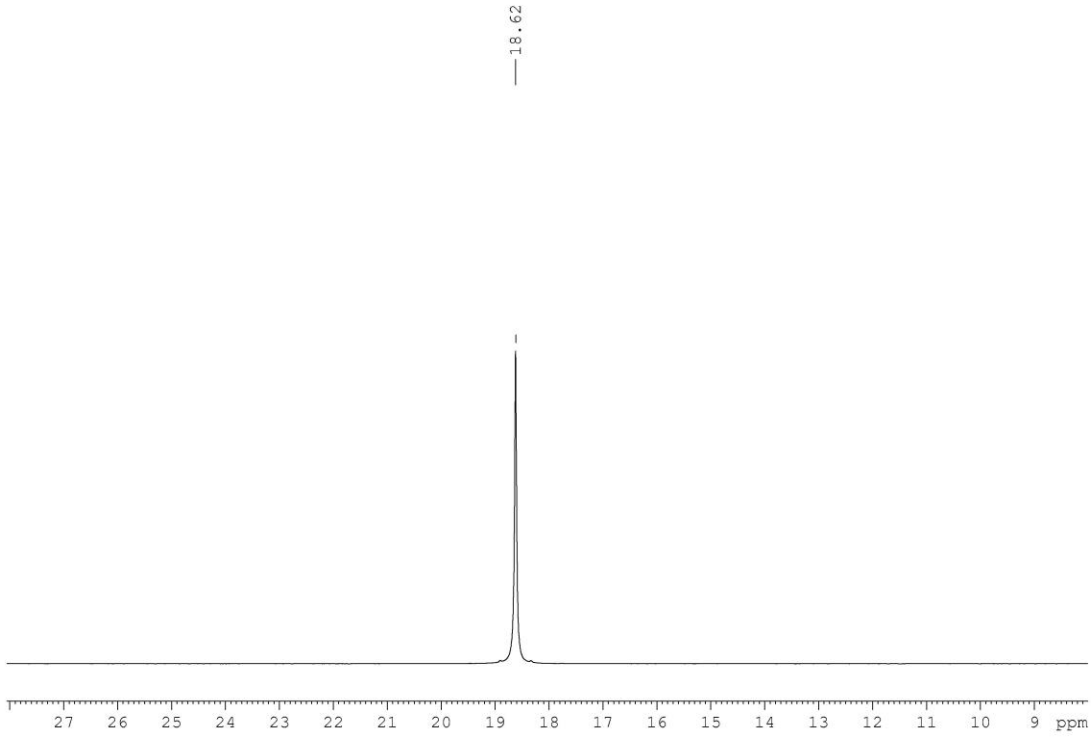


**Figure S 6.20** $^{31}$P NMR spectrum ($D_2O$, 242 MHz) of **10a**.

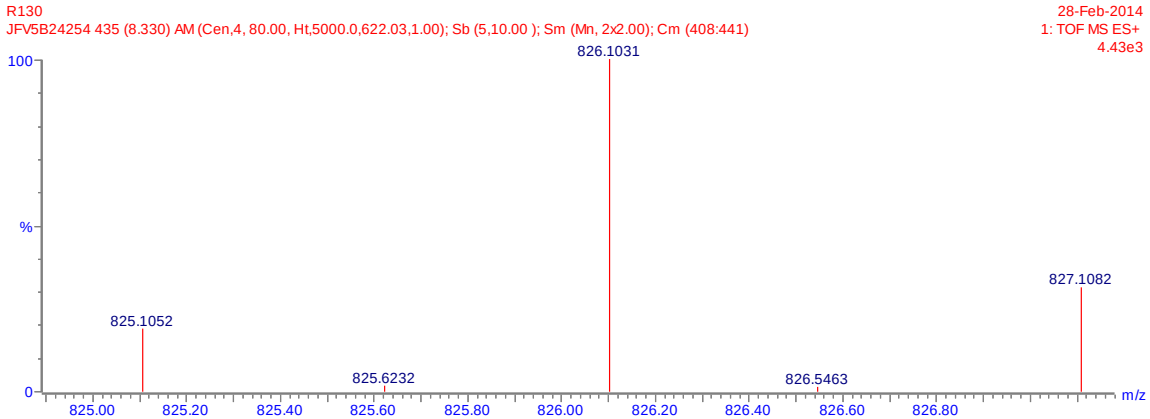


**Figure S 6.21** HRMS of **10a**.

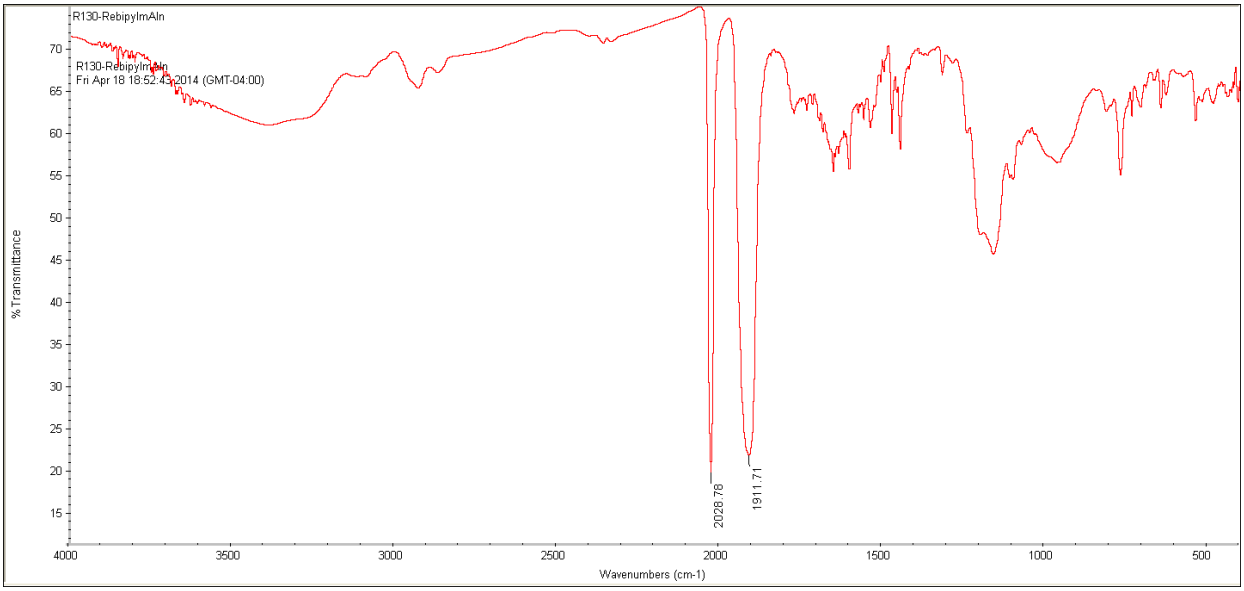


**Figure S 6.22** IR spectrum of **10a**.

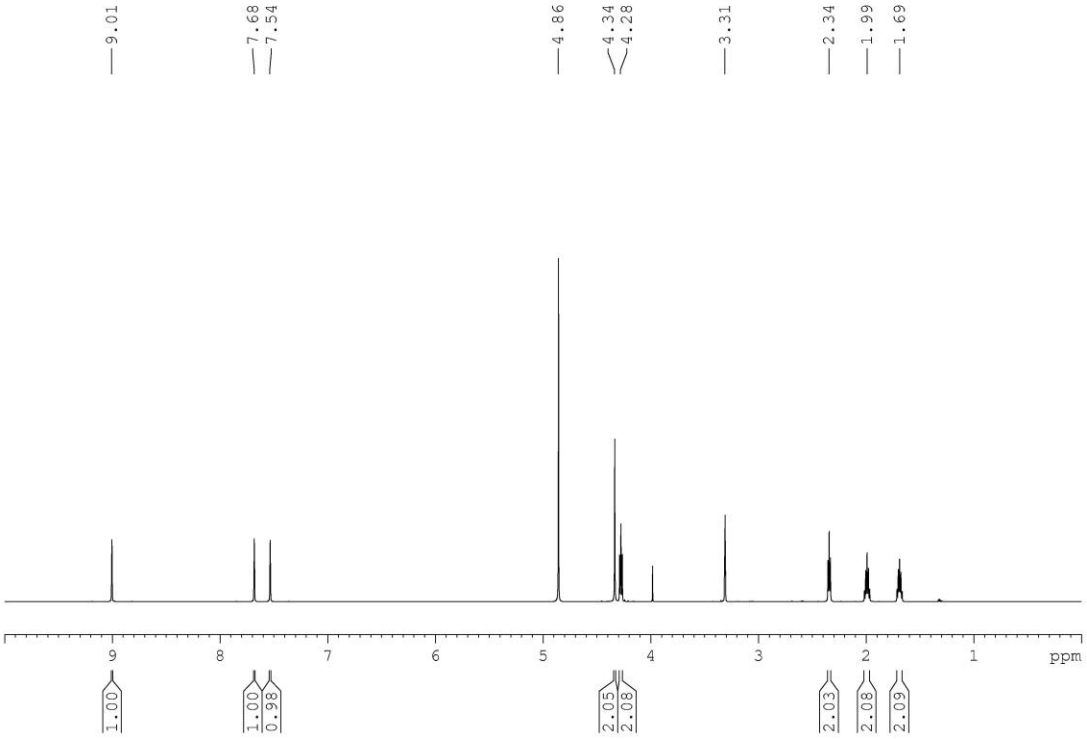


**Figure S 6.23** $^{1}$H NMR spectrum ($CD_3OD$, 600 MHz) of **12**.

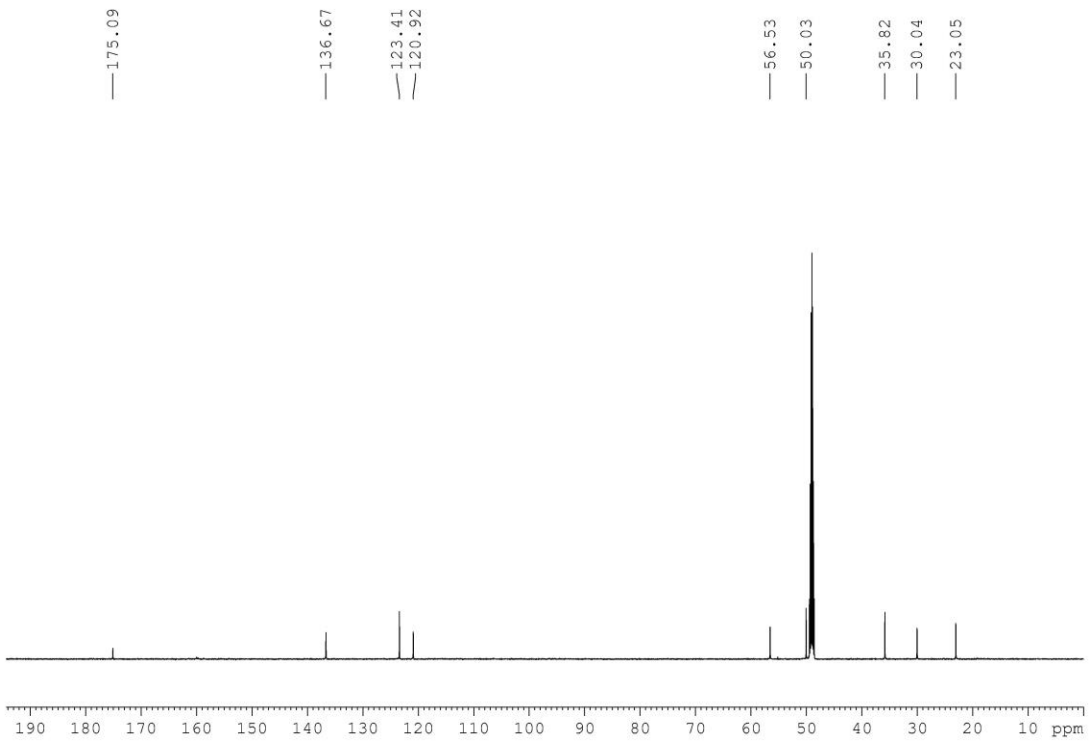


**Figure S 6.24** $^{13}C$ NMR spectrum ($CD_3OD$, 150 MHz) of **12.**

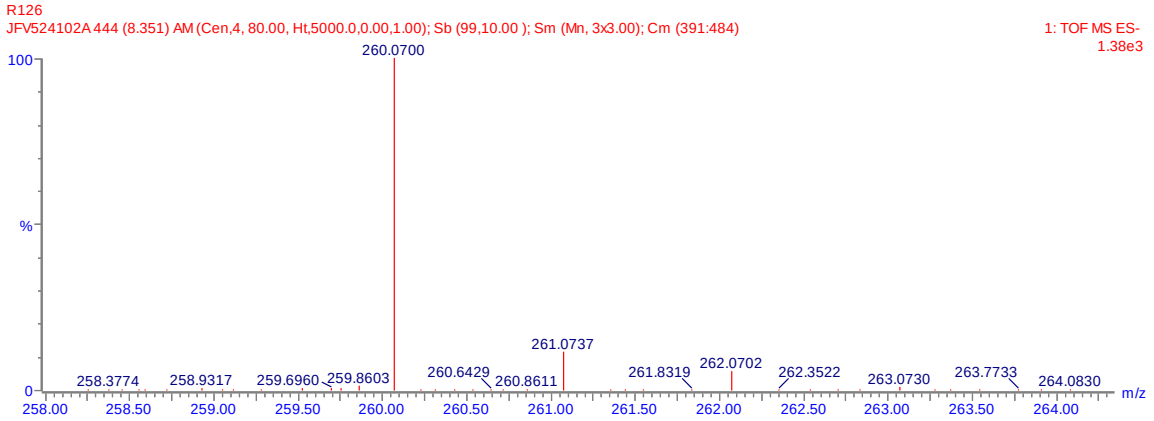


**Figure S 6.25** HRMS of **12**.

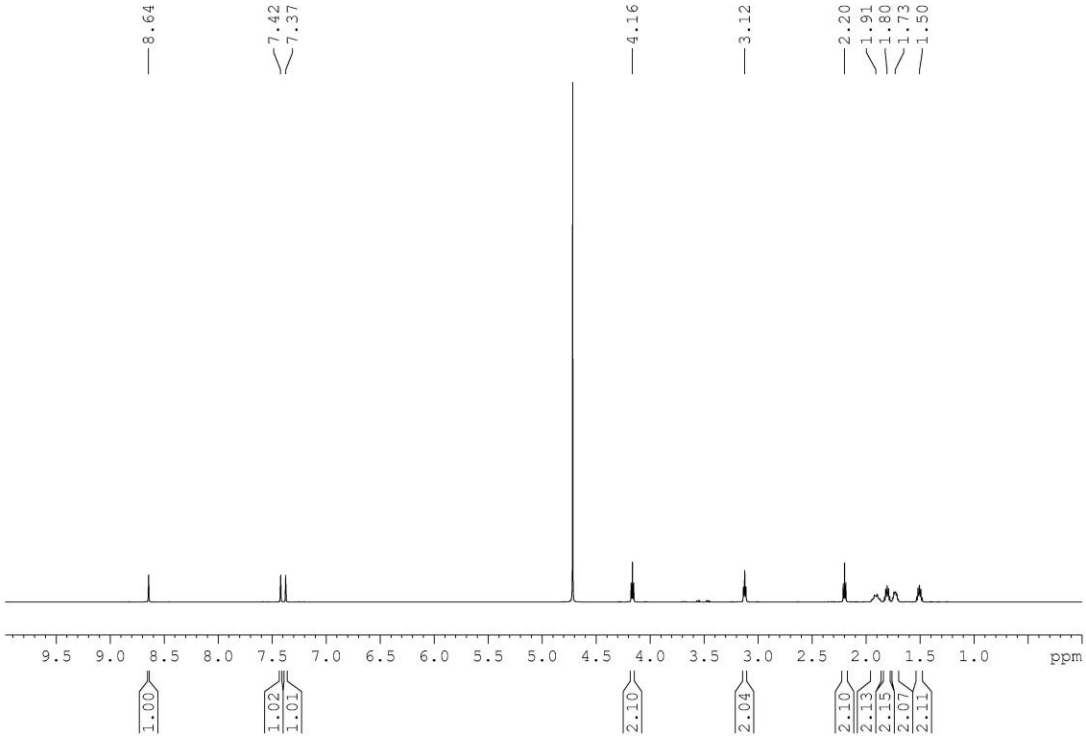


**Figure S 6.26** $^{1}$H NMR spectrum ($D_2O$, 600 MHz) of **13**.

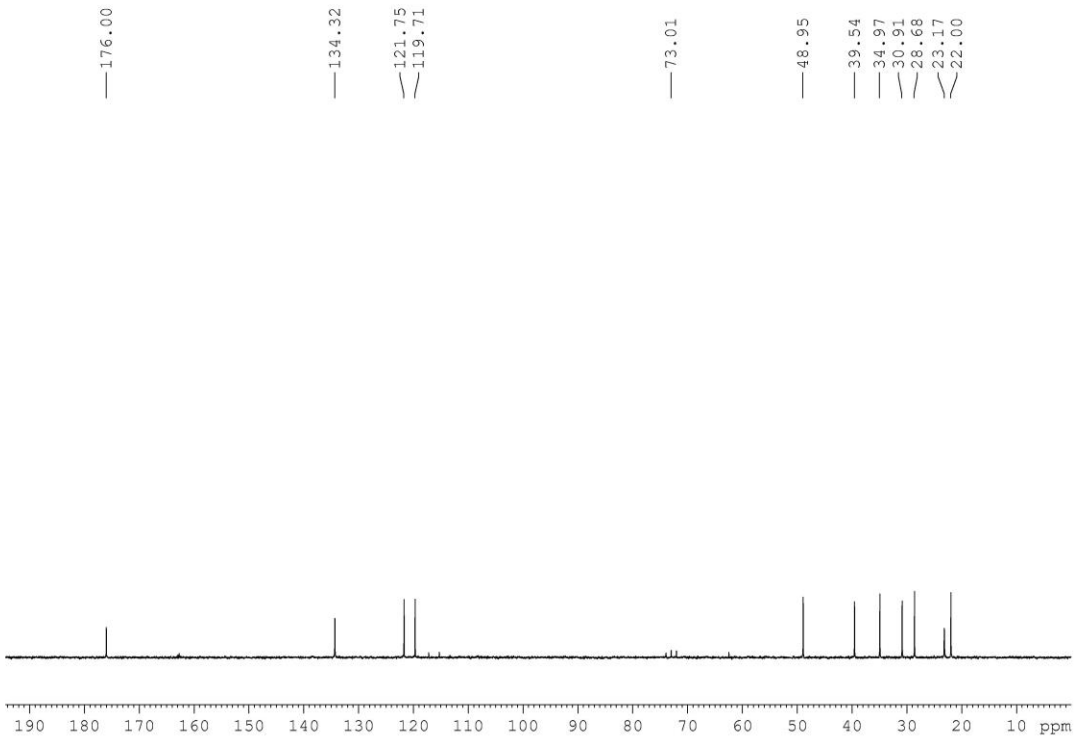


**Figure S 6.27** $^{13}C$ NMR spectrum ($D_2O$, 150 MHz) of **13**.

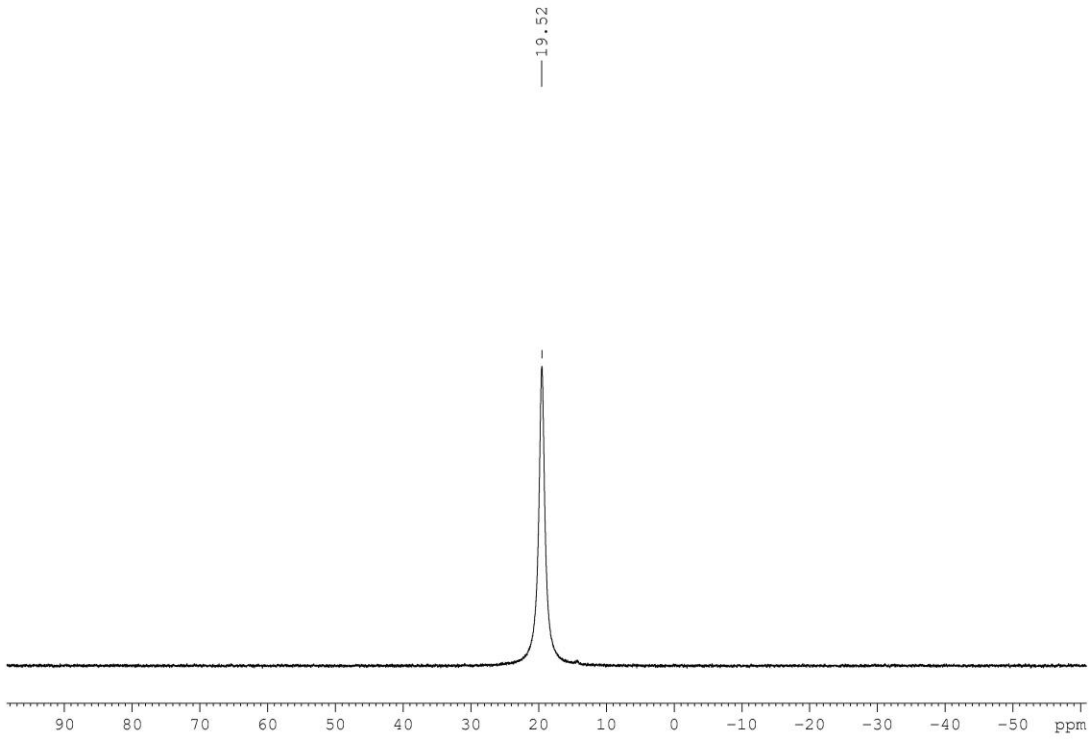


**Figure S 6.28** $^{31}$P NMR spectrum ($D_2O$, 242 MHz) of **13**.

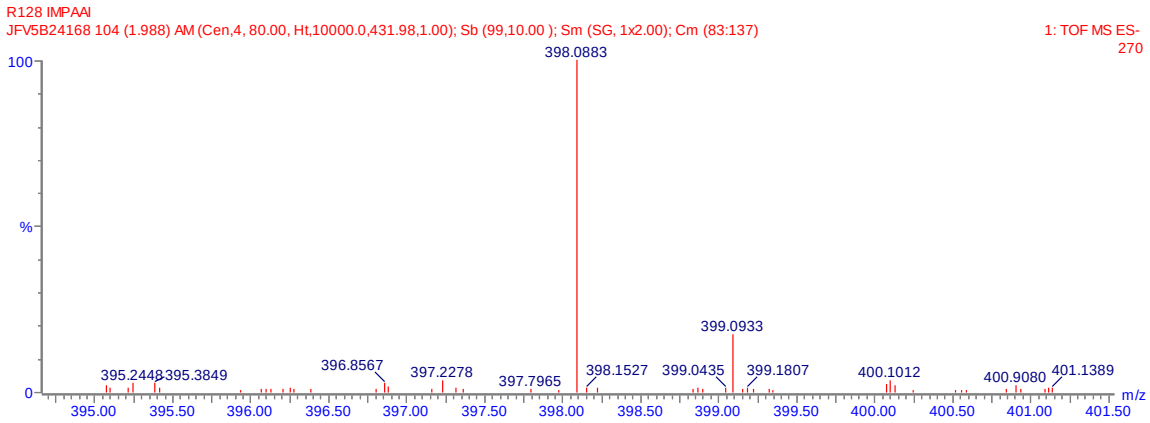


**Figure S 6.29** HRMS of **13**.

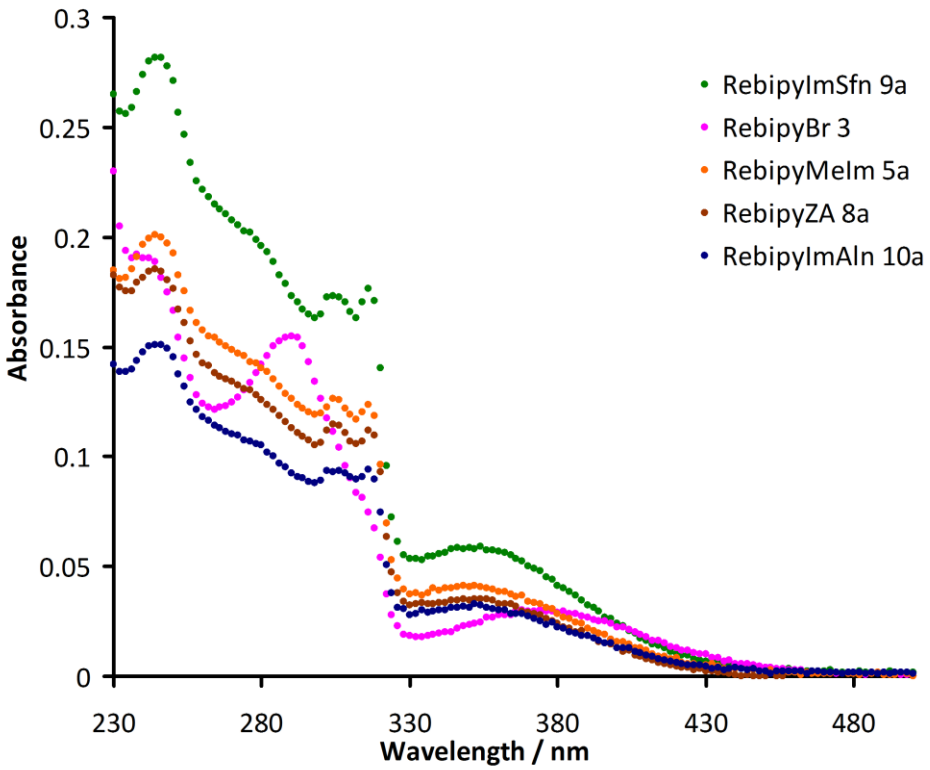


**Figure S 6.30** Absorption spectra for compounds **3**, **5a**, **8a**, **9a**, **10a** (50 µM in $H_2O$).

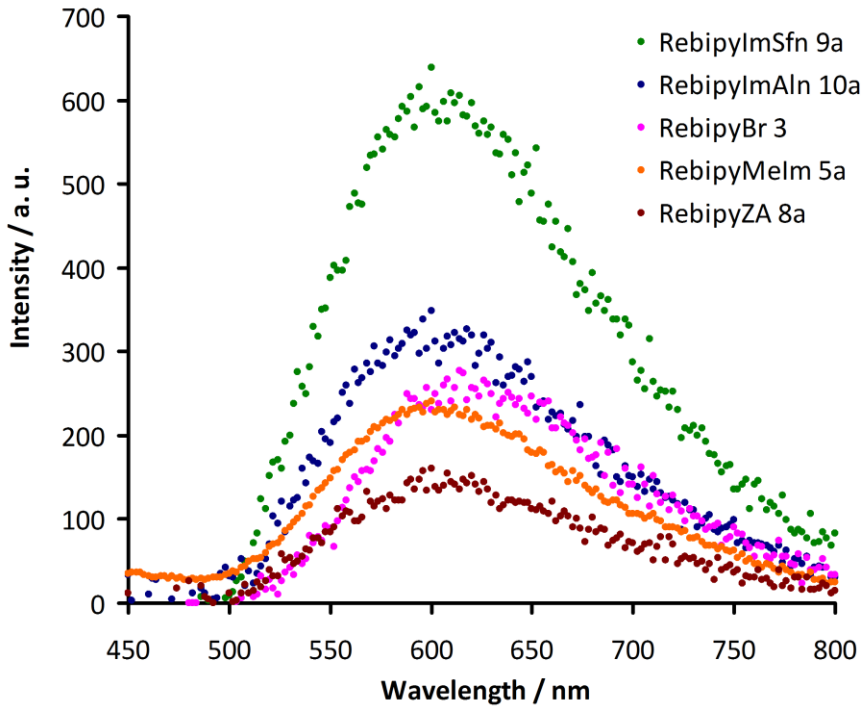


**Figure S 6.31** Emission spectra for compounds **3**, **5a**, **8a**, **9a**, **10a** (50 µM in $H_2O$).

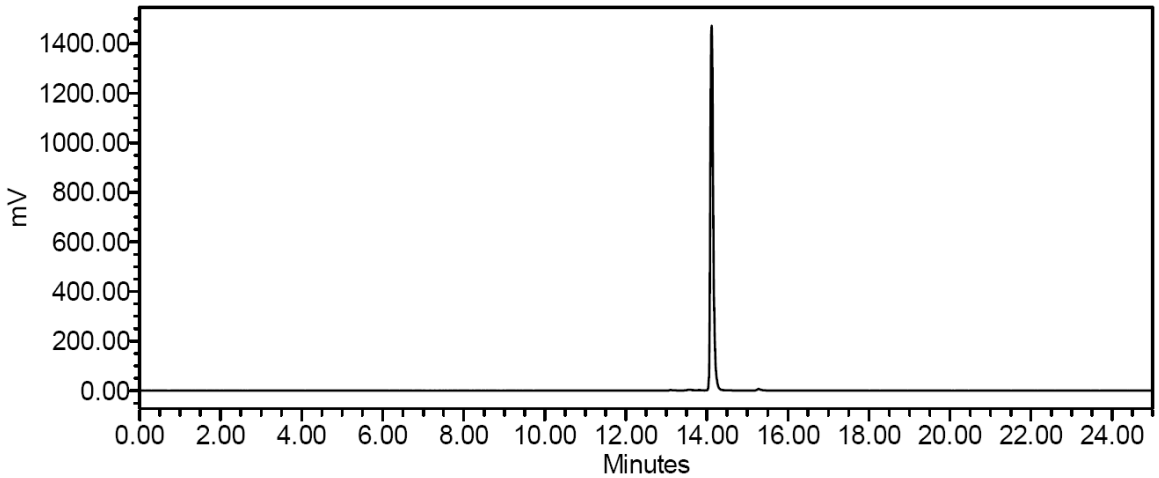


**Figure S 6.32** γ-HPLC chromatogram at 1 h following histidine challenge to $[^{99m}Tc(CO)_3(bipy)(MeIm)]^+$ **5b**.

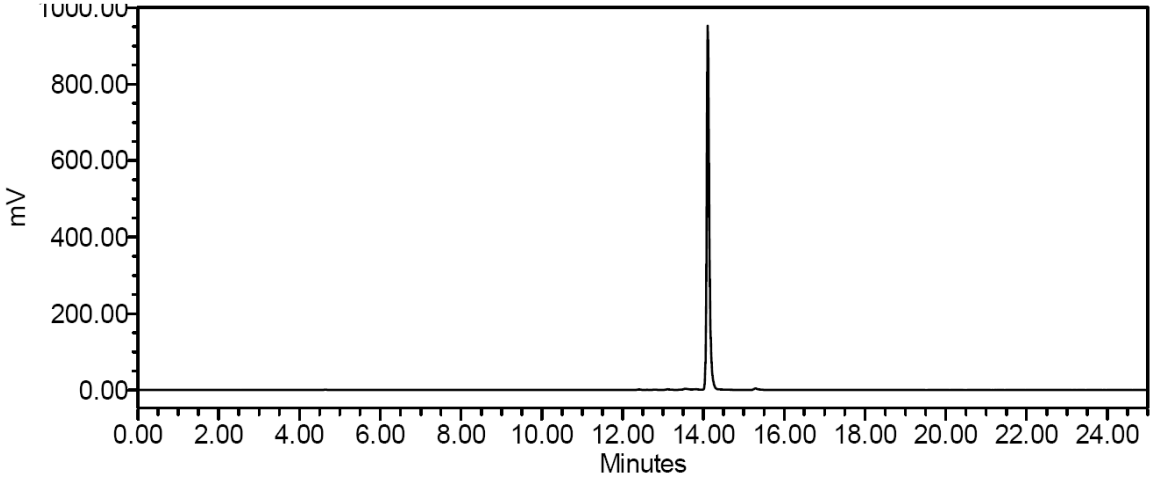


**Figure S 6.33** γ-HPLC chromatogram at 2 h following histidine challenge to $[^{99m}Tc(CO)_3(bipy)(MeIm)]^+$ **5b**.

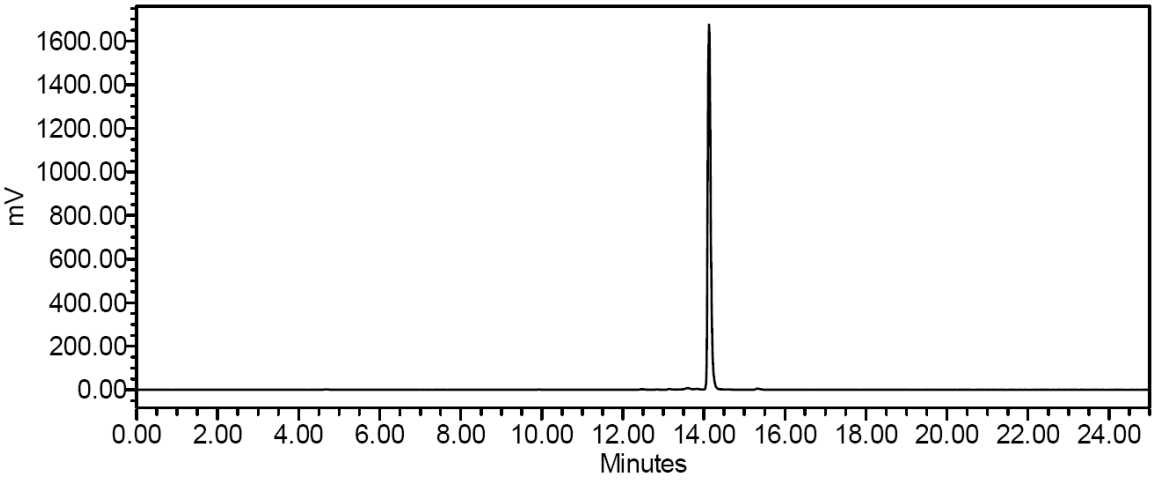


**Figure S 6.34** γ-HPLC chromatogram at 3 h following histidine challenge to $[^{99m}Tc(CO)_3(bipy)(MeIm)]^+$ **5b**.

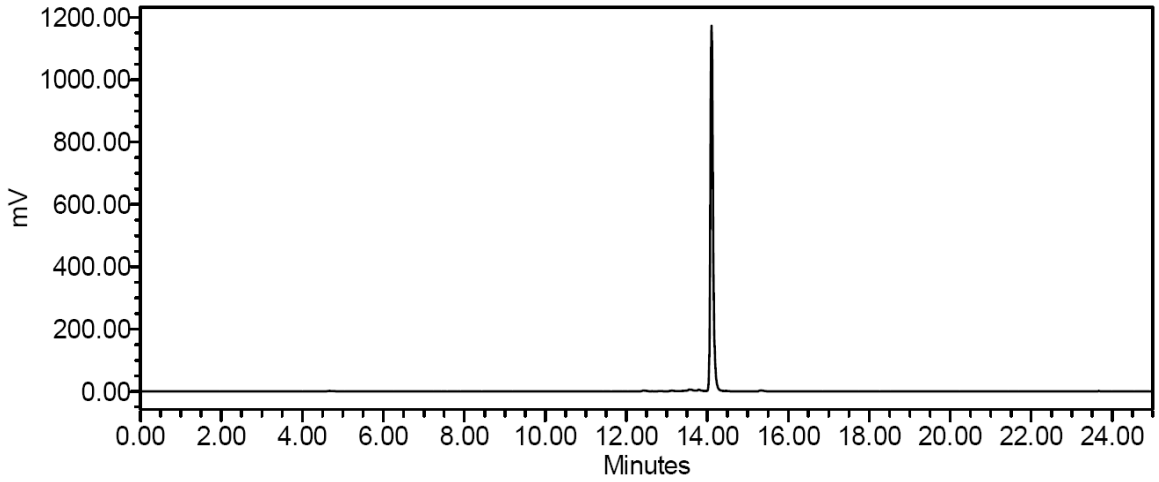


**Figure S 6.35** γ-HPLC chromatogram at 6 h following histidine challenge to $[^{99m}Tc(CO)_3(bipy)(MeIm)]^+$ **5b.**

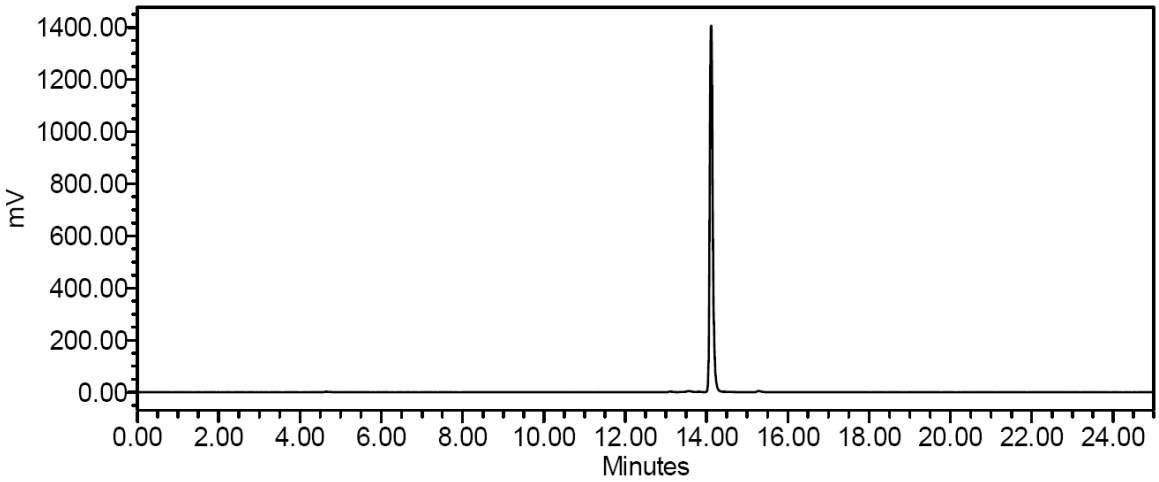


**Figure S 6.36** γ-HPLC chromatogram at 1 h following cysteine challenge to $[^{99m}Tc(CO)_3(bipy)(MeIm)]^+$ **5b**.

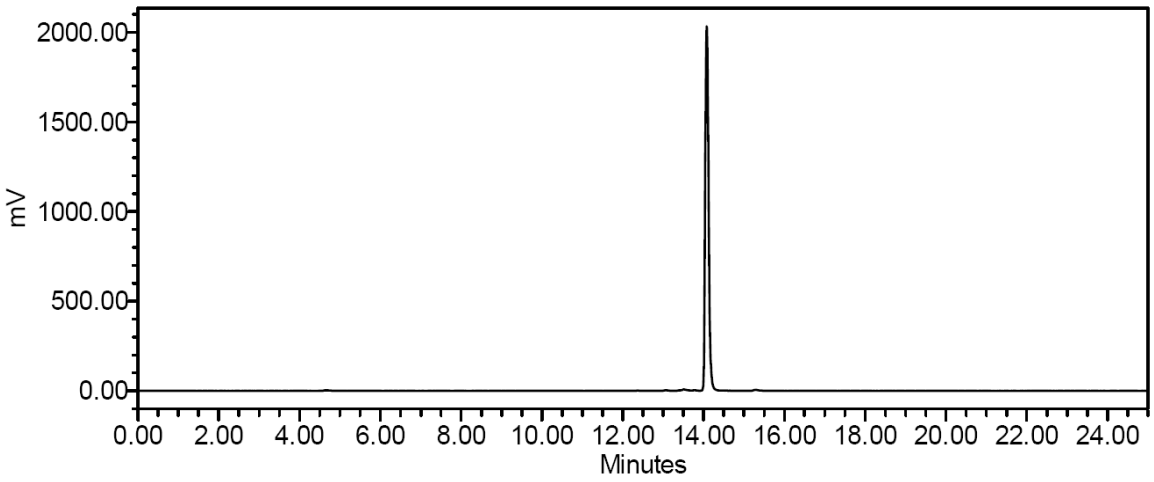


**Figure S 6.37** γ-HPLC chromatogram at 3 h following cysteine challenge to $[^{99m}Tc(CO)_3(bipy)(MeIm)]^+$ **5b**.

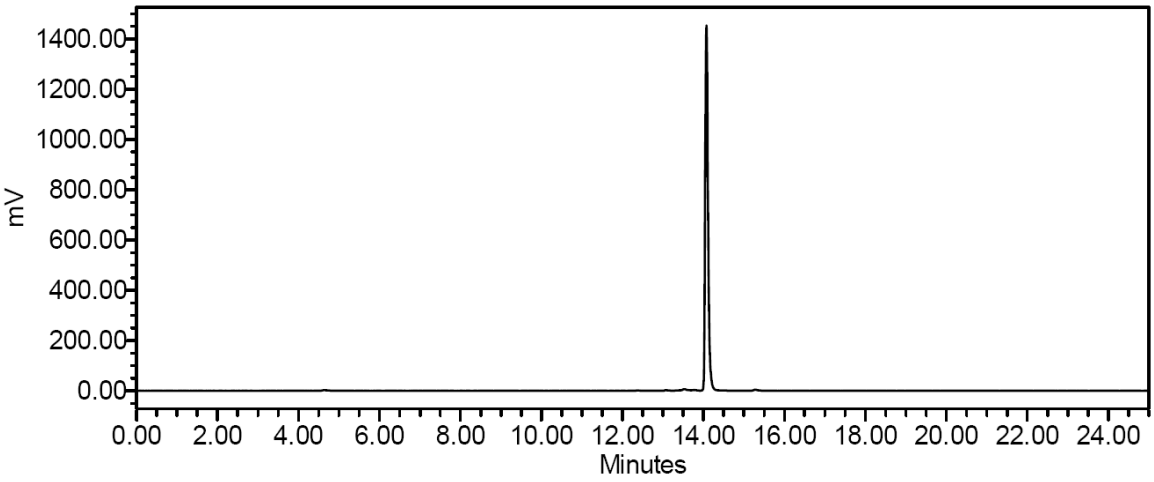


**Figure S 6.38** γ-HPLC chromatogram at 6 h following cysteine challenge to $[^{99m}Tc(CO)_3(bipy)(MeIm)]^+$ **5b**.

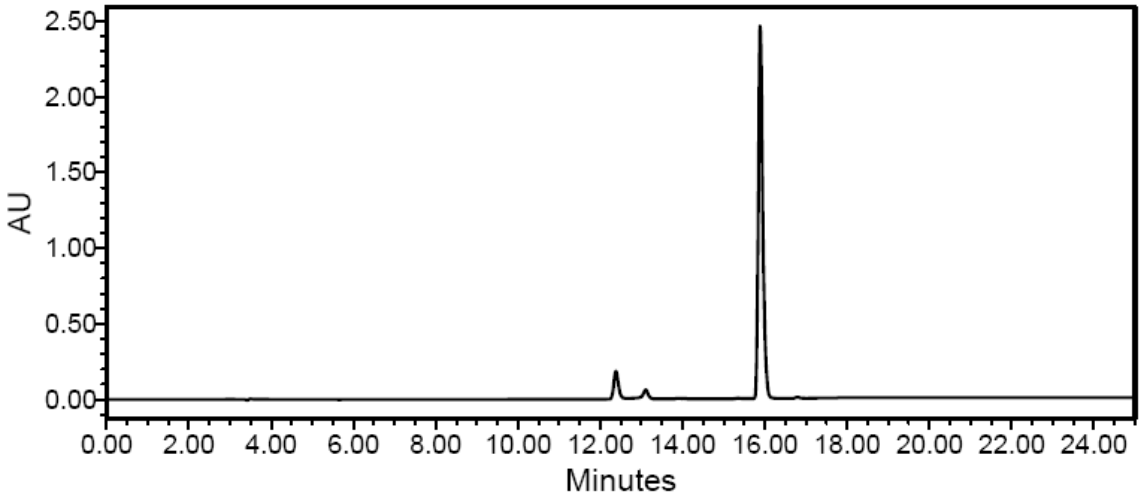


**Figure S 6.39** UV-HPLC chromatogram of $[Re(CO)_3(bipy)Cl]$.

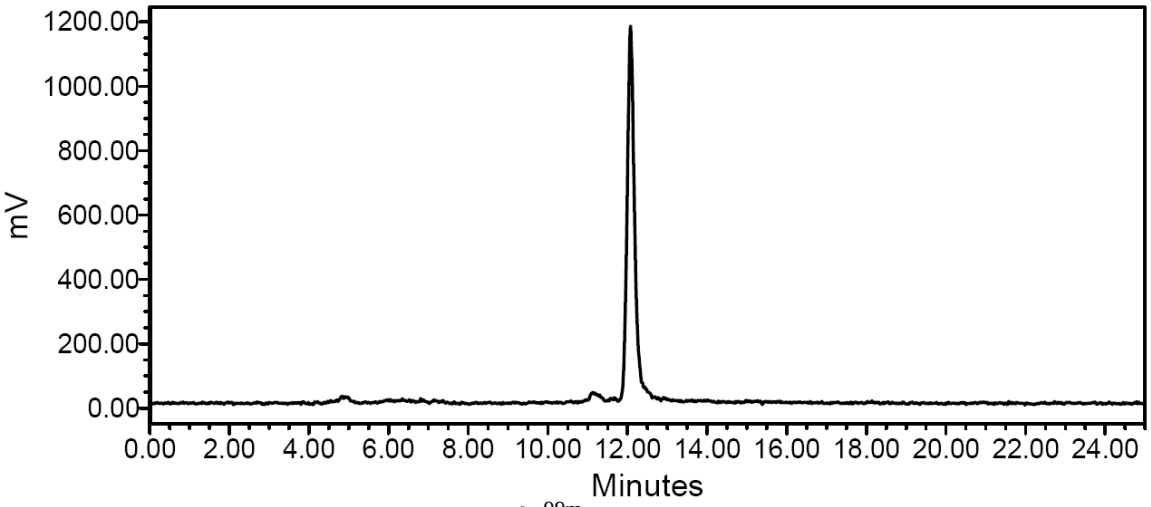


**Figure S 6.40** γ-HPLC chromatogram of $[^{99m}Tc(CO)_3(bipy)ImPA]$ **6b.**

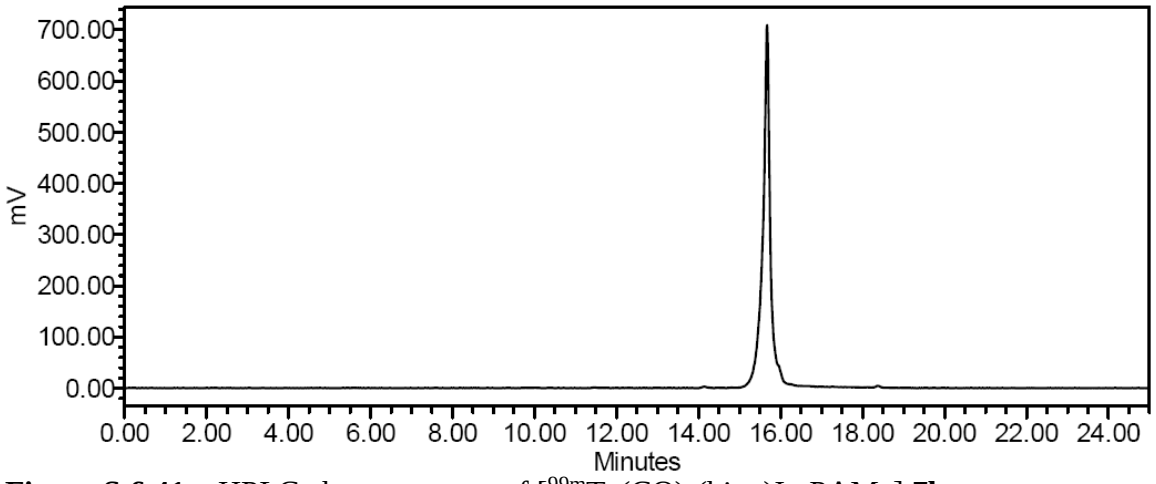


**Figure S 6.41** γ-HPLC chromatogram of [$^{99m}$Tc(CO)$_3$(bipy)ImPAMe] **7b**.

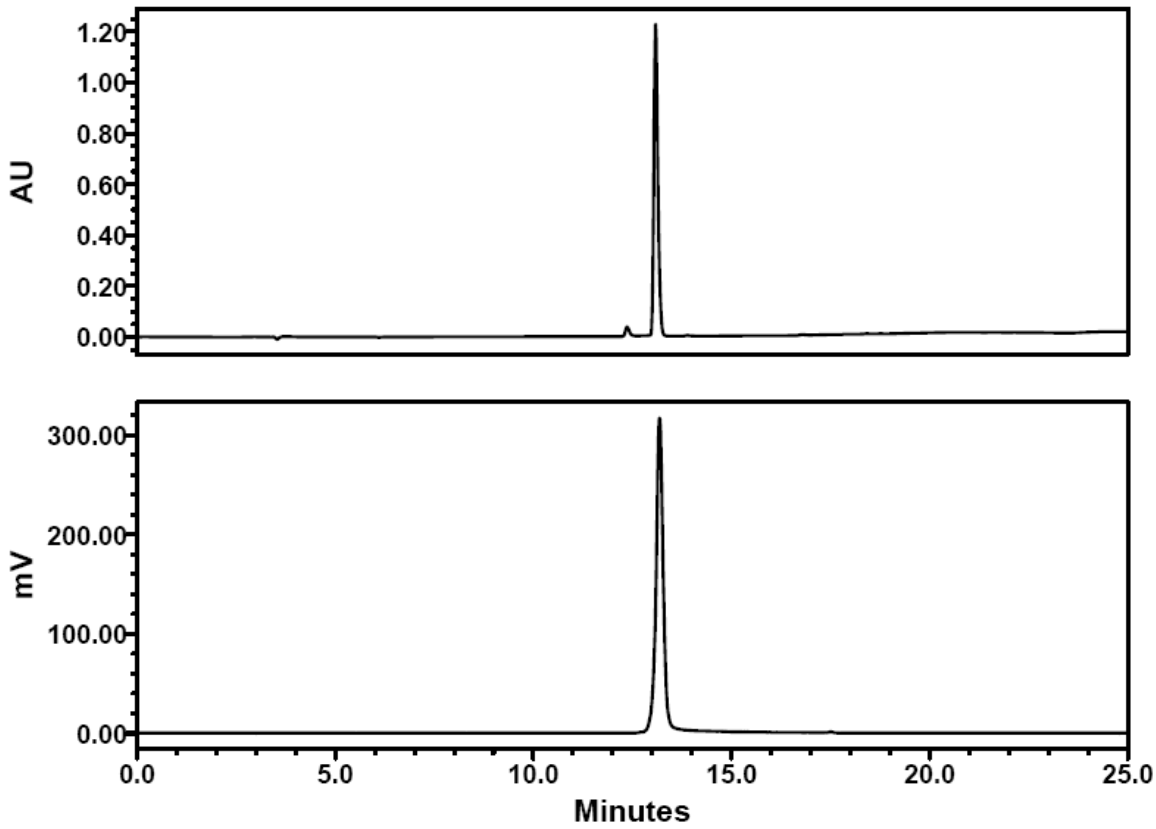


**Figure S 6.42** HPLC chromatograms (UV and γ) of the isolated [Re(CO)$_3$(bipy)(H$_2$O)]$^+$ **4a** complex co-injected with $^{99m}$Tc complex **4b**.

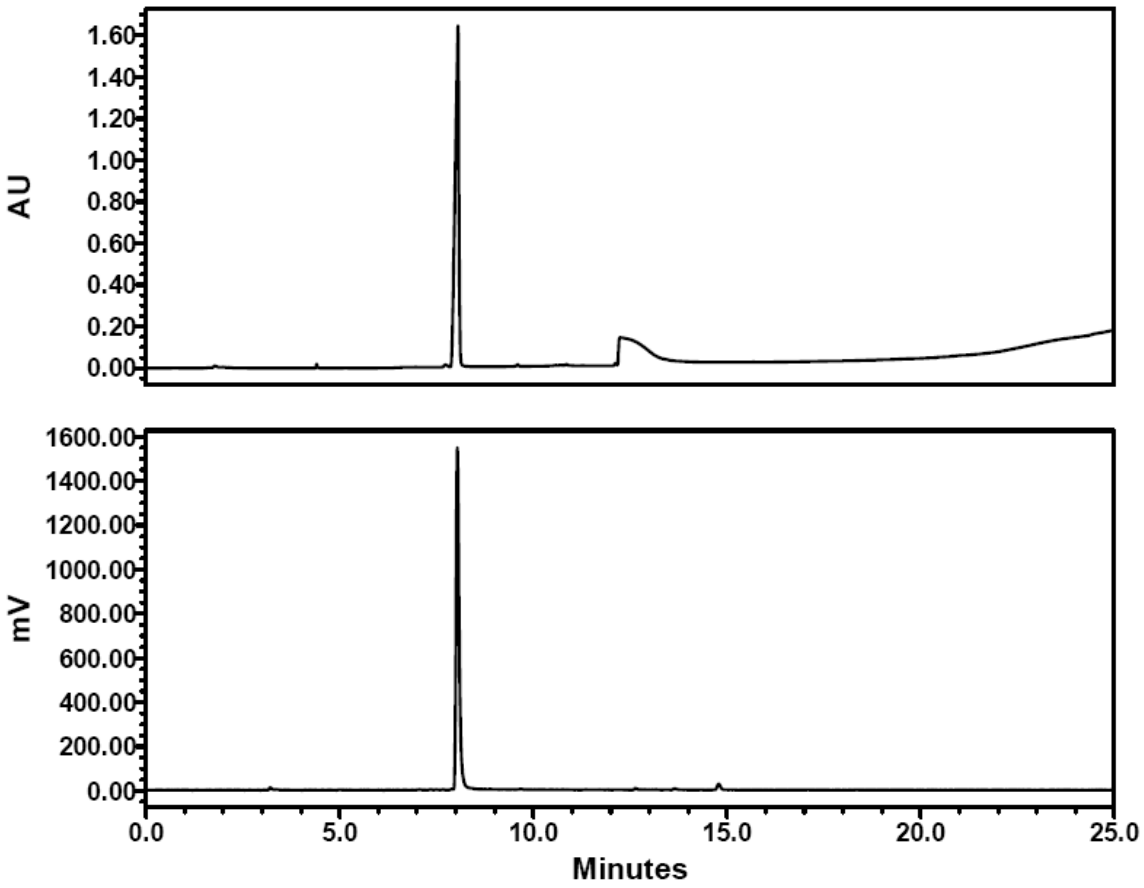


**Figure S 6.43** HPLC chromatograms (UV and γ) of the isolated [$Re(CO)_3$(bipy)(ZA)] **8a** complex co-injected with $^{99m}$Tc complex **8b**.

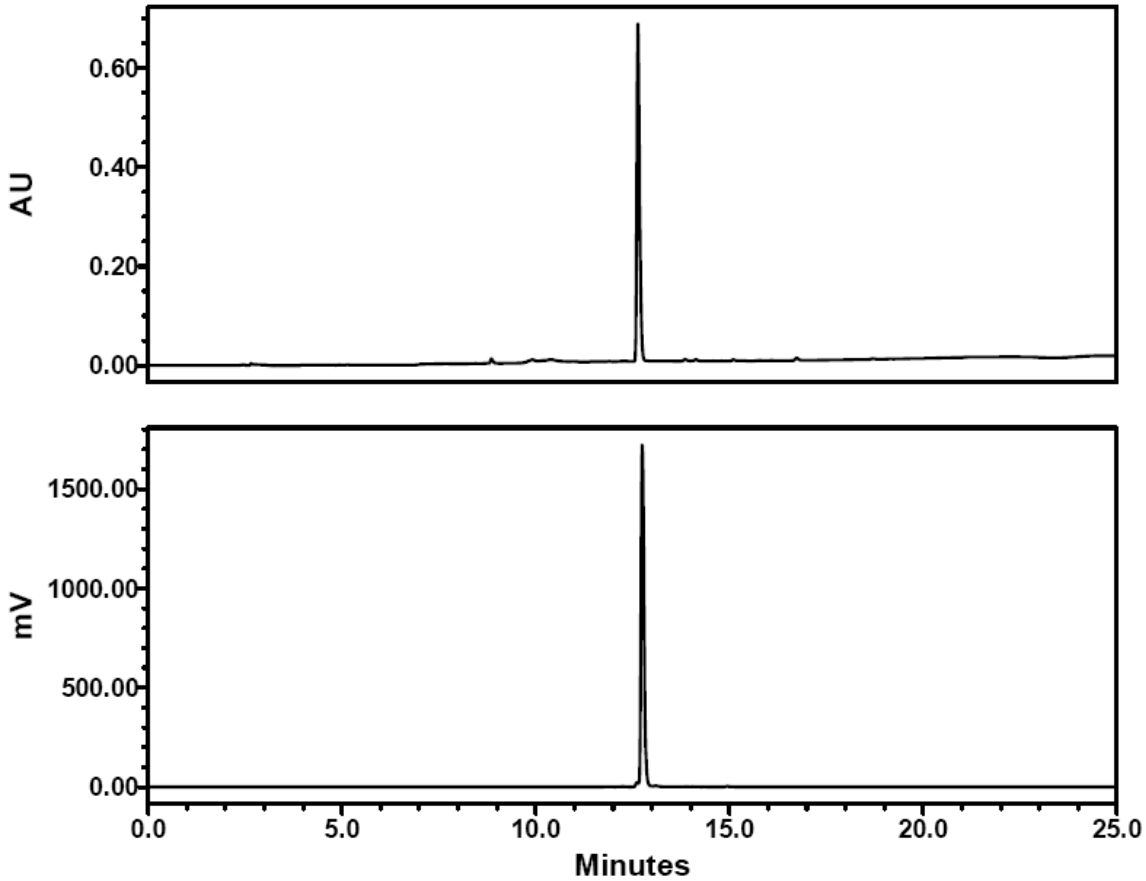


**Figure S 6.44** HPLC chromatograms (UV and γ) of the isolated $[Re(CO)_3(bipy)(ImSfn)]$ **9a** complex co-injected with $^{99m}Tc$ complex **9b**.

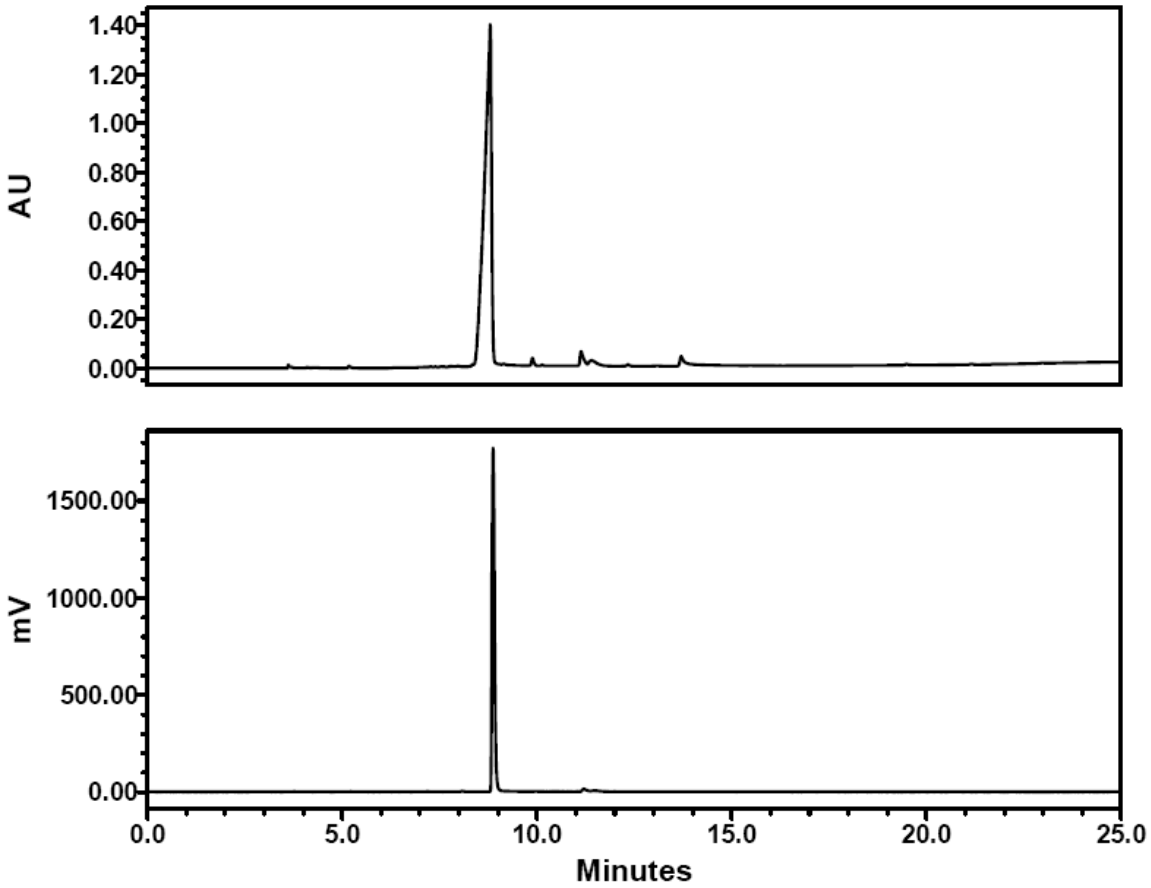


**Figure S 6.45** HPLC chromatograms (UV and γ) of the isolated $[Re(CO)_3(bipy)(ImAln)]$ **10a** complex co-injected with $^{99m}Tc$ complex **10b**.

**Table S 6.1** Crystal/refinement data

| Complex | **8a** | **9a** |
|---|---|---|
| Empirical formula | $C_{18}H_{30}C_{l3}N_4Na_2O_{18}P_2Re$ | $C_{22}H_{22}N_5O_7ReS$ |
| Formula weight | 989.92 $gmol^{-1}$ | 686.70 $gmol^{-1}$ |
| Temperature | 173(2) K | 173(2) K |
| Wavelength | 0.71073 Å | 0.71073 Å |
| Crystal system | Triclinic | Monoclinic |
| Space group | P -1 | P 21/c |
| Unit cell dimensions | a = 7.8523(9) Å | a = 12.8456(4) Å |
| | b = 8.8092(9) Å | b = 9.6955(3) Å |
| | c = 23.923(3) Å | c = 21.2199(7) Å |
| | α = 92.108(2)° | α = 90° |
| | β = 92.974(2)° | β = 101.3040(18)° |
| | γ = 94.718(2)° | γ = 90° |
| Volume | 1645.6(3) $Å^3$ | 2591.55(14) Å3 |
| Z | 2 | 4 |
| Density (calculated) | 1.998 $Mg/m^3$ | 1.760 $Mg/m^3$ |
| Absorption coefficient | 4.141 $mm^{-1}$ | 4.819 $mm^{-1}$ |
| Reflections collected | 17373 | 67536 |
| Independent reflections | 5794 [R(int) = 0.0260] | 5294 [R(int) = 0.0353] |
| Data / restraints / parameters | 5794 / 54 / 469 | 5294 / 36 / 362 |
| Goodness-of-fit on $F^2$ | 1.063 | 1.057 |
| Final R indices [I>2sigma(I)] | R1 = 0.0374, wR2 = 0.1048 | R1 = 0.0197, wR2 = 0.0422 |
| R indices (all data) | R1 = 0.0416, wR2 = 0.1065 | R1 = 0.0265, wR2 = 0.0451 |

**Table S 6.2** Selected bond lengths [Å] and angles [°] for **8a** and **9a**

| | | | |
|---|---|---|---|
| **8a** | | | |
| Re(1)-C(3) | 1.921(7) | Re(1)-N(3) | 2.180(5) |
| Re(1)-C(1) | 1.929(8) | O(3)-C(3) | 1.164(9) |
| Re(1)-C(2) | 1.930(7) | O(1)-C(1) | 1.147(9) |
| Re(1)-N(4) | 2.173(8) | O(2)-C(2) | 1.156(9) |
| Re(1)-N(1) | 2.175(6) | | |
| C(3)-Re(1)-C(1) | 91.9(3) | C(2)-Re(1)-N(1) | 92.1(3) |
| C(3)-Re(1)-C(2) | 89.0(3) | N(4)-Re(1)-N(1) | 80.1(17) |
| C(1)-Re(1)-C(2) | 89.5(3) | C(3)-Re(1)-N(3) | 94.9(2) |
| C(3)-Re(1)-N(4) | 95.5(18) | C(1)-Re(1)-N(3) | 97.3(3) |
| C(2)-Re(1)-N(4) | 98.2(4) | N(4)-Re(1)-N(3) | 74.6(3) |
| C(3)-Re(1)-N(1) | 175.5(3) | N(1)-Re(1)-N(3) | 83.4(2) |
| C(1)-Re(1)-N(1) | 92.4(3) | | |
| **9a** | | | |
| Re(1)-C(1) | 1.913(3) | Re(1)-N(1) | 2.182(3) |
| Re(1)-C(2) | 1.919(3) | O(1)-C(1) | 1.144(4) |
| Re(1)-C(3) | 1.923(3) | O(2)-C(2) | 1.149(4) |
| Re(1)-N(4) | 2.163(2) | O(3)-C(3) | 1.148(4) |
| Re(1)-N(5) | 2.171(2) | | |
| C(1)-Re(1)-C(2) | 90.15(15) | C(3)-Re(1)-N(5) | 174.10(11) |
| C(1)-Re(1)-C(3) | 87.42(13) | N(4)-Re(1)-N(5) | 74.90(9) |
| C(2)-Re(1)-C(3) | 88.90(13) | C(1)-Re(1)-N(1) | 91.05(13) |
| C(1)-Re(1)-N(4) | 172.35(11) | C(2)-Re(1)-N(1) | 178.13(11) |
| C(2)-Re(1)-N(4) | 93.57(11) | C(3)-Re(1)-N(1) | 92.58(11) |
| C(3)-Re(1)-N(4) | 99.32(11) | N(4)-Re(1)-N(1) | 85.07(9) |
| C(1)-Re(1)-N(5) | 98.26(12) | N(5)-Re(1)-N(1) | 85.78(10) |
| C(2)-Re(1)-N(5) | 92.63(11) | | |

# 7 Appendix 2 (Supporting Information for Chapter 3)

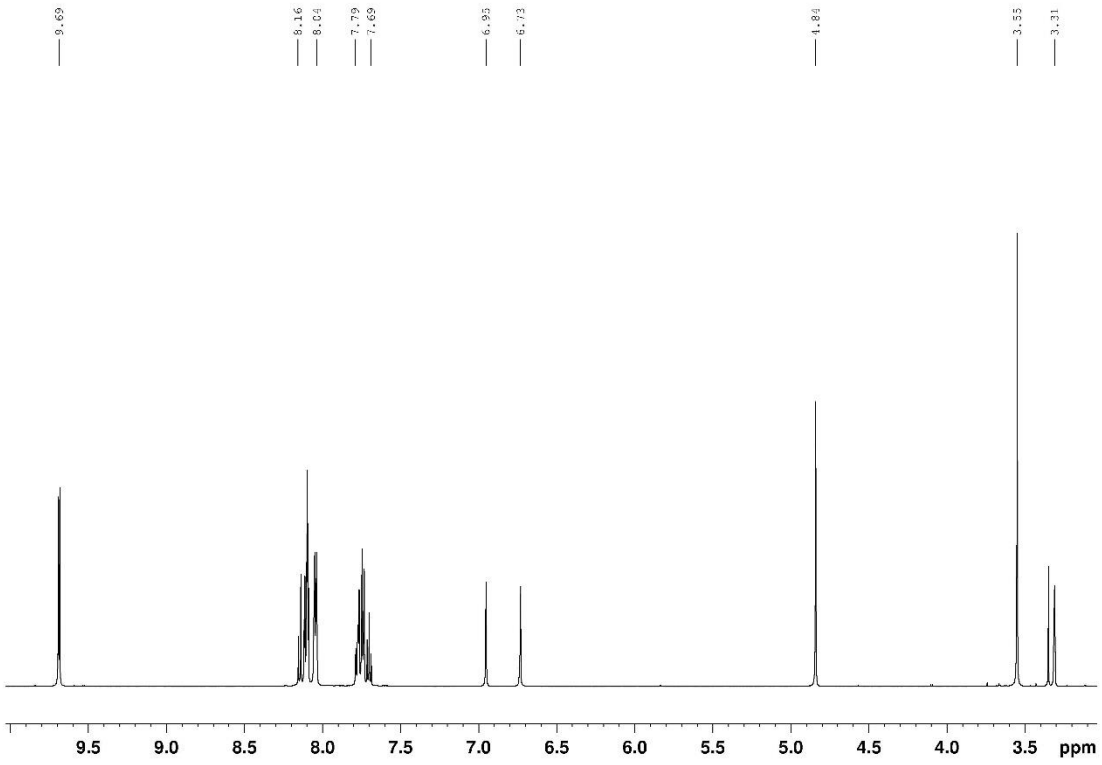


**Figure S 7.1** $^{1}$H NMR spectrum (MeOD, 600 MHz) of **3a**.

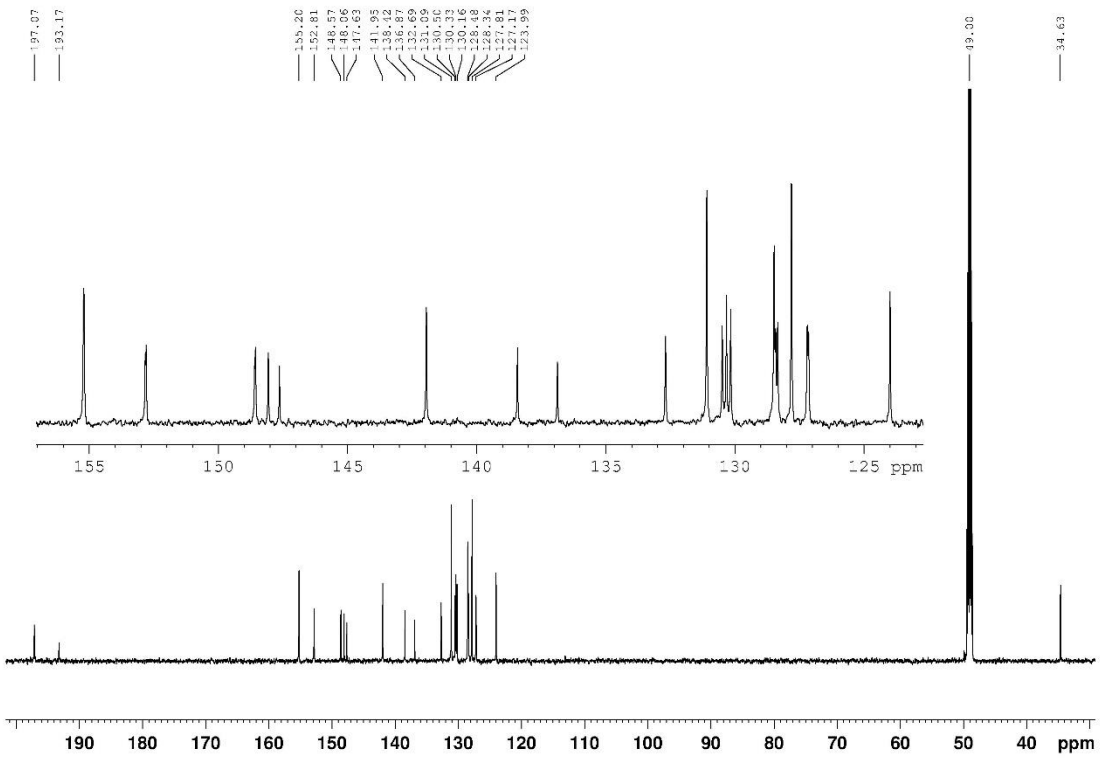


**Figure S 7.2** $^{13}$C NMR spectrum (MeOD, 150 MHz) of **3a**.

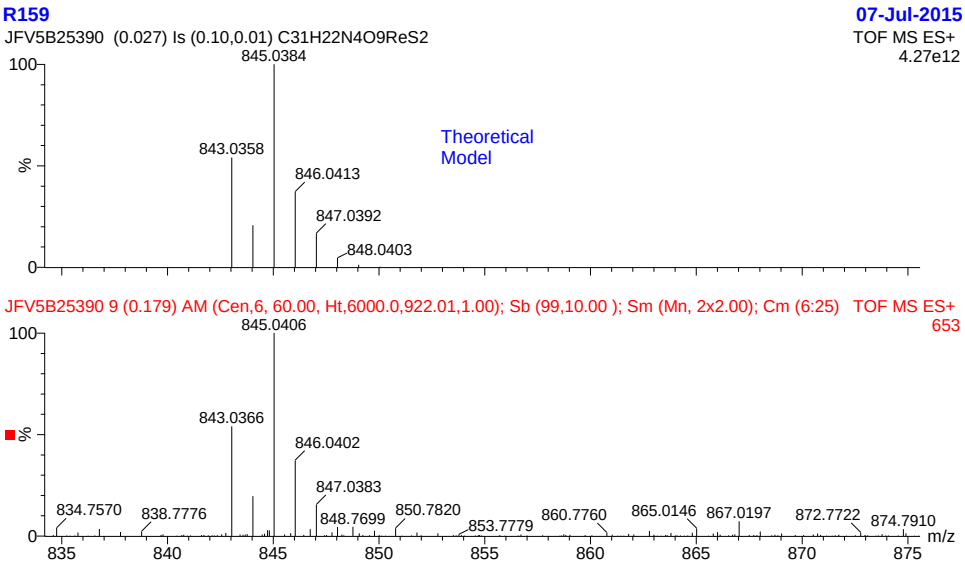


**Figure S 7.3** HRMS of **3a**.

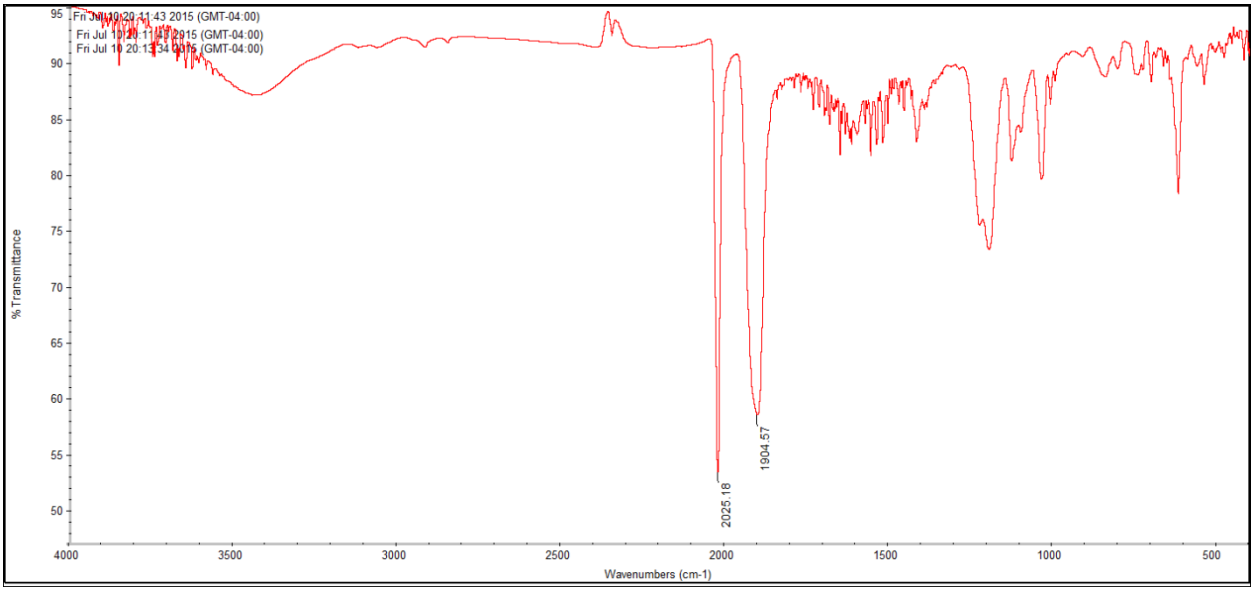


**Figure S 7.4** IR spectrum of **3a**.

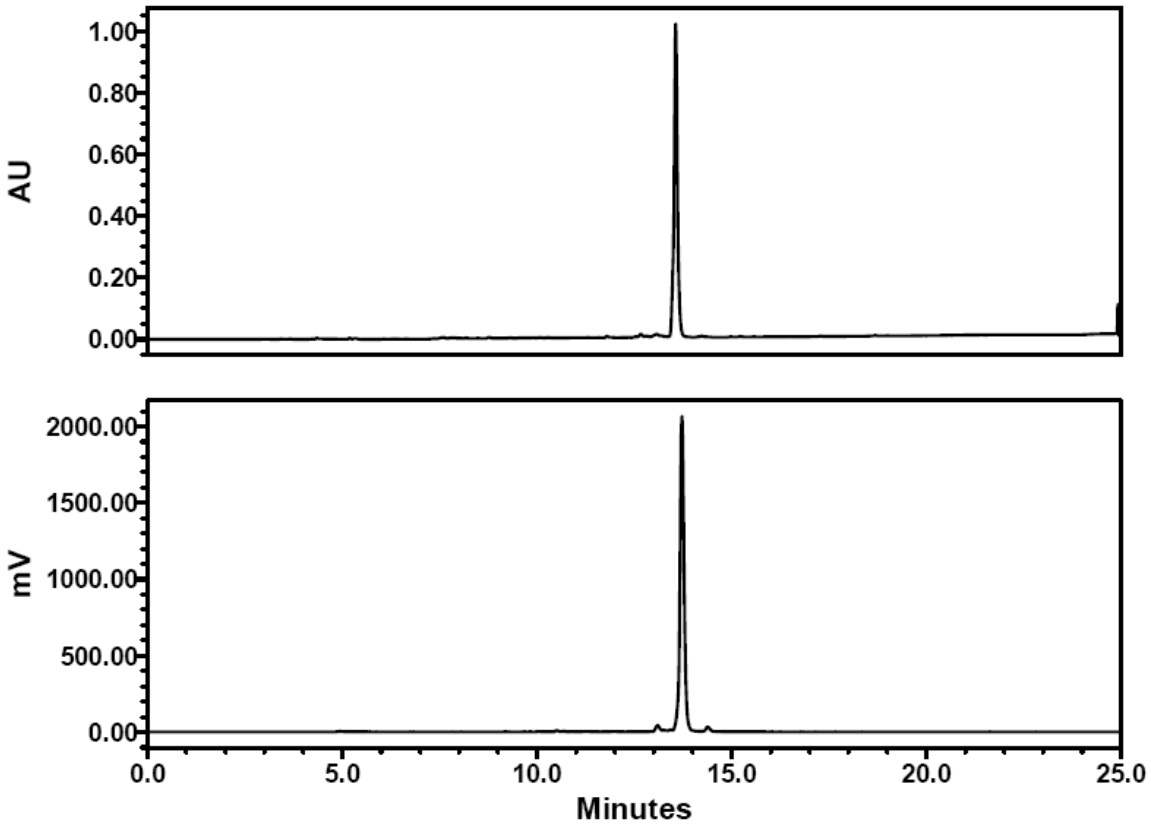


**Figure S 7.5** HPLC chromatograms (UV and γ) of $[Re(CO)_3(BPS)MeIm]^-$ **3a** co-injected with **3b.**

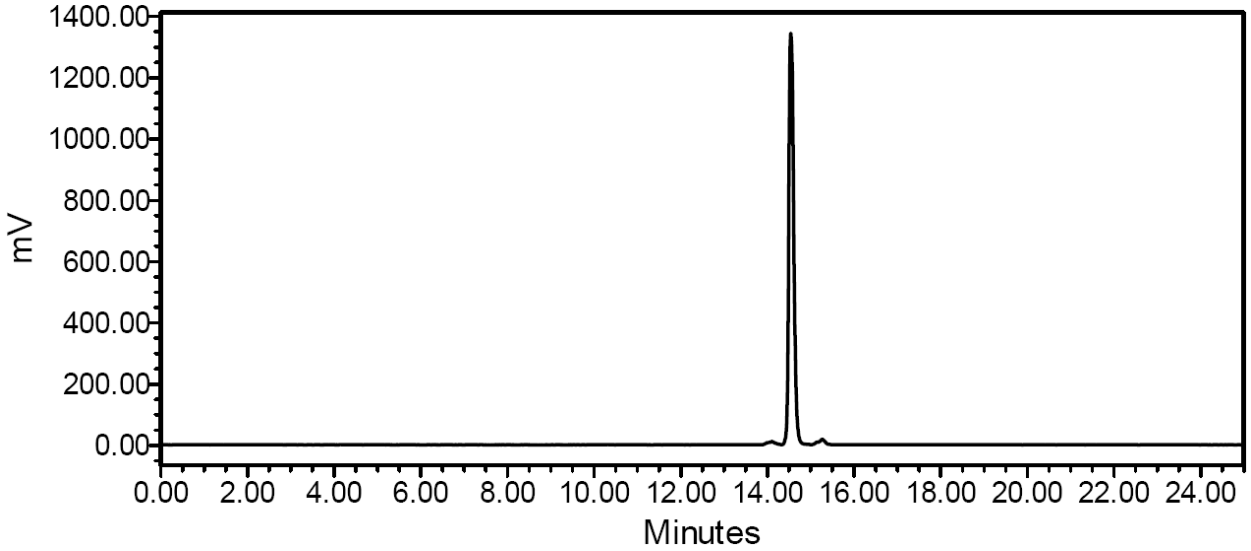


**Figure S 7.6** γ-HPLC chromatogram of [$^{99m}$Tc(CO)$_3$(BPS)(MeIm)]$^-$ **3b** at 0.5 h following histidine challenge (2 mM).

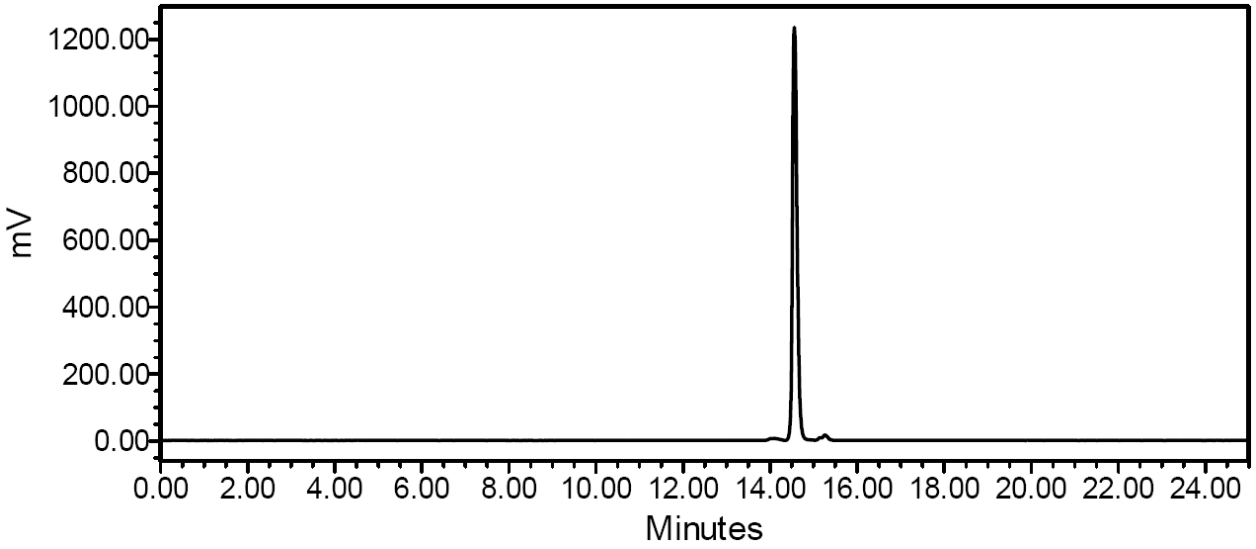


**Figure S 7.7** γ-HPLC chromatogram of [$^{99m}$Tc(CO)$_3$(BPS)(MeIm)]$^-$ **3b** at 1 h following histidine challenge (2 mM).

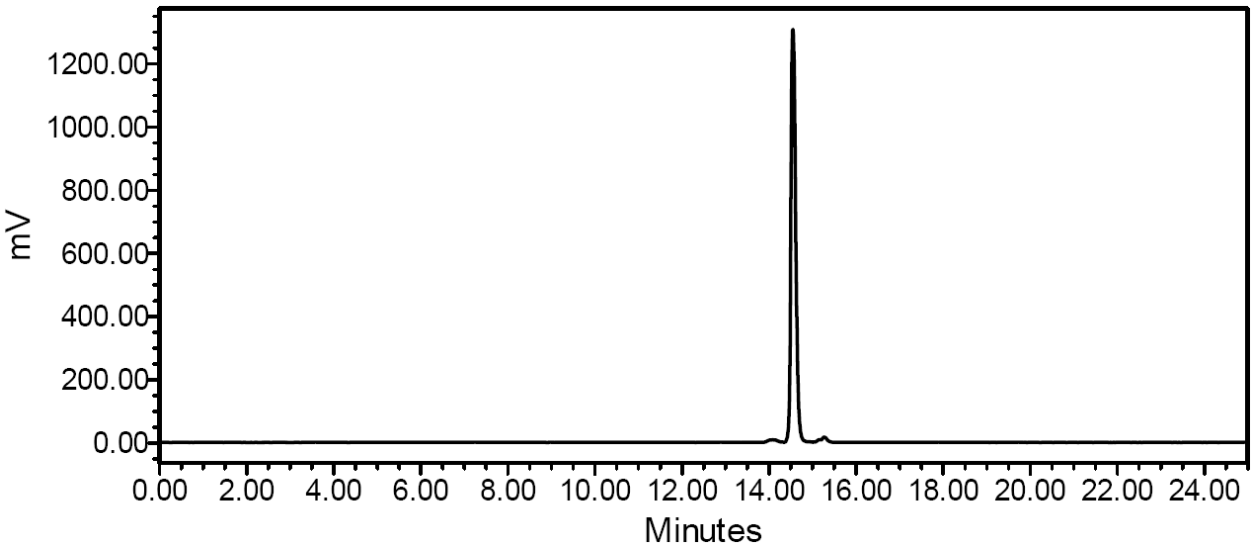


**Figure S 7.8** γ-HPLC chromatogram of [$^{99m}$Tc(CO)$_3$(BPS)(MeIm)]$^-$ **3b** at 2 h following histidine challenge (2 mM).

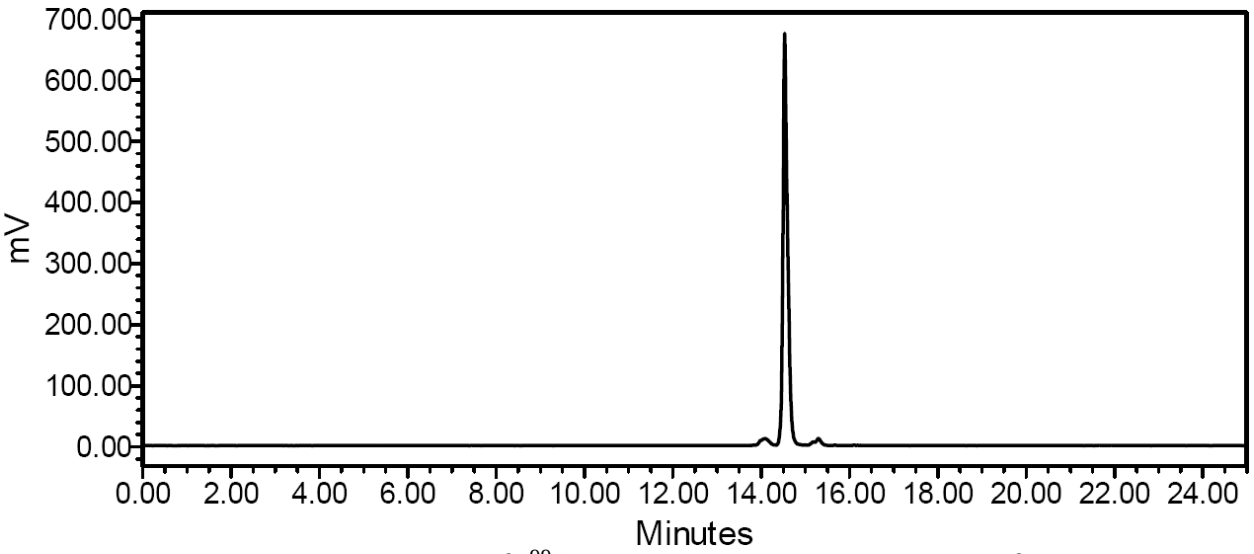


**Figure S 7.9** γ-HPLC chromatogram of [$^{99m}$Tc(CO)$_3$(BPS)(MeIm)]$^-$ **3b** at 3 h following histidine challenge (2 mM).

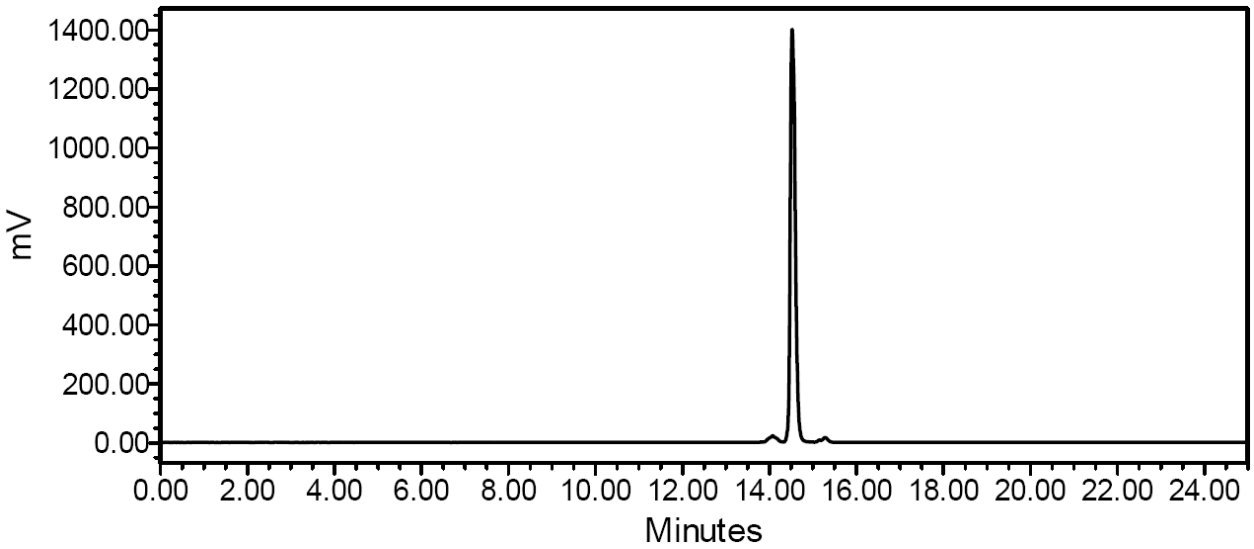


**Figure S 7.10** γ-HPLC chromatogram of [$^{99m}$Tc(CO)$_3$(BPS)(MeIm)]$^-$ **3b** at 6 h following histidine challenge (2 mM).

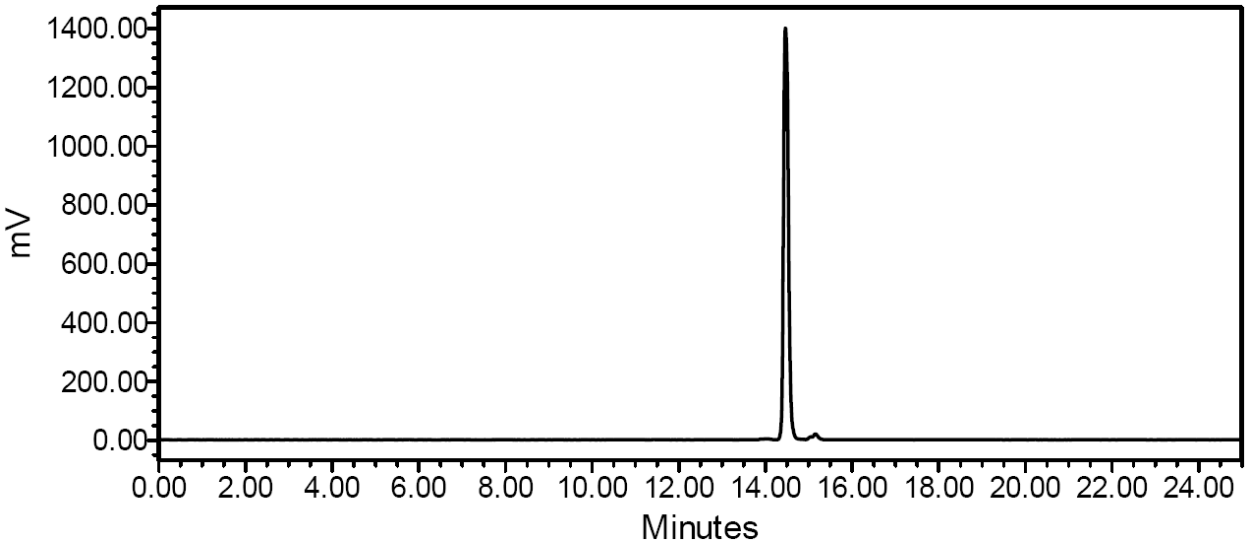


**Figure S 7.11** γ-HPLC chromatogram of [$^{99m}$Tc(CO)$_3$(BPS)(MeIm)]$^-$ **3b** at 0.5 h following cysteine challenge (2 mM).

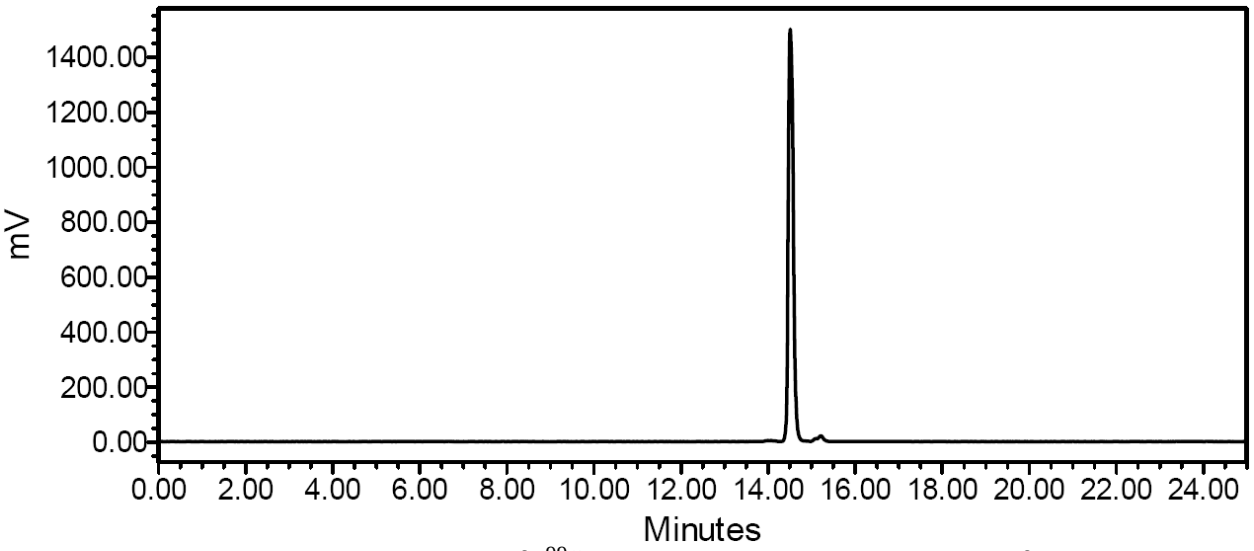


**Figure S 7.12** γ-HPLC chromatogram of [$^{99m}$Tc(CO)$_3$(BPS)(MeIm)]$^-$ **3b** at 1 h following cysteine challenge (2 mM).

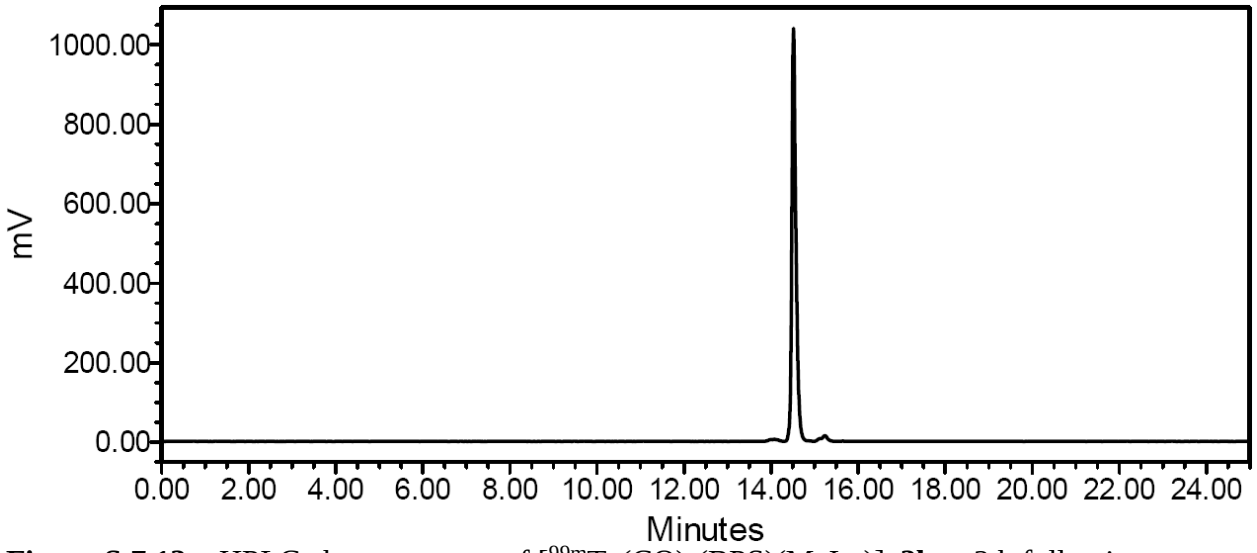


**Figure S 7.13** γ-HPLC chromatogram of [$^{99m}$Tc(CO)$_3$(BPS)(MeIm)]$^-$ **3b** at 2 h following cysteine challenge (2 mM).

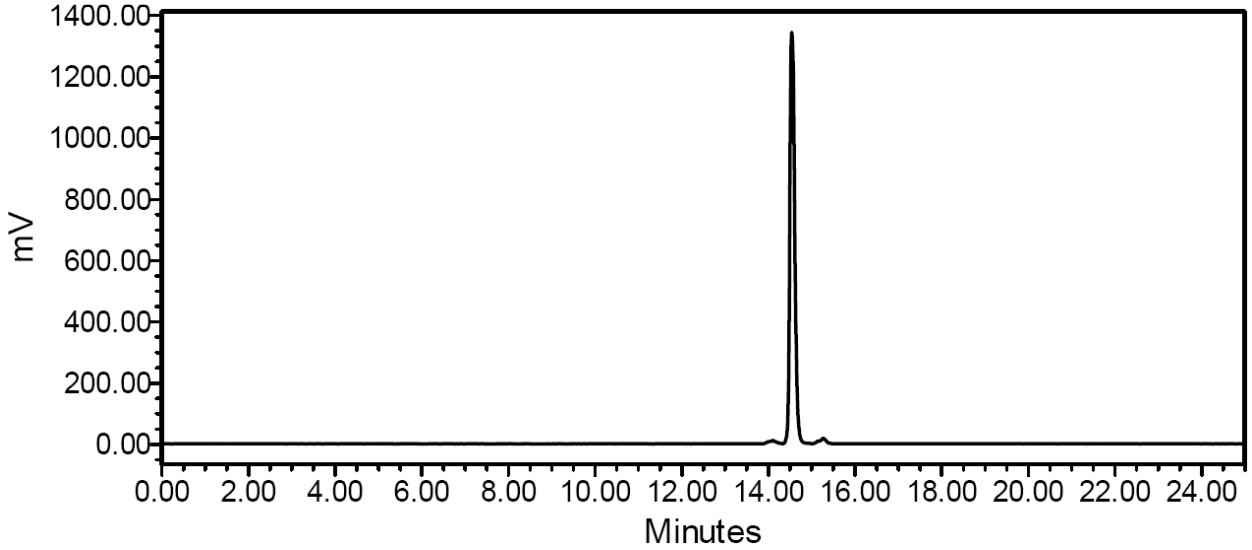


**Figure S 7.14** γ-HPLC chromatogram of [$^{99m}$Tc(CO)$_3$(BPS)(MeIm)]$^-$ **3b** at 3 h following cysteine challenge (2 mM).

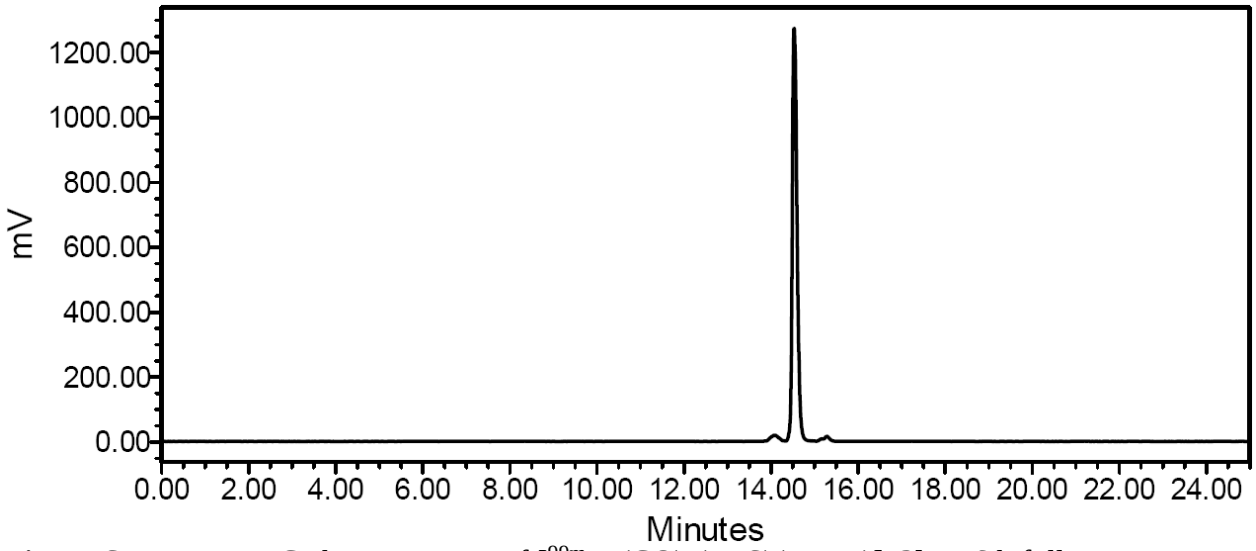


**Figure S 7.15** γ-HPLC chromatogram of [$^{99m}$Tc(CO)$_3$(BPS)(MeIm)]$^-$ **3b** at 6 h following cysteine challenge (2 mM).

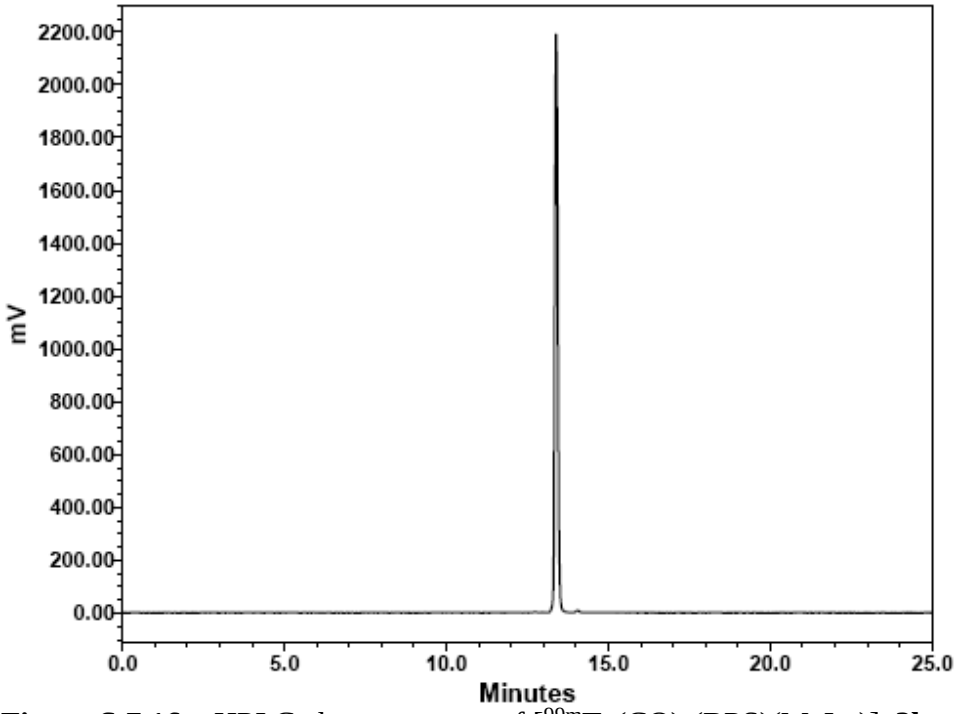


**Figure S 7.16** γ-HPLC chromatogram of [$^{99m}$Tc(CO)$_3$(BPS)(MeIm)]$^-$ **3b** at 0.5 h following histidine challenge (0.2 M).

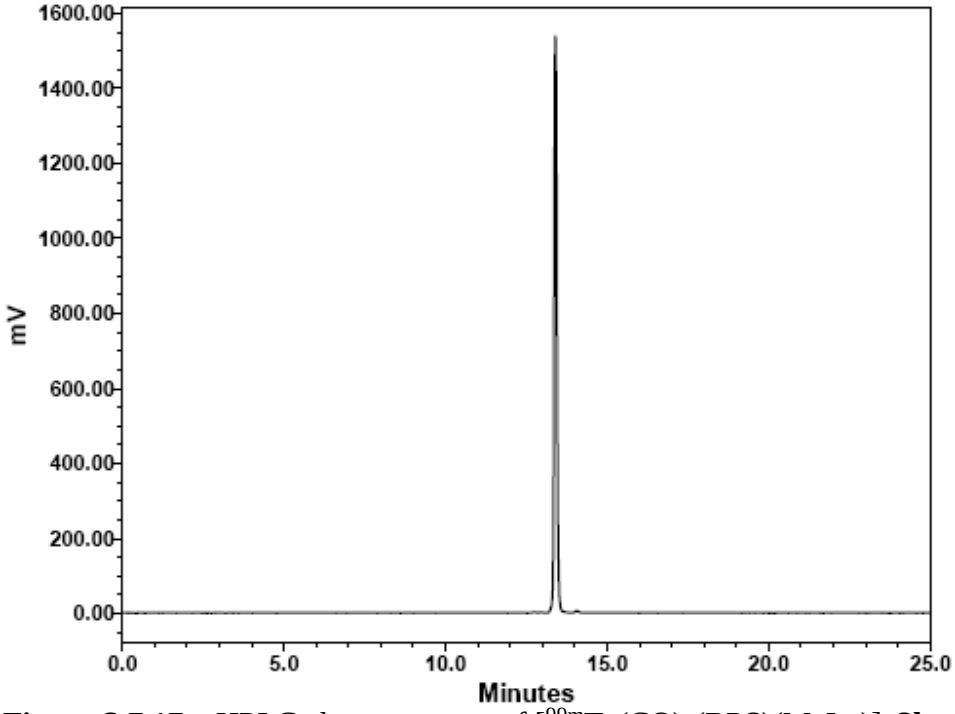


**Figure S 7.17** γ-HPLC chromatogram of [$^{99m}$Tc(CO)$_3$(BPS)(MeIm)]$^-$ **3b** at 1 h following histidine challenge (0.2 M).

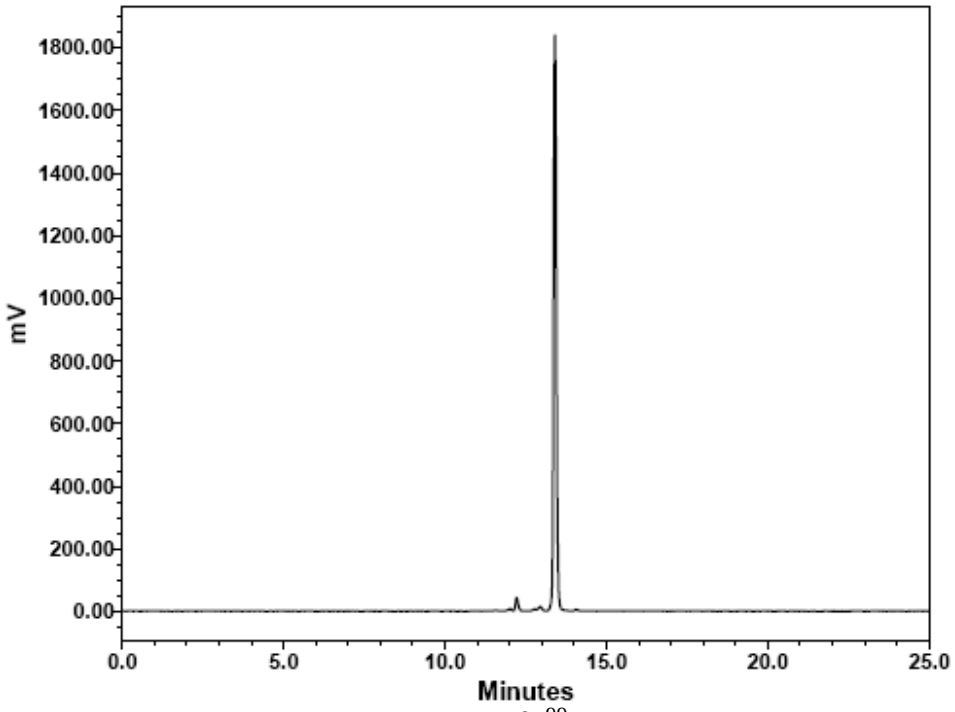


**Figure S 7.18** γ-HPLC chromatogram of [$^{99m}$Tc(CO)$_3$(BPS)(MeIm)]$^-$ **3b** at 2 h following histidine challenge (0.2 M).

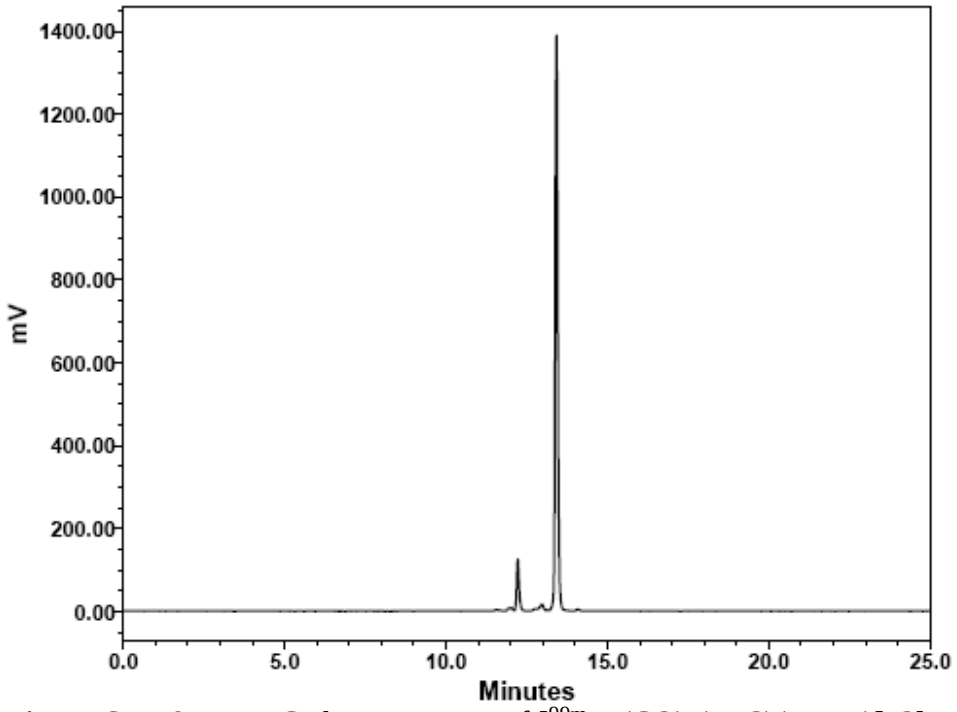


**Figure S 7.19** γ-HPLC chromatogram of [$^{99m}$Tc(CO)$_3$(BPS)(MeIm)]$^-$ **3b** at 3 h following histidine challenge (0.2 M).

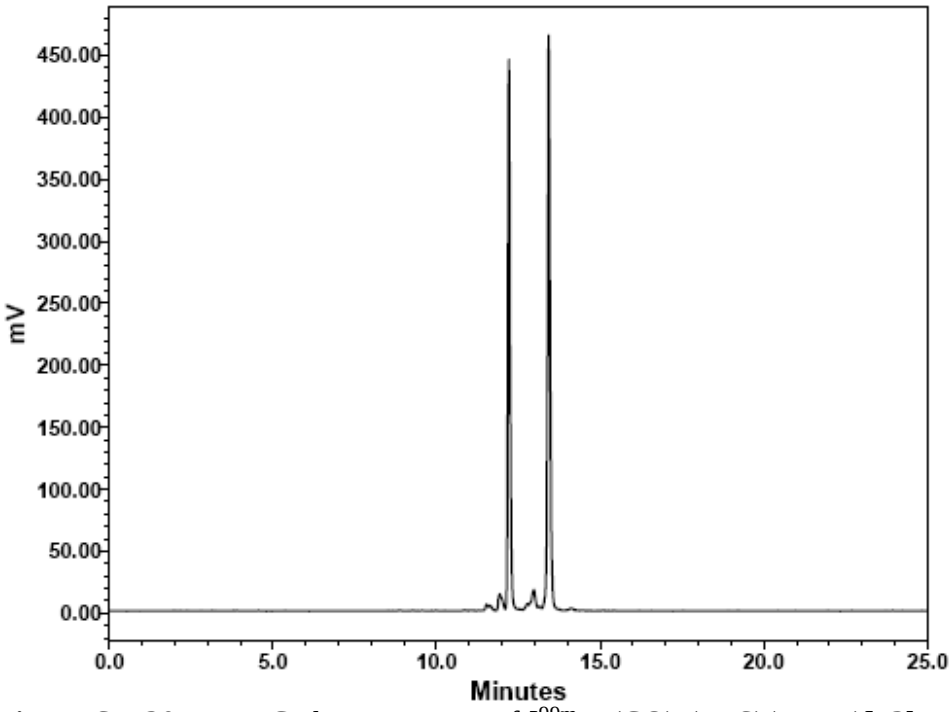


**Figure S 7.20** γ-HPLC chromatogram of [$^{99m}$Tc(CO)$_3$(BPS)(MeIm)]$^-$ **3b** at 6 h following histidine challenge (0.2 M).

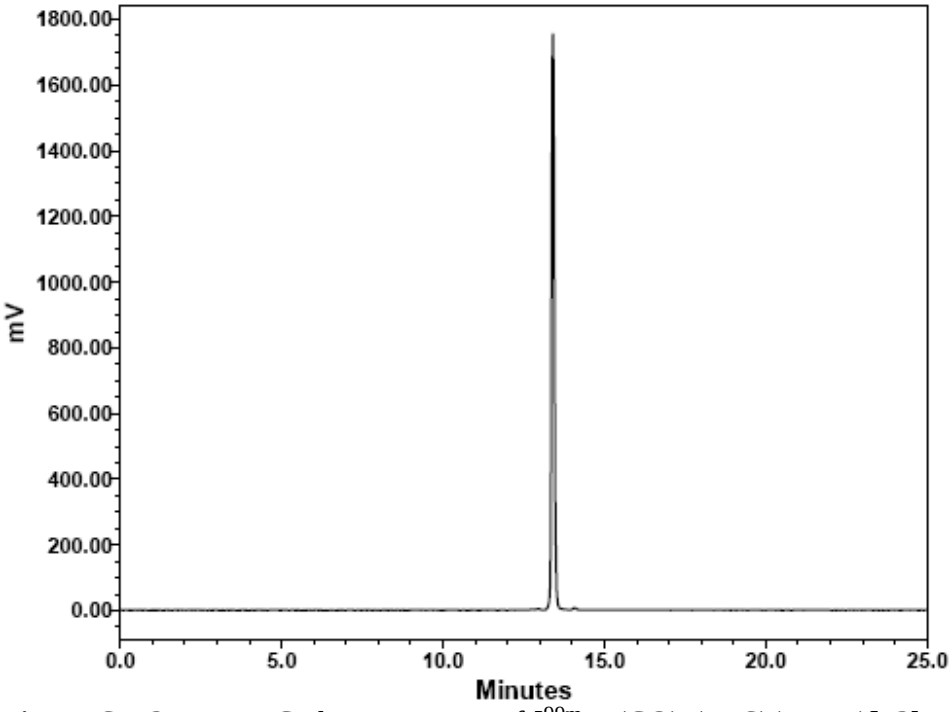


**Figure S 7.21** γ-HPLC chromatogram of [$^{99m}$Tc(CO)$_3$(BPS)(MeIm)]$^-$ **3b** at 0.5 h following cysteine challenge (0.2 M).

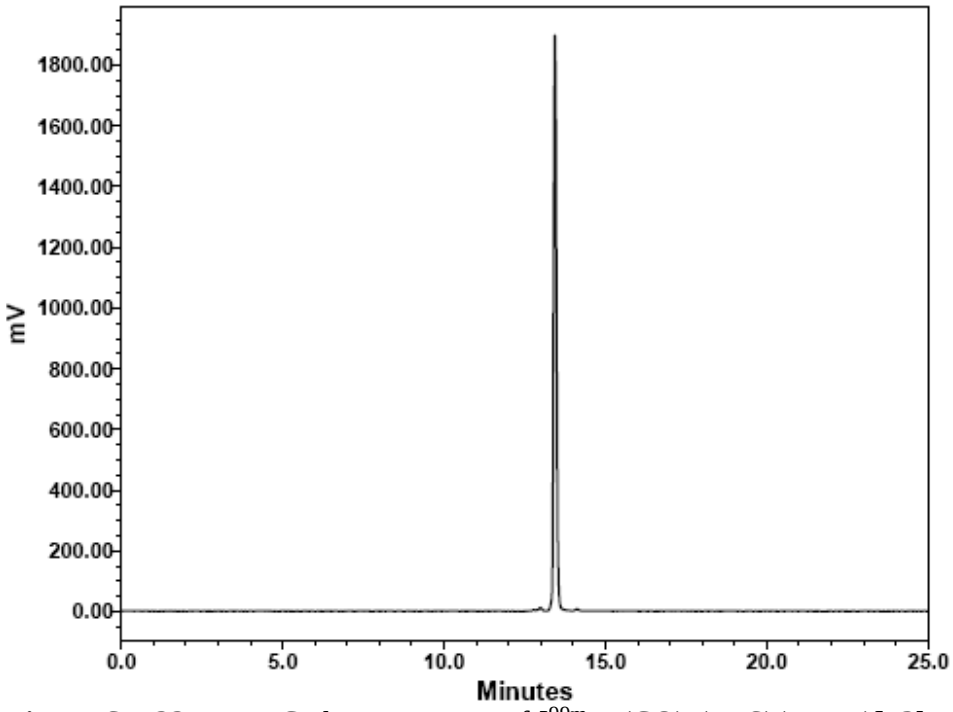


**Figure S 7.22** γ-HPLC chromatogram of [$^{99m}$Tc(CO)$_3$(BPS)(MeIm)]$^-$ **3b** at 1 h following cysteine challenge (0.2 M).

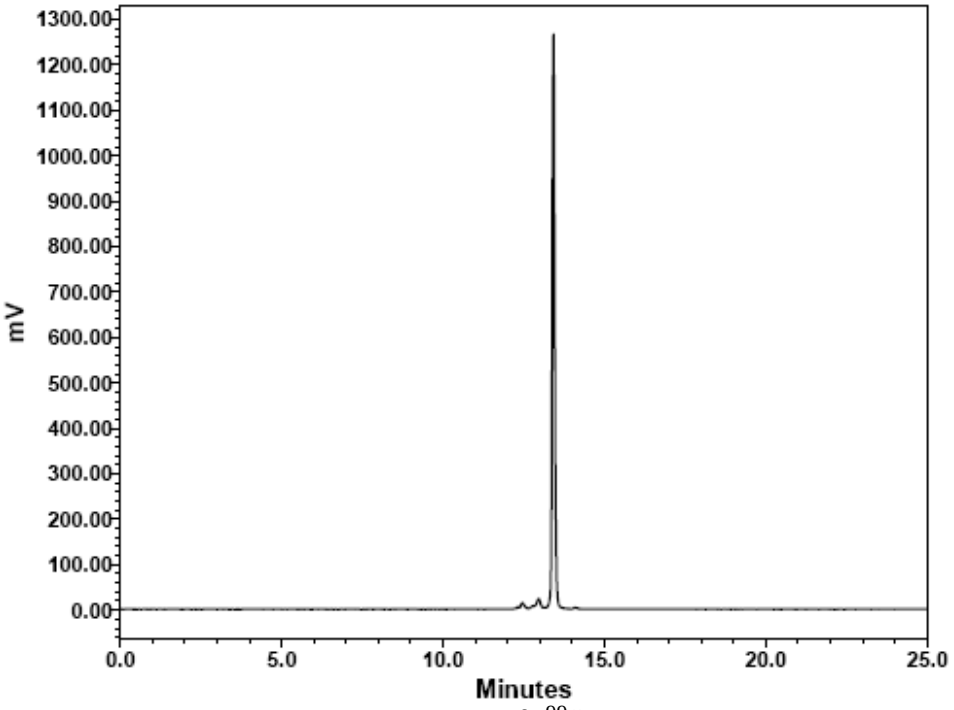


**Figure S 7.23** γ-HPLC chromatogram of [$^{99m}$Tc(CO)$_3$(BPS)(MeIm)]$^-$ **3b** at 2 h following cysteine challenge (0.2 M).

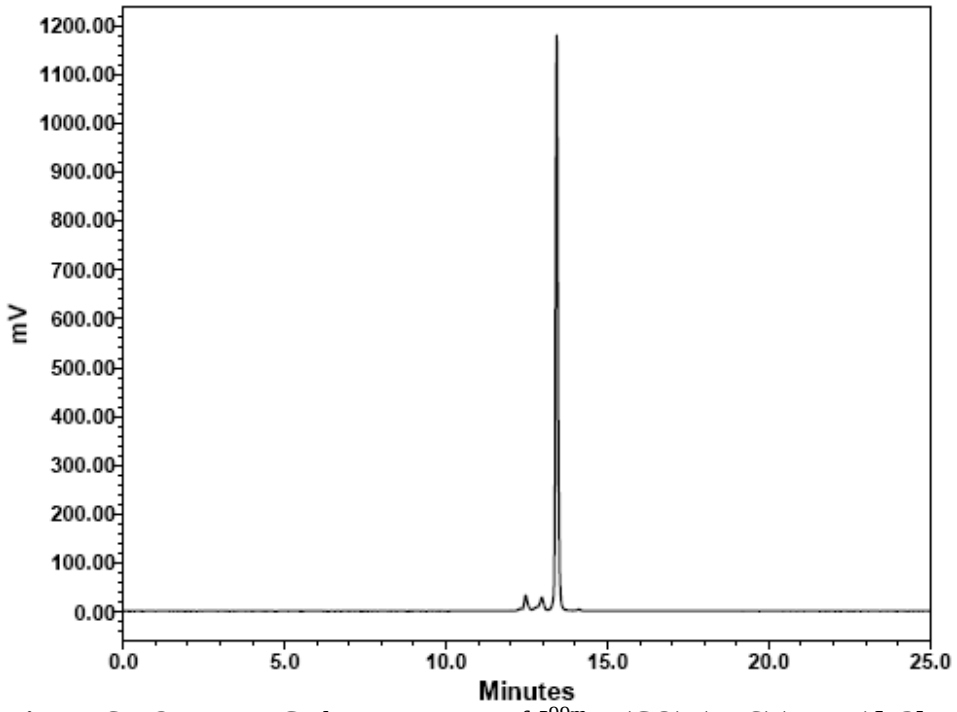


**Figure S 7.24** γ-HPLC chromatogram of [$^{99m}$Tc(CO)$_3$(BPS)(MeIm)]$^-$ **3b** at 3 h following cysteine challenge (0.2 M).

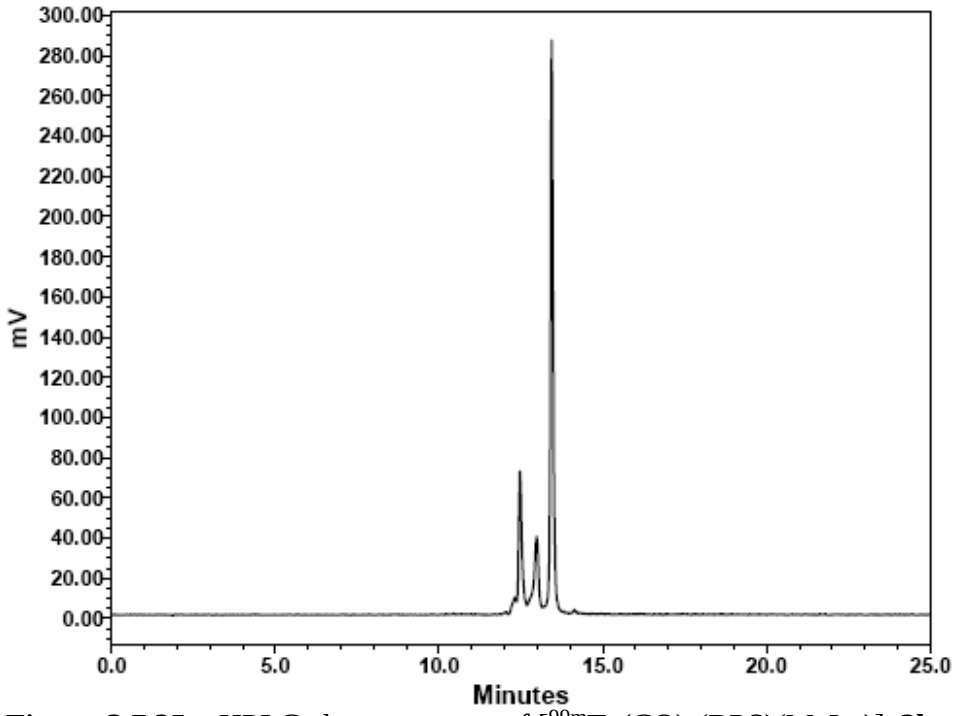


**Figure S 7.25** γ-HPLC chromatogram of [$^{99m}$Tc(CO)$_3$(BPS)(MeIm)]$^-$ **3b** at 6 h following cysteine challenge (0.2 M).

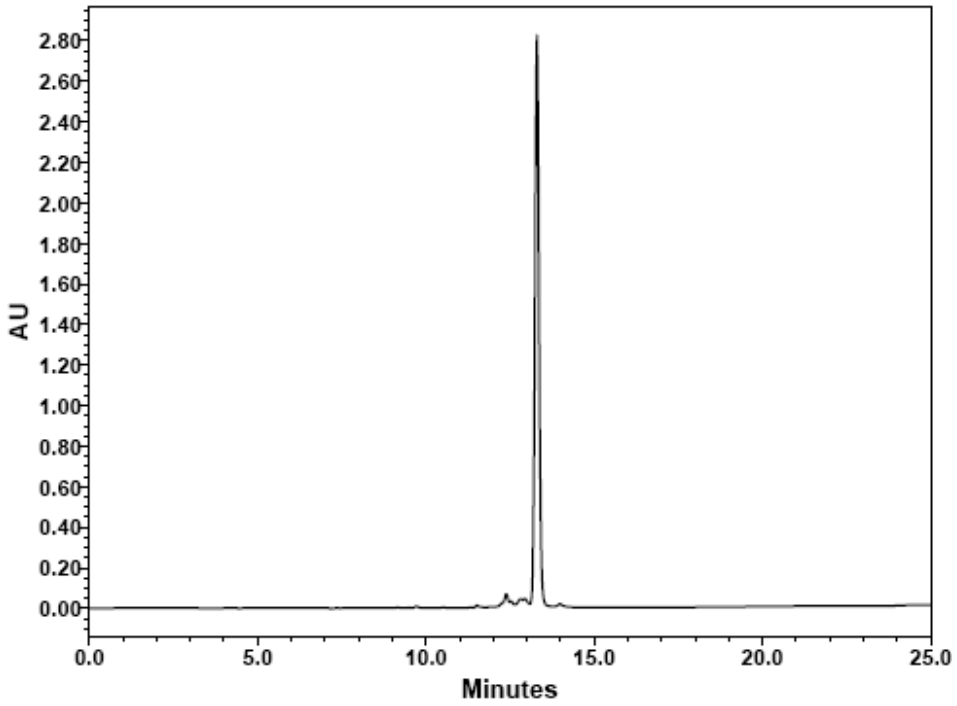


**Figure S 7.26** UV-HPLC chromatogram at 1 h incubation of $[Re(CO)_3(BPS)(MeIm)]^-$ **3a** in $H_2O$ (50 μM).

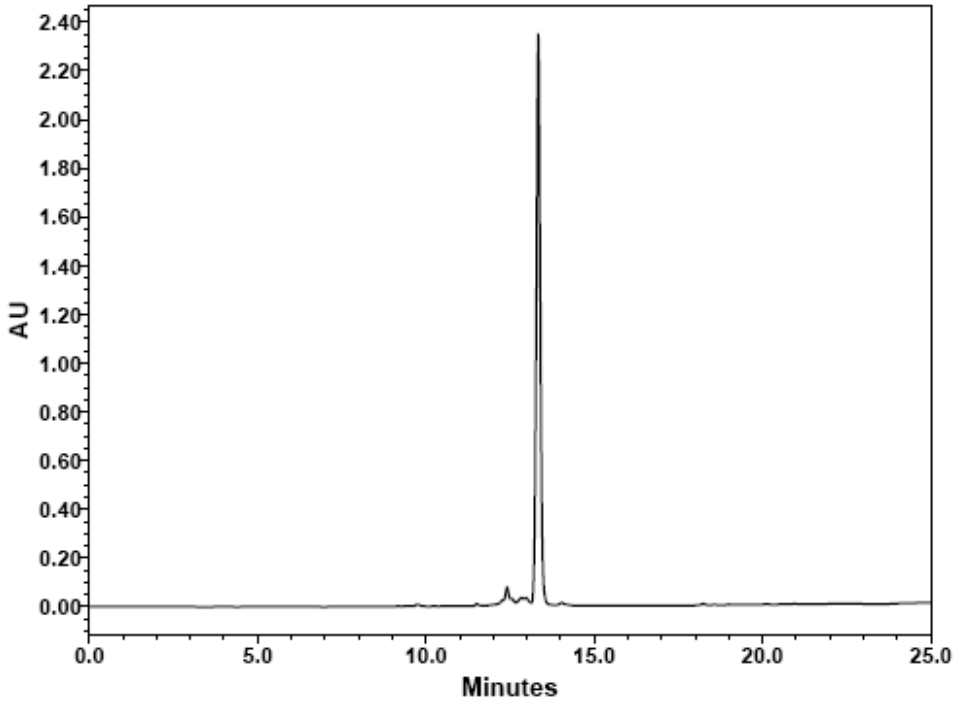


**Figure S 7.27** UV-HPLC chromatogram at 3 h incubation of $[Re(CO)_3(BPS)(MeIm)]^-$ **3a** in $H_2O$ (50 μM).

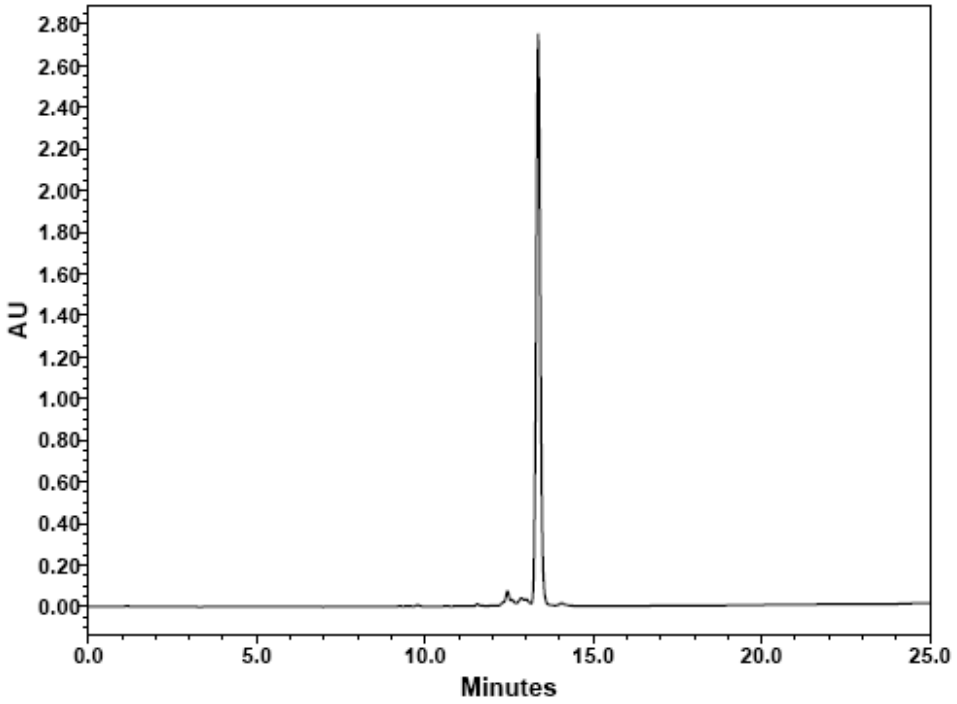


**Figure S 7.28** UV-HPLC chromatogram at 6 h incubation of $[Re(CO)_3(BPS)(MeIm)]^-$ **3a** in $H_2O$ (50 μM).

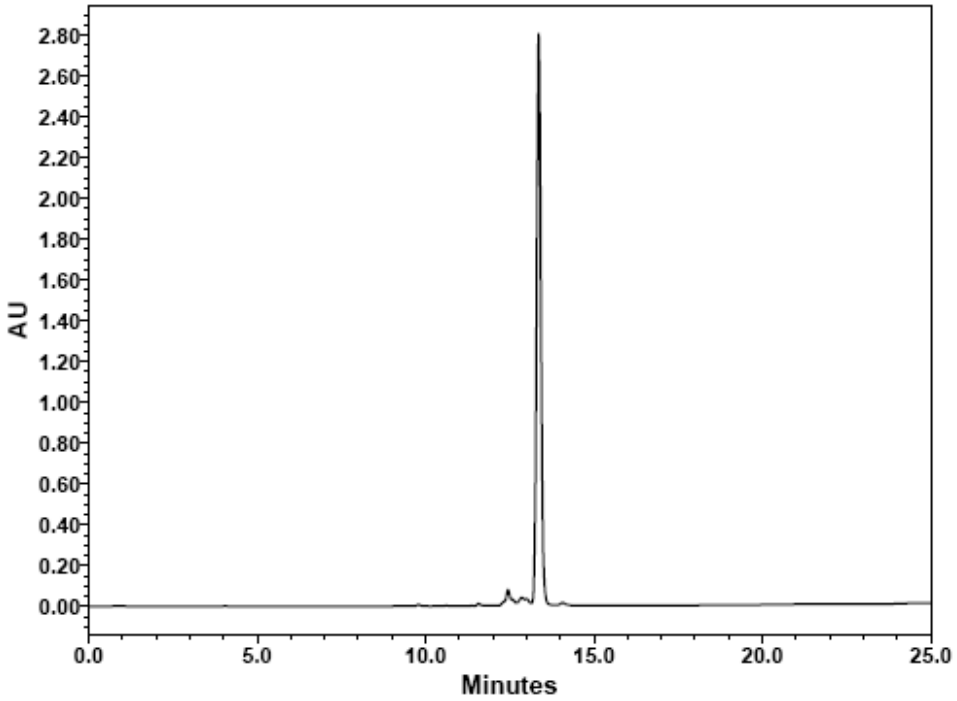


**Figure S 7.29** UV-HPLC chromatogram at 12 h incubation of $[Re(CO)_3(BPS)(MeIm)]^-$ **3a** in $H_2O$ (50 µM).

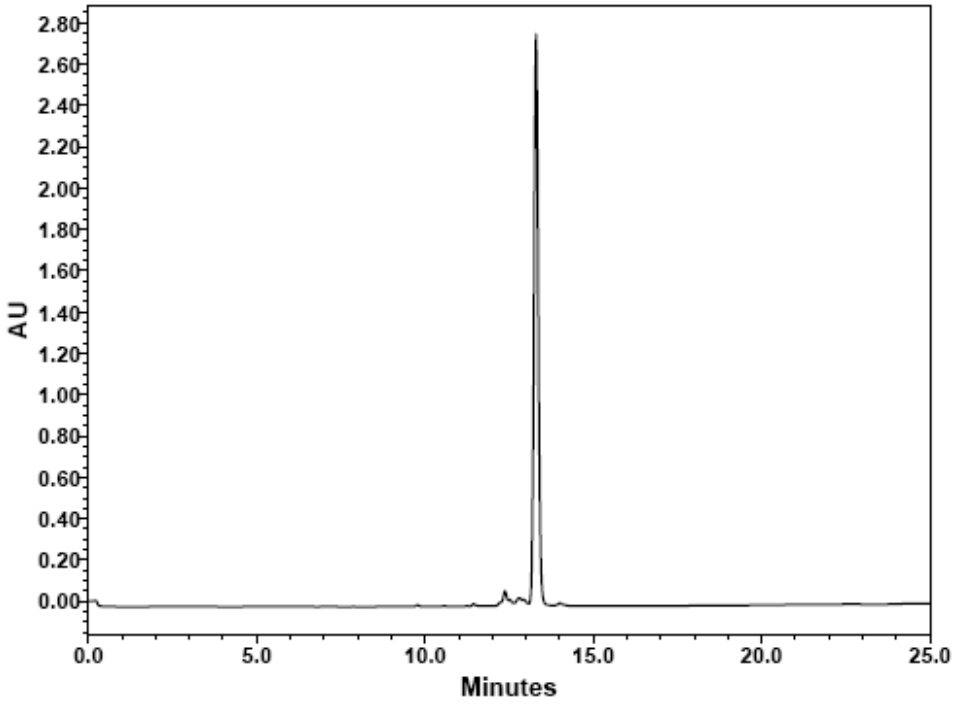


**Figure S 7.30** UV-HPLC chromatogram at 24 h incubation of $[Re(CO)_3(BPS)(MeIm)]^-$ **3a** in $H_2O$ (50 µM).

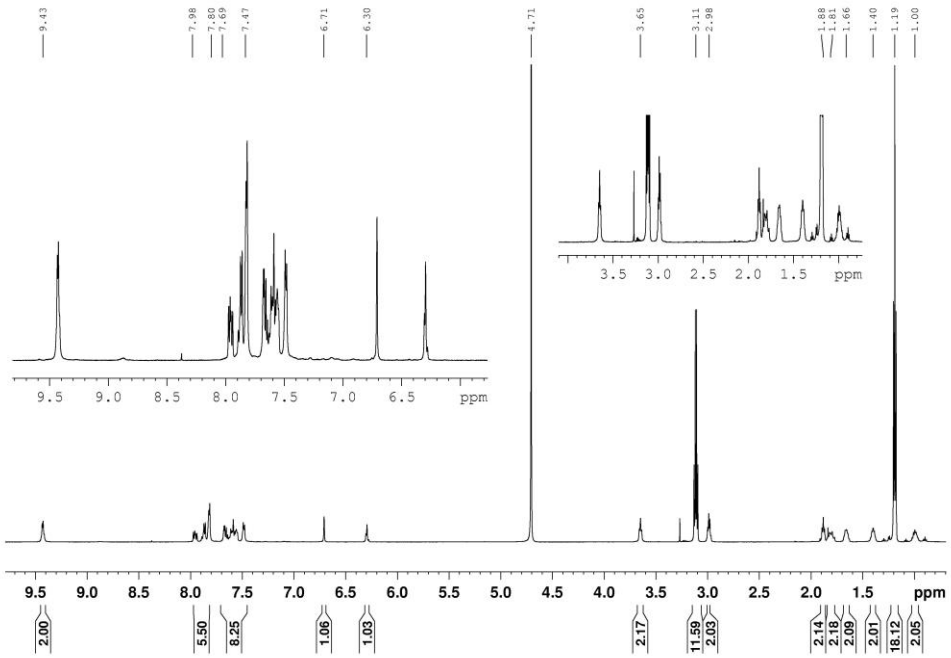


**Figure S 7.31** $^{1}$H NMR spectrum ($D_2O$, 600 MHz) of **4a**.

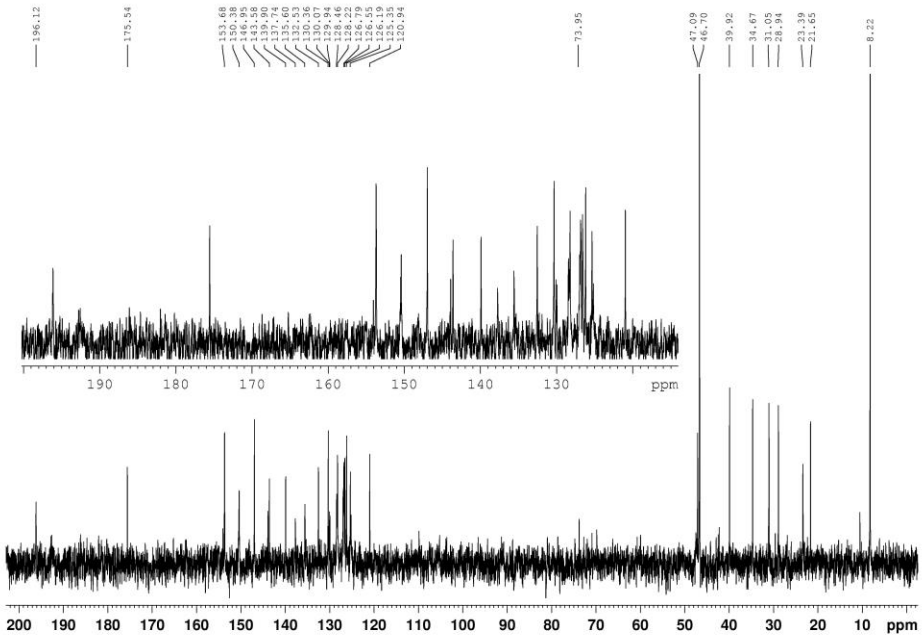


**Figure S 7.32** $^{13}C$ NMR spectrum ($D_2O$, 150 MHz) of **4a**.

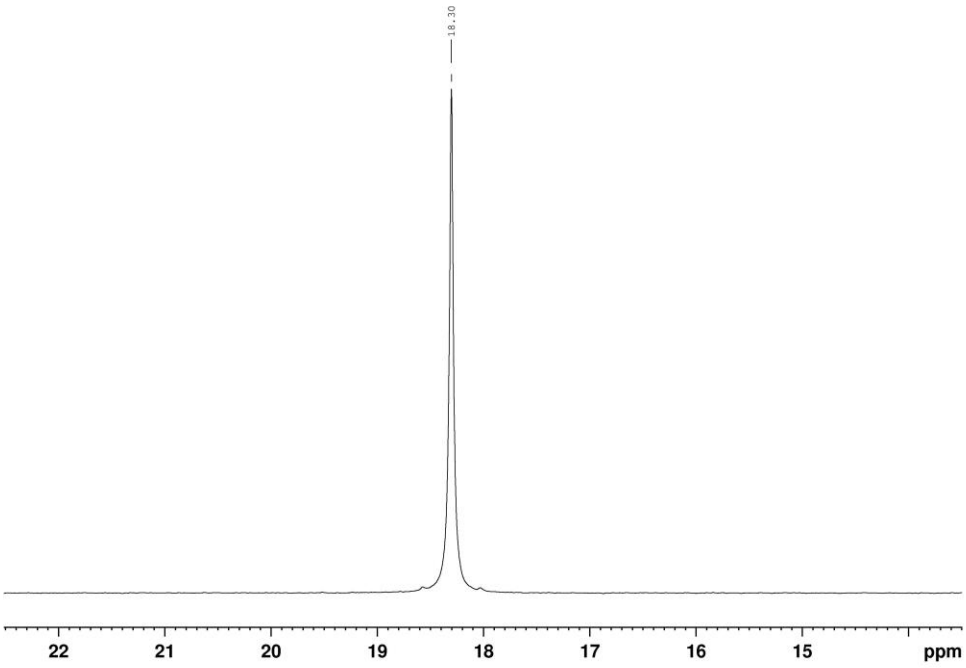


**Figure S 7.33** $^{31}P\{^{1}H\}$ NMR spectrum ($D_2O$, 242 MHz) of **4a**.

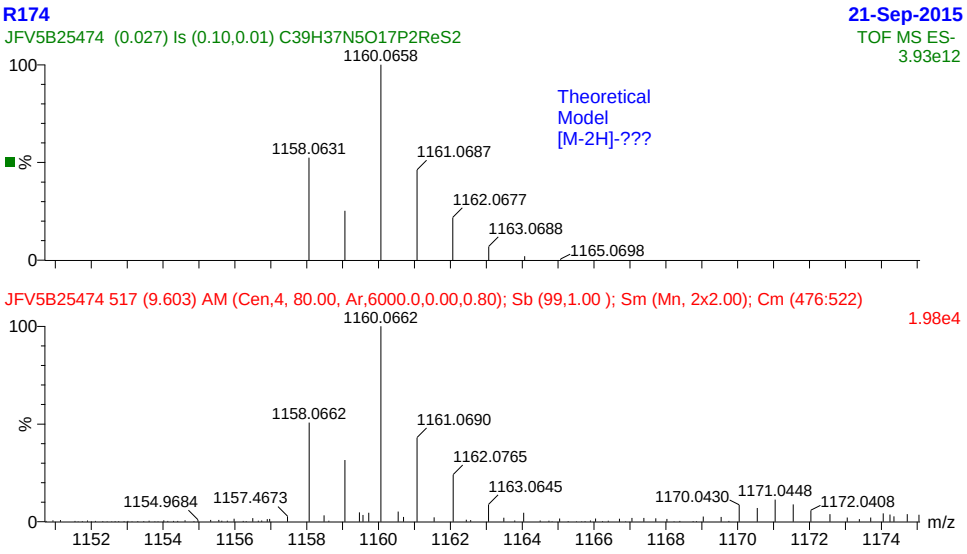


**Figure S 7.34** HRMS of **4a**.

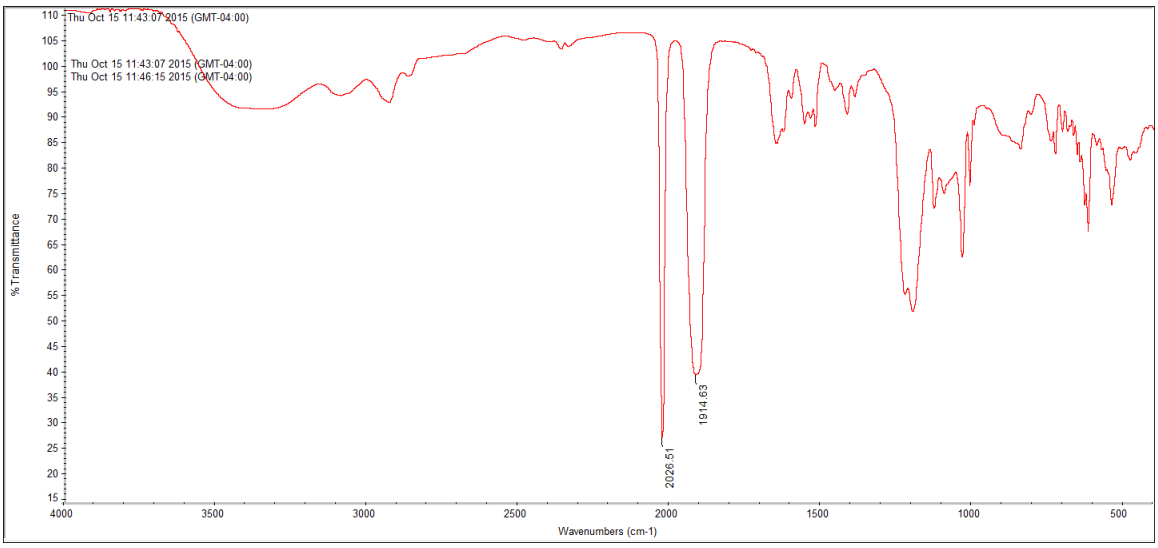


**Figure S 7.35** IR spectrum of **4a**.

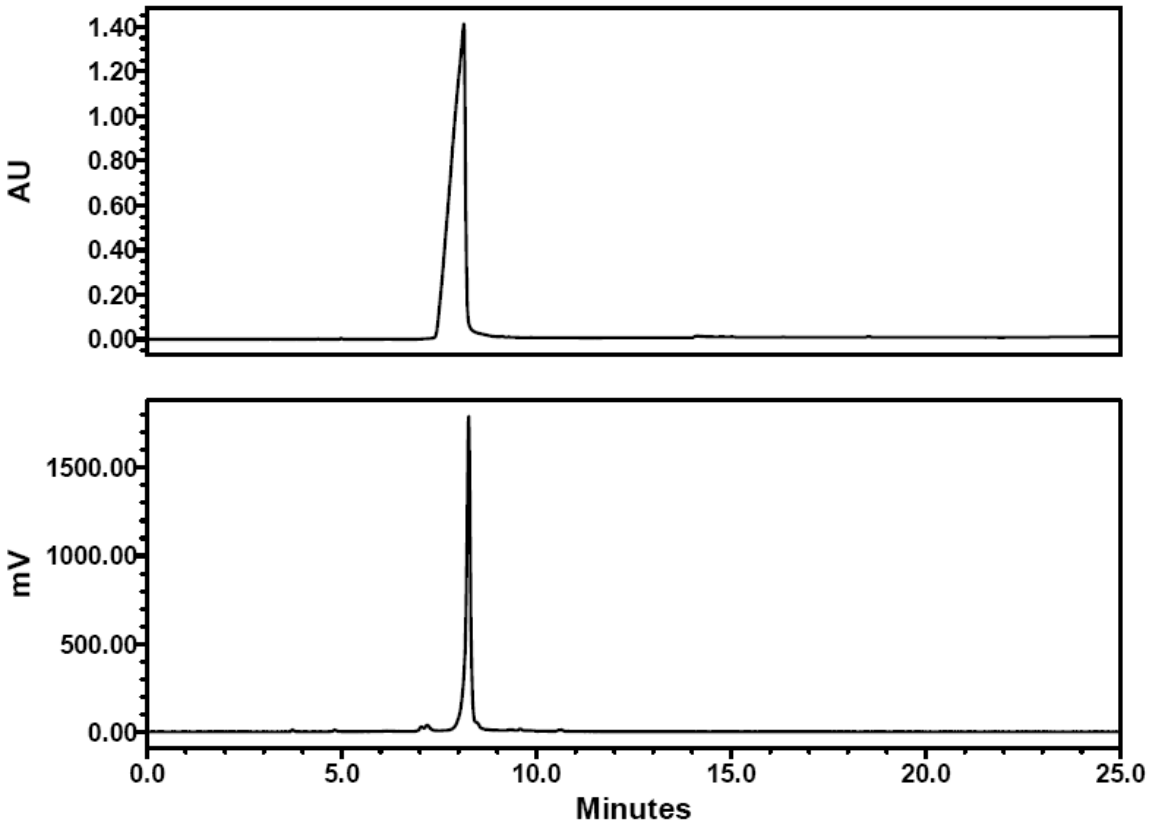


**Figure S 7.36** HPLC chromatograms (UV and γ) of $[Re(CO)_3(BPS)(ImAln)]^{2-}$ **4a** co-injected with **4b**.

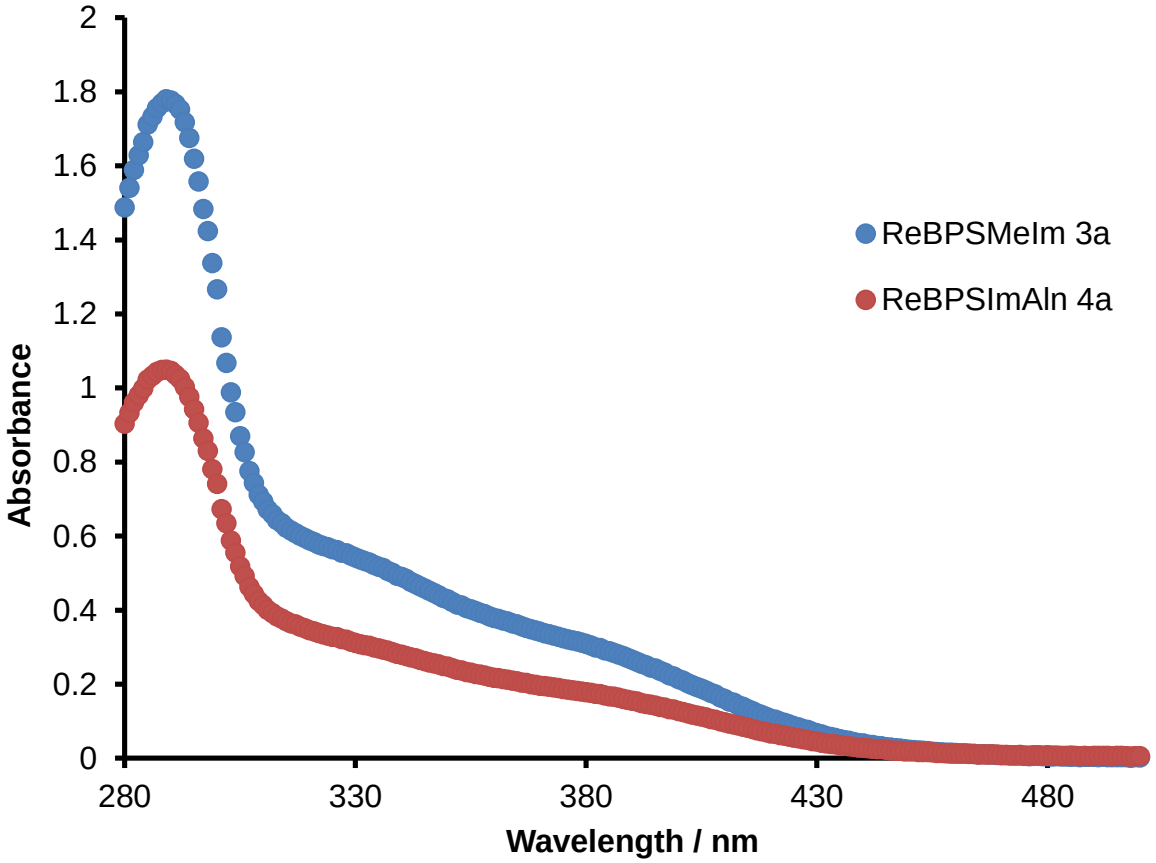


**Figure S 7.37** Absorption spectra for compounds **3a** and **4a** (50µM in $H_2O$).

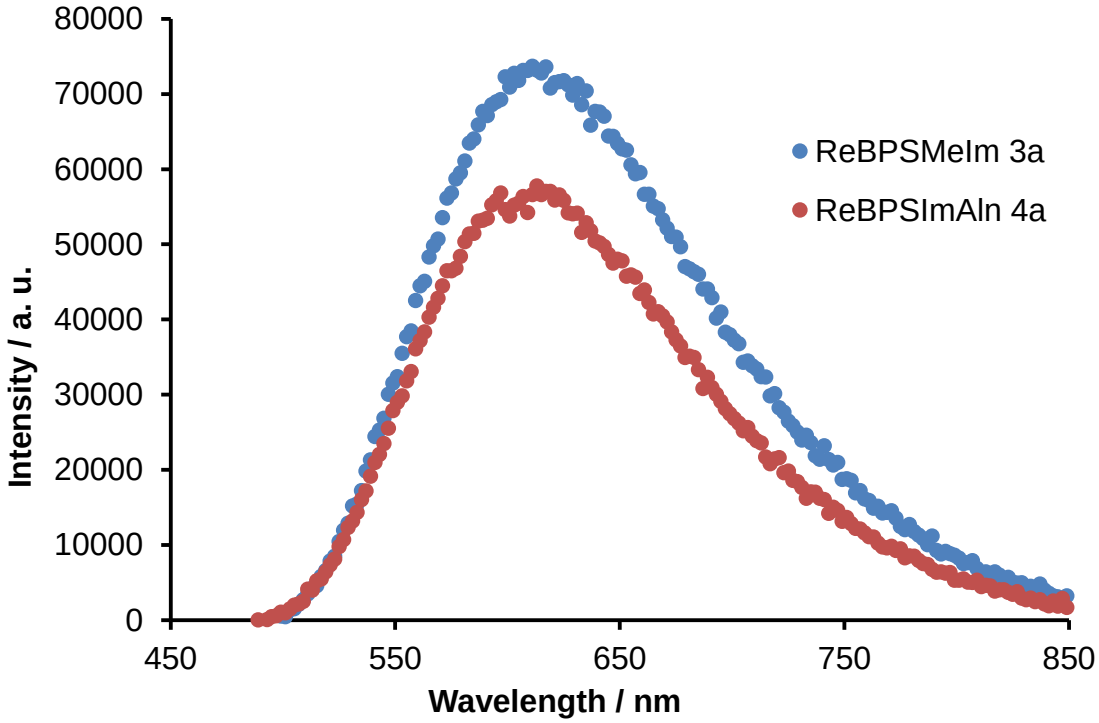


**Figure S 7.38** Emission spectra for compounds **3a** and **4a** (50µM in $H_2O$).

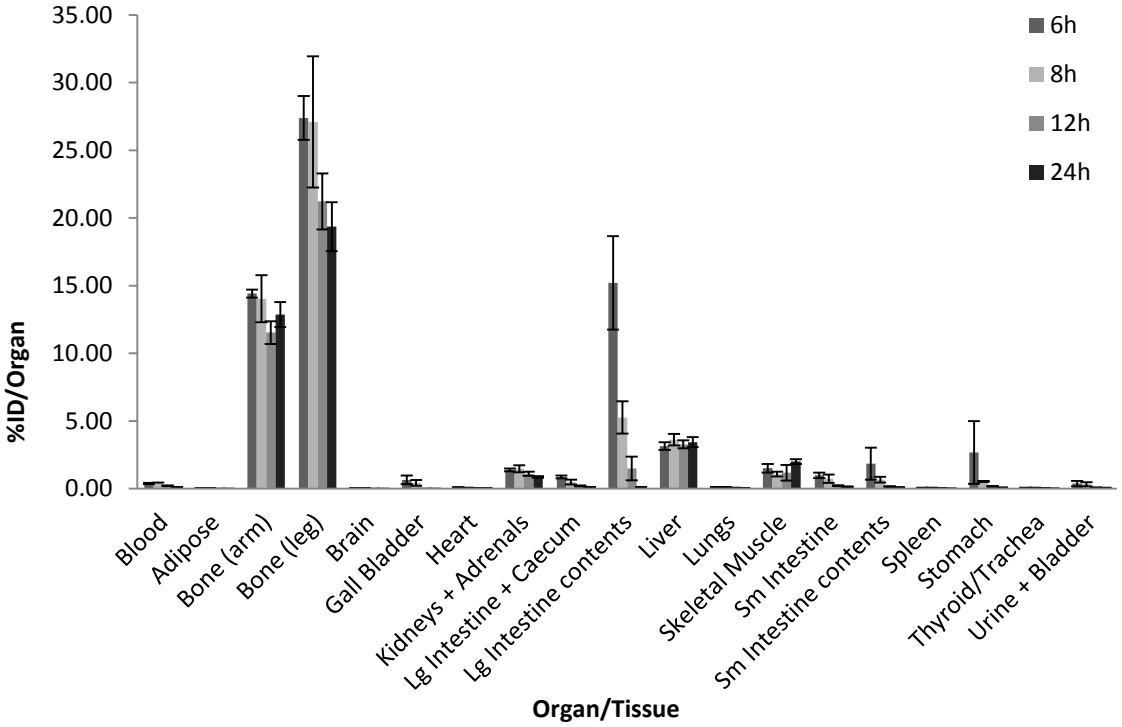


**Figure S 7.39** Biodistrubution profile of **4b** (%ID/O) at different time points performed on healthy female Balb/c mice.

# 8 Appendix 3 (Supporting Information for Chapter 4)

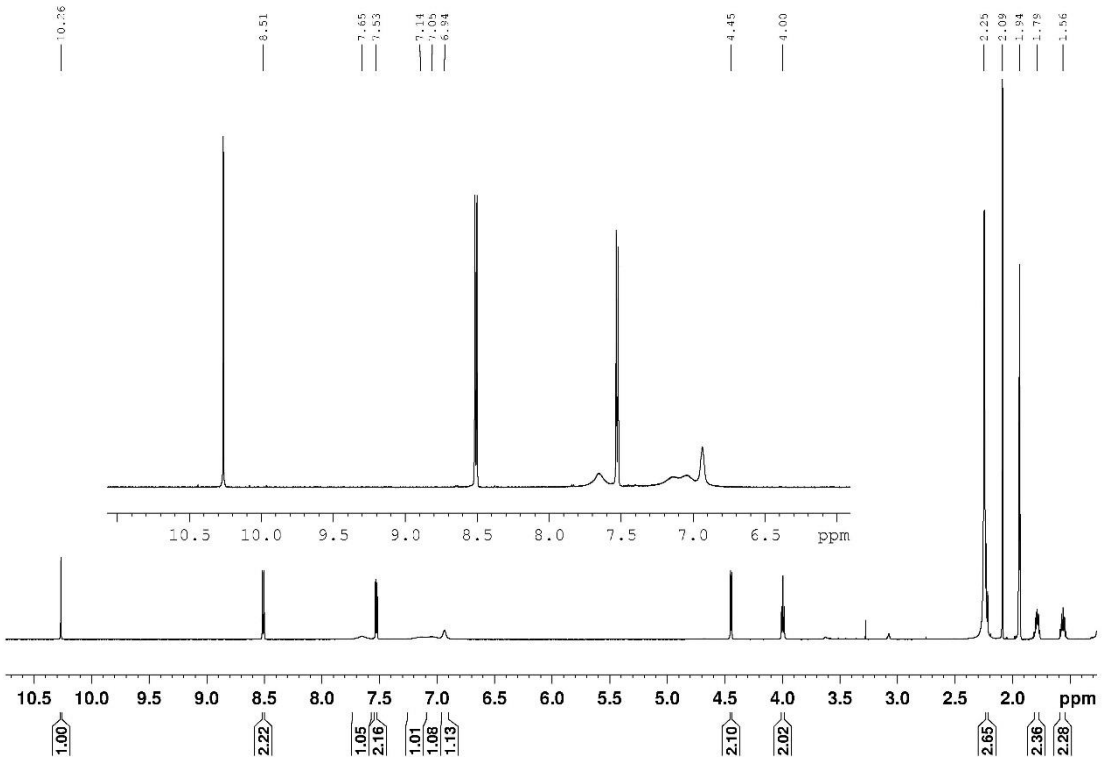


**Figure S 8.1** $^{1}$H NMR spectrum ($CD_3CN$, 600 MHz) of **6**.

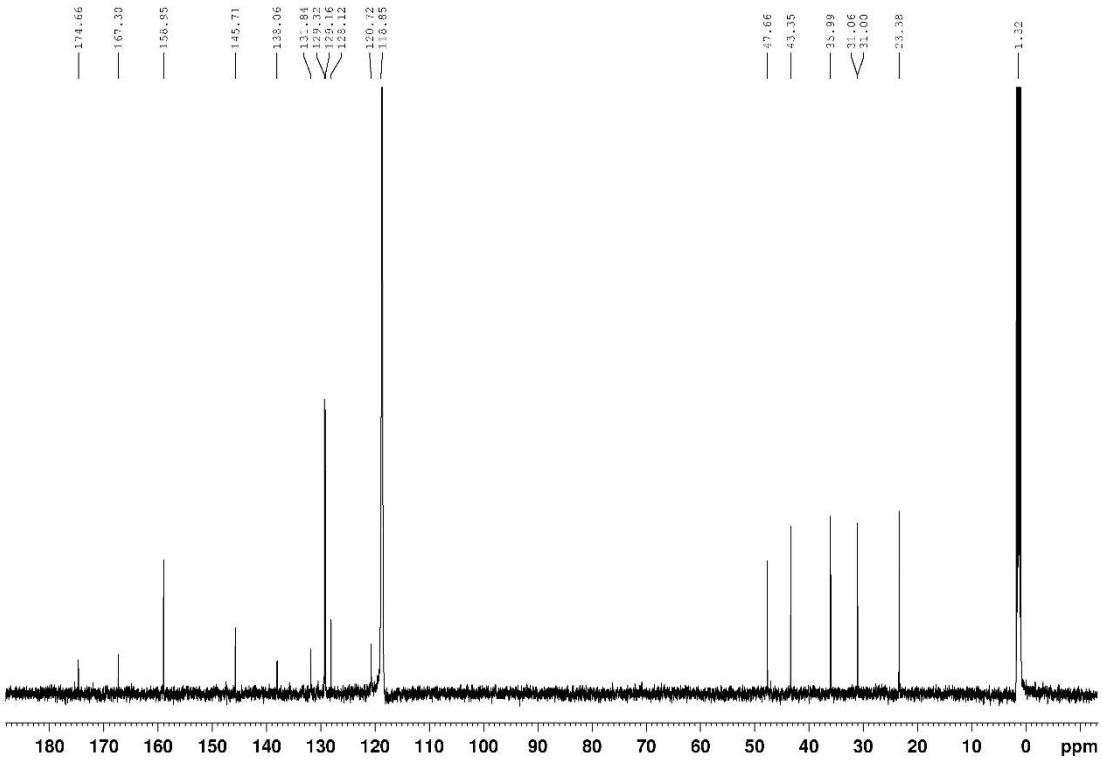


**Figure S 8.2** $^{13}C$ NMR spectrum ($CD_3CN$, 150 MHz) of **6**.

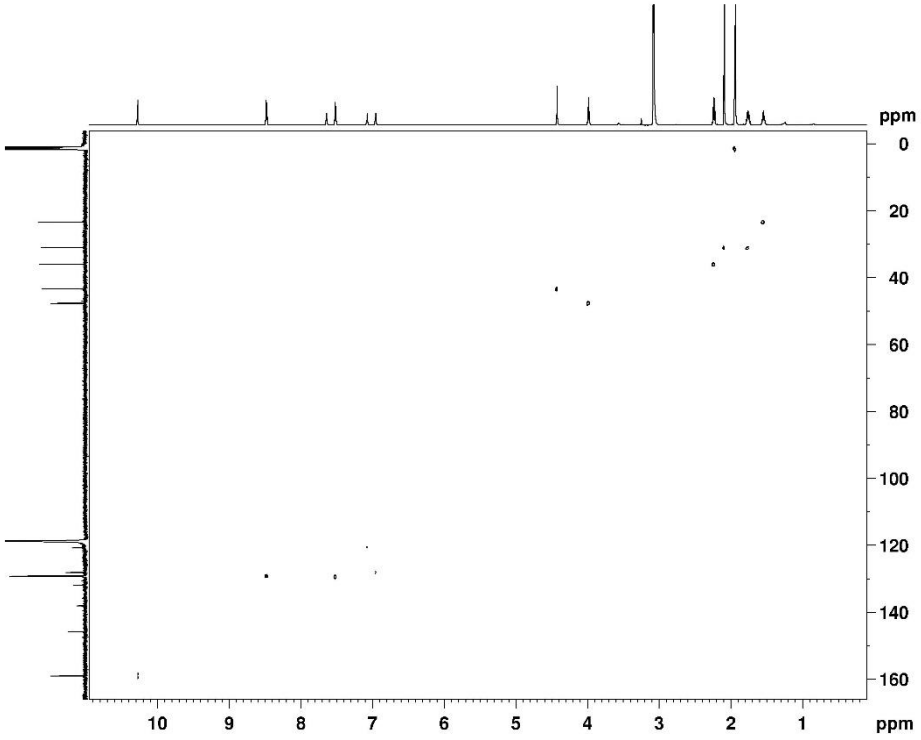


**Figure S 8.3** $^{1}H$-$^{13}C$ HSQC NMR spectrum ($CD_3CN$) of **6**.

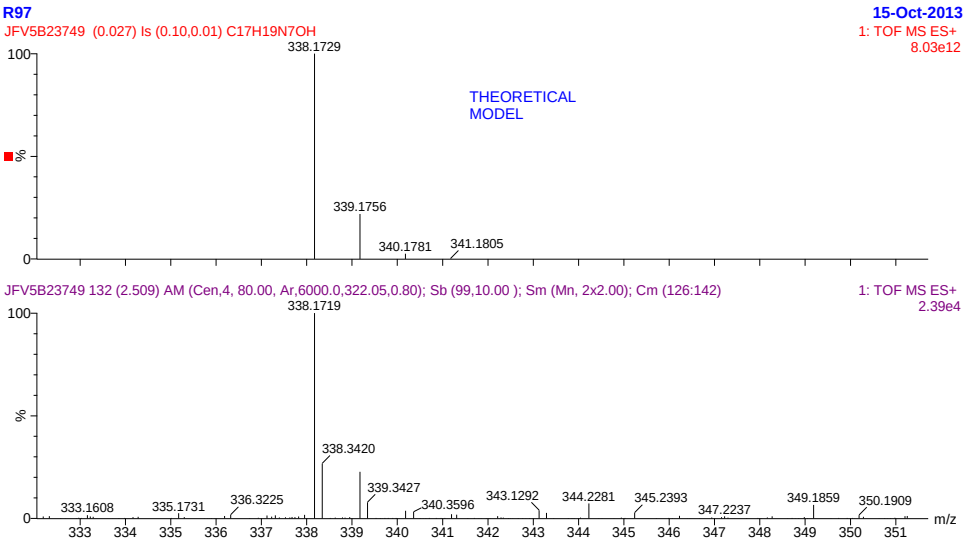


**Figure S 8.4** HRMS of **6**.

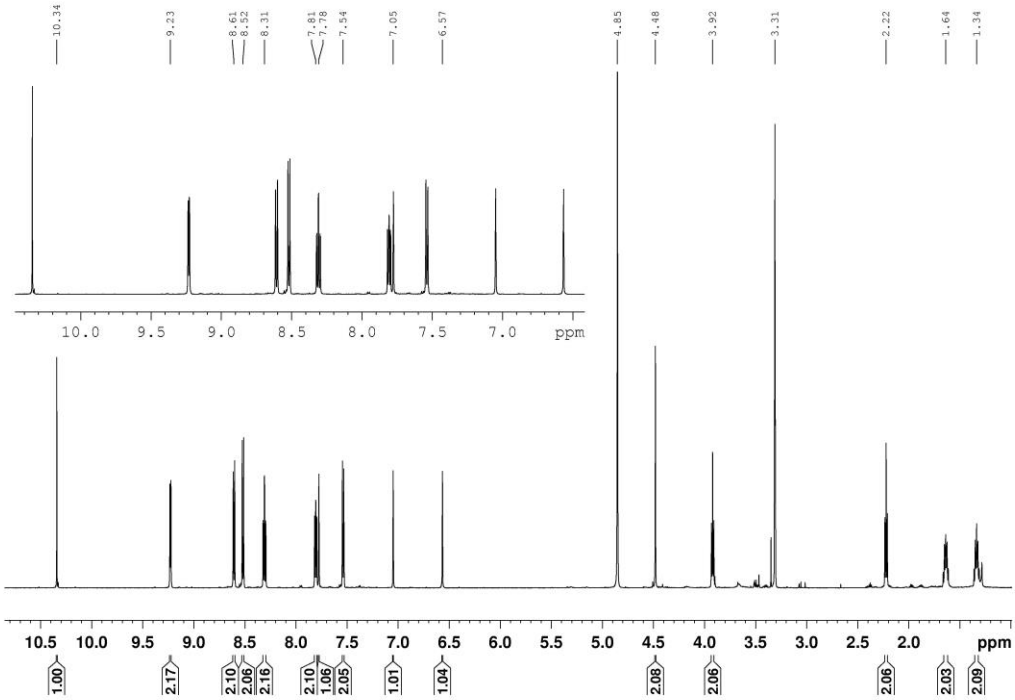


**Figure S 8.5** $^{1}$H NMR spectrum (MeOD, 600 MHz) of **10a**.

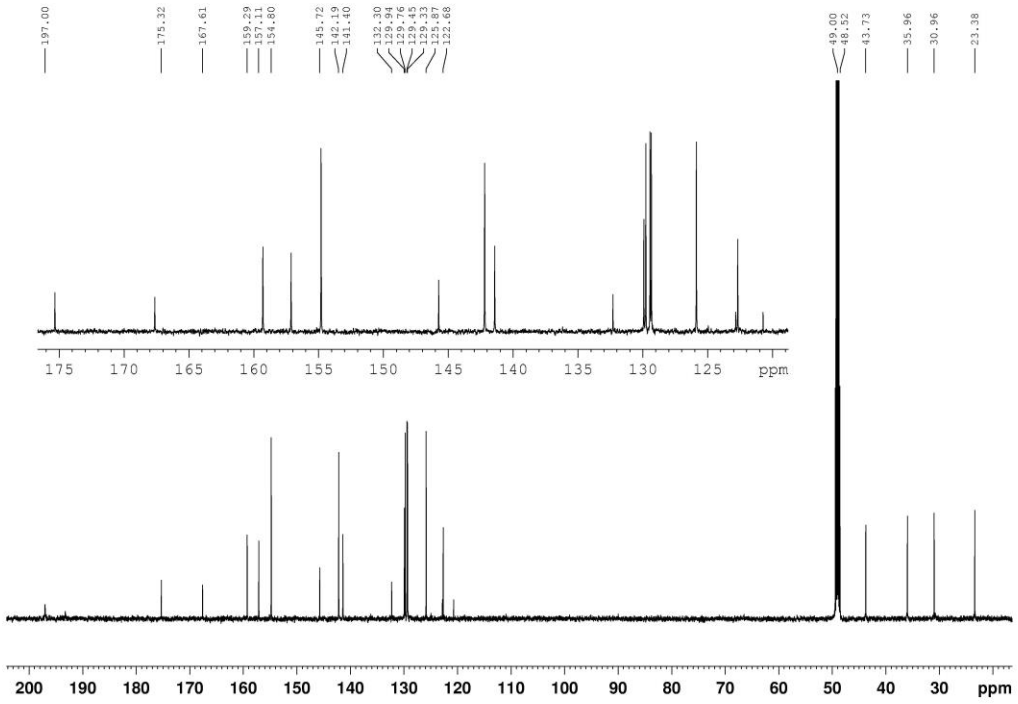


**Figure S 8.6** $^{13}$C NMR spectrum (MeOD, 150 MHz) of **10a**.

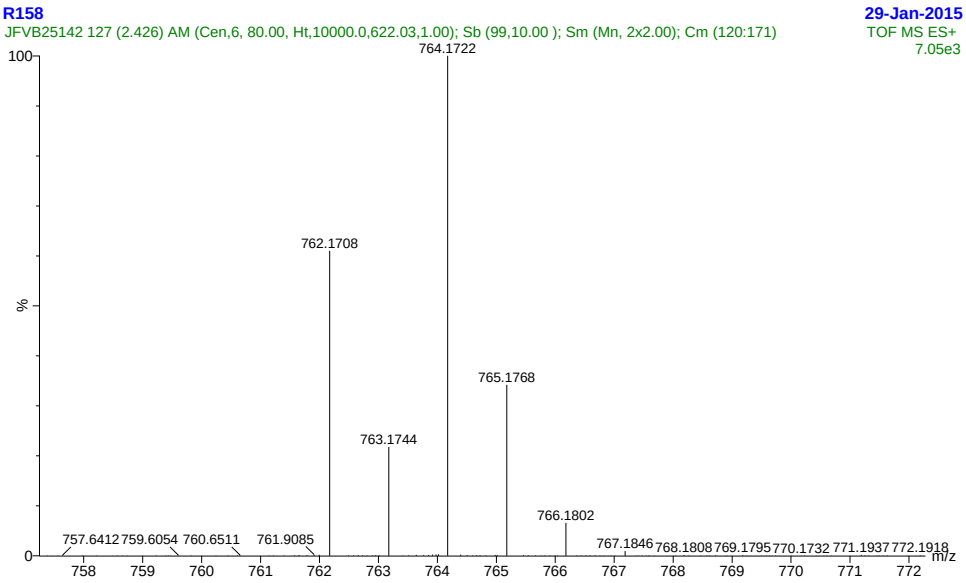


**Figure S 8.7** HRMS of **10a**.

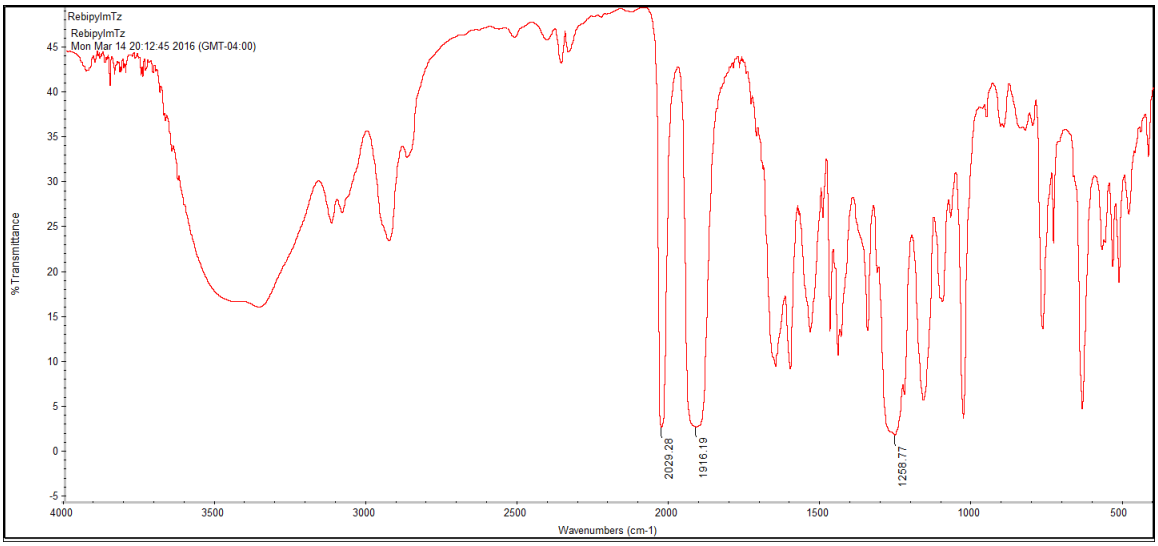


**Figure S 8.8** IR spectrum of **10a**.

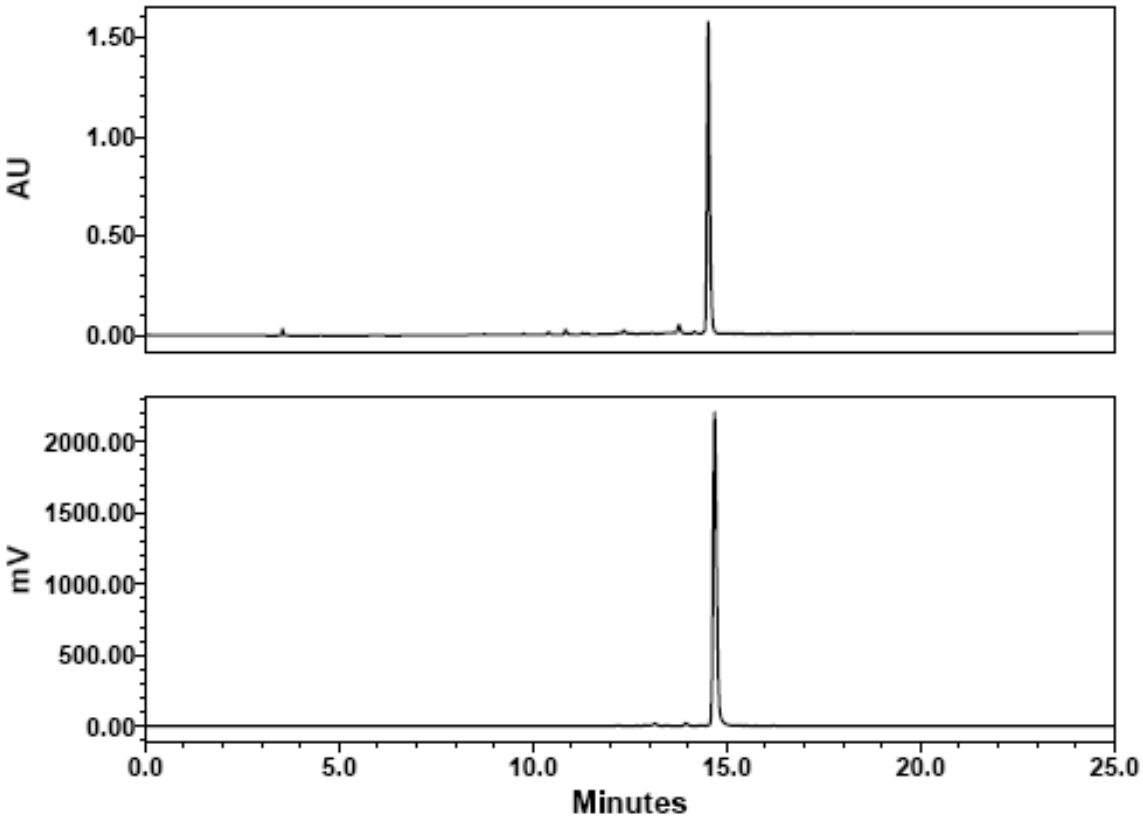


**Figure S 8.9** HPLC chromatograms (UV and γ) of $[Re(CO)_3(bipy)(ImTz)]^+$ co-injected with **10b**.

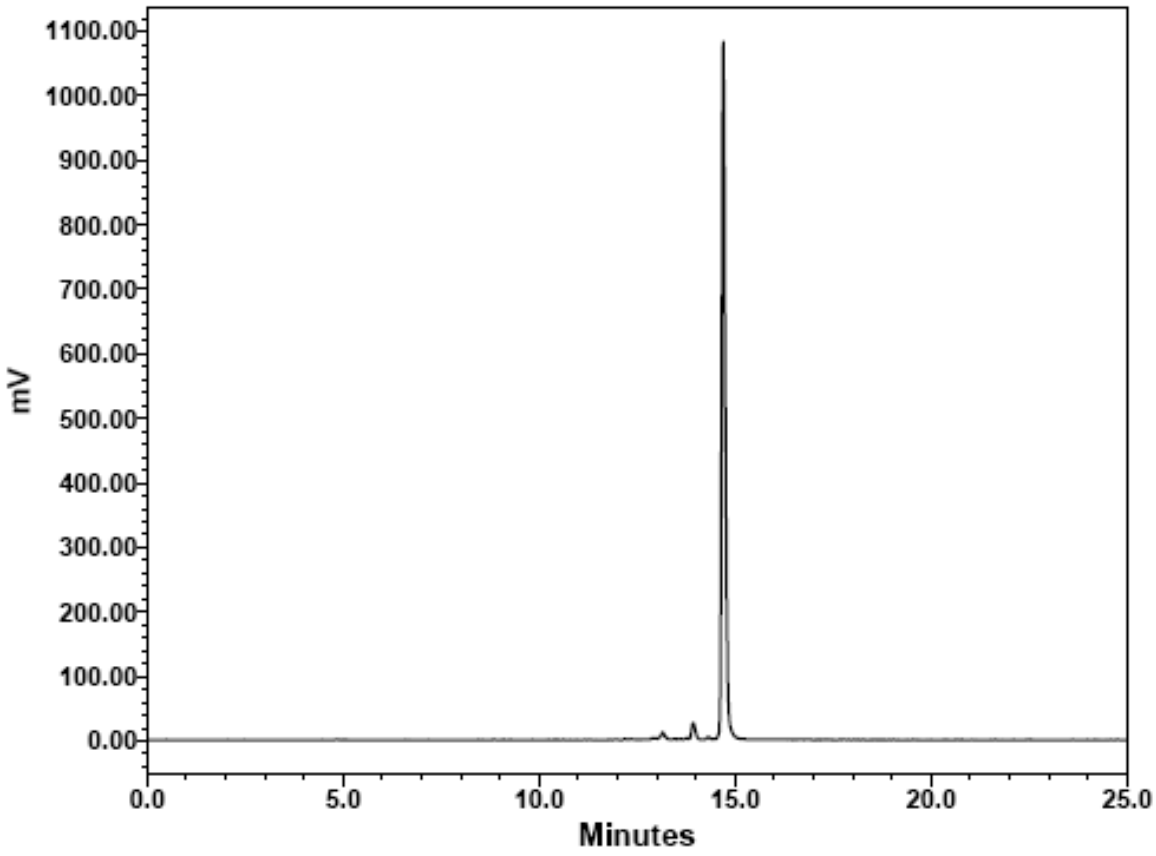


**Figure S 8.10** γ-HPLC chromatogram at 0.5 h following cysteine challenge to $[^{99m}Tc(CO)_3(bipy)(ImTz)]^+$ **10b**.

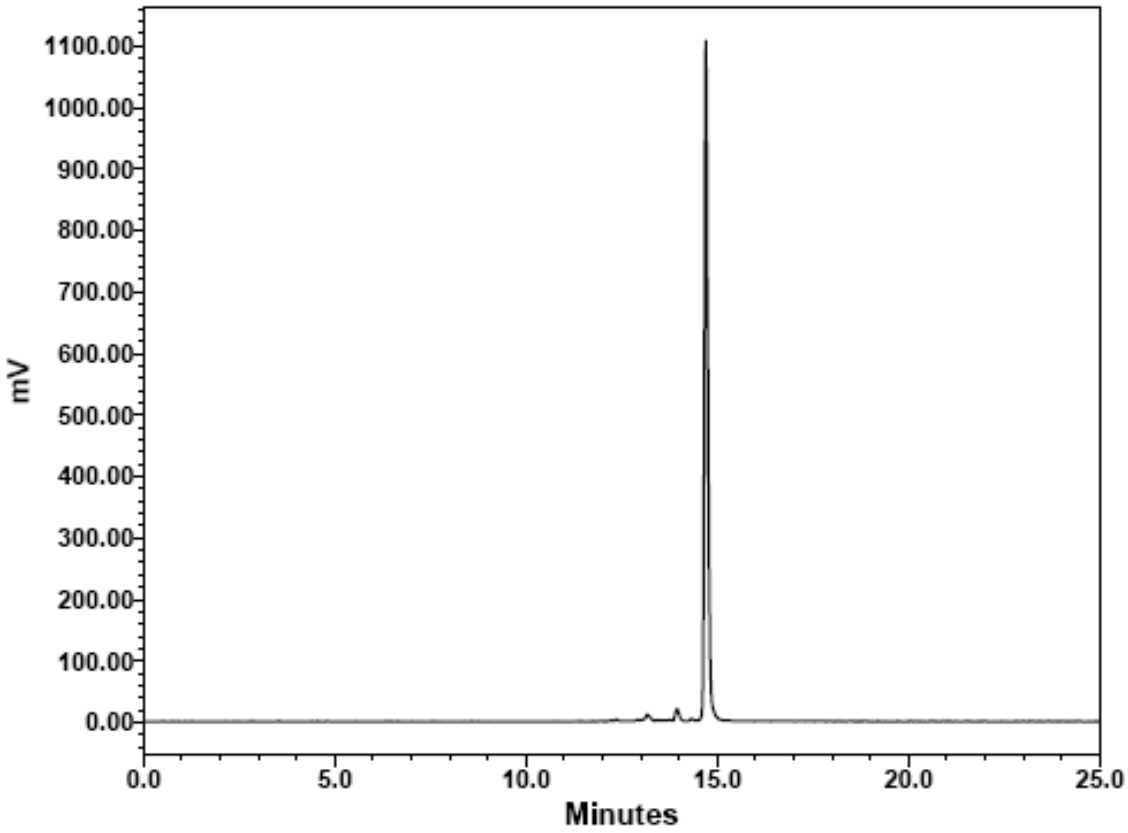


**Figure S 8.11** γ-HPLC chromatogram at 1 h following cysteine challenge to $[^{99m}Tc(CO)_3(bipy)(ImTz)]^+$ **10b**.

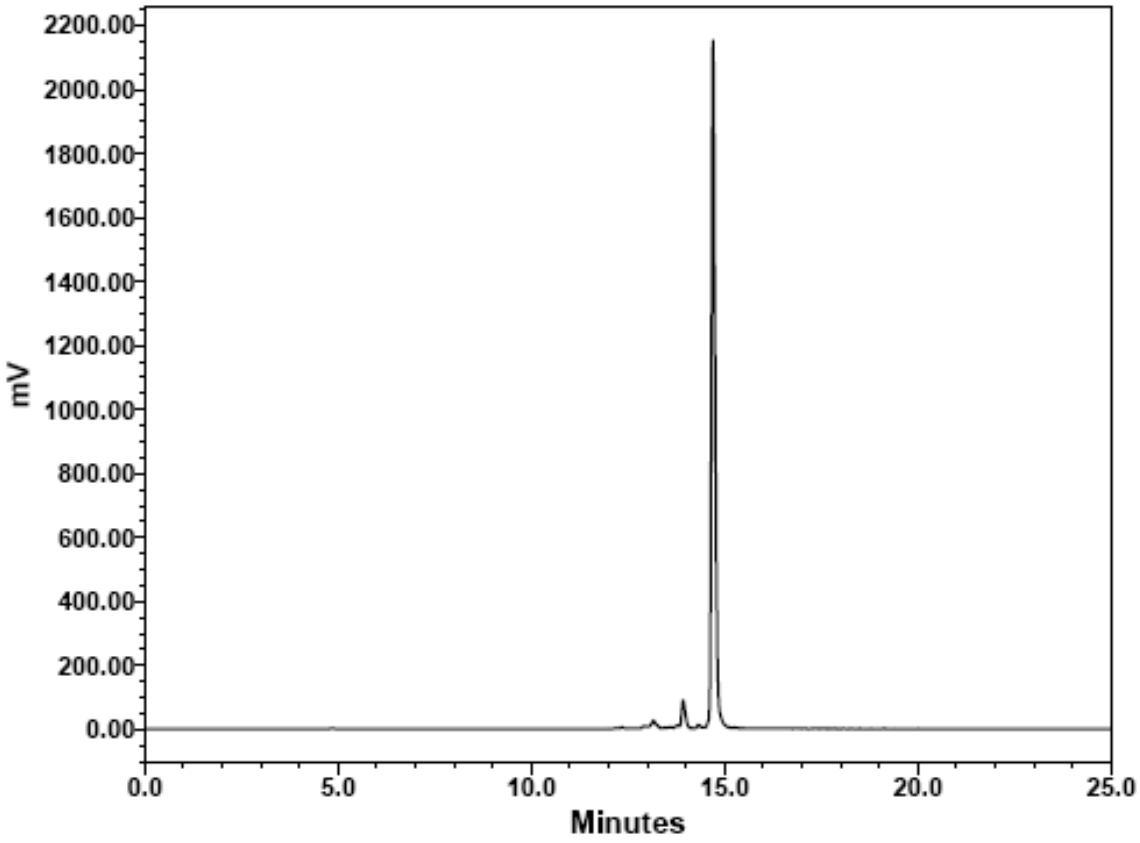


**Figure S 8.12** γ-HPLC chromatogram at 2 h following cysteine challenge to $[^{99m}Tc(CO)_3(bipy)(ImTz)]^+$ **10b**.

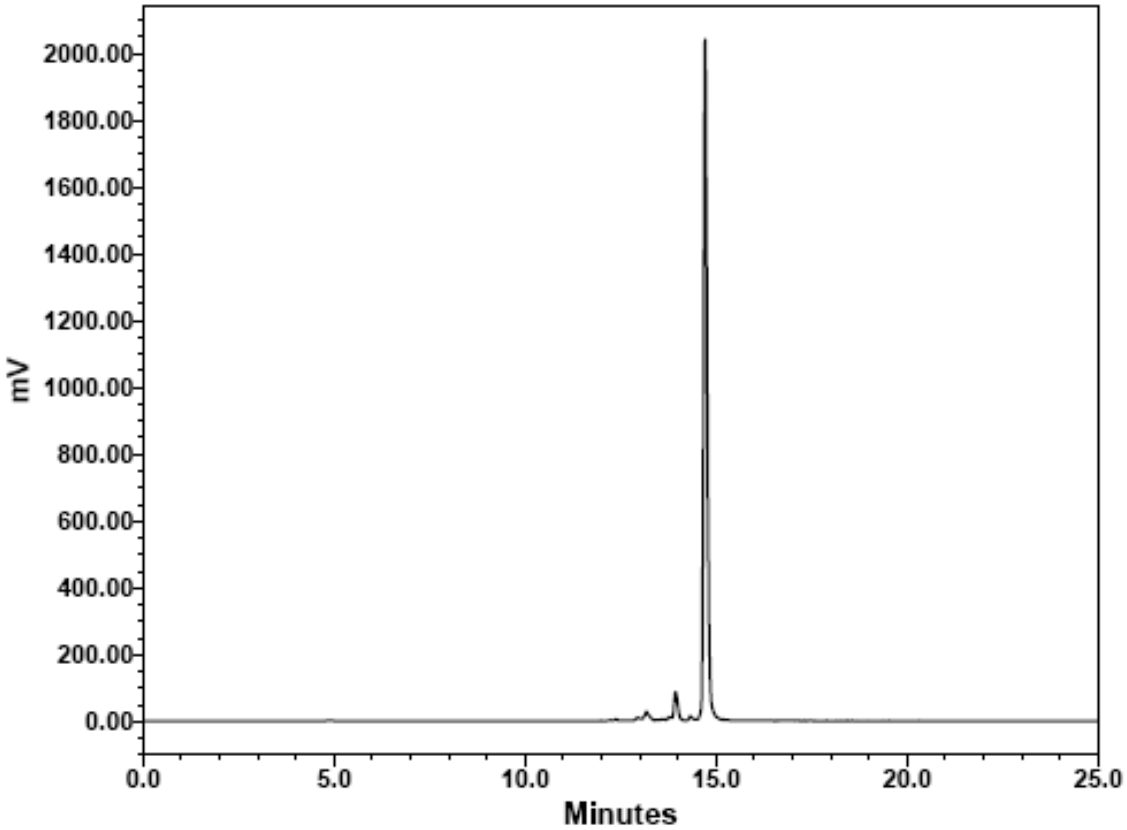


**Figure S 8.13** γ-HPLC chromatogram at 3 h following cysteine challenge to $[^{99m}Tc(CO)_3(bipy)(ImTz)]^+$ **10b**.

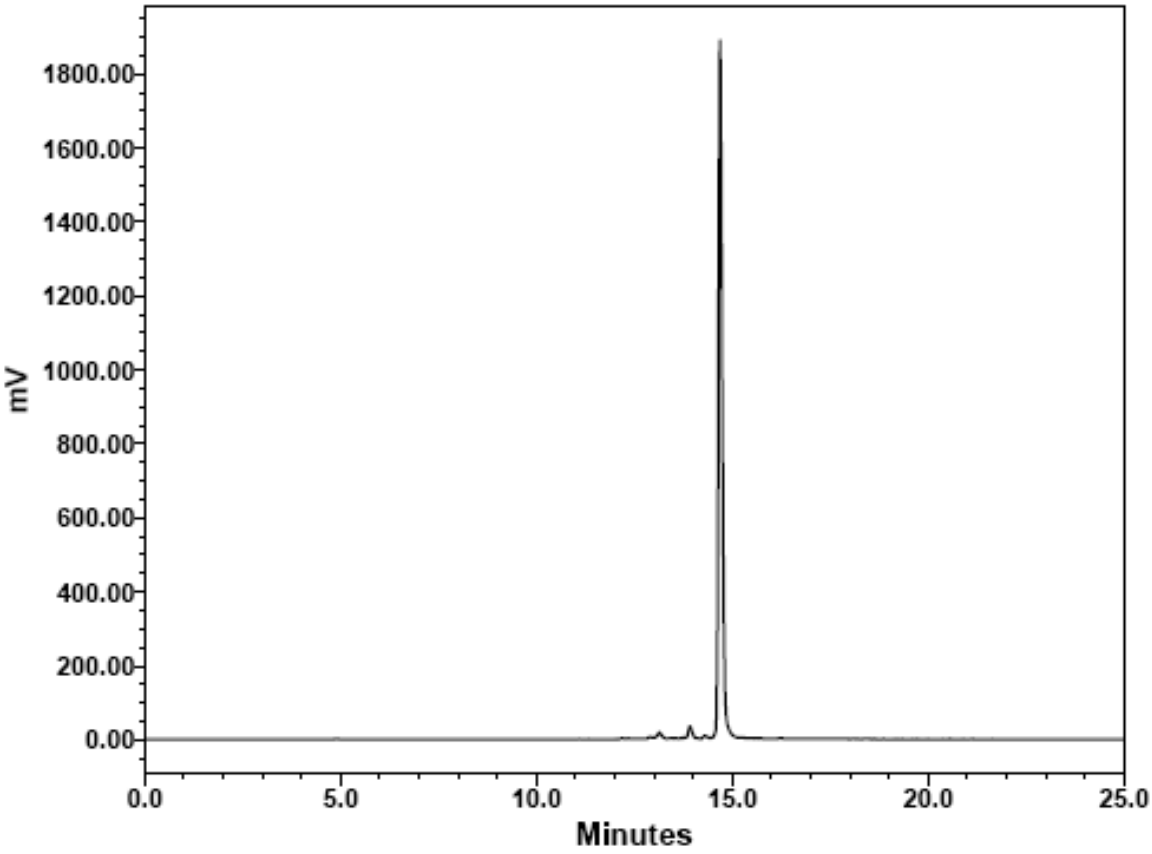


**Figure S 8.14** γ-HPLC chromatogram at 6 h following cysteine challenge to $[^{99m}Tc(CO)_3(bipy)(ImTz)]^+$ **10b**.

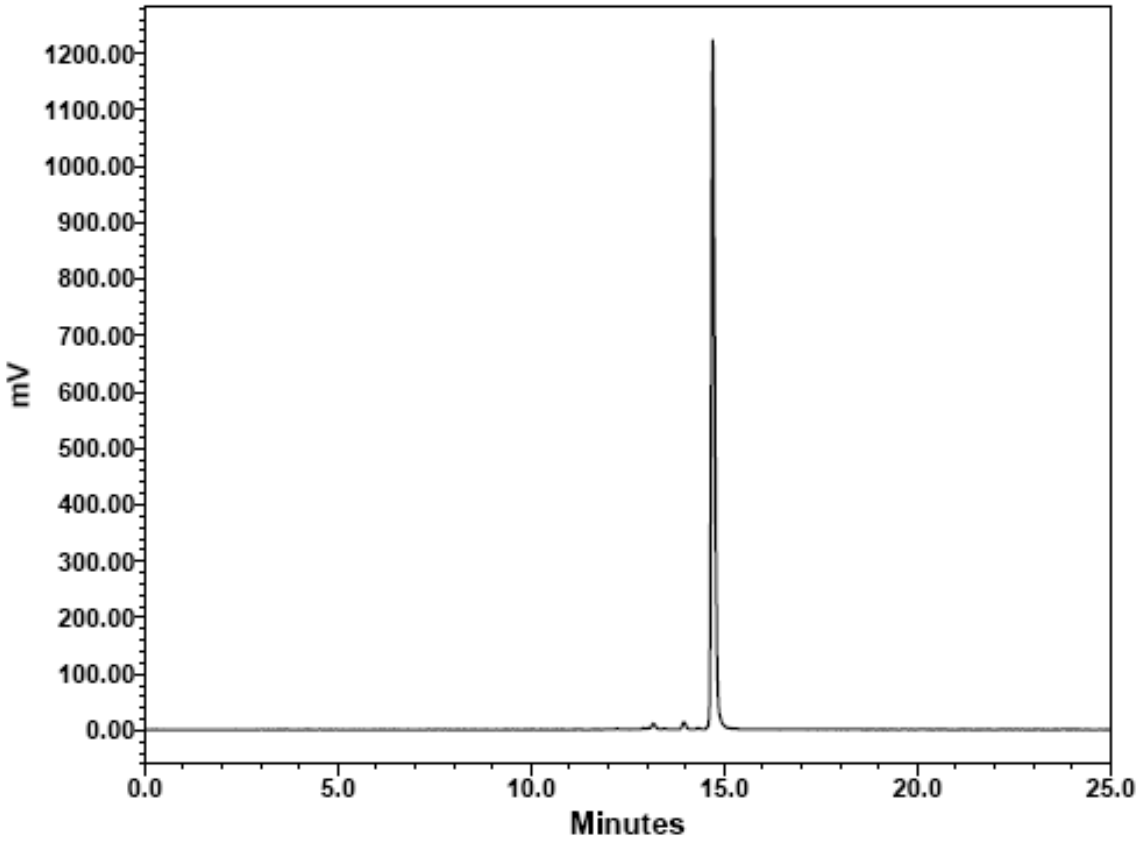


**Figure S 8.15** γ-HPLC chromatogram at 0.5 h following histidine challenge to $[^{99m}Tc(CO)_3(bipy)(ImTz)]^+$ **10b**.

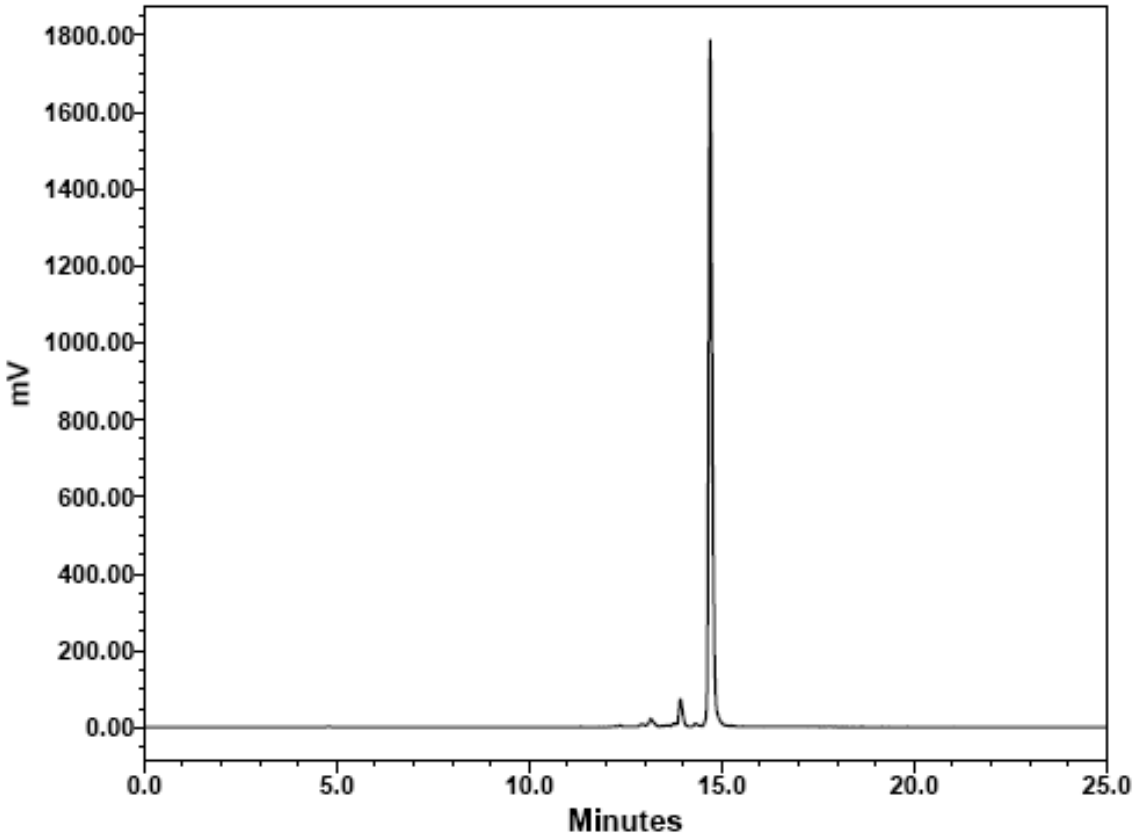


**Figure S 8.16** γ-HPLC chromatogram at 1 h following histidine challenge to $[^{99m}Tc(CO)_3(bipy)(ImTz)]^+$ **10b**.

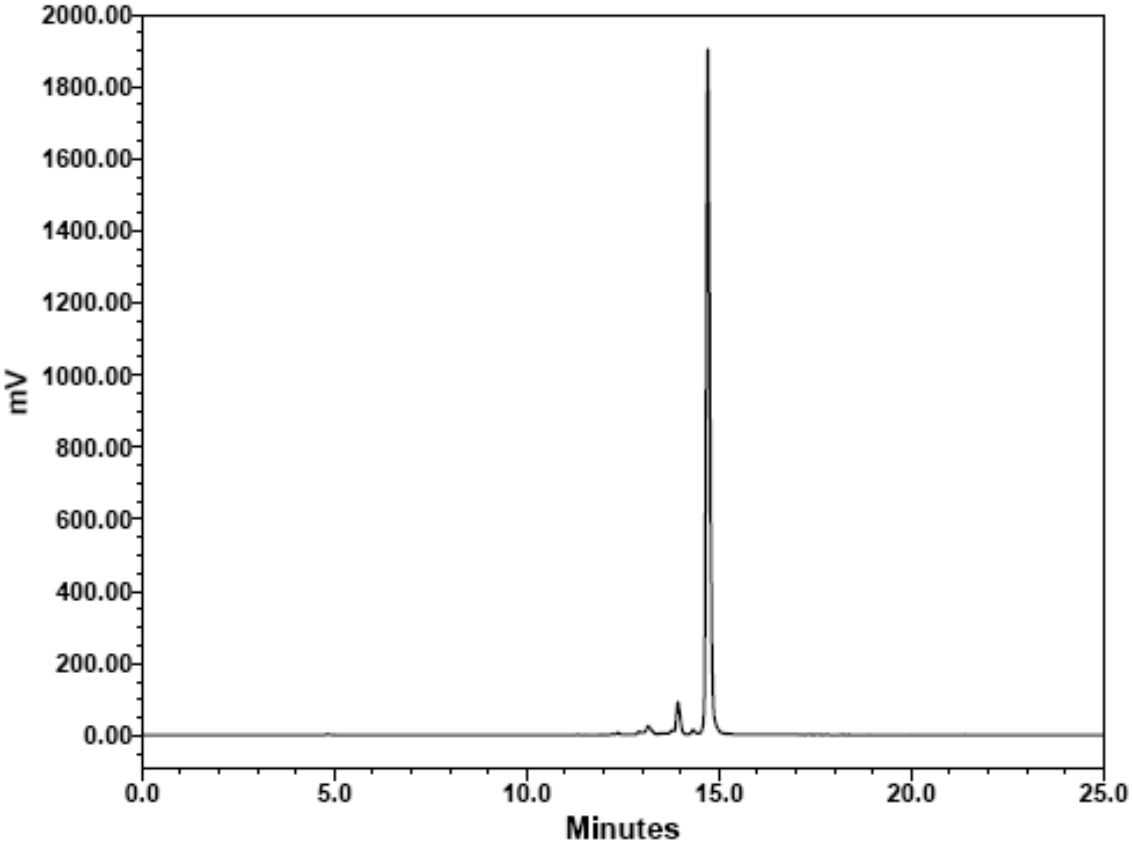


**Figure S 8.17** γ-HPLC chromatogram at 2 h following histidine challenge to $[^{99m}Tc(CO)_3(bipy)(ImTz)]^+$ **10b**.

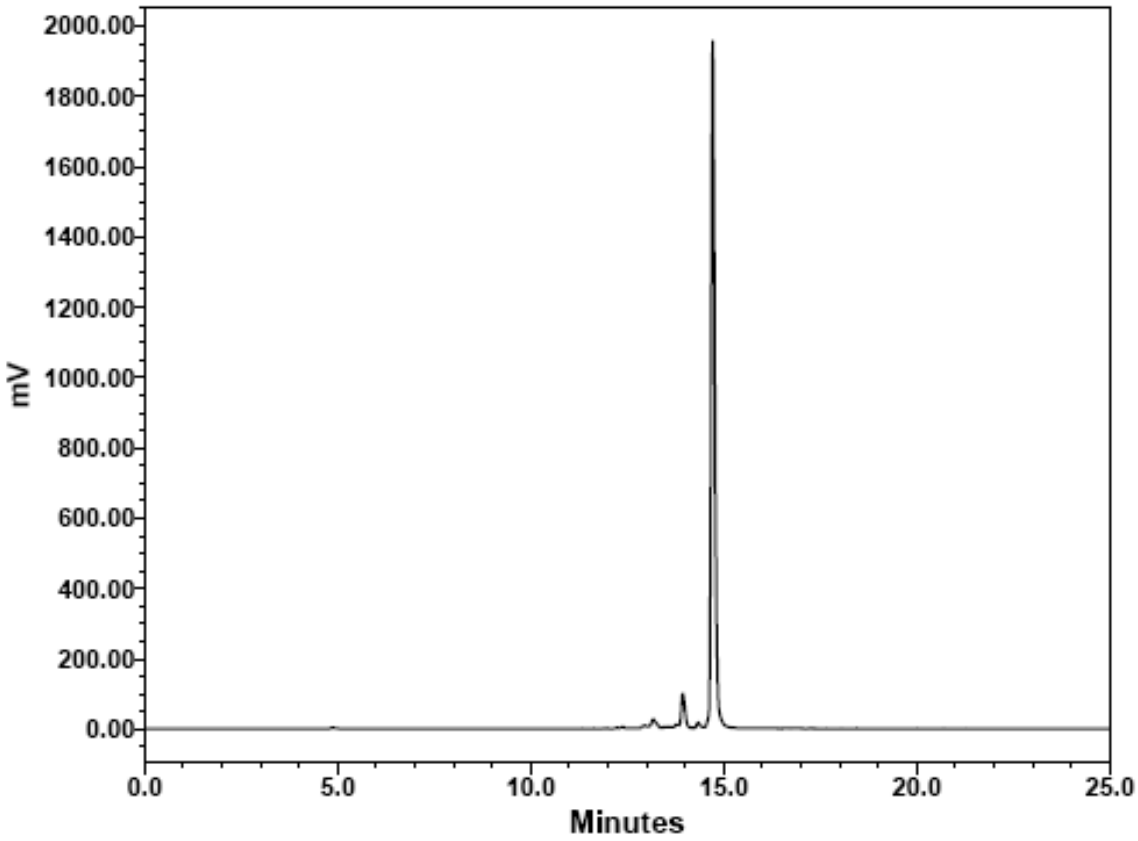


**Figure S 8.18** γ-HPLC chromatogram at 3 h following histidine challenge to $[^{99m}Tc(CO)_3(bipy)(ImTz)]^+$ **10b**.

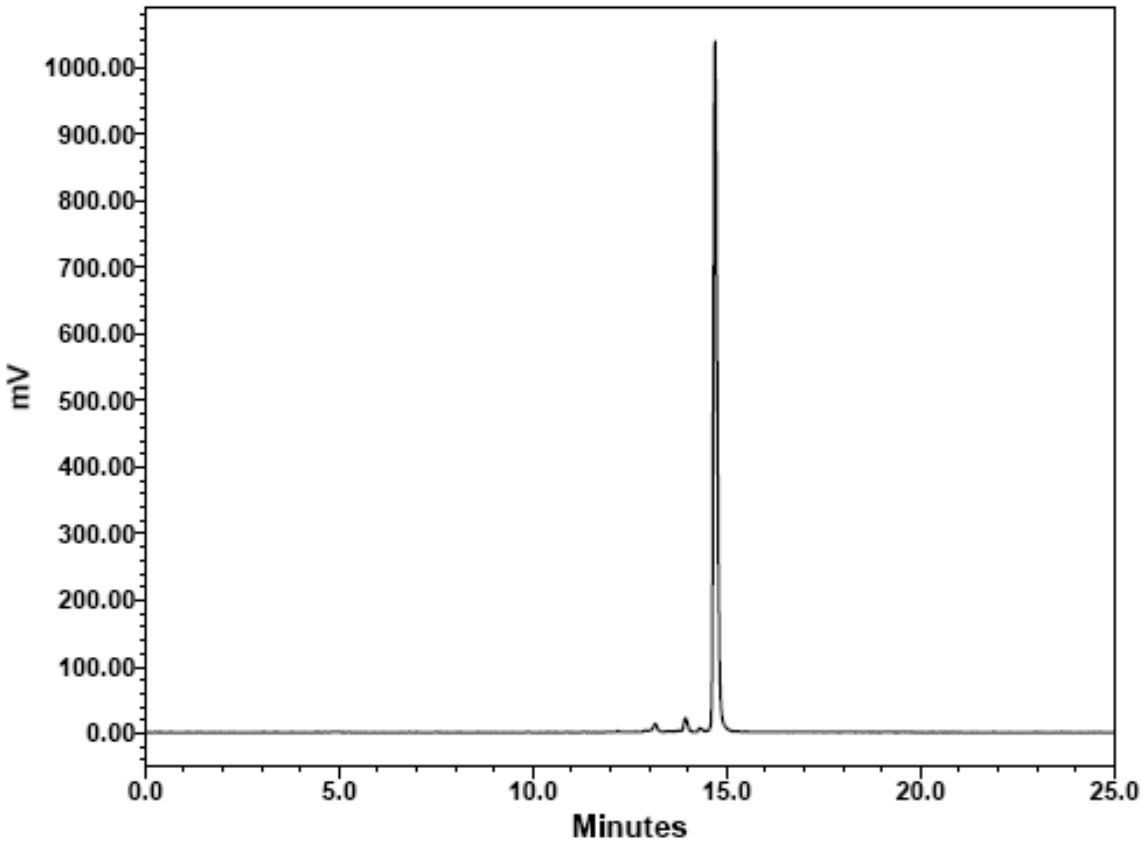


**Figure S 8.19** γ-HPLC chromatogram at 6 h following histidine challenge to $[^{99m}Tc(CO)_3(bipy)(ImTz)]^+$ **10b**.

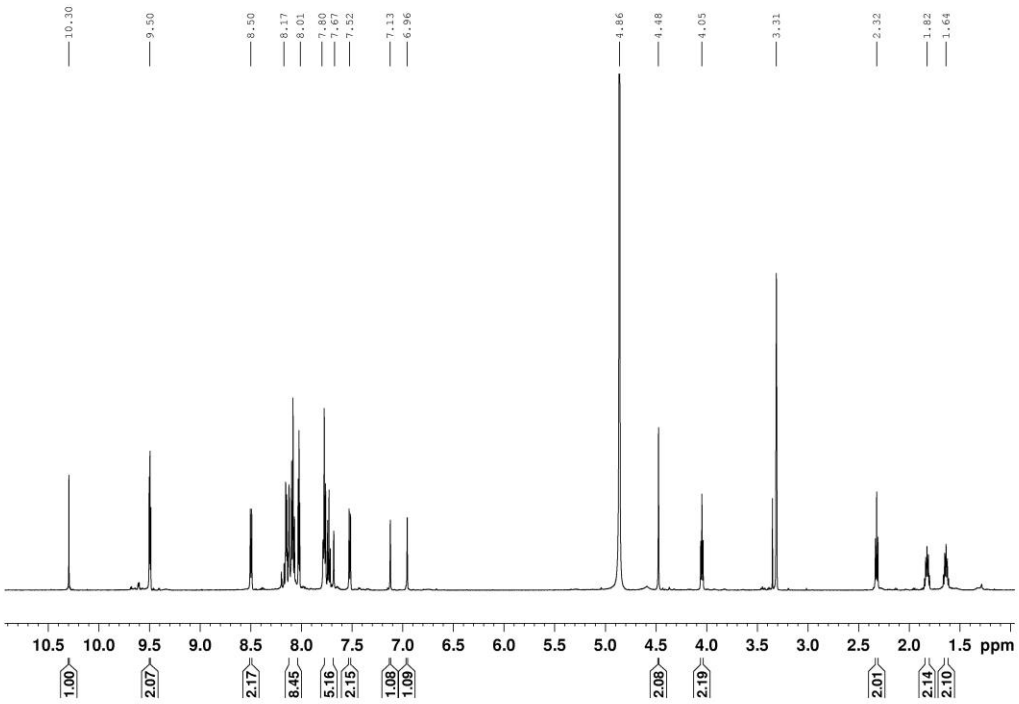


**Figure S 8.20** $^{1}$H NMR spectrum (MeOD, 600 MHz) of **11a**.

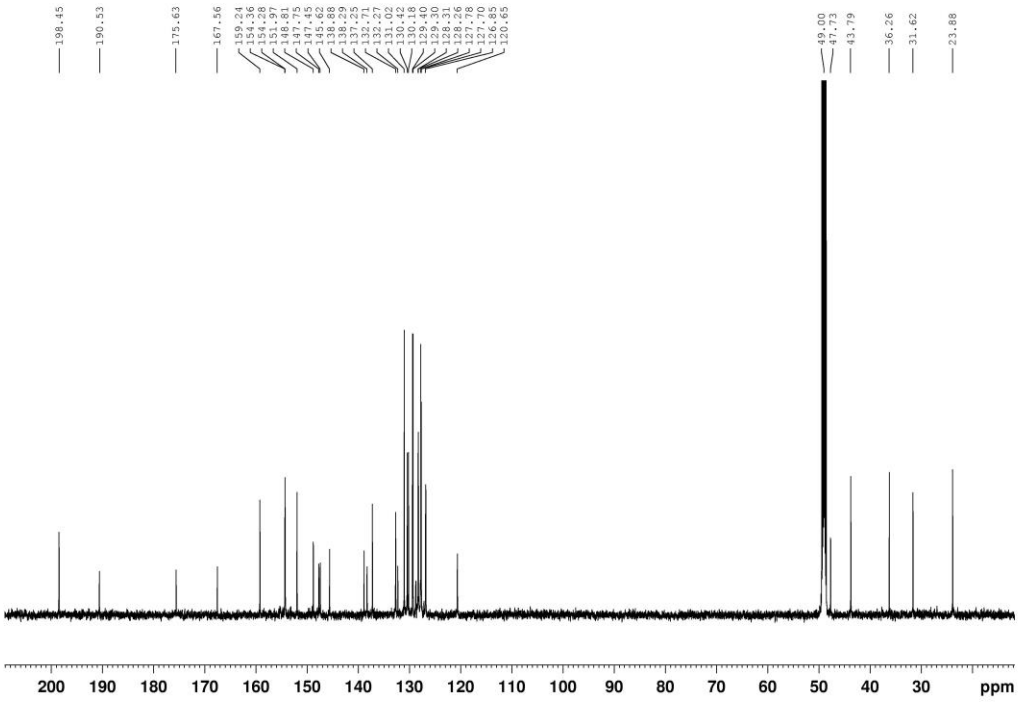


**Figure S 8.21** $^{13}$C NMR spectrum (MeOD, 150 MHz) of **11a**.

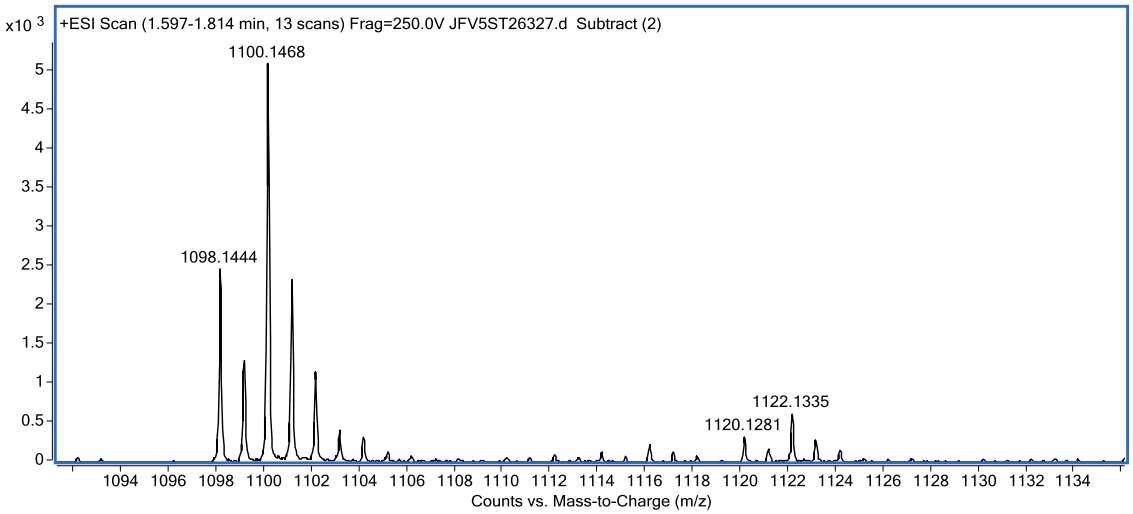


**Figure S 8.22** HRMS of **11a**.

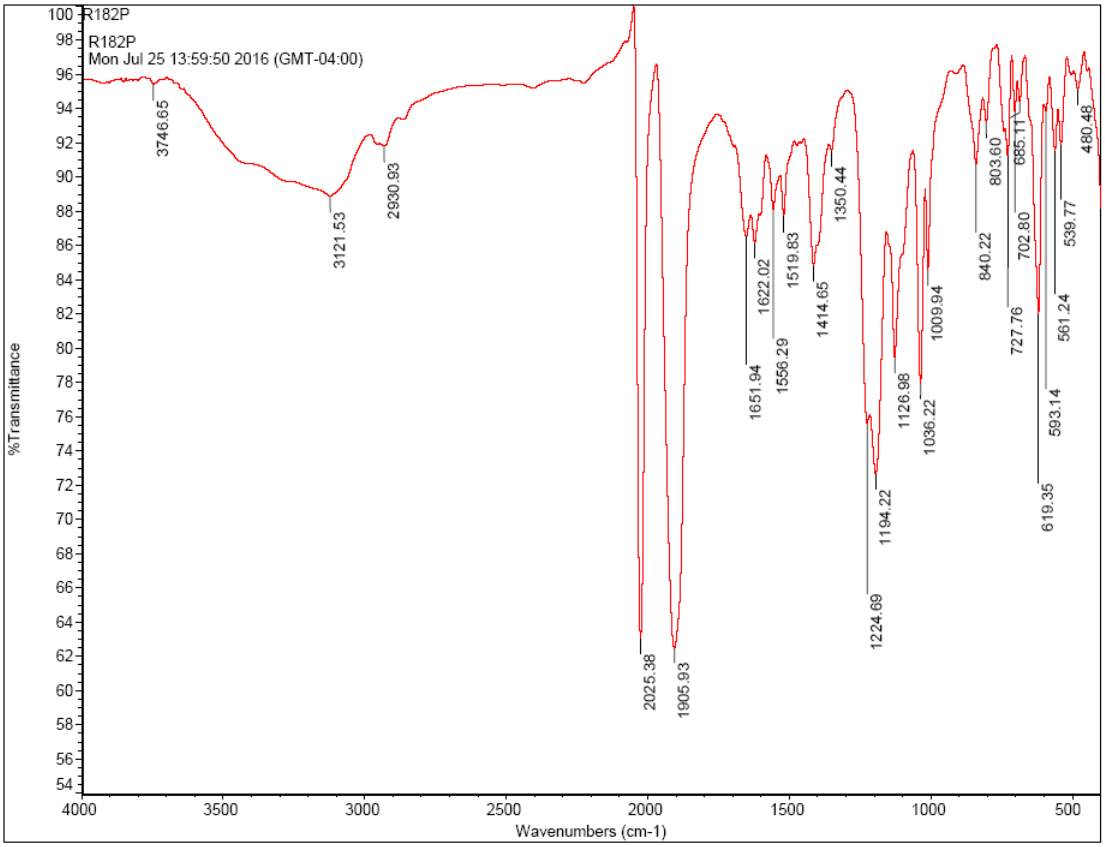


**Figure S 8.23** IR spectrum of **11a**.

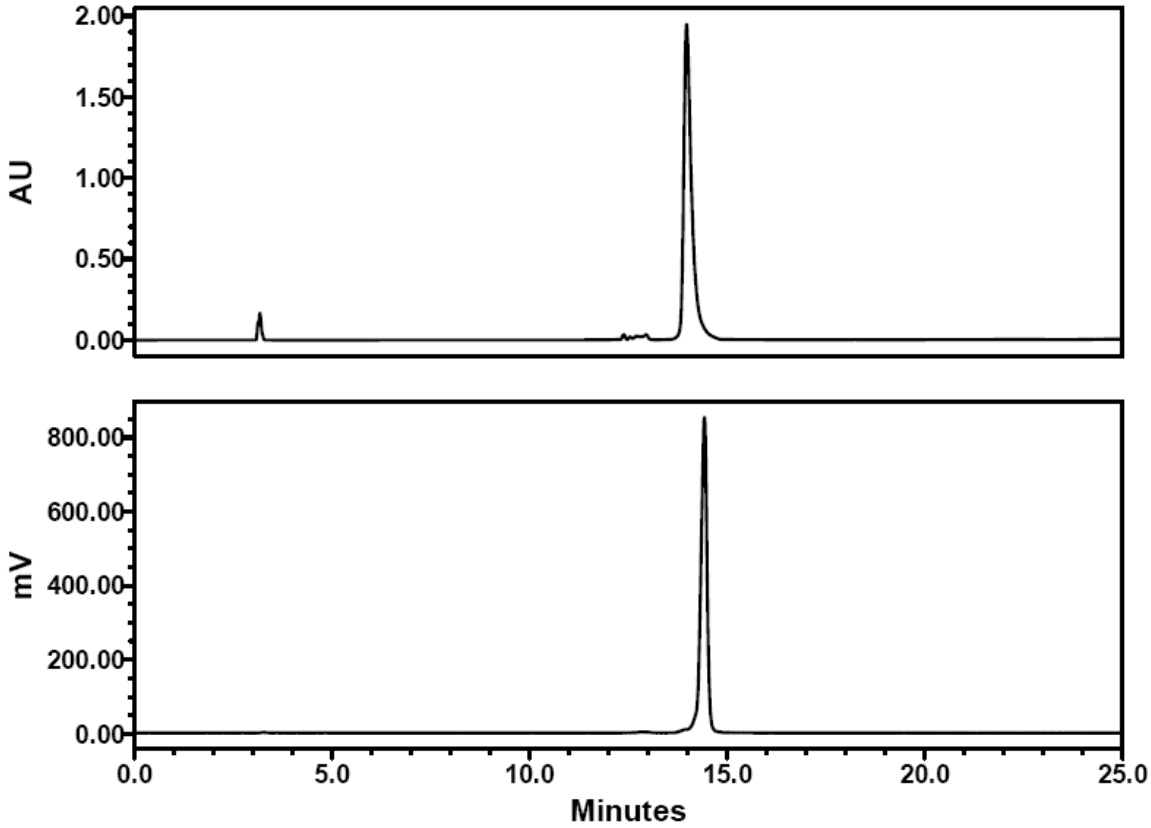


**Figure S 8.24** HPLC chromatograms (UV and γ) of $[Re(CO)_3(BPS)(ImTz)]^-$ co-injected with **11b**.

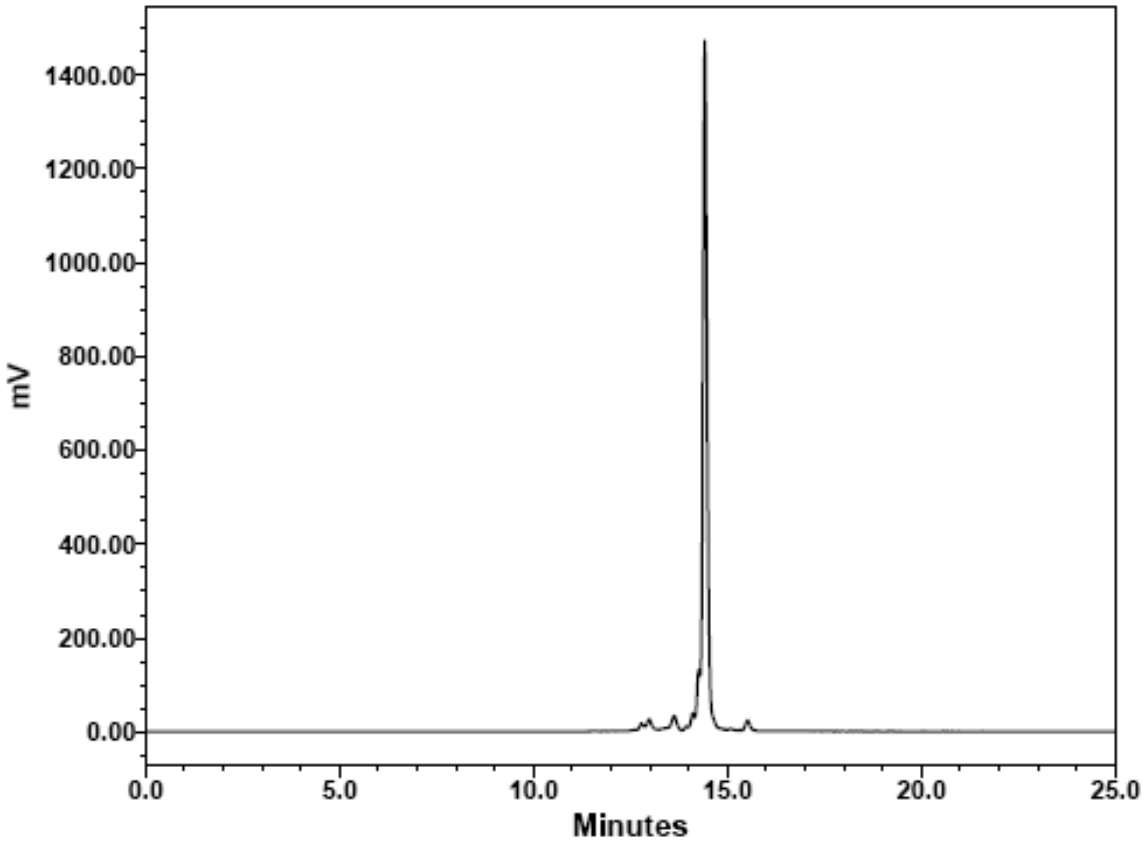


**Figure S 8.25** γ-HPLC chromatogram at 0.5 h following cysteine challenge to $[^{99m}Tc(CO)_3(BPS)(ImTz)]^-$ **11b**.

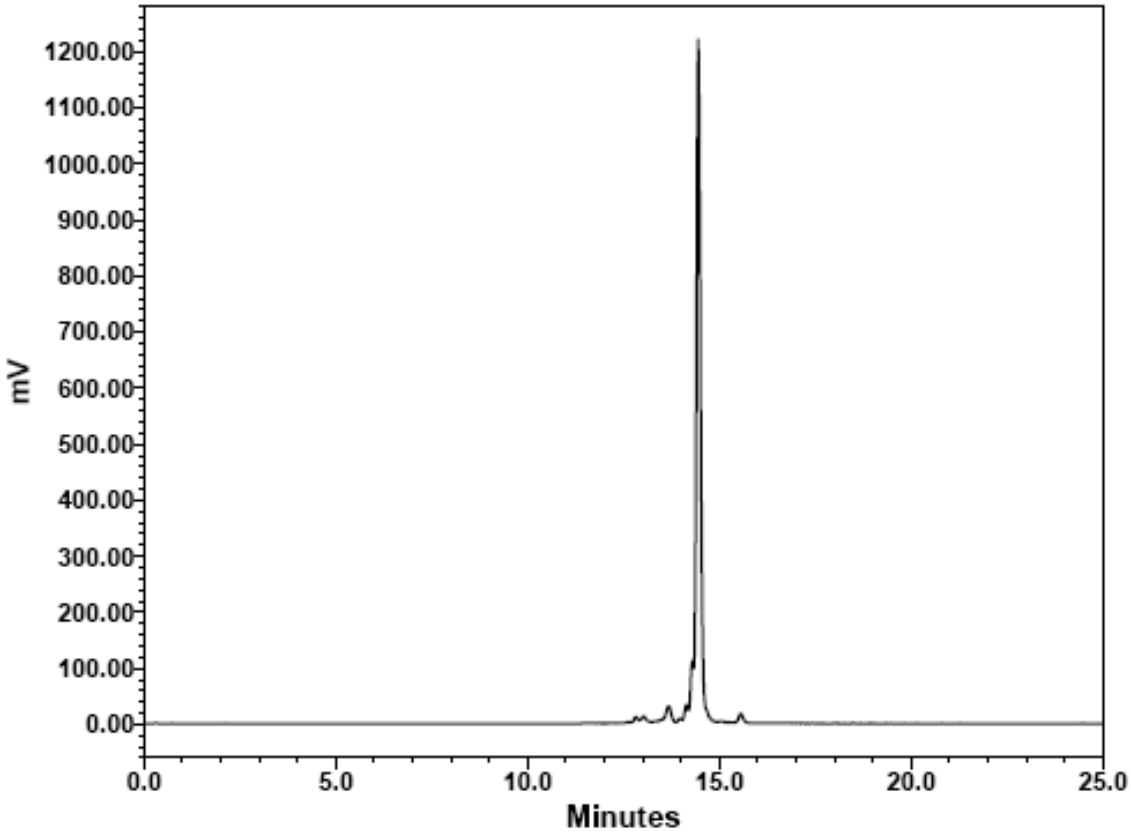


**Figure S 8.26** γ-HPLC chromatogram at 1 h following cysteine challenge to $[^{99m}Tc(CO)_3(BPS)(ImTz)]^-$ **11b**.

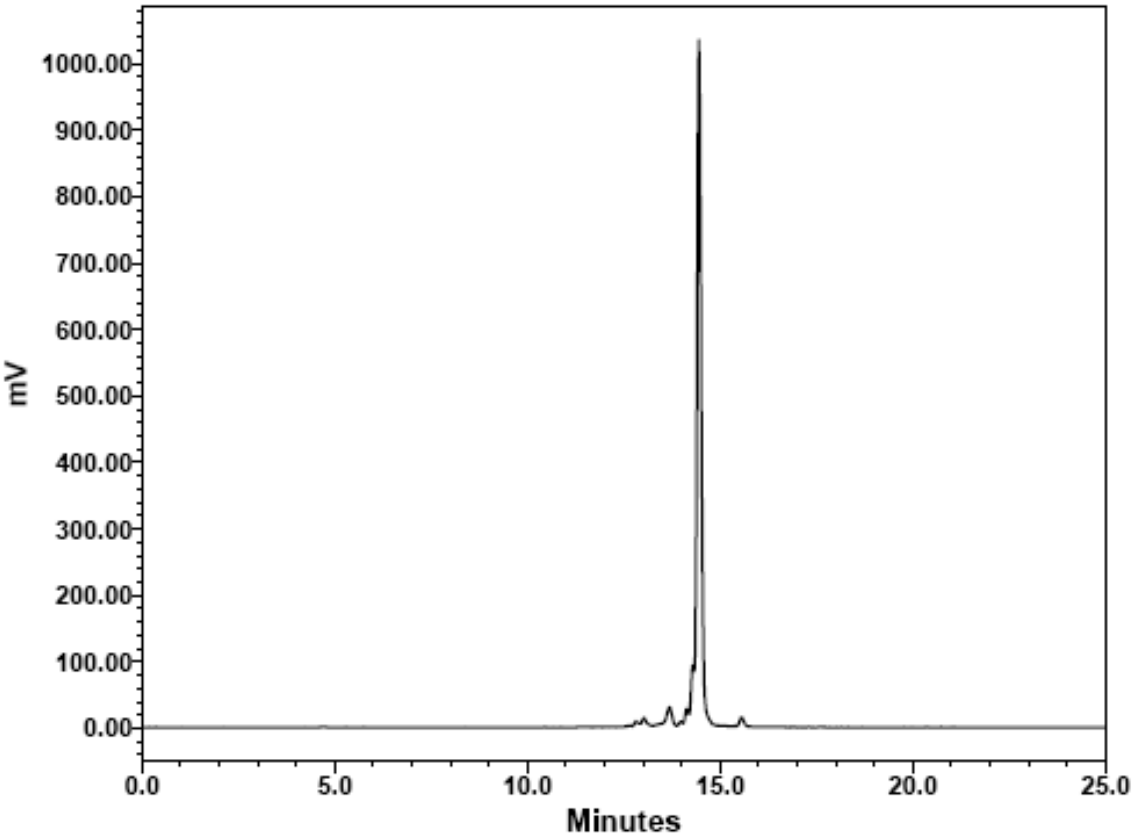


**Figure S 8.27** γ-HPLC chromatogram at 2 h following cysteine challenge to $[^{99m}Tc(CO)_3(BPS)(ImTz)]^-$ **11b**.

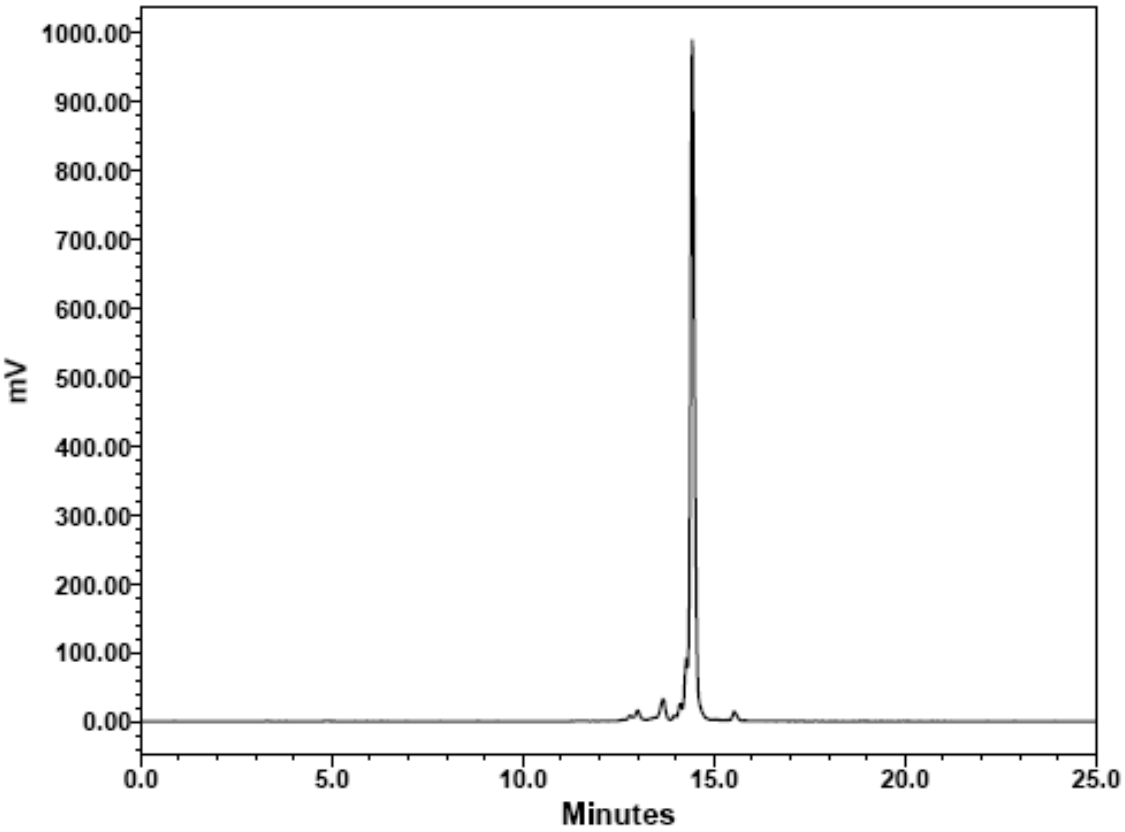


**Figure S 8.28** γ-HPLC chromatogram at 3 h following cysteine challenge to $[^{99m}Tc(CO)_3(BPS)(ImTz)]^-$ **11b**.

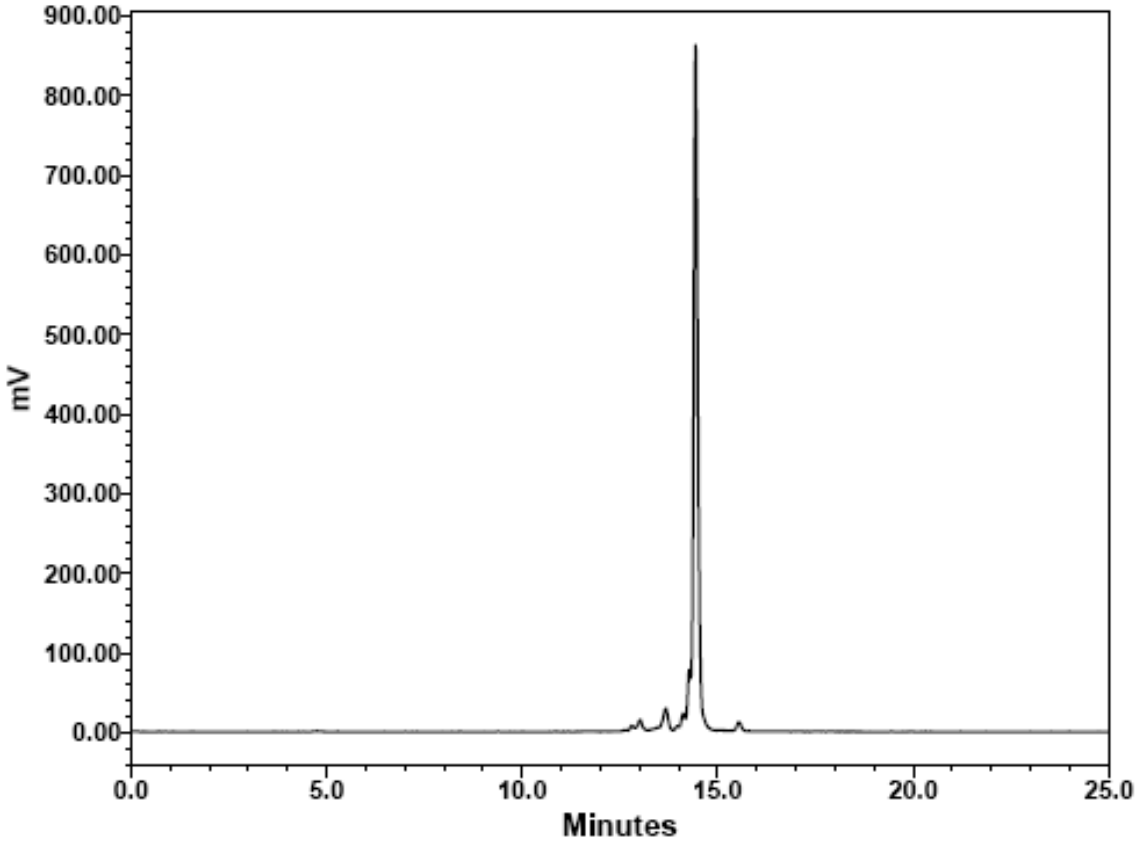


**Figure S 8.29** γ-HPLC chromatogram at 6 h following cysteine challenge to $[^{99m}Tc(CO)_3(BPS)(ImTz)]^-$ **11b**.

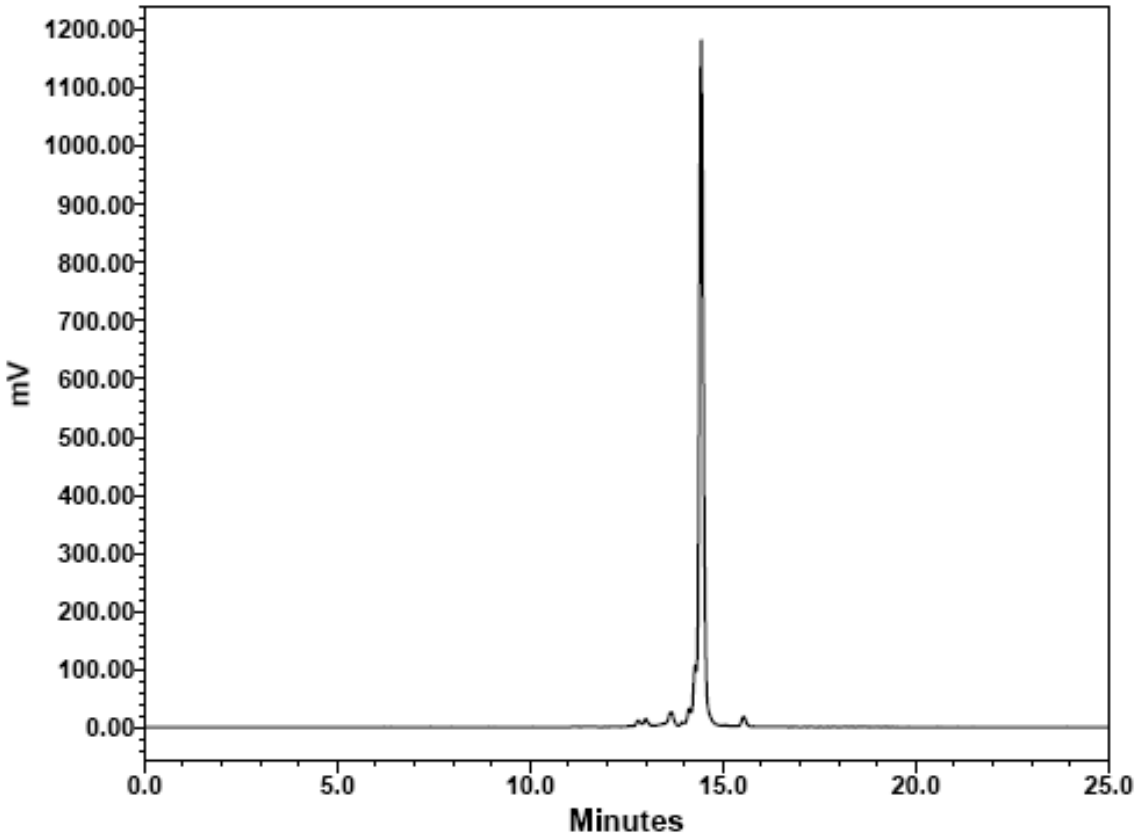


**Figure S 8.30** γ-HPLC chromatogram at 0.5 h following histidine challenge to $[^{99m}Tc(CO)_3(BPS)(ImTz)]^-$ **11b**.

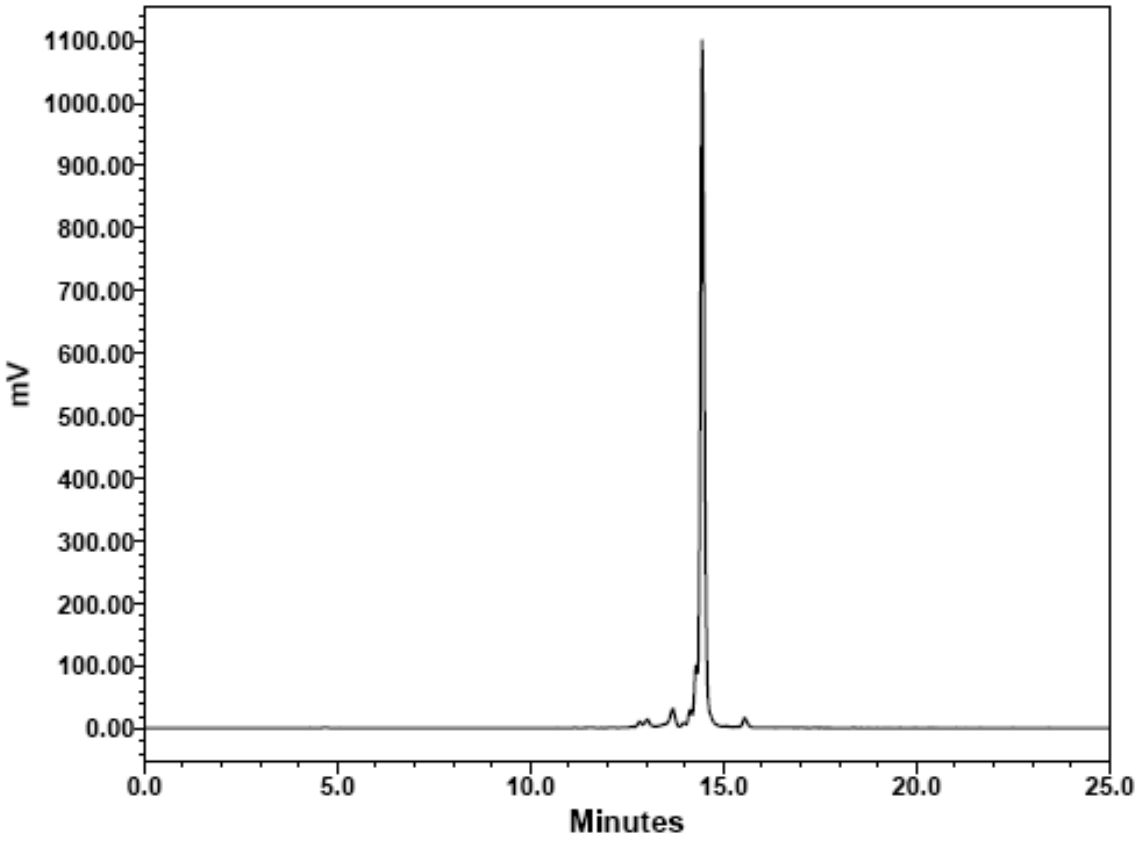


**Figure S 8.31** γ-HPLC chromatogram at 1 h following histidine challenge to $[^{99m}Tc(CO)_3(BPS)(ImTz)]^-$ **11b**.

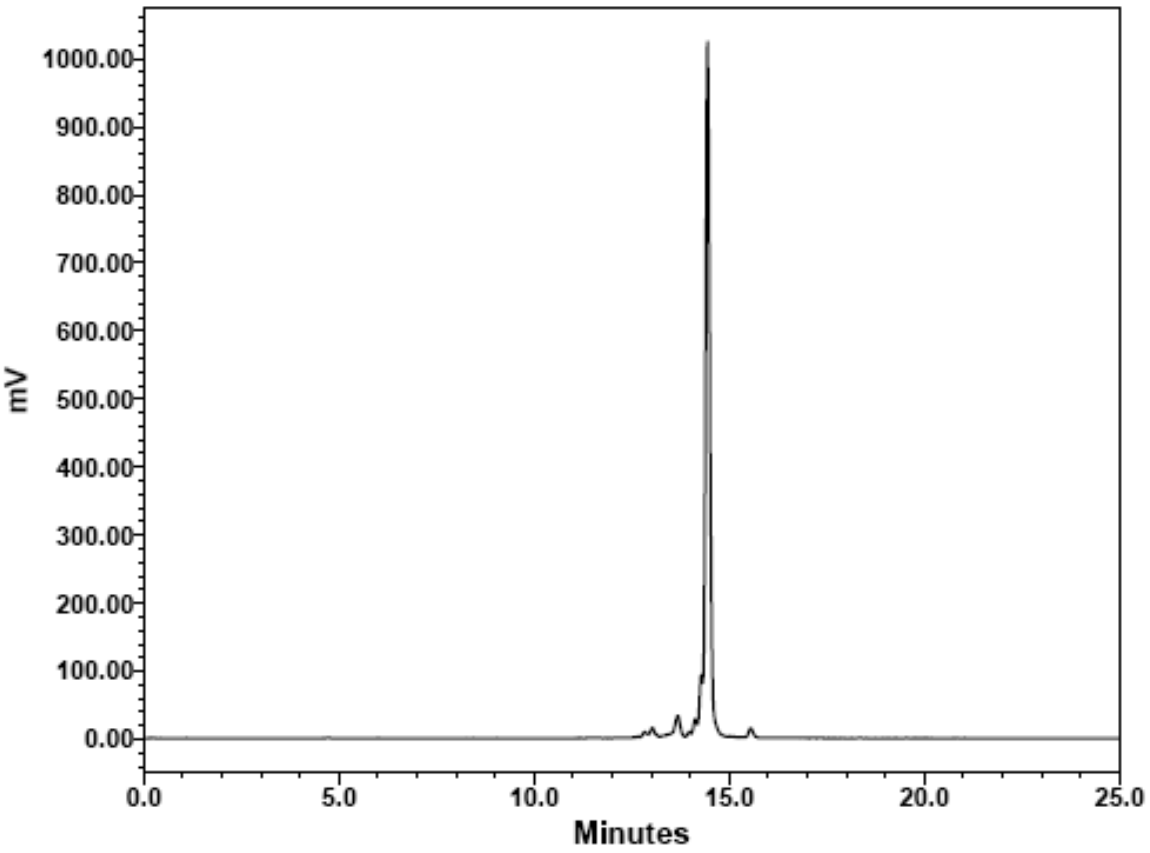


**Figure S 8.32** γ-HPLC chromatogram at 2 h following histidine challenge to $[^{99m}Tc(CO)_3(BPS)(ImTz)]^-$ **11b**.

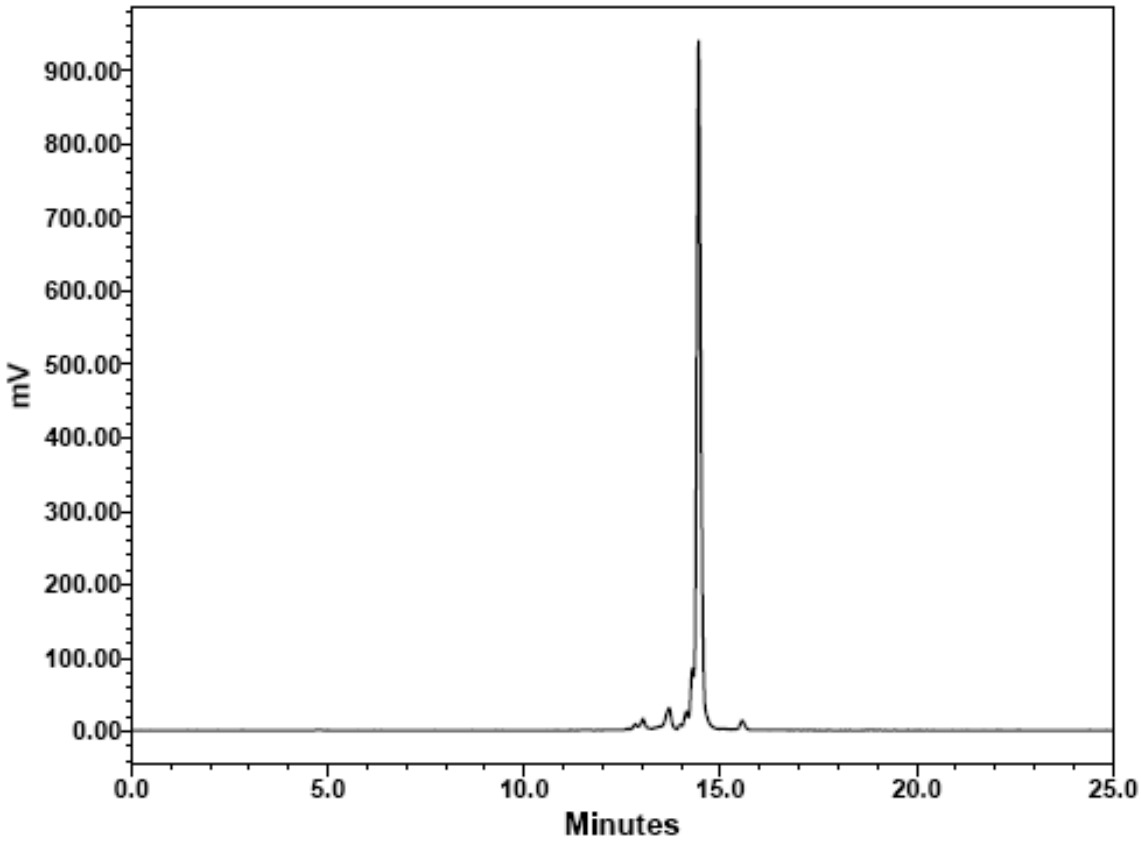


**Figure S 8.33** γ-HPLC chromatogram at 3 h following histidine challenge to $[^{99m}Tc(CO)_3(BPS)(ImTz)]^-$ **11b**.

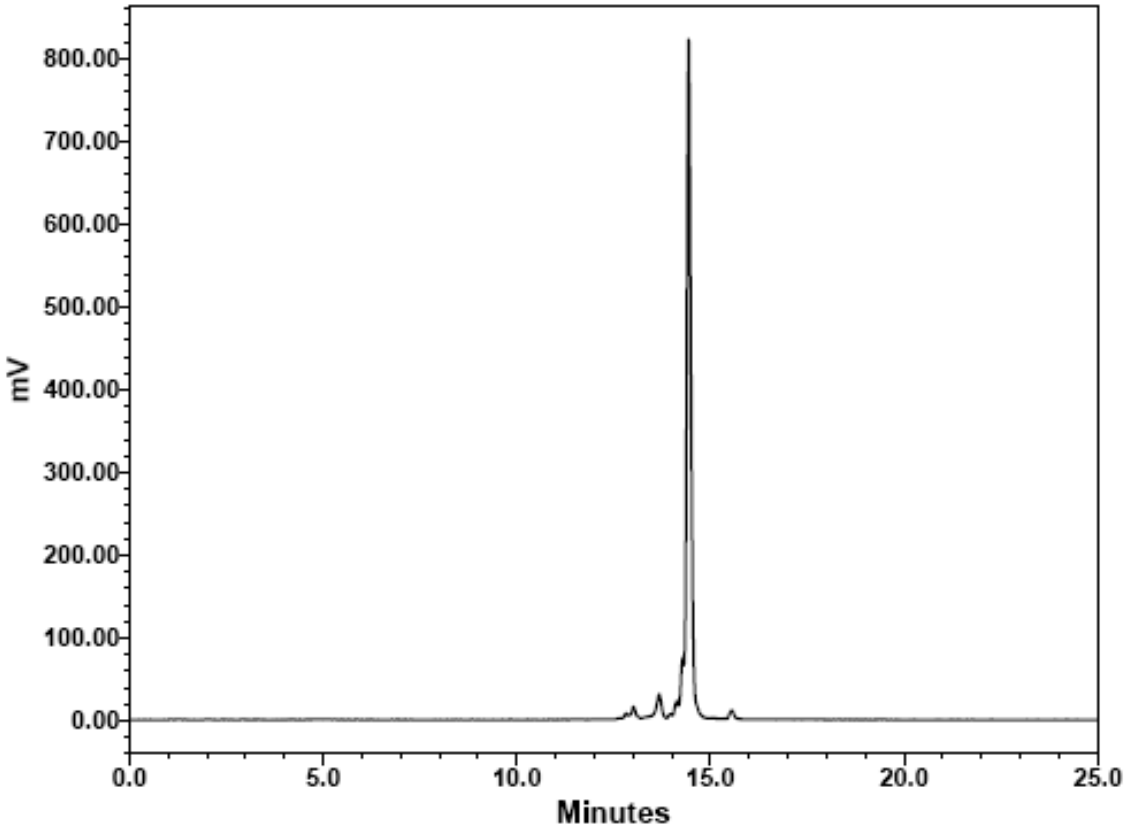


**Figure S 8.34** γ-HPLC chromatogram at 6 h following histidine challenge to $[^{99m}Tc(CO)_3(BPS)(ImTz)]^-$ **11b**.

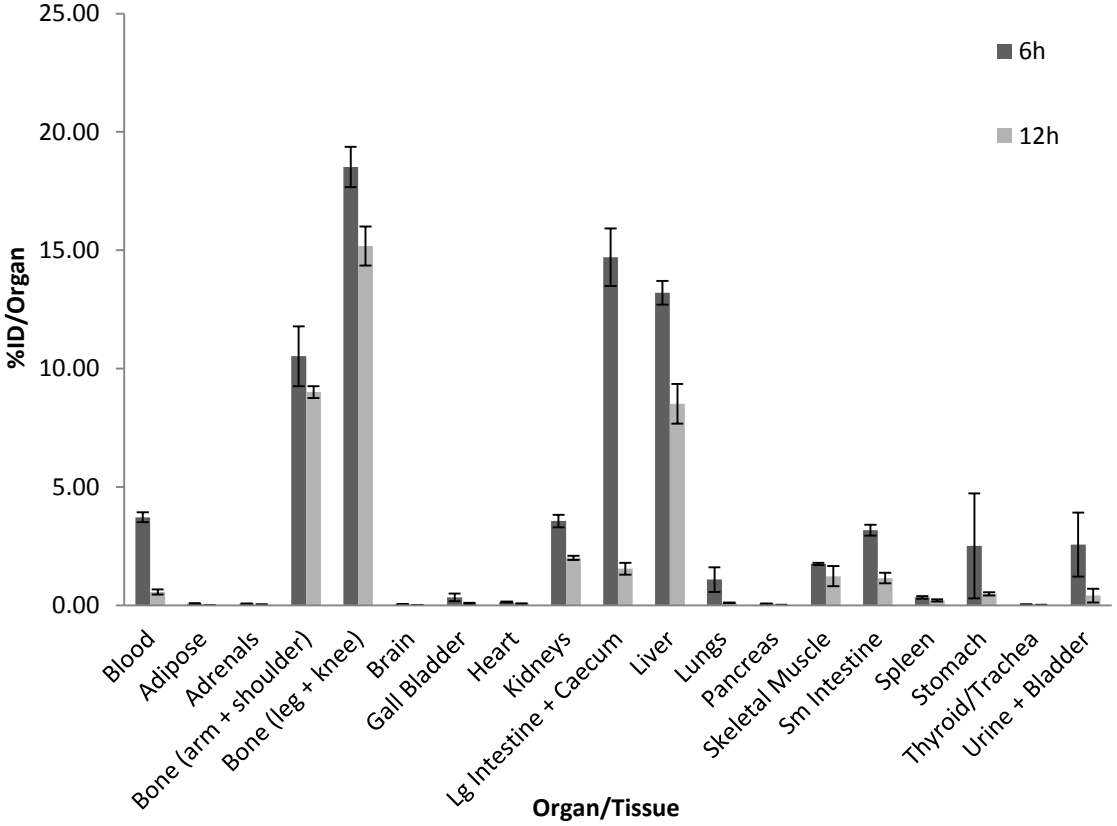


**Figure S 8.35** Biodistribution data for select fluids and tissues for pretargeting with 20 mg/kg of TCO-BP administered 1 h prior to **11b**. Experiments were performed using Balb/c mice (n = 3 per time point) with tissues collected at 6 h and 12 h post administration of the labeled compound. Data are expressed as mean percent injected dose per gram (%ID/o) ± SEM.

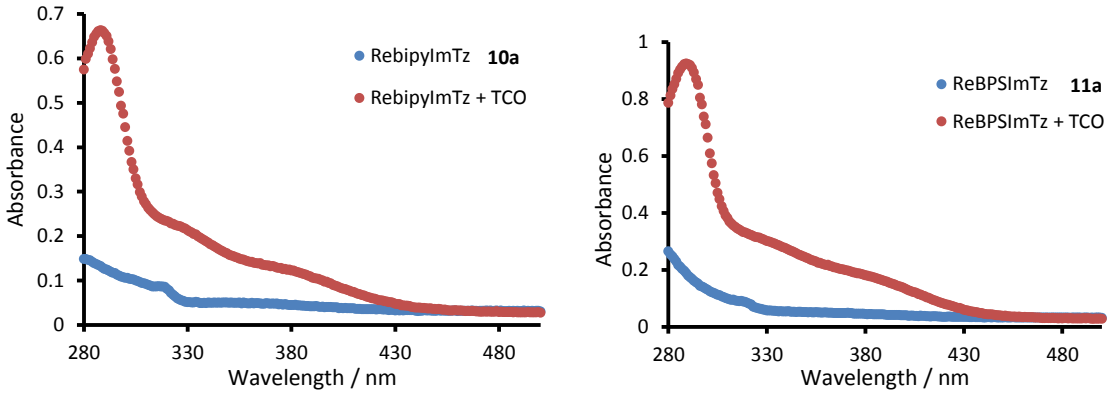


**Figure S 8.36** Absorption spectra for compounds **10a** and **11a** (50 µM in MeOH) in the presence of 0 (blue) and 500 µM (red) TCO-OH.

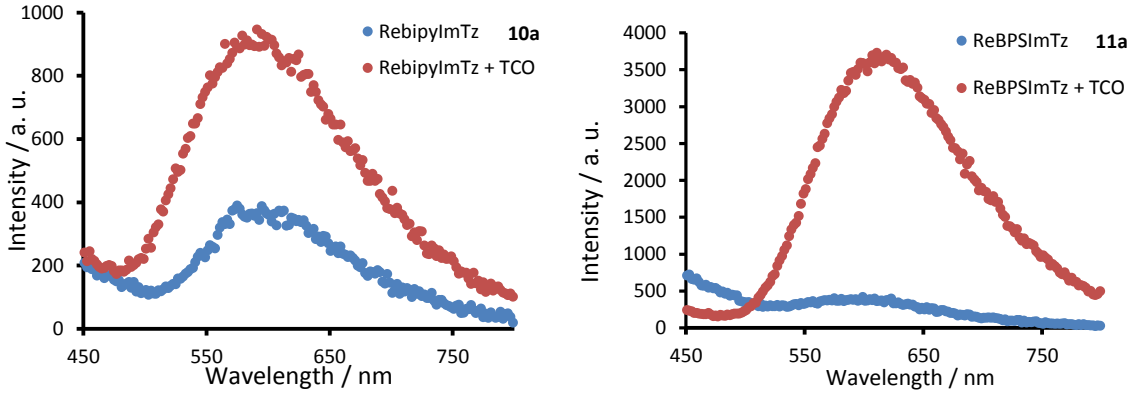


**Figure S 8.37** Emission spectra for compounds **10a** and **11a** (50 µM in MeOH) in the presence of 0 (blue) and 500 µM (red) TCO-OH.

**Table S 8.1** Biodistribution data expressed as (top) percent injected dose per gram (%ID/g) and (bottom) percent injected dose per organ (%ID/O) for select fluids and tissues for pretargeting with 20 mg/kg of TCO-BP administered 1 h prior to **11b**. Experiments were performed using Balb/c mice (n = 3 per time point) with tissues collected at 6 h and 12 h post administration of the labeled compound.

| %ID/g | n=3 6h | | n=3 12h | |
|---|---|---|---|---|
| **Organs** | avg | SEM | avg | SEM |
| **Blood** | 4.06 | 0.16 | 0.62 | 0.10 |
| **Adipose** | 1.04 | 0.31 | 0.15 | 0.02 |
| **Adrenals** | 4.96 | 0.65 | 2.56 | 0.74 |
| **Bone (arm + shoulder)** | 5.28 | 0.67 | 4.51 | 0.08 |
| **Bone (leg + knee)** | 9.27 | 0.32 | 7.62 | 0.49 |
| **Brain** | 0.10 | 0.02 | 0.02 | 0.00 |
| **Gall Bladder** | 54.32 | 5.45 | 7.94 | 2.75 |
| **Heart** | 1.53 | 0.12 | 0.86 | 0.05 |
| **Kidneys** | 13.43 | 0.33 | 7.76 | 0.95 |
| **Lg Intestine + Caecum** | 27.70 | 4.63 | 2.95 | 0.68 |
| **Liver** | 12.95 | 0.63 | 8.09 | 0.67 |
| **Lungs** | 7.54 | 3.25 | 0.89 | 0.13 |
| **Pancreas** | 0.45 | 0.07 | 0.19 | 0.01 |
| **Skeletal Muscle** | 0.24 | 0.00 | 0.17 | 0.06 |
| **Sm Intestine** | 3.34 | 0.22 | 1.20 | 0.28 |
| **Spleen** | 3.21 | 0.40 | 2.34 | 0.49 |
| **Stomach** | 9.09 | 7.92 | 1.58 | 0.45 |
| **Thyroid/Trachea** | 2.16 | 0.19 | 1.76 | 0.06 |
| **Urine + Bladder** | 23.58 | 6.67 | 3.01 | 0.19 |

| %ID/O | n=3 6h | | n=3 12h | |
|---|---|---|---|---|
| **Organs** | avg | SEM | avg | SEM |
| **Blood** | 3.72 | 0.21 | 0.57 | 0.11 |

| | | | | |
|---|---|---|---|---|
| **Adipose** | 0.07 | 0.02 | 0.01 | 0.00 |
| **Adrenals** | 0.07 | 0.01 | 0.03 | 0.01 |
| **Bone (arm + shoulder)** | 10.52 | 1.26 | 9.01 | 0.26 |
| **Bone (leg + knee)** | 18.52 | 0.85 | 15.18 | 0.82 |
| **Brain** | 0.04 | 0.01 | 0.01 | 0.00 |
| **Gall Bladder** | 0.33 | 0.16 | 0.07 | 0.03 |
| **Heart** | 0.14 | 0.02 | 0.08 | 0.01 |
| **Kidneys** | 3.56 | 0.26 | 2.01 | 0.09 |
| **Lg Intestine + Caecum** | 14.71 | 1.21 | 1.55 | 0.25 |
| **Liver** | 13.21 | 0.50 | 8.51 | 0.84 |
| **Lungs** | 1.09 | 0.52 | 0.11 | 0.01 |
| **Pancreas** | 0.06 | 0.02 | 0.03 | 0.00 |
| **Skeletal Muscle** | 1.75 | 0.05 | 1.23 | 0.42 |
| **Sm Intestine** | 3.18 | 0.23 | 1.15 | 0.22 |
| **Spleen** | 0.34 | 0.06 | 0.21 | 0.05 |
| **Stomach** | 2.51 | 2.21 | 0.49 | 0.06 |
| **Thyroid/Trachea** | 0.03 | 0.00 | 0.03 | 0.00 |
| **Urine + Bladder** | 2.57 | 1.35 | 0.41 | 0.29 |

# 9 Appendix 4 (Supporting Information for Chapter 5)

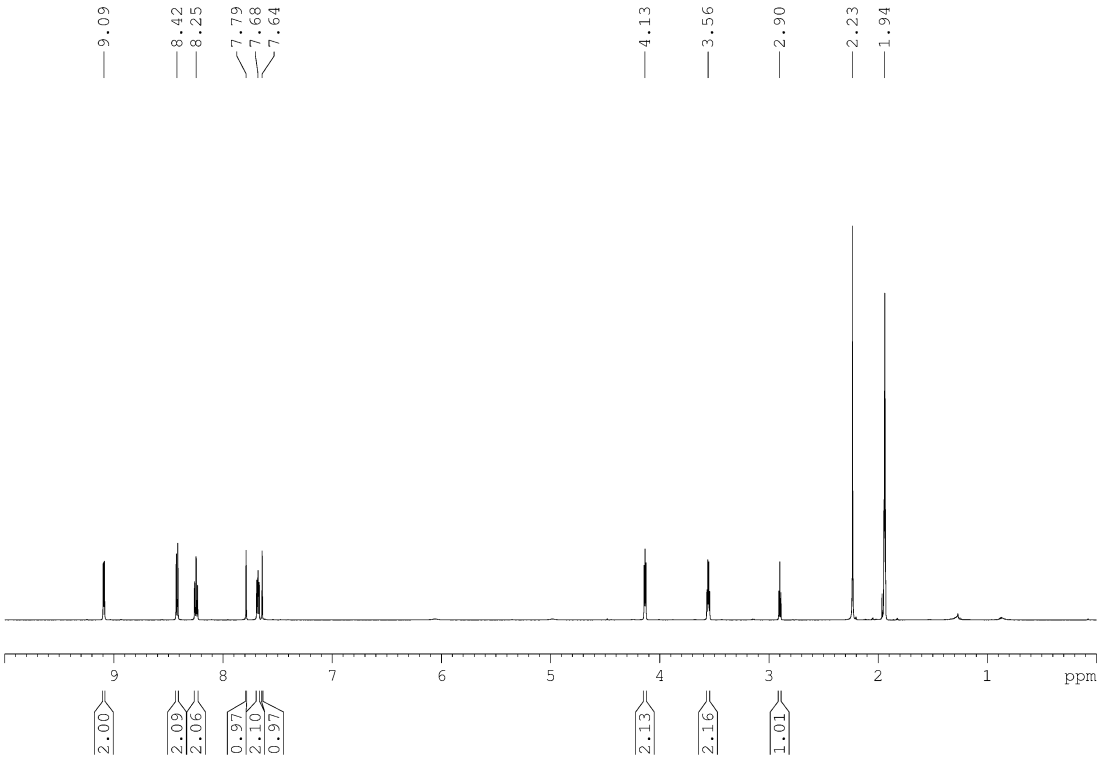


**Figure S 9.1** $^{1}$H NMR spectrum ($CD_3CN$, 600 MHz) of **3a**.

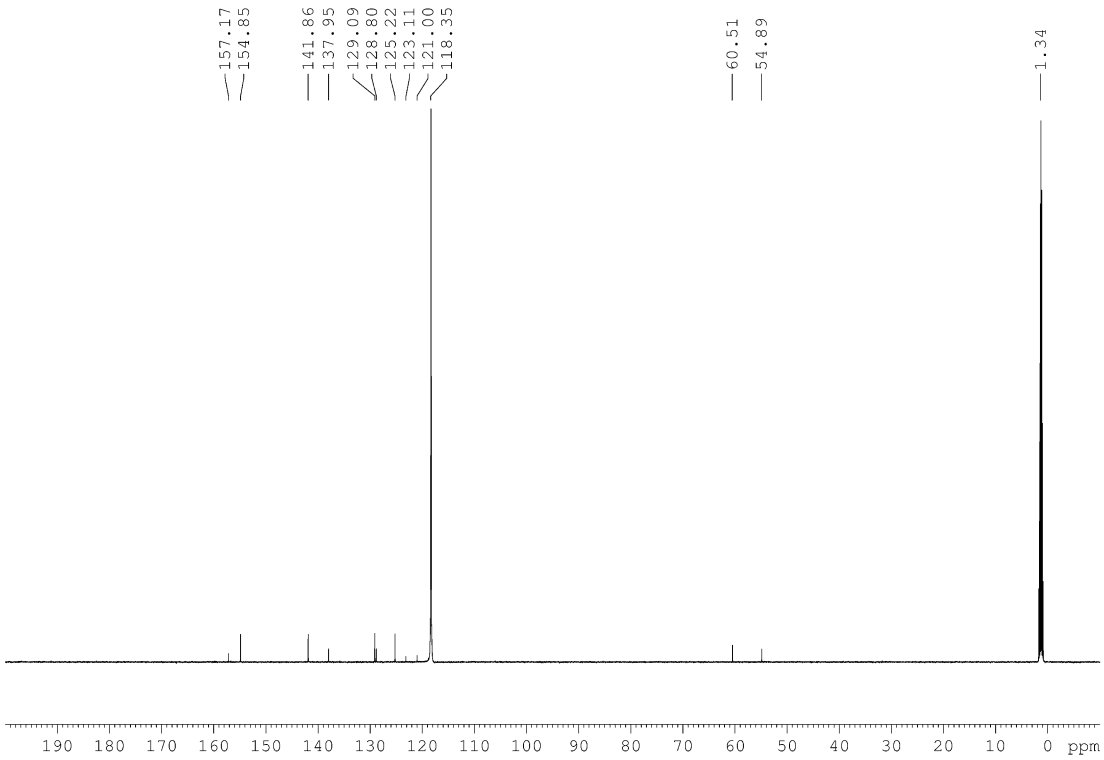


**Figure S 9.2** $^{13}C$ NMR spectrum ($CD_3CN$, 150 MHz) of **3a**.

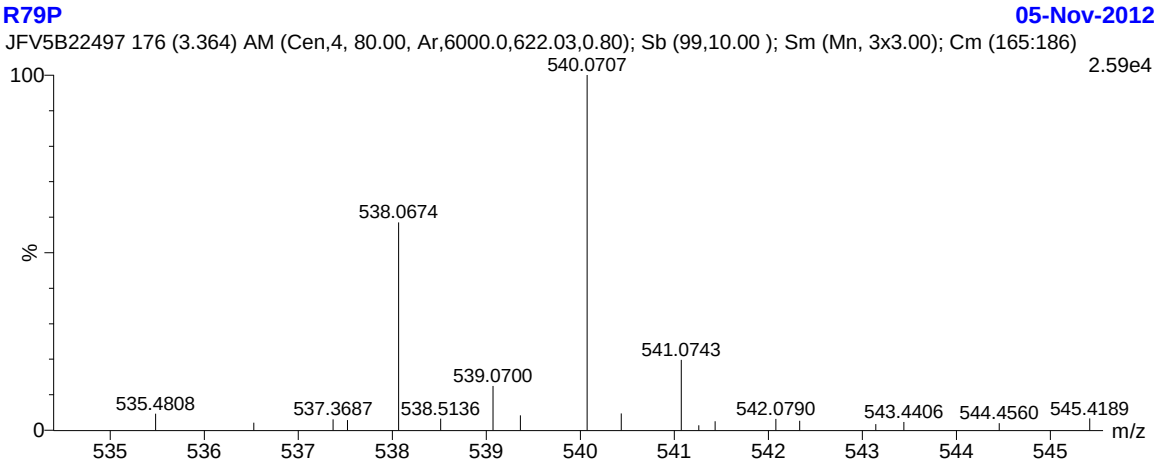


**Figure S 9.3** Positive ion HR-ESI MS of **3a**.

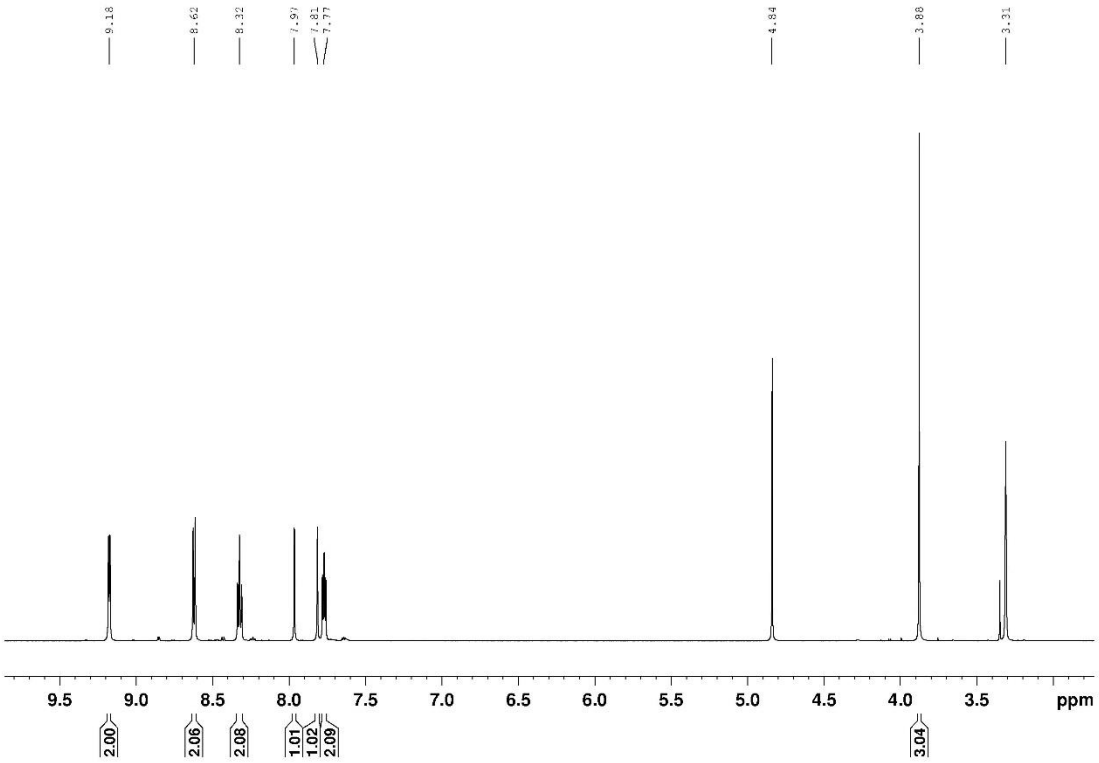


**Figure S 9.4** $^{1}$H NMR spectrum ($CD_3OD$, 600 MHz) of **5a**.

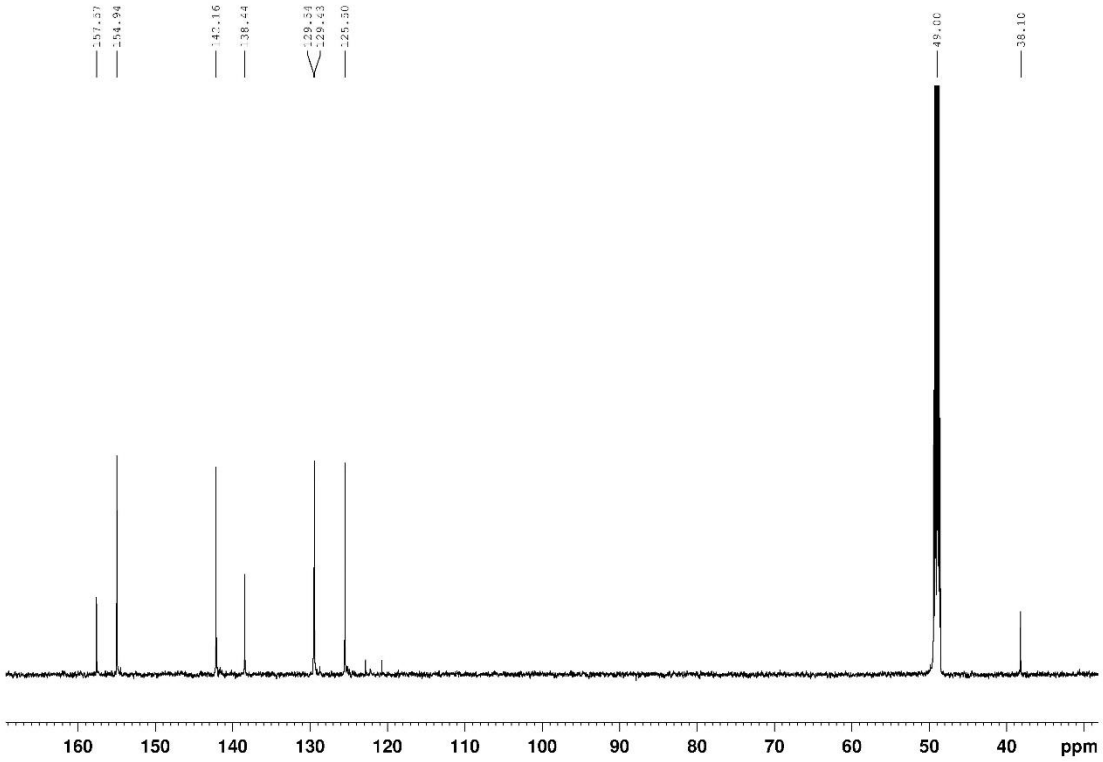


**Figure S 9.5** $^{13}C$ NMR spectrum ($CD_3OD$, 150 MHz) of **5a**.

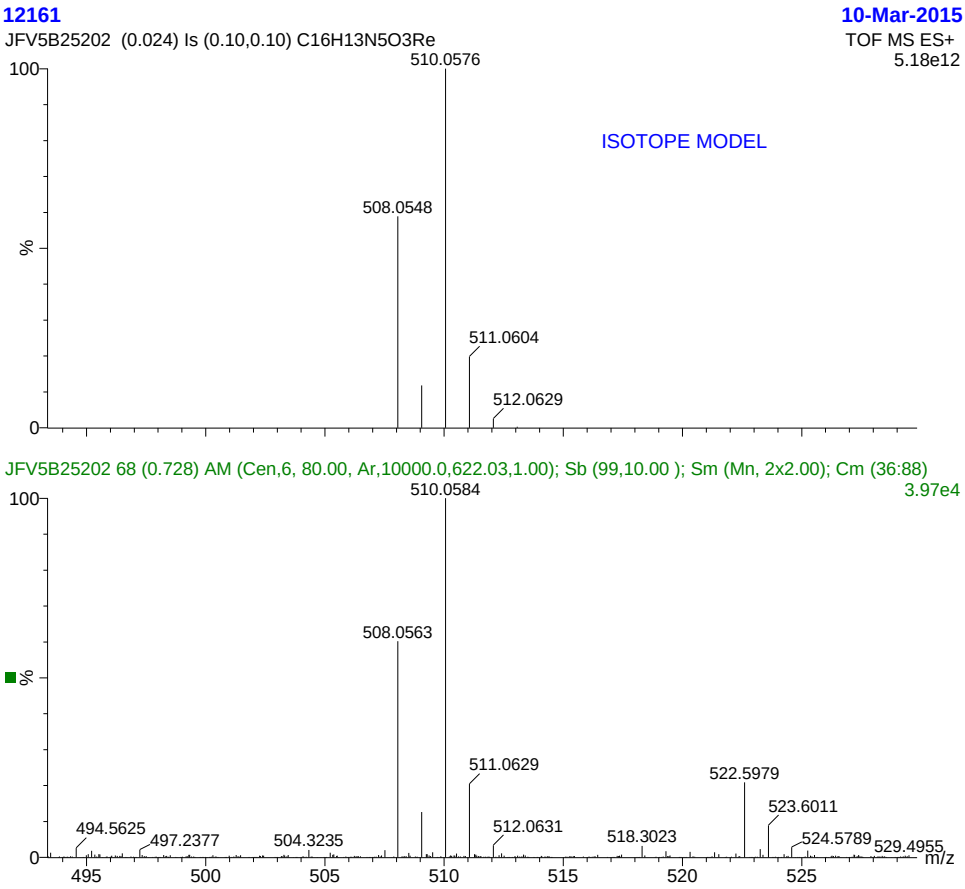


**Figure S 9.6** Positive ion HR-ESI MS of **5a**.

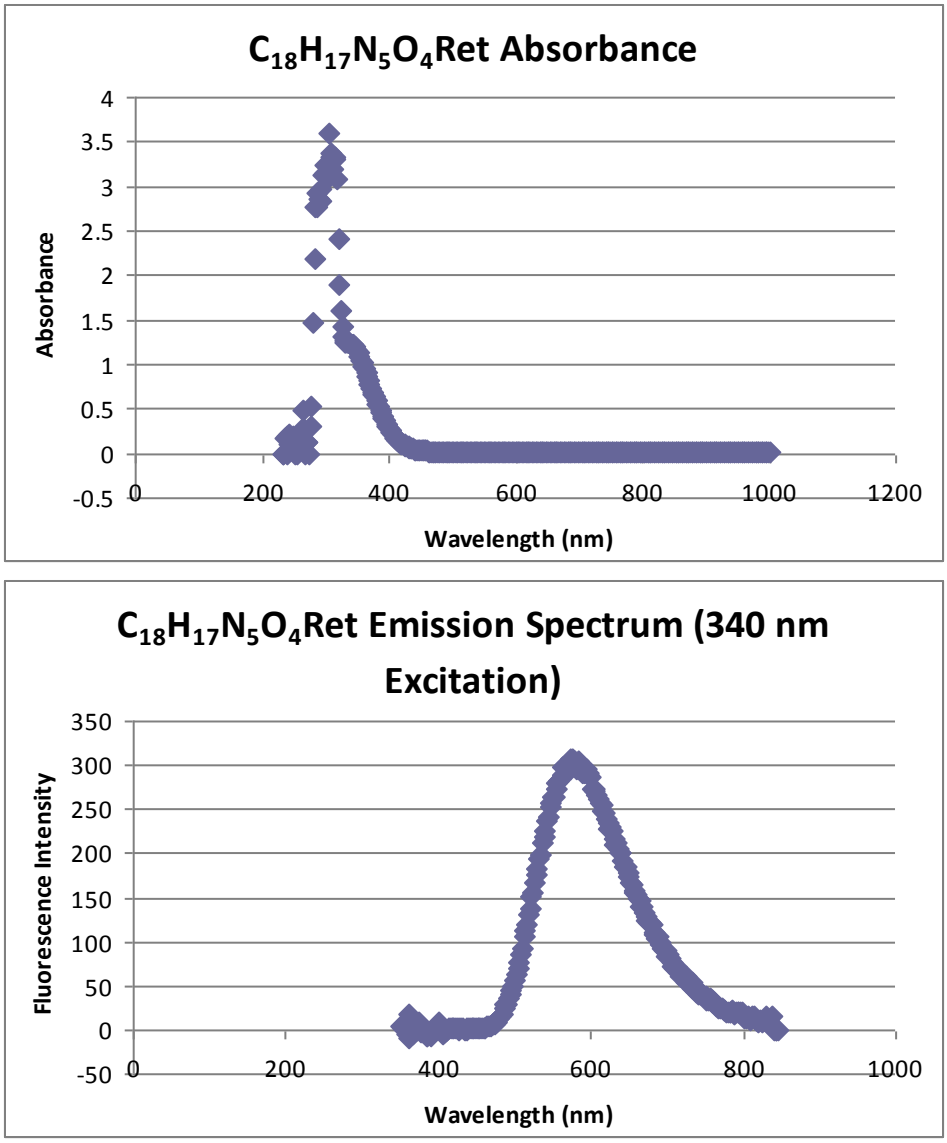


**Figure S 9.7** Absorption (top) and emission (bottom) spectrum of **3a**.

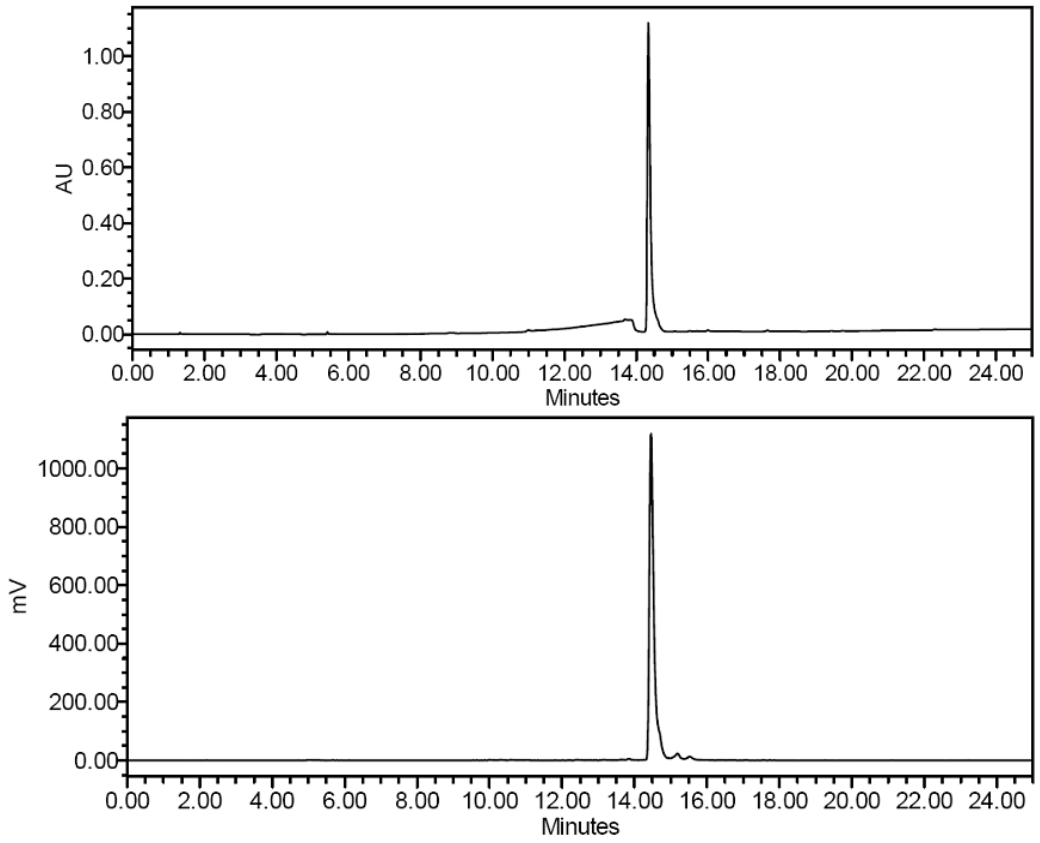


**Figure S 9.8** HPLC chromatograms (UV and γ) of the isolated

$[Re(CO)_3(bipy)(EtOHTrz)]^+$ **3a** complex co-injected with $^{99m}Tc$ complex **3b**.

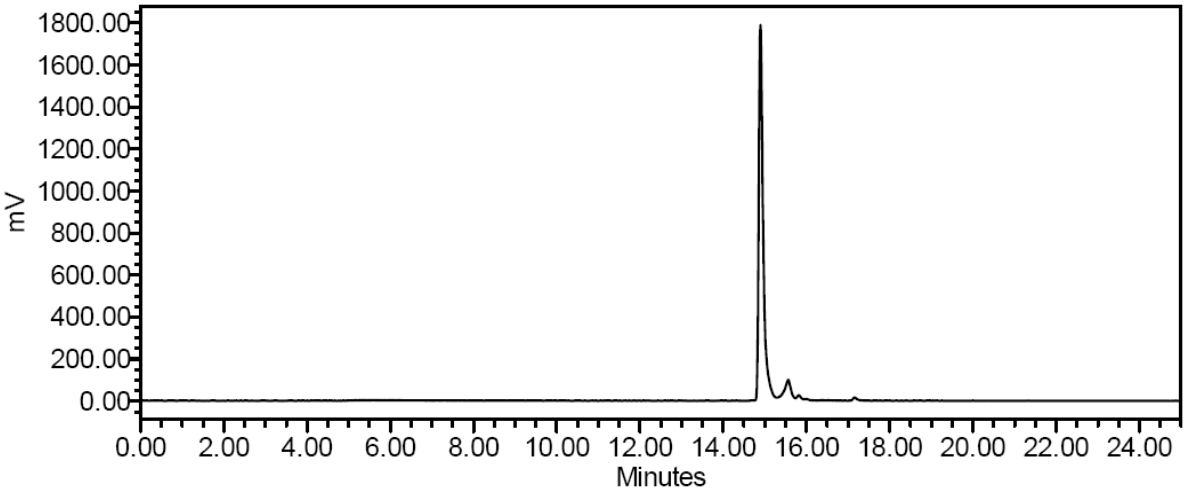


**Figure S 9.9** γ-HPLC chromatogram at 0.5 h following incubation in saline to $[^{99m}Tc(CO)_3(bipy)(EtOHTrz)]^+$ **3b**.

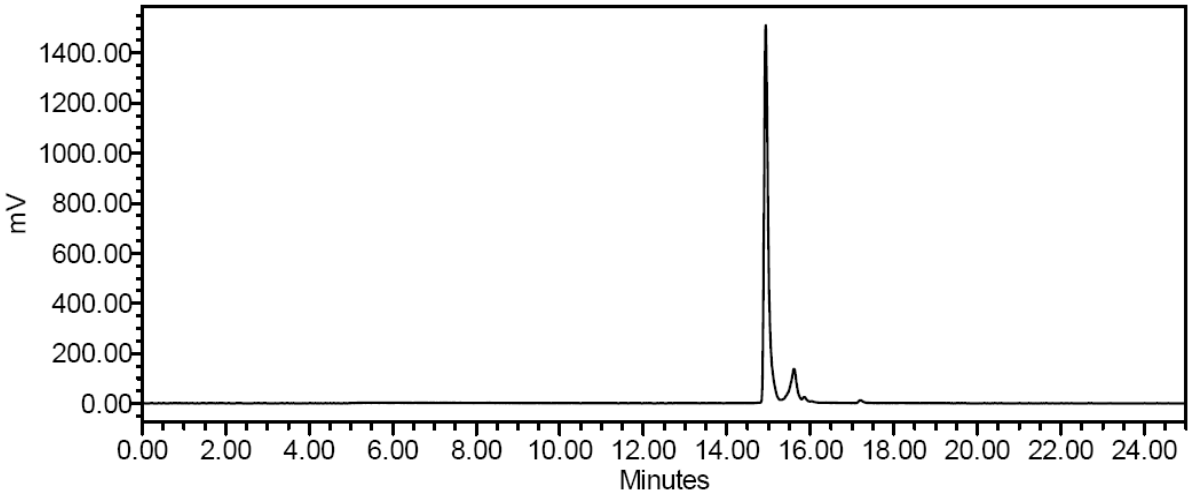


**Figure S 9.10** γ-HPLC chromatogram at 1 h following incubation in saline to $[^{99m}Tc(CO)_3(bipy)(EtOHTrz)]^+$ **3b**.

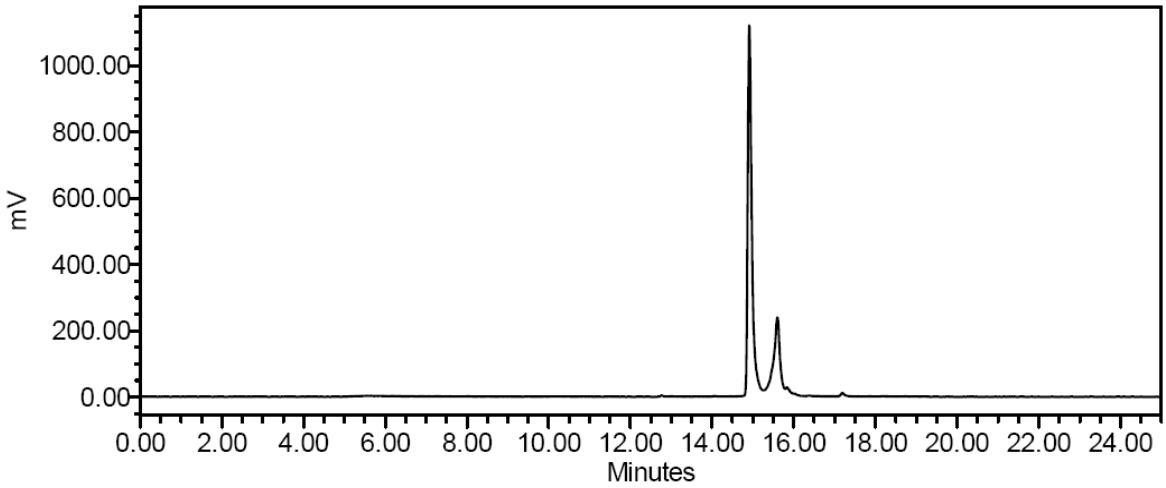


**Figure S 9.11** γ-HPLC chromatogram at 2 h following incubation in saline to $[^{99m}Tc(CO)_3(bipy)(EtOHTrz)]^+$ **3b**.

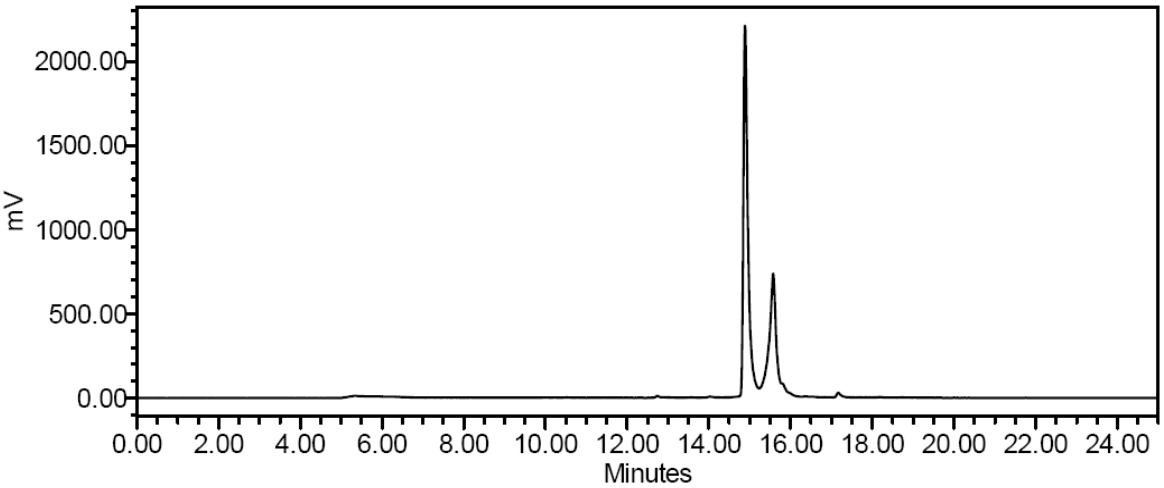


**Figure S 9.12** γ-HPLC chromatogram at 3 h following incubation in saline to $[^{99m}Tc(CO)_3(bipy)(EtOHTrz)]^+$ **3b**.

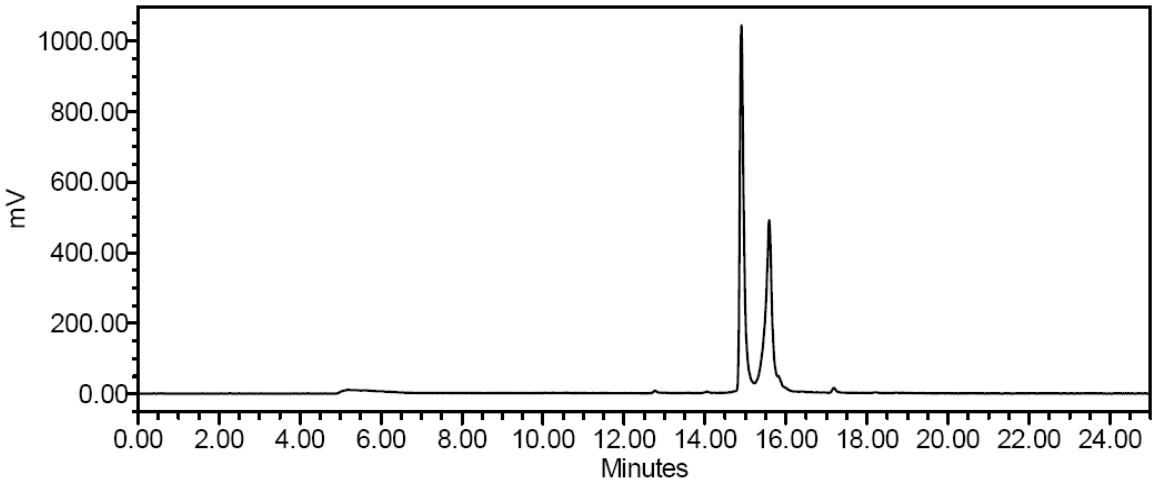


**Figure S 9.13** γ-HPLC chromatogram at 6 h following incubation in saline to $[^{99m}Tc(CO)_3(bipy)(EtOHTrz)]^+$ **3b**.

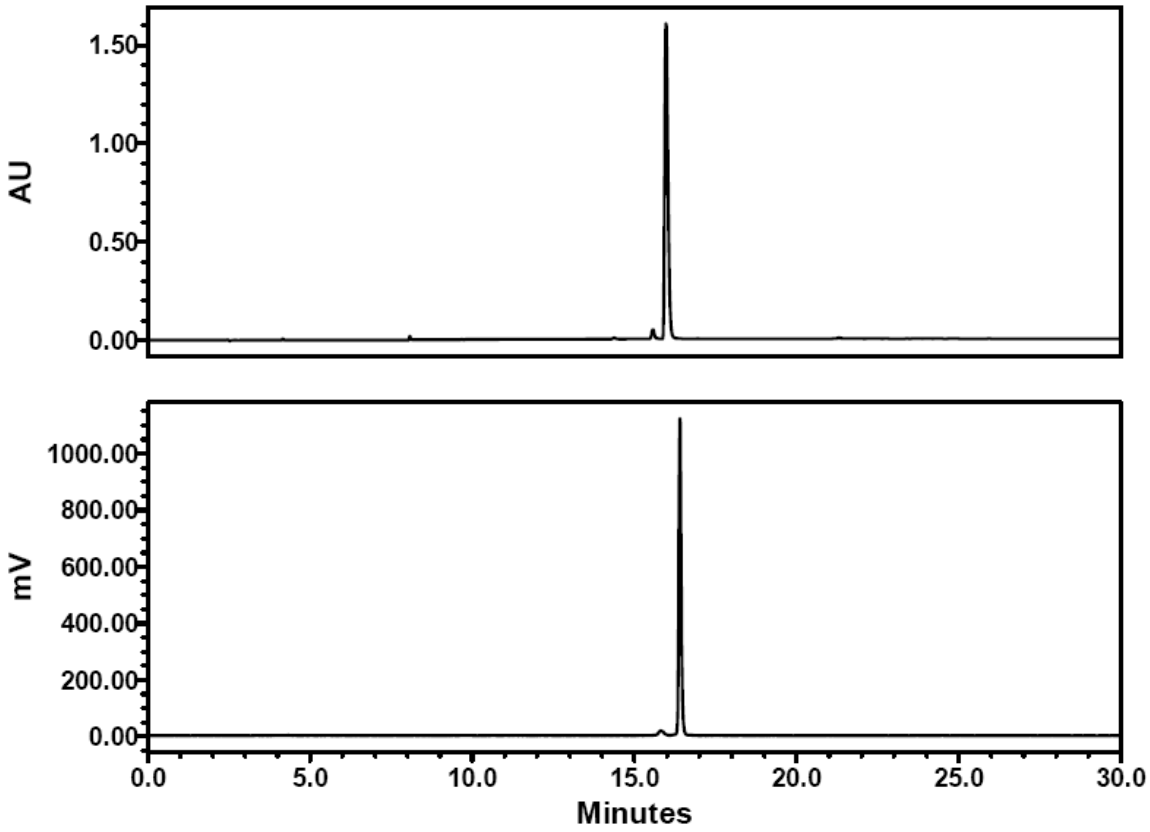


**Figure S 9.14** HPLC chromatograms (UV and γ) of the isolated

$[Re(CO)_3(bipy)(MeTrz)]^+$ **5a** complex co-injected with $^{99m}Tc$ complex **5b**.

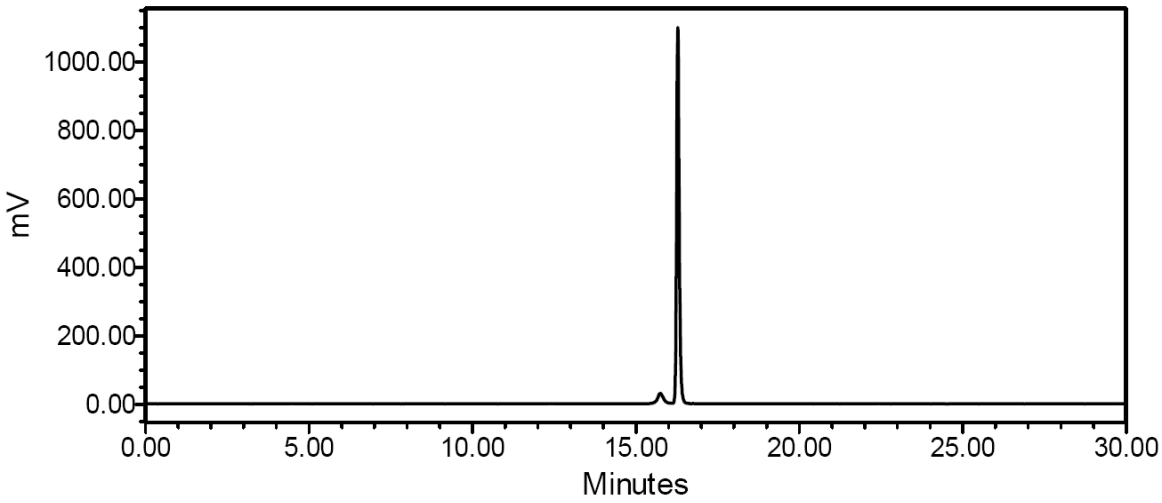


**Figure S 9.15** γ-HPLC chromatogram at 0.5 h following incubation in saline to $[^{99m}Tc(CO)_3(bipy)(MeTrz)]^+$ **5b**.

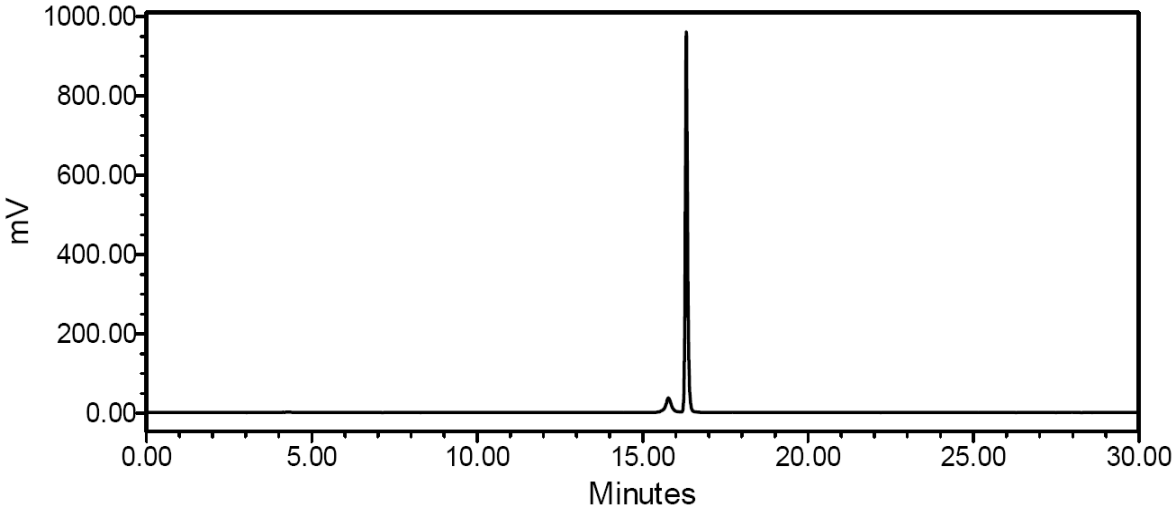


**Figure S 9.16** γ-HPLC chromatogram at 1 h following incubation in saline to $[^{99m}Tc(CO)_3(bipy)(MeTrz)]^+$ **5b**.

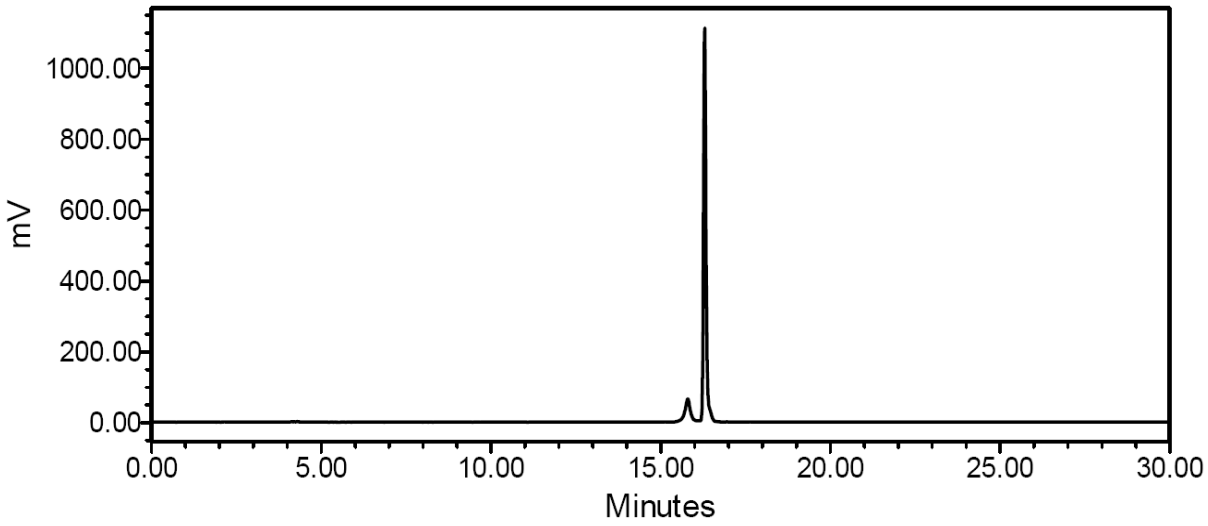


**Figure S 9.17** γ-HPLC chromatogram at 2 h following incubation in saline to $[^{99m}Tc(CO)_3(bipy)(MeTrz)]^+$ **5b**.

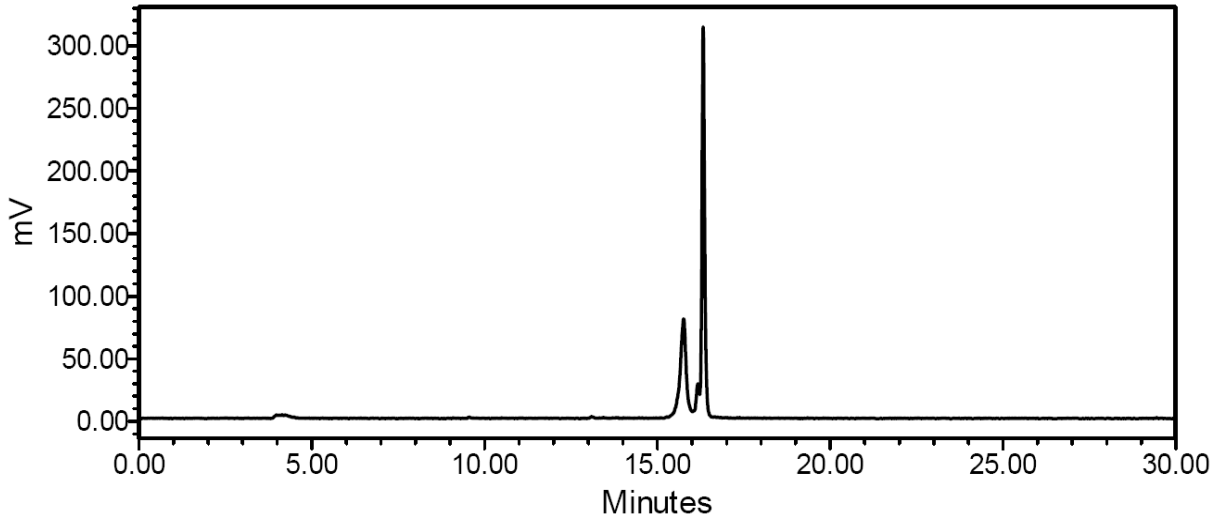


**Figure S 9.18** γ-HPLC chromatogram at 3 h following incubation in saline to $[^{99m}Tc(CO)_3(bipy)(MeTrz)]^+$ **5b**.

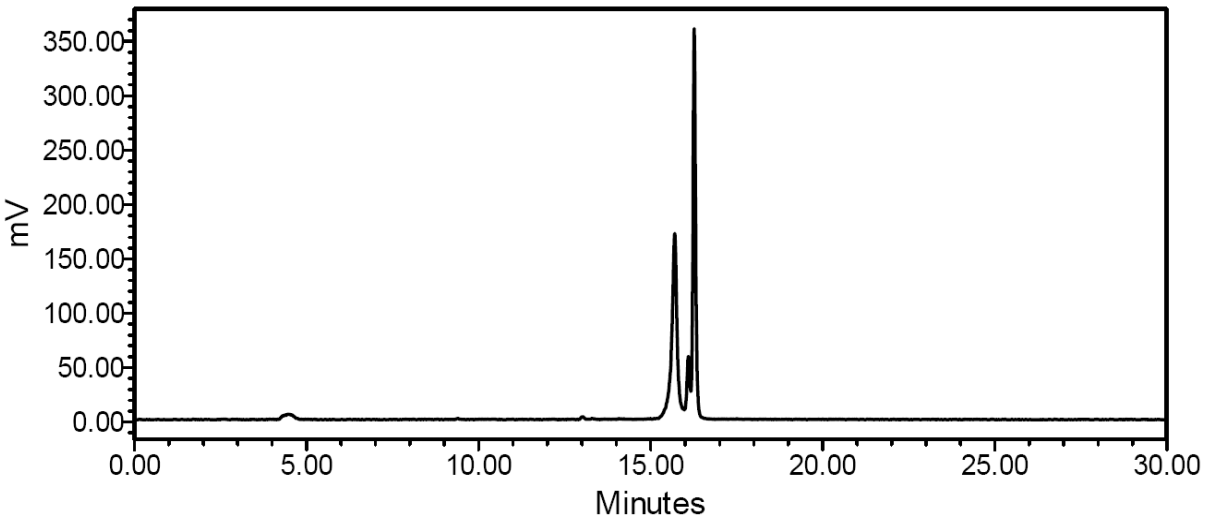


**Figure S 9.19** γ-HPLC chromatogram at 6 h following incubation in saline to $[^{99m}Tc(CO)_3(bipy)(MeTrz)]^+$ **5b**.

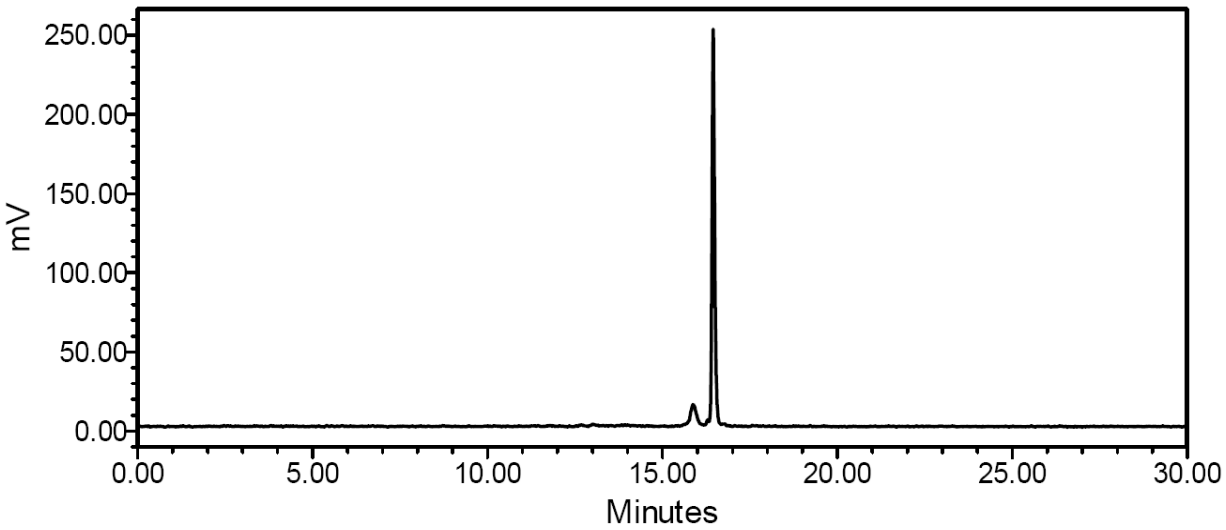


**Figure S 9.20** γ-HPLC chromatogram at 0.5 h following cysteine challenge to $[^{99m}Tc(CO)_3(bipy)(MeTrz)]^+$ **5b**.

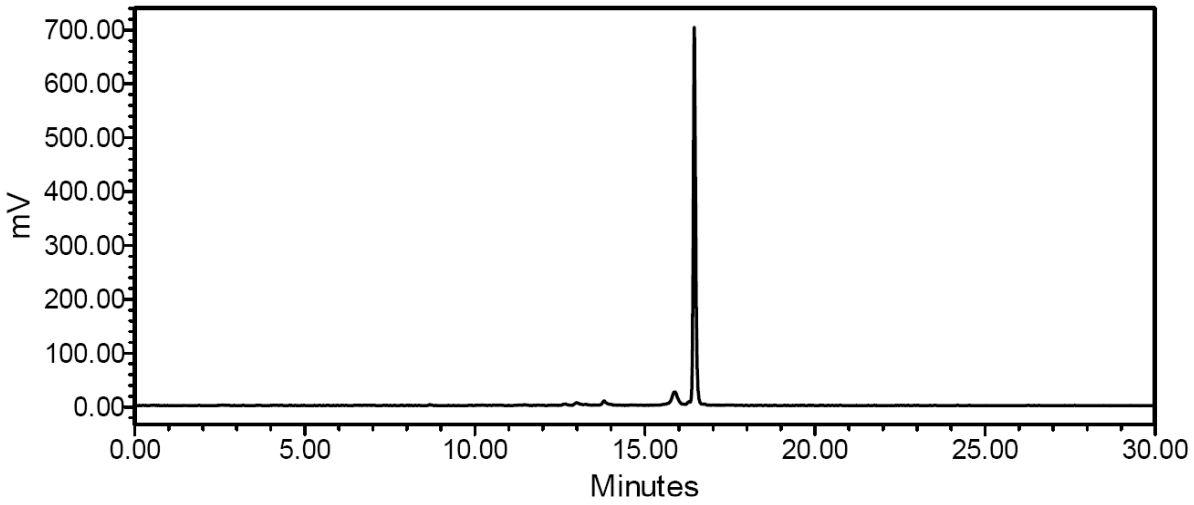


**Figure S 9.21** γ-HPLC chromatogram at 1 h following cysteine challenge to $[^{99m}Tc(CO)_3(bipy)(MeTrz)]^+$ **5b**.

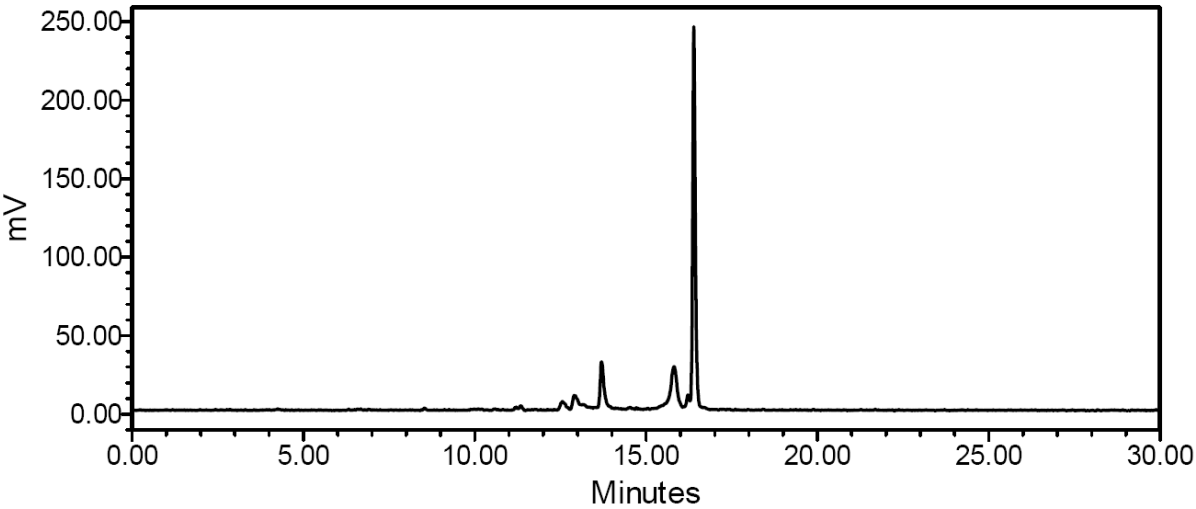


**Figure S 9.22** γ-HPLC chromatogram at 2 h following cysteine challenge to $[^{99m}Tc(CO)_3(bipy)(MeTrz)]^+$ **5b**.

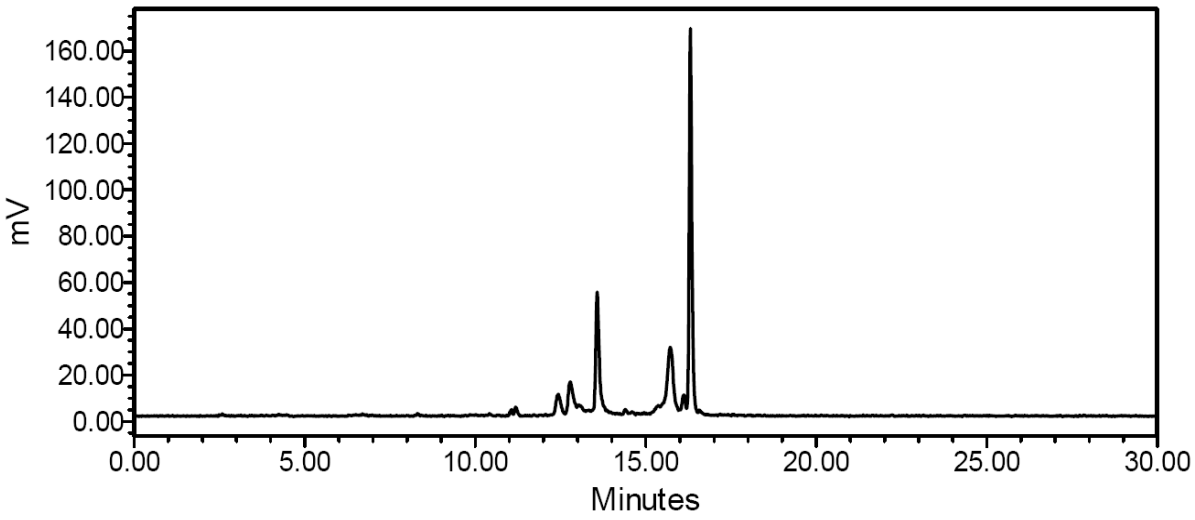


**Figure S 9.23** γ-HPLC chromatogram at 3 h following cysteine challenge to $[^{99m}Tc(CO)_3(bipy)(MeTrz)]^+$ **5b**.

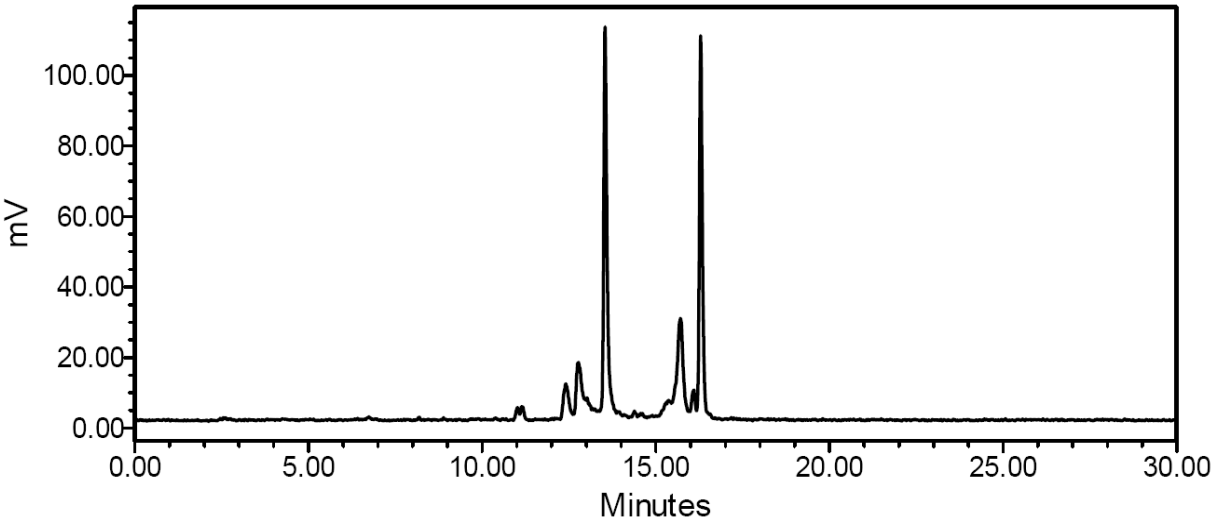


**Figure S 9.24** γ-HPLC chromatogram at 6 h following cysteine challenge to $[^{99m}Tc(CO)_3(bipy)(MeTrz)]^+$ **5b**.

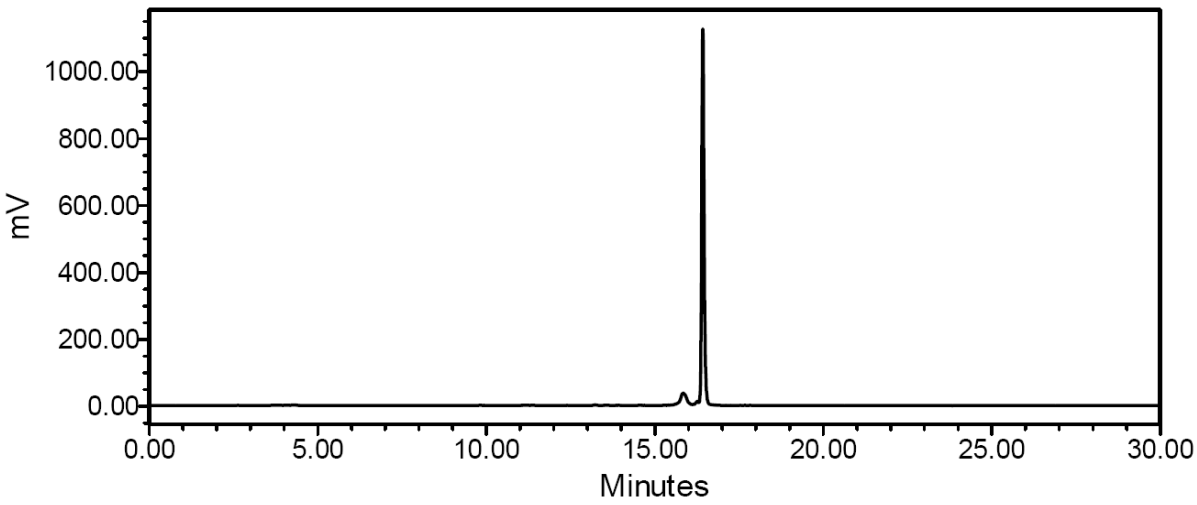


**Figure S 9.25** γ-HPLC chromatogram at 0.5 h following histidine challenge to $[^{99m}Tc(CO)_3(bipy)(MeTrz)]^+$ **5b**.

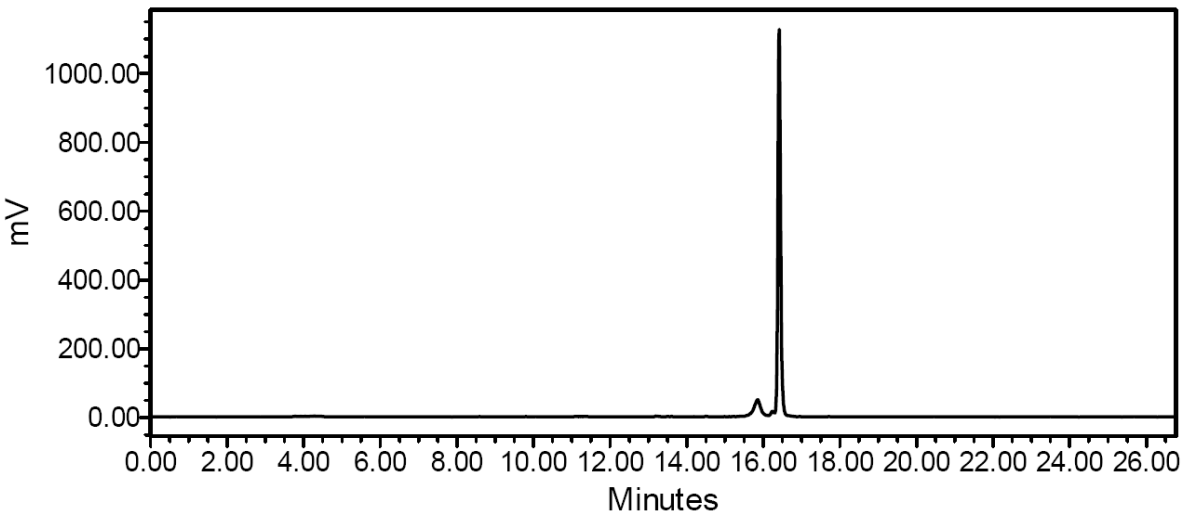


**Figure S 9.26** γ-HPLC chromatogram at 1 h following histidine challenge to $[^{99m}Tc(CO)_3(bipy)(MeTrz)]^+$ **5b**.

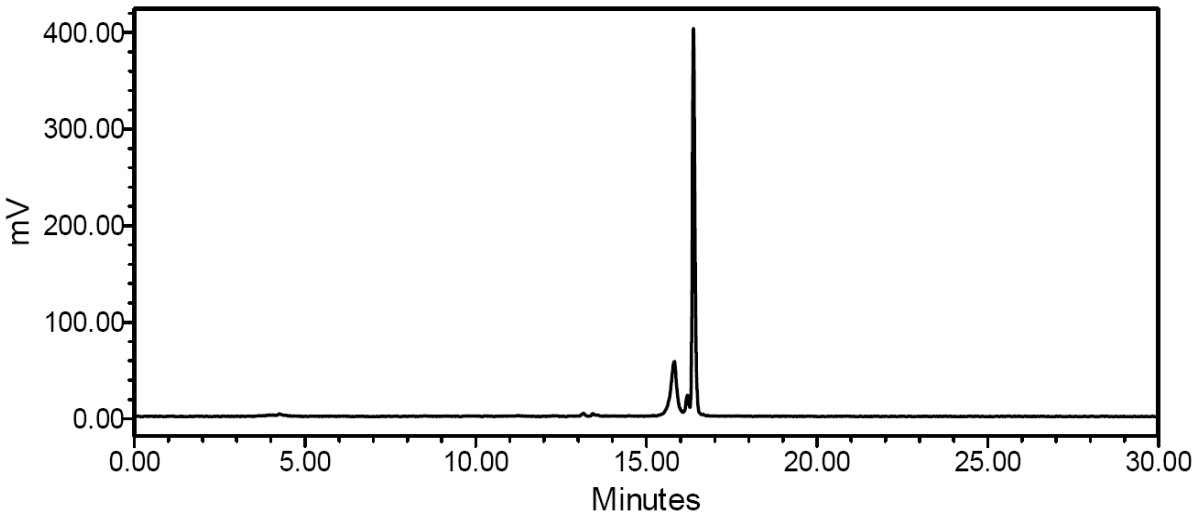


**Figure S 9.27** γ-HPLC chromatogram at 2 h following histidine challenge to $[^{99m}Tc(CO)_3(bipy)(MeTrz)]^+$ **5b**.

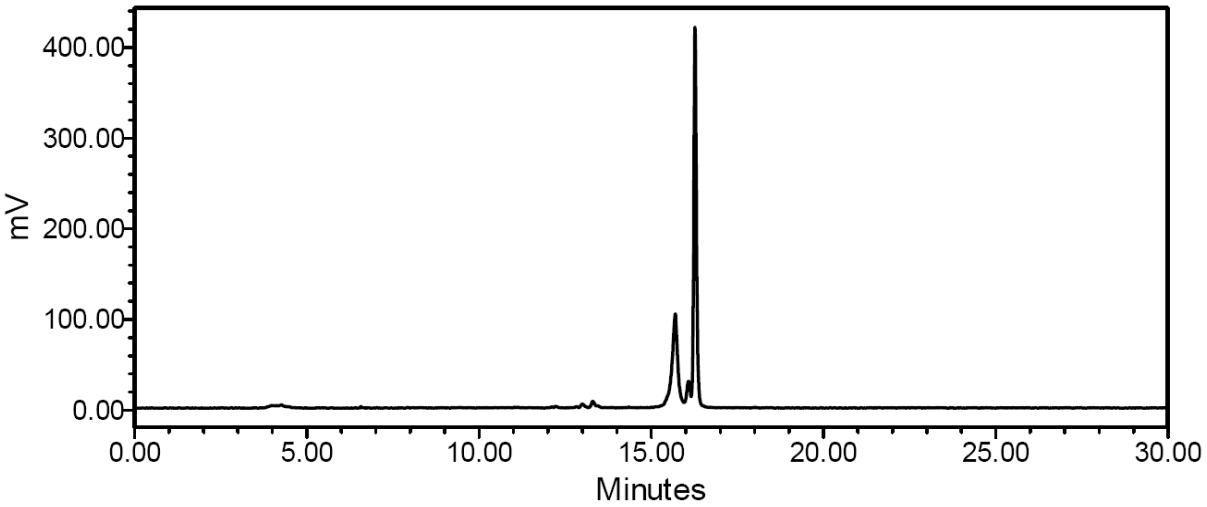


**Figure S 9.28** γ-HPLC chromatogram at 3 h following histidine challenge to $[^{99m}Tc(CO)_3(bipy)(MeTrz)]^+$ **5b**.

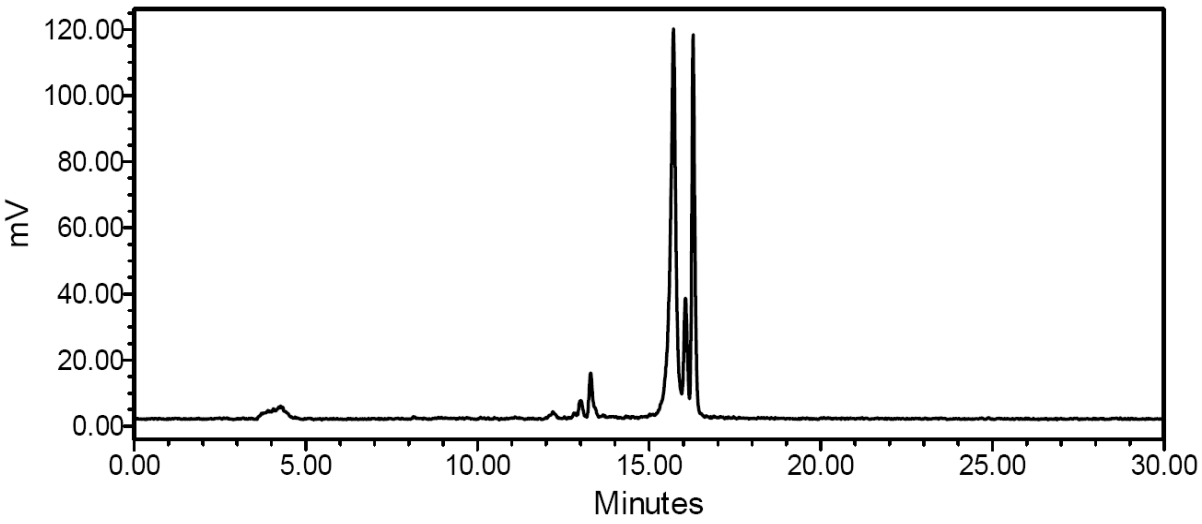


**Figure S 9.29** γ-HPLC chromatogram at 6 h following histidine challenge to $[^{99m}Tc(CO)_3(bipy)(MeTrz)]^+$ **5b**.